



Final Report for the Liquid Motion in a Rotating Tank Experiment (LME)

D.M. Deffenbaugh, F.T. Dodge, and S.T. Green
Southwest Research Institute, San Antonio, Texas

Prepared under Contract NAS3-27252

National Aeronautics and
Space Administration

Lewis Research Center

September 1998

Acknowledgments

The authors wish to acknowledge the valuable contributions to and support for this project by our sponsors at NASA Lewis Research Center (LeRC). While there was broad support from the whole team at LeRC, we would especially like to acknowledge the insight and encouragement from Penni Dalton, Richard Knoll, Erich Kroeger, and David Chato. Since the Preliminary Design Phase of the project was supported by NASA Goddard Space Flight Center, we would also like to acknowledge Jeffery Didion for his guidance and support. We would also like to thank the support teams at NASA Johnson Space Center Flight Safety, NASA Kennedy Space Center Ground Safety, Robert Stuckey in Flight Integration, and McDonnell Douglas Aerospace's SpaceHab Customer Integrations Group. Most of all we like to express our gratitude for the extraordinary efforts on-orbit by the two mission specialists, Astronauts Carlos Noriega and Edward Lu. Without their efforts onboard STS-84, we might never have produced the unique results represented in this report.

The authors wish to express our appreciation for the valuable support from the Southwest Research Institute team as well: the design efforts of Edgar Schroeder, Steve Green, Steve Petullo, Greg Dirks, and Don Shirley; the software efforts by Terry Grimley and Marty Menchaca; the electronic troubleshooting efforts of Lindy Ahr and Benjamin Piepgrass; the fabrication efforts by Marion Burzynski and Bill McLaren; the quality assurance effort of Ken Jones; and the qualification testing efforts by Rick Pitman. Finally, this report and all of the documentation on this project could not have been produced without the skill and patience of Mrs. Julie Valle, who prepared this report.

Available from

NASA Center for Aerospace Information
7121 Standard Drive
Hanover, MD 21076
Price Code: A06

National Technical Information Service
5285 Port Royal Road
Springfield, VA 22100
Price Code: A06

FINAL REPORT FOR THE LIQUID MOTION IN A ROTATING TANK EXPERIMENT (LME)

SwRI Project 04-6322
Document No. 6322-FNL-01, Original
NASA Contract NAS3-27252

Prepared by: D. M. Deffenbaugh
F. T. Dodge
S. T. Green

Date: May 31, 1998


Approved by:


SwRI Project Manager
Department of Fluids Engineering

Date:

5-22-98

Approved by:


SwRI Division Vice President
Division of Mechanical and Fluids Engineering

Date:

5/25/98

Mechanical and Fluids Engineering Division
Southwest Research Institute
P.O. Drawer 28510
6220 Culebra Road
San Antonio, Texas 78228-0510
(210) 684-5111

This page left intentionally blank.

REVISION RECORD

REVISION/ CHANGE	DATE	DESCRIPTION	APPROVAL ¹
Original	May 1998		

¹Document "changes" require approval on this page. Document "revisions" require the re-release of the cover page with approval signatures.

This page left intentionally blank.

EXECUTIVE SUMMARY

The Liquid Motion Experiment (LME), which flew on STS 84 in May 1997, was an investigation of liquid motions in spinning, nutating tanks. LME was designed to quantify the effects of such liquid motions on the stability of spinning spacecraft, which are known to be adversely affected by the energy dissipated by the liquid motions.

The LME hardware was essentially a spin table which could be forced to nutate at specified frequencies at a constant cone angle, independently of the spin rate. Cylindrical and spherical test tanks, partially filled with liquids of different viscosities, were located at the periphery of the spin table to simulate a spacecraft with off-axis propellant tanks; one set of tanks contained generic propellant management devices (PMDs). The primary quantitative data from the flight tests were the liquid-induced torques exerted on the tanks about radial and tangential axes through the center of the tank. Visual recordings of the liquid oscillations also provided qualitative information.

The flight program incorporated two types of tests: *sine sweep* tests, in which the spin rate was held constant and the nutation frequency varied over a wide range; and *sine dwell* tests, in which both the spin rate and the nutation frequency were held constant. The sine sweep tests were meant to investigate all the prominent liquid resonant oscillations and the damping of the resonances, and the sine dwell tests were meant to quantify the viscous energy dissipation rate of the liquid oscillations for steady state conditions.

The *sine sweep tests* showed that liquid resonances occurred in the cylindrical tanks in a range of nutation frequencies between 0.56 and 0.78 times the spin rate. Somewhat unexpectedly, resonances were also excited in the spherical tanks, for a nutation frequency range between 0.74 and 0.78 times the spin rate, although the amplitude of the resonant torques was smaller than for the cylindrical tanks. The damping of the resonances for the cylindrical tanks was found to be about 1% to 2% of critical, and the damping for the spherical tank resonances was found to be slightly larger. The PMDs tended to increase the resonant damping for cylindrical tanks and decrease it for spherical tanks. The *sine dwell tests* showed that the liquid energy dissipation rates tended to increase with spin rate and fill level. Also, PMDs tended to reduce the energy dissipation rate for cylindrical tanks and usually, but not always, increase the rate for spherical tanks. The energy dissipation rate data were not entirely consistent, sometimes being negative for some tanks or some torque axes, mainly as the result of difficulties in computing accurate values of the phase angle between the torque sinusoidal signal and the table angular velocity. The positive energy dissipation data did, however, agree well with previous ground test results and predicted the available flight data acquired from spacecraft fairly closely.

The LME flight data were compared to analytical results obtained from two companion IR&D programs at Southwest Research Institute. The comparisons indicated that the models predicted the observed liquid resonances, damping, and energy dissipation rates for many test conditions but not for all. It was concluded that improved models and CFD simulations are needed to resolve the differences. This work is ongoing under a current IR&D program.

Further flight tests are needed to help resolve the questions raised by the first flight. Future flight tests should employ a better method of isolating the load cells from various sources of noise. In addition, other tank geometries and locations should be investigated; for example, some spacecraft designs employ tanks on the spin axis rather than offset from the spin axis. Furthermore, the first flight showed that the effect of PMDs on liquid oscillations is not easy to predict, sometimes enhancing the resonant oscillations and sometimes damping them, depending on tank shape and PMD design. Future LME flights could investigate specific proposed PMD designs for current spacecraft and thereby eliminate unexpected interactions between the liquid resonances and the PMD.

This page left intentionally blank.

ACKNOWLEDGMENTS

The authors wish to acknowledge the valuable contributions to and support for this project by our sponsors at NASA Lewis Research Center (LeRC). While there was broad support from the whole team at LeRC, we would especially like to acknowledge the insight and encouragement from Penni Dalton, Richard Knoll, Erich Kroeger, and David Chato. Since the Preliminary Design Phase of the project was supported by NASA Goddard Space Flight Center, we would like to acknowledge Jeffery Didion for his guidance and support. We would also like to thank the support teams at NASA Johnson Space Center Flight Safety, NASA Kennedy Space Center Ground Safety, Robert Stuckey in Flight Integration, and McDonnell Douglas Aerospace's SpaceHab Customer Integrations Group. Most of all we would like to express our gratitude for the extraordinary efforts on-orbit by the two mission specialists, Astronauts Carlos Noriega and Edward Lu. Without their efforts onboard STS-84, we might never have produced the unique results represented in this report.

The authors wish to express our appreciation for the valuable support from the Southwest Research Institute team as well: the design efforts of Edgar Schroeder, Steve Green, Steve Petullo, Greg Dirks, and Don Shirley; the software efforts by Terry Grimley and Marty Menchaca; the electronic troubleshooting efforts of Lindy Ahr and Benjamin Piepgrass; the fabrication efforts by Marion Burzynski and Bill McLaren; the quality assurance effort of Ken Jones; and the qualification testing efforts by Rick Pitman. Finally, this report and all of the documentation on this project could not have been produced without the skill and patience of Mrs. Julie Valle, who prepared this report.

This page left intentionally blank.

TABLE OF CONTENTS

<u>Section</u>	<u>Page</u>
LIST OF FIGURES	xii
LIST OF TABLES	xiv
LIST OF ACRONYMS	xv
1. INTRODUCTION	1
1.1 DESCRIPTION OF PROBLEM	1
1.2 IMPORTANCE OF PROBLEM ADDRESSED BY LME	1
1.3 LME OBJECTIVES	3
1.4 BRIEF DESCRIPTION OF LME.....	4
1.5 LME SUCCESS CRITERIA	5
2. LME BACKGROUND	7
2.1 FORM OF LIQUID OSCILLATIONS IN SPINNING TANKS	7
2.2 ANALYTICAL MODELING OF LIQUID OSCILLATIONS IN SPINNING TANKS	8
2.2.1 Numerical Models	8
2.2.2 Approximate Analytical Models.....	8
2.3 LIMITATIONS OF GROUND EXPERIMENTATION.....	9
2.3.1 Spin Table Test Method.....	9
2.3.2 Drop Tower Spin Test Method.....	10
2.3.3 Forced Motion Spin Tables.....	10
2.4 NEED FOR THE LME IN-SPACE EXPERIMENT	11
3. DESIGN AND FABRICATION	13
3.1 DESIGN RATIONALE.....	13
3.1.1 Introduction.....	13
3.1.2 Design Requirements for Model Validation	13
3.1.3 Design Requirements for Applicability to Spacecraft	13
3.1.4 Response Parameters	14
3.2 TECHNICAL REQUIREMENTS	15
3.2.1 Choice of Carrier	15
3.2.2 General Configuration and Middeck Constraints	15
3.2.3 LME Experiment Requirements and Rationale.....	15
3.2.3.1 Tanks	16
3.2.3.2 Tank Fill Levels.....	16
3.2.3.3 Liquids.....	16
3.2.3.4 Spin Rates and Nutation Frequencies	17
3.2.3.5 Cone Angle.....	17
3.2.4 Environmental Controls.....	17
3.2.4.1 Tank Pressure and Liquid Temperature.....	17
3.2.4.2 G-jitter	18
3.2.5 LME Instrumentation Requirements.....	18
3.2.5.1 Electric Power.....	18
3.2.5.2 Data Transmission.....	18
3.2.5.3 Load Cells	18
3.2.5.4 Spin Rate and Nutation Frequency Counters.....	19
3.2.5.5 Spin Table Motion Instrumentation.....	19
3.2.5.6 Ambient Acceleration Instrumentation.....	19
3.2.5.7 Visual Recording and Lighting System.....	19
3.2.5.8 Time	20

TABLE OF CONTENTS (cont'd)

<u>Section</u>	<u>Page</u>
3.2.6 Data Acquisition System	20
3.2.7 Data Storage	20
3.2.8 Recorded Quantities	20
3.2.9 Summary of Technical Requirements	21
3.3 LME DESIGN	21
3.3.1 Overview	21
3.3.2 LME Tanks	22
3.3.3 Tank Propellant Management Devices	23
3.3.4 Load Cells and Tank Mounting Structures	24
3.3.5 Spin Table	26
3.3.6 Pedestal System	28
3.3.7 Accelerometer	29
3.3.8 Baseplate and Enclosure	29
3.3.9 Enclosure and Pedestal Cooling Systems	30
3.3.10 Enclosure Access Panel Electrical Interlock	31
3.3.11 LME Electrical System	31
3.3.12 Motor Speed Control	31
3.3.13 Strain Gauge Amplifier (SGA)	32
3.3.14 Data Acquisition System (DAS)	33
3.3.15 Optical Data Link	34
3.3.16 Experiment Interface Unit (EIU)	34
3.3.17 Power Distribution Module (PDM)	34
3.3.18 LME 28VDC Power Interconnection	35
3.4 FABRICATION AND ASSEMBLY	36
4. VERIFICATION TESTING	39
4.1 SCIENCE REQUIREMENTS VERIFICATION	39
4.2 INTEGRATION VERIFICATION	40
4.3 SAFETY VERIFICATION	42
4.4 GROUND SAFETY TESTS	45
4.5 ACCEPTANCE TESTS	46
5. FLIGHT OPERATIONS	47
5.1 OVERVIEW	47
5.2 EXPERIMENT ASSEMBLY AND CHECKOUT	47
5.3 OPERATIONS DURING TESTING	54
5.3.1 Loading Software	54
5.3.2 Test Selection	54
5.3.3 Instrumentation Verification and Observation	55
5.3.4 Fluid Tank Set Change	55
5.3.5 Ground Communications	56
5.3.6 Test Matrix	56
5.4 RAPID SAFING	57
5.5 DEVIATIONS DURING FLIGHT OPERATIONS	57
6. FLIGHT DATA ANALYSIS	61
6.1 INTRODUCTION	61
6.1.1 Sine Sweep Tests Characteristics	61
6.1.2 Sine Dwell Test Characteristics	62
6.1.3 Spin and Nutation Rates	63
6.1.4 Liquid Properties	64

TABLE OF CONTENTS (cont'd)

<u>Section</u>	<u>Page</u>
6.1.5 Flight Test Matrix Descriptors	64
6.2 DATA ANALYSIS.....	65
6.2.1 Data Reduction	65
6.2.2 Sine Sweep Test Results.....	66
6.2.3 Sine Dwell Test Data	72
6.2.4 Comparison of Energy Dissipation Rates to Ground and Spacecraft Flight Results	75
7. CONCLUSIONS AND RECOMMENDATIONS	79
8. REFERENCES	83
APPENDIX A	
Mechanical Assembly Drawings	A-1
APPENDIX B	
Software User's Guide	B-1
APPENDIX C	
Summary of Radial and Tangential Torque Histories for Cylindrical Tanks	C-1
APPENDIX D	
Summary of Radial and Tangential Torque Histories for Spherical Tanks.....	D-1

LIST OF FIGURES

Figure		Page
1-1	Idealized Spinning Spacecraft.....	1
1-2	INTELSAT IV On-Orbit Instability Tests.....	3
1-3	Nutation Control Design Process.....	4
1-4	LME Layout.	5
2-1	Free Surface Oscillations.....	7
2-2	Inertial Oscillations	7
3-1	Estimated Moment for Half-Full LME Cylindrical Tank. $\Omega_0 = 20$ rpm.....	19
3-2	LME Liquid Test Tanks.	22
3-3	LME Propellant Management Devices.	23
3-4	Tank Mounting Structure.....	24
3-5	LME Load Cell Design.	25
3-6	LME Spin Table.....	26
3-7	LME Spin Table.....	26
3-8	LME Tank/Load Cell Assembly.....	27
3-9	LME Pedestal Assembly.	28
3-10	Pedestal Drive System.....	28
3-11	Schematic of LME Enclosure.....	29
3-12	LME Enclosure.	29
3-13	LME Cooling System Electrical Block Diagram.....	30
3-14	LME Electrical System Block Diagram.	31
3-15	LME MSC Block Diagram.	32
3-16	LME SGA Block Diagram.....	33
3-17	LME DAS/EIU Block Diagram.....	33
3-18	LME PDM Block Diagram.	35
3-19	LME Power Wiring and Fusing Diagram	37
5-1	LME On-Orbit in SpaceHab Aboard STS-84.....	47
5-2	LME Enclosure Assembly.....	48
5-3	LME Stow Configuration.	49
5-4	LME Run Configuration.....	50
5-5	View of Enclosure and Lid Showing Locations of ¼-Turn Fasteners.	52
5-6	Hub Alignment Mark.....	52
5-7	Spin Table Latch Pin with Alignment Marks.	53
5-8	Spin Table Latch Pin, Cross-Section View.	53

LIST OF FIGURES (cont'd)

<u>Figure</u>	<u>Page</u>
5-9 LME During Operation.	54
5-10 LME Rapid Safing Timeline.	59
6-1 Predicted Resonant Frequency for a Spinning, Nutating Cylindrical Tank.	62
6-2 Predicted Resonant Frequency for a Spinning, Nutating Spherical Tank.....	62
6-3 Half Power Damping Computation.	62
6-4 Sample Data Time History for a Sine Sweep Test.....	65
6-5 Sample Filtered Torque Data for a Sine Sweep Test.....	65
6-6 Wobble Motor Rotation Rate for Test A0002 (20 rpm spin rate).	66
6-7 Radial Torque for Tank 1 (2/3 full cylinder) in Test A0101.....	66
6-8 Normalized Radial Torque for Tank 1 2/3 full cylinder) in Test A0101.	67
6-9 Expansion of Radial Torque for Tank 1 (2/3 full cylinder) in the Region of the Most Prominent Resonance..	68
6-10 Damping of Liquid Resonances for Both Cylinders and Spheres.....	68
6-11 Radial Torque for Tank 1 (2/3 full cylinder) in Test A0101.....	69
6-12 Comparison of Predicted Resonant Frequencies to Test Results for Cylindrical Tanks.....	69
6-13 Comparison of Predicted Resonant Frequencies to Test Results for Spherical Tanks.	71
6-14 Energy Dissipation Rates for Cylindrical Tanks.....	72
6-15 Energy Dissipation Rates for Spherical Tanks.	75

LIST OF TABLES

<u>Table</u>	<u>Page</u>
3-1 LME MSC Specifications.....	32
4-1 Science Requirement Verification.....	39
4-2 Integration Verification.....	41
4-3 Flight Safety Verification.....	42
4-4 Ground Safety Verification.	45
4-5 Project Requirement Verification.	46
5-1 Fluid Tank Identification List.....	54
5-2 LME Sweep Test Matrix.....	56
5-3 Timeline of Test Runs.	58
6-1 Summary of Resonant Frequency λ_{res} and Damping λ Data for Cylindrical Tanks.....	70
6-2 Summary of Resonant Frequency λ_{res} and Damping λ Data for Spherical Tanks	73
6-3 Summary of Energy Dissipation Rate Data for Cylindrical Tanks.....	74
6-4 Summary of Energy Dissipation Rate Data for Spherical Tanks.	76
7-1 Data Quality Test Matrix.....	80

LIST OF ACRONYMS

ADC	Analog-to-Digital Converter
BCD	Binary-Coded Decimal
CDR	Critical Design Review
CFM	Cubic Feet per Minute
DAC	Digital-to-Analog Converter
DAS	Data Acquisition System
ECDC	Electronically Commutated DC
EIU	Experiment Interface Unit
EMI	Electromagnetic Interference
HVM	Homogeneous Vortex Model
LSWD	Low Speed Warning Detector
MDP	Maximum Design Pressure
MODE	Middeck Orbital Dynamics Experiment
MPS	Manufacturing Planning Sheet
MSC	Motor Speed Controller
MUX	Multiplexer
NAR	Non-Advocate Review
ODL	Optical Data Link
PDM	Power Distribution Module
PDR	Preliminary Design Review
PGA	Programmable Gain Amplifier
PGSC	Payload and General Support Computer
PMD	Propellant Management Device
QA	Quality Assurance
SGA	Strain Gauge Amplifier

This page left intentionally blank.

1. INTRODUCTION

1.1 DESCRIPTION OF PROBLEM

The Liquid Motion in a Rotating Tank Experiment (LME) was a flight investigation of the characteristics of liquid motions in spinning, nutating tanks. The data from the flight tests will aid in determining the effects of such motions on the stability of spinning spacecraft.

Spacecraft are made to spin for a number of reasons, including gyroscopic stiffness, equal distribution of solar thermal loads, and positioning of the liquids in a tank over the outlet. Just as for any freely-spinning body, a spinning spacecraft can have a nutation motion superimposed on its steady spin; this nutation is sometimes called "coning." During nutation, the spin axis of a spacecraft rotates around its angular momentum vector, which is fixed in inertial space in the absence of any external torques or forces. Figure 1-1 illustrates such a motion for an idealized spacecraft containing liquid in two off-axis tanks. The angle between the spin axis and the angular momentum vector is the cone angle θ , which is a measure of the magnitude of the nutation. The angular rate at which the spin axis rotates around the angular momentum vector is called the nutation frequency λ . In a spacecraft-fixed coordinate system, λ is proportional to the spin rate Ω_0 according to:

$$\lambda = \Omega_0 \left(1 - \frac{I_{spin}}{I_{trans}} \right) \quad (1-1)$$

where I_{spin} is the mass moment of inertia of the spacecraft about the spin axis and I_{trans} is the mass moment of inertia about a transverse axis through the center of mass. The spacecraft is assumed to be axisymmetric. Since $I_{trans} > I_{spin}$ is the common mass distribution for a spinning spacecraft, Eq. (1-1) shows that the nutation frequency is smaller than the spin rate, $\lambda < \Omega_0$.

The nutation motion produces an oscillatory motion of the liquids in the tanks, which is the subject of LME.

1.2 IMPORTANCE OF PROBLEM ADDRESSED BY LME

The dynamic effects of liquid oscillations in a nutating spacecraft can form a positive feedback loop with the nutation and thereby cause the attitude control thrusters to consume fuel faster than planned, or in some cases, cause a loss of spacecraft stability. Although these dynamic effects are well recognized [Agrawal, 1984], there is a lack of quantitative knowledge about the oscillations that would permit the effects to be treated in the design of spacecraft. Consequently, spacecraft attitude control systems are usually designed quite conservatively.

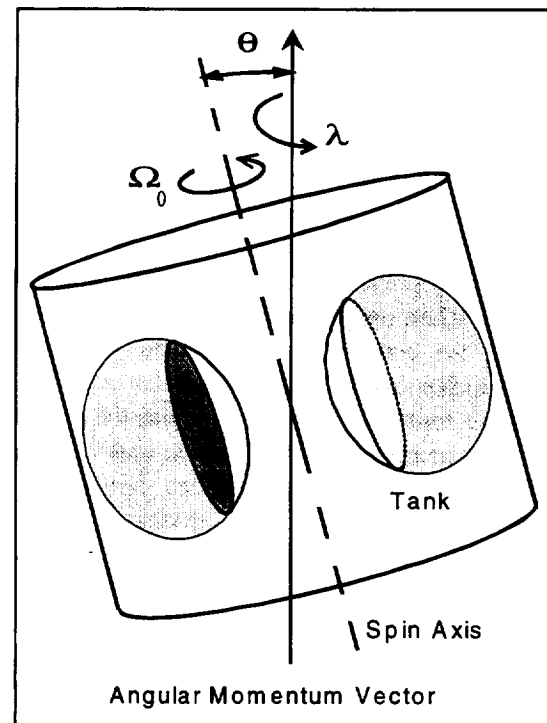


Figure 1-1. Idealized Spinning Spacecraft.

The spin axis rotates around the angular momentum vector, setting the liquid into motion.

Spacecraft stability and control. The spin axis of many modern spacecraft coincides with the axis of one of the smaller mass moments of inertia of the spacecraft [as assumed in Eq. (1-1)]; this configuration is a result of the need to fit the spacecraft in the Space Shuttle cargo bay or in the fairing of an expendable rocket, or merely because of the large mass of the apogee motor used for the transfer orbit. Such spacecraft are called "prolate" spinners. A dynamic peculiarity of prolate spinners is that energy dissipation causes the coning amplitude θ to increase rather than decrease as might be expected [Thomson, 1961]. The rate of increase of θ is predicted by:

$$\theta \frac{d\theta}{dt} = \frac{\Omega_0^2 (I_{trans} - I_{spin})}{E} \quad (1-2)$$

and $d\theta/dt > 0$ when $I_{trans} > I_{spin}$, which is the case for a prolate spinner. The nutation itself produces the liquid oscillations that create the viscous energy dissipation.

Equation (1-2) assumes that the liquid is merely a passive source of energy dissipation, which does not otherwise affect the spacecraft dynamics. This is a reasonable assumption when the liquid mass is small, but the liquid mass fraction of many current spacecraft approaches 50% of the total spacecraft mass [Agrawal, 1990]. The dynamics of the oscillations of such a large mass will interact with the nutation, especially if a liquid resonant oscillation is excited by the nutation, and may cause the cone angle to change rapidly even without considering energy dissipation. Since the energy dissipation rate of a resonant liquid oscillation is large, the combined effects of dynamics and energy dissipation from liquid resonances can lead to extremely rapid increases in the coning amplitude.

If the coning amplitude is not controlled by the attitude control motors, it will eventually increase to the point that the spacecraft spins about one of its transverse axes — the disastrous "flat spin" instability — and when this occurs the spacecraft usually cannot carry out its mission. The problem of rapid increase in coning amplitude is especially critical for spacecraft launched from the Space Shuttle, because they are uncontrolled during the first 100 seconds or so after being ejected from the shuttle bay when thruster firings are prohibited. The spacecraft's "time constant" τ for divergent nutation (i.e., defined as the time required for a given coning amplitude to increase by $e = 2.71828$) must be considerably larger than this coasting duration to prevent a flat spin. As an example of the problem, the Eurostar spacecraft (which is a prolate spinner when the apogee motor is attached) was initially estimated to have a τ well in excess of 100 seconds during the coasting period [Pocha, 1987]. However, preliminary drop tests of a scale model of the spacecraft showed that the time constant for the design liquid fill level was only about 30 seconds. The only credible source of the small τ 's was the onboard liquid, which constituted about 55% of the mass. Further drop tower investigations showed that τ could be more than doubled by removing the flexible vanes in the cylindrical-like tanks (needed to control the liquid location in low gravity when the spacecraft is not spinning). At that point, an extensive set of drop tower tests was initiated to find a design of anti-slosh baffles to damp the liquid motions. Eventually, a suitable design was found empirically, although the characteristics of the liquid motion causing the problem were never diagnosed.

As another example of the detrimental effects of liquid resonances, INTELSAT IV encountered coning motions in flight that had a much faster growth rate than ground tests predicted. To discover the cause of this, the spacecraft itself was used to conduct a series of *in-space* experiments by rotating the antenna platform to vary the nutation frequency. Figure 1-2 shows some representative test results. Large values of dedamping occurred when λ was in the range of 0.65 to 0.75 times Ω_0 . (Dedamping is the inverse of the divergent time constant.) As discussed later, this range coincides with the frequency range where

LME Final Report

"inertial wave" resonances of the liquid might be excited, although apparently that was not detected during ground tests or predicted by analysis. In this case, it was later discovered that the conical spherical tanks used in the spacecraft tended to magnify the effects of liquid resonances, and such tanks are no longer common.

The initial designs of many other commercial, NASA, and DOD spacecraft have been found by ground testing to be susceptible to liquid resonances and undesirably short divergent time constants.

Even when liquid resonances do not occur, energy dissipation caused by liquid motions is a major concern for prolate spinners since, as shown by Eq. (1-2), it causes the coning motion to diverge. This *unavoidable* source of θ growth must be controlled by the attitude control thrusters, and the rate at which propellant is consumed to do so is one of the factors that determines the life of the spacecraft [Hubert and Goodzeit, 1984]. The resulting uncertainty in end-of-life predictions for communications satellites, based on information available before launch, can be in excess of one year, often far exceeding customer requirements [Chobotov and Purohit, 1993].

1.3 LME OBJECTIVES

The above discussion demonstrates the need for practical and scientific benefits that can be realized by acquiring data on liquid oscillations in spinning tanks in a realistic low-gravity environment. The Liquid Motion in a Rotating Tank Experiment was designed to fulfill these objectives. The specific objectives of LME were to:

1. Obtain data in a realistic low-g environment to validate and provide physical guidance for improved analytical models of liquid motions in the tanks of spinning spacecraft.
2. Obtain data in a realistic low-g environment to validate and improve, if necessary, procedures for scaling ground test data from spacecraft physical models to flight conditions.

The first objective required the acquisition of data over a wide range of the relevant dimensionless parameters. The second objective required the acquisition of data for a range of dimensionless parameters that are representative of actual spacecraft.

The ultimate goal of LME, as illustrated by the flow chart in Figure 1-3, was to develop a better design process for the nutation control of spinning spacecraft. The chart also indicates that LME's *scientific*

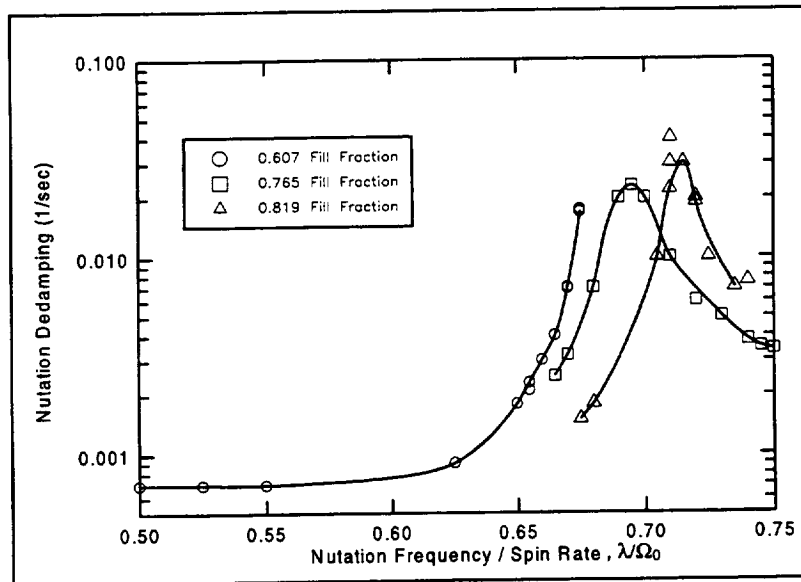


Figure 1-2. INTELSAT IV On-Orbit Instability Tests.

Liquid resonances near $\lambda/\Omega_0 \approx 0.7$ caused a rapid increase in coning amplitude.

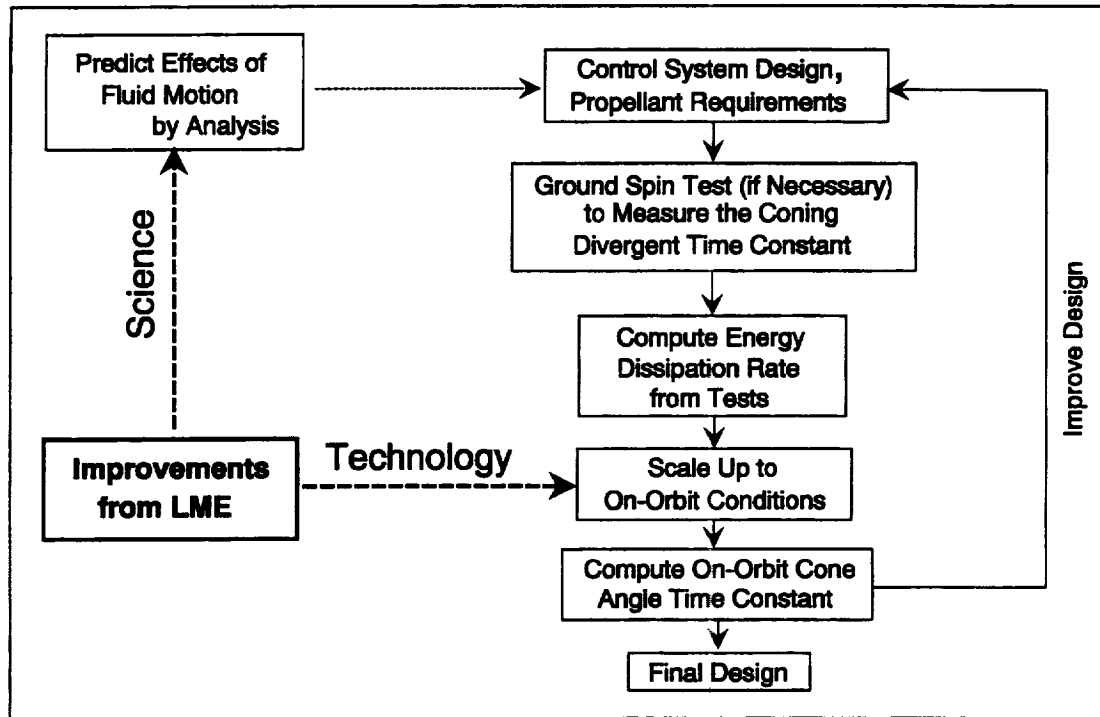


Figure 1-3. Nutation Control Design Process.

LME was designed to have both technological (ability to scale up ground tests to on-orbit conditions) and scientific benefits (better predictions of the effects of fluid motions).

benefits would lead to a better initiation of the design process, and LME's *technological benefits* would lead to better and more reliable use of ground testing.

1.4 BRIEF DESCRIPTION OF LME

As shown by Figure 1-4, LME is essentially a spin table that creates a nutation motion of tanks containing liquid mounted on the table. The table is driven by two independently controllable electric motors; one of the motors provides a steady rotation, and the other provides a nutation with an independently adjustable nutation frequency. The inclination of the spin table to the spin axis (i.e., the cone angle θ) is constant. The experiment was designed to be mounted on a SpaceHab double adapter plate, with a separate locker used for storage of tanks and other items. Four tanks of two different shapes and fill levels were mounted on the spin table for each test.

The primary LME test variables were tank shape, liquid fill level, liquid viscosity, spin rate, nutation frequency, and PMD design. Three sets of four tanks were used in the tests, with one set containing typical propellant management devices (PMDs). Three spin rates were used for each tank set. Two of the spin rates were sufficiently high to make surface tension effects negligible compared to the centrifugal acceleration imposed on the test tanks; these "high g" tests were meant to investigate the scaling of liquid motions with respect to spin rate. The third spin rate was low enough to make surface tension effects significant; these tests were meant to investigate liquid motions under "low g" conditions. The primary test measurements were the liquid torque exerted on the tanks and the phase angle of the torque relative to the table motion. In addition, visual recordings were made of the liquid motions.

LME Final Report

1.5 LME SUCCESS CRITERIA

LME's objectives could be realized and the experiment would be deemed a complete success if:

- ❑ Torque time-history data with an acceptable signal-to-noise ratio were acquired for all four tanks of all three tank sets over the full range of high and low spin rates, and visual recordings could be made of the liquid motion in one tank of each set.

All objectives, except the investigation of surface tension effects, would be realized, but over a smaller parameter range, by a more limited success criterion:

- ❑ Torque time-history data with an acceptable signal-to-noise ratio were acquired for both tanks of a given shape with a single fluid for the two highest spin rates.

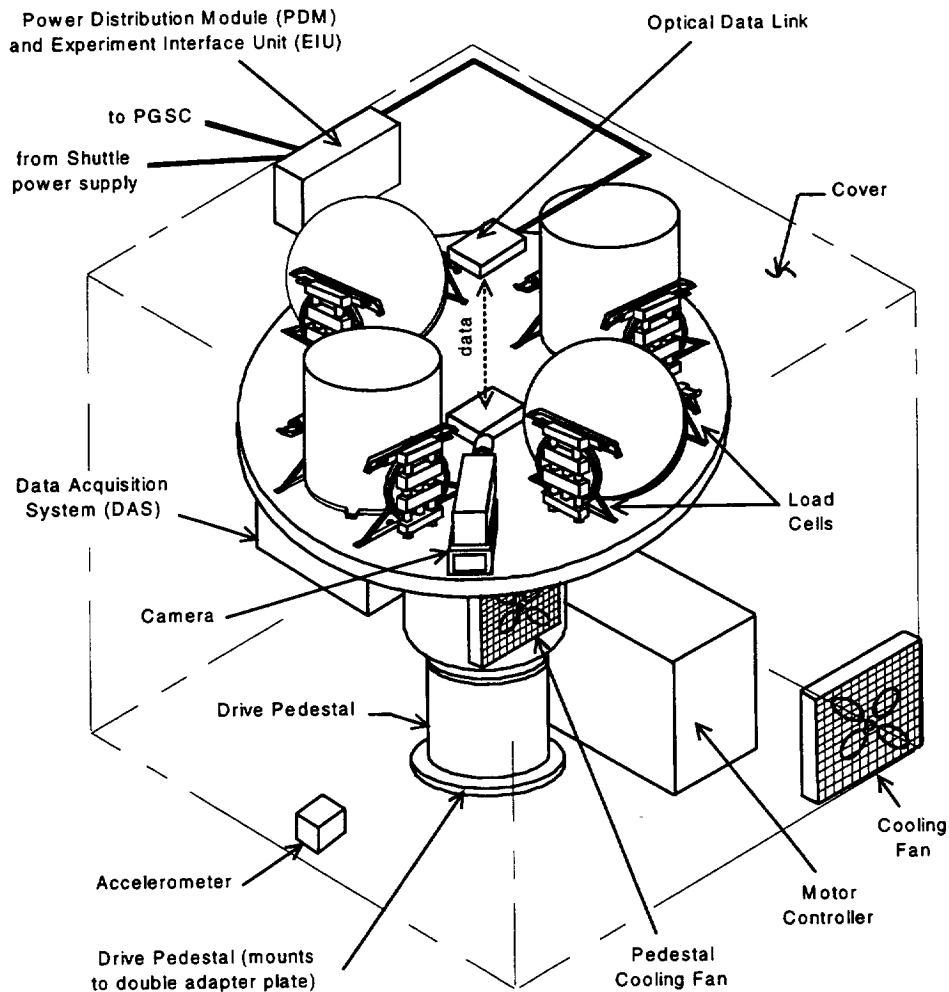


Figure 1-4. LME Layout.

LME simulates the nutation dynamics of a spinning spacecraft.

This page left intentionally blank.

2. LME BACKGROUND

2.1 FORM OF LIQUID OSCILLATIONS IN SPINNING TANKS

Liquid in a partially-full spinning tank can oscillate in two distinctly different modes: **free surface waves**, and **inertial (internal) waves**. Of these two, the inertial wave mode is the more important because the resonant frequency of such modes are in the range that can be excited by nutation.

Free surface waves are similar to the sloshing that occurs in non-spinning tanks, as shown in Figure 2-1. In a spinning tank, the centrifugal acceleration $R(\Omega_0)^2$ (R is the distance from the spin axis to the free surface) is analogous to a steady acceleration g (such as gravity), so the resonant frequency is proportional to $\Omega_0(R/d)^{1/2}$ where d is the tank diameter [Abramson, 1966]. Since $R > d$ and the proportionality constant is greater than one, the resonant frequency is greater than the spin rate; in fact, unless the fill level is very small, the resonant frequency is greater than twice the spin rate [Weihs and Dodge, 1991]. Thus, the resonant frequency of free surface waves is always higher than the frequency of the nutation motion that excites them. Free surface waves cause an oscillation of the liquid center of mass, so in general, both a torque and a force on the tank are produced.

Inertial waves are vortex-like oscillations of the liquid interior, as shown in Figure 2-2, and can occur even in the absence of a liquid free surface. The oscillations are excited by Coriolis accelerations induced by nutation of a spinning tank [Greenspan, 1969]. For a symmetrical tank spinning about its z -symmetry axis, the theory shows, for example, that the liquid pressure field $p(r, \theta, z)$ corresponding to a liquid oscillation at a frequency λ is governed by:

$$\frac{\partial^2 p}{\partial r^2} + \frac{\partial^2 p}{r^2 \partial \theta^2} + \left(1 - \frac{4\Omega_0^2}{\lambda^2}\right) \frac{\partial^2 p}{\partial z^2} = 0 \quad (2-1)$$

When the oscillation frequency $\lambda > 2\Omega_0$, this differential equation is "elliptic" and the oscillations are the free surface sloshing oscillations mentioned above. But, when $\lambda < 2\Omega_0$, the equation is "hyperbolic" and the oscillations are inertial waves [Greenspan, 1969]. No general theory is available for tanks spinning about an axis outside the tank, but approximate analytical models indicate that even for this nonaxisymmetric geometry, all the inertial wave resonances occur in the frequency range between 0 and $2\Omega_0$, and the most prominent resonances have frequencies less than Ω_0 [Pfeiffer, 1974; El-Rahab and Wagner, 1981; Agrawal, 1993; Dodge, *et al.*, 1994]. Since the motion of the free surface is a secondary effect for an inertial wave,

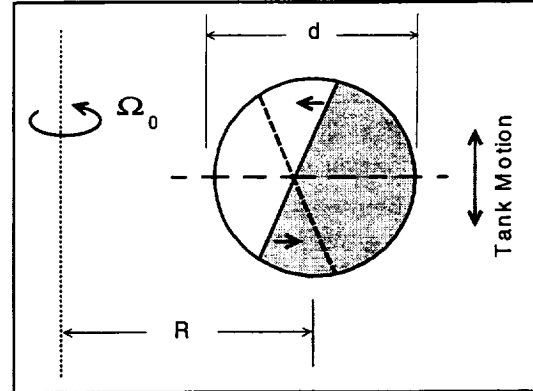


Figure 2-1. Free Surface Oscillations.
Resonant frequency is greater than $2\Omega_0$.

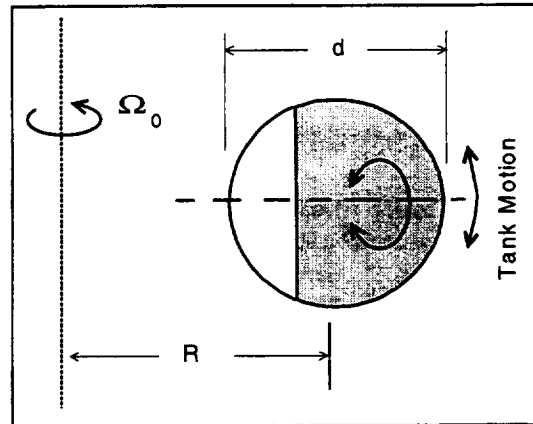


Figure 2-2. Inertial Oscillations.
Resonant frequency is less than $2\Omega_0$.

the liquid center of mass does not necessarily oscillate, in which case the liquid motion exerts only a torque on the tank.

2.2 ANALYTICAL MODELING OF LIQUID OSCILLATIONS IN SPINNING TANKS

2.2.1 Numerical Models

Analytical solutions of the general fluid dynamics equations for a spinning, nutating tank are not feasible. For that reason, various numerical schemes have been developed specifically for nutating tanks containing liquid, but, at present, they can only be applied to cases in which the centrifugal acceleration is smaller than gravity, or else they only simulate the free surface motion or contain other assumptions that limit their usefulness for spacecraft applications [Chen and Pletcher, 1991; Hill, *et al.*, 1988].

General purpose computational fluid dynamics codes, such as FLOW-3D and NASA-RIPPLE, can, in principle, be applied to nutating tanks containing a liquid having a free surface and are not restricted to linearized or small amplitude motions. Unfortunately, test cases using these codes do not always yield realistic simulations [McIntyre, *et al.*, 1990]. The reasons for the failures are not clear but may be related to the solution algorithm, which is based on elliptic equations. Furthermore, the codes simulate transient motions, so the natural frequencies of the liquid motions cannot be found directly but instead must be discovered by the numerical equivalent of sweeping over a range of excitation frequencies.

2.2.2 Approximate Analytical Models

Since neither exact analytical nor numerical methods can generally be applied to all situations of interest, several approximate, linearized analytical theories have been developed for low viscosity liquids [Selmi and Herbert, 1992] and for high viscosity liquids [Pfeiffer, 1974; El-Rahab and Wagner, 1981; Dodge, *et al.*, 1994]. Spacecraft propellants have a low viscosity, so the most applicable of these approximate theories is one based on the inviscid Euler equations called the *Homogeneous Vortex Model*. This model is summarized below since it forms the basis for the design of LME.

The essential features of the Homogeneous Vortex Model (HVM) are:

- ❑ The vorticity of the liquid motion, which is a major complication in the analysis of spinning liquids, is averaged over the volume of the liquid, with the result that it is only a function of time (i.e., is homogeneous) rather than of space and time.
- ❑ A reasonable assumption is made about the liquid velocity: the velocity field is assumed to be composed of a rotational part due to the homogeneous vortex, plus a second part due to a vector velocity potential that corrects the vorticity-induced motion such that the combination "fits" into the geometric shape of the liquid volume, plus a third part due to a scalar velocity potential that allows for oscillations of the free surface.

There are enough free parameters in the HVM to satisfy all the requirements imposed by Euler's equations and the boundary conditions at the tank walls and the liquid free surface. The model also lends itself well to numerical solution using commercially-available finite element codes [Everstine, 1981], so special computer programs are not needed. The solution yields the liquid natural frequencies of the inertial oscillations and the free surface oscillations, as well as the liquid motion produced by any specified motion of the tank

[Guibert, 1984; Pfeiffer, 1984]. Only one inertial oscillation mode is predicted, however, so it is assumed to be the dominant mode. When the motion is forced at this liquid natural frequency, the amplitude of the liquid motion becomes infinitely large since viscosity and nonlinear effects are both neglected in the model. But, a boundary layer analysis can be readily added to the basic flow to estimate energy dissipation rates and to limit the amplitude of resonant motions [Ebert, 1984a; Dodge, *et al.*, 1998]. In addition, surface tension can be included when the centrifugal acceleration is small, as it may be for a slowly spinning spacecraft [Ebert, 1984b; Dodge, *et al.*, 1994].

Implications from the HVM. Example numerical results obtained from the HVM show that free surface oscillations are only lightly coupled to the inertial mode of oscillation. This again demonstrates the need to consider the inertial mode as predominant. With respect to ground tests on spacecraft dynamics, another conclusion from the HVM is that when the centrifugal acceleration is large compared to gravity (i.e., analogous to low gravity), the natural frequencies of *all* liquid oscillations are proportional to the spin rate, just as the nutation frequency.*

HVM Validation. The HVM simplifies the physics of the liquid motion in ways that make it difficult to judge the realism of its predictions or to determine its range of reliability. For example, the fundamental assumption of a stable homogeneous vortex may not be physically realizable for all tank shapes and configurations (apparently, the vortex will be stable only in tanks that permit geostrophic contours to fit completely within the liquid [Pederson, 1984]). Also, only one inertial wave resonance is predicted. In the absence of confirming data over a wide range of parameters, there is thus no assurance that the HVM predictions are reliable. This lack of accurate and detailed experimental data to provide physical insight has, in fact, greatly hampered the development of *all* analytical and numerical models.

2.3 LIMITATIONS OF GROUND EXPERIMENTATION

Because of the lack of a validated analytical model of liquid oscillation effects, ground-based testing is now used to confirm the operation of specific spinning spacecraft before flight and to make empirical re-designs when the initial design is unsatisfactory. The most common types of ground tests are: (1) a dynamically-scaled prototypical spacecraft model mounted on an air-bearing spin table, and (2) a small, dynamically-scaled spacecraft model allowed to fall freely (drop test). Each method is discussed below.

2.3.1 Spin Table Test Method

For this method, a prototypical-size spacecraft model containing tanks and simulated propellants is mounted on a spin table supported on a low friction air bearing. The entire apparatus is housed in a vacuum chamber to minimize aerodynamic drag. The model is spun up, the restraints are released, and the apparatus is allowed to spin freely on the air bearing [Wilson, *et al.*, 1972]. The growth rate of the cone angle in time is monitored, from which the effective energy dissipation due to all causes is computed by an "energy sink" model, such as given by Eq. (1-2).

* In some spin-table ground tests of spacecraft models, system resonant frequencies have been found that are not strictly proportional to the spin rate [Agrawal, 1984]. These resonances are thought to be nonlinear interactions of the liquid resonances with the spacecraft precession.

To overcome Earth's gravity, the spin rate of the model must be very large, usually much larger than the design spin rate. Otherwise, the liquid configuration is not geometrically the same as for flight conditions, and moreover spurious free surface oscillations (caused by changing the direction of the gravity vector when the model nutates) will be excited, with the result that the test data will be invalid. But, the required high spin rates have the drawback that the model's Reynolds number $R\Omega_0 d/\nu$ is much larger than the flight value (ν is the liquid kinematic viscosity.) Since the energy dissipation rate is a strong function of Reynolds number, the results of a spin table test must be scaled up to flight conditions, based on Reynolds number considerations and an assumption about how energy dissipation is related to cone angle divergence. Furthermore, the ground-test Reynolds number is usually so large that the liquid oscillations are turbulent, whereas the flight Reynolds number is generally small and the flow is laminar, in which case there is no valid way to relate one energy dissipation rate to the other. (The turbulent nature of the oscillations in ground tests has been confirmed visually [Zedd and Dodge, 1985].) Energy dissipation rates are so large, in fact, for most air-bearing tests that inertial wave resonances are overdamped compared to space conditions, and thus their effects are less than may occur in space.

2.3.2 Drop Tower Spin Test Method

The influence of gravity can be eliminated by conducting free fall tests of small dynamically-scaled spinning spacecraft models in a drop tower [Harrison, 1984]. This kind of test allows the model spin rate and the model liquid viscosity to be chosen so as to duplicate the full-scale value of the Reynolds number, thereby permitting the divergent time constant of the coning to be interpreted directly as the flight value. High spin rates are still required, however, to accumulate enough nutation cycles during the short period of free fall to estimate the coning growth rate reliably. The drop tower test method is not without other drawbacks, such as the existence of an upper bound on measurable time constants, difficulty in duplicating tank details in small models, and the need to change the moment of inertia ratios of the model and then re-balance it to conduct resonance searches in which the nutation frequency is varied. The major drawback of a free fall method is, however, its short test duration; this makes it practically impossible to investigate the fundamental characteristics of liquid oscillations.

Because of the reasonably good accuracy with which drop tower tests of a specific spacecraft design correlate with flight measurements, this method has tended to become the standard in recent years.

2.3.3 Forced Motion Spin Tables

Since neither air-bearing spin tables nor drop tower tests can conveniently determine the fundamental aspects of liquid oscillations, several investigations have been conducted with *forced motion* spin tables [Zedd and Dodge, 1985; Guibert, 1984; Guibert, 1986]. For this method, the test tanks are mounted on a spin table that simulates a coning motion over a range of nutation frequencies and spin rates. The main advantage of the method is that resonance searches can be accomplished without any need to alter moment of inertia ratios or re-balance the model. (LME is an adaptation of this method to in-space testing.) The oscillating torque exerted by the liquid on the tank is the primary test measurement. Liquid motion can be observed by video cameras spinning with the spin table, although the turbulent, chaotic motion due to the high spin rates generally obscures the underlying oscillations. When the cone angle is large enough, such that the forced motion can overcome the high values of turbulent damping, inertial wave resonances are *sometimes* evident in the torque measurements. Generally, however, the high spin rates required for ground testing make it impossible to measure oscillatory torques accurately and to visualize any inertial waves

imbedded in the turbulent, chaotic flow. Thus, in this respect, the method suffers from the same limitations as the air bearing and free fall methods.

2.4 NEED FOR THE LME IN-SPACE EXPERIMENT

It is evident from the above discussion that ground tests are not generally an adequate method for acquiring data to validate analytical models of liquid motions in spinning tanks or to provide physical guidance for improved models. Experiments in space can overcome the limitations of ground-based testing. Specifically, experimentation in a low-gravity environment for a reasonable period of time is the *only method* that can simultaneously obtain the following desirable test characteristics:

1. Eliminate the unwanted and spurious effects of gravity and thereby obtain the correct geometric liquid-tank configuration and diminish to a negligible level the once-per-nutation-cycle gravitational excitation of the free surface.
2. Allow low spin rates to be used and thus reduce energy dissipation rates to values typical of spacecraft flight, eliminate overdamping of inertial waves, permit visual observation of liquid oscillations, investigate the importance of surface tension, and acquire parametric design data.
3. Permit sufficiently long test times to obtain data and physical understanding to guide analytical model development.

This page left intentionally blank.

3. DESIGN AND FABRICATION

3.1 DESIGN RATIONALE

3.1.1 Introduction

As its objectives indicated, LME was meant to acquire data that would (1) validate analytical models and provide guidance for improved models, and (2) aid in the attitude control system design and operation of future spacecraft. To accomplish the model validation objective, a wide range of parameters was varied and controlled in the tests. To accomplish the spacecraft design objective, the values of the test parameters were chosen in accordance with the principles of dynamic similarity.

3.1.2 Design Requirements for Model Validation

To be applicable for validating models and providing physical guidance for improved models, the LME tests had to cover a wide range of parameters. The design of LME allowed the following important parameters to be varied:

- ☐ **Tank shape** — spheres and cylinders
- ☐ **Tank fill level** — one-third and two-thirds full
- ☐ **Tank internal hardware** — “bare” tanks and tanks containing typical propellant management devices
- ☐ **Liquid properties** — viscosity variation over an order of magnitude, including a value typical of common spacecraft propellants
- ☐ **Tank motion** — spin rate variation from a low value to high values; and nutation frequency variation from a value well below the spin rate to a value slightly more than the spin rate.

3.1.3 Design Requirements for Applicability to Spacecraft

Dynamic similarity between the LME tests and representative spacecraft required *geometric* similarity, *kinematic* similarity, and *physical effect* similarity [Baker, *et al.*, 1991]. These requirements were incorporated into the design of LME, as discussed below.

Geometric similarity. LME incorporated spherical tanks that were geometrically similar to typical spacecraft tanks at about 1/6 to 1/10 scale. The ratio of the spin axis offset from the tank center to the LME tank diameter was about 1.4, also representative of many spacecraft.

Kinematic similarity. The motion imparted to the LME tanks was similar to the nutation of a spinning spacecraft. The ratio of the LME nutation frequency to spin rate was varied over a range from near zero to more than one, thus simulating spinning spacecraft with a wide range of inertia ratios. The LME coning angle was within the range of spacecraft values.

Physical effects similarity. The physical effects that govern the motion of liquid in spinning tanks are (a) centrifugal forces, (b) Coriolis forces, (c) viscous forces, (d) inertia forces, (e) surface tension forces, and (f) gravitationally-induced (or equivalent) body forces. These six forces can be grouped into five

LME Final Report

independent non-dimensional ratios which impose the requirements of physical effects similarity. LME used values for all five ratios that are typical of representative spacecraft, as discussed below.

- ❑ **Reynolds number.** This ratio of *inertia* and *viscous* forces determines the rate of energy dissipation and the resonant amplitude of fluid oscillations. The characteristic liquid velocity in nutating tanks is proportional to $\lambda\theta d$, so the relevant Reynolds number is proportional to $\lambda\theta d^2/\nu$. For the values of the parameters chosen for LME (discussed in Section 3.3), the Reynolds number was varied from about 1/100 to 1/2 of representative spacecraft.
- ❑ **Rossby number.** This ratio of *inertia* and *Coriolis* forces determines the fluid dynamic characteristics of the liquid oscillations. It can be expressed as $\lambda\theta d/R\Omega_0$, which is a combination of the geometric and kinematic parameters d/R , λ/Ω_0 , and θ . Because of the geometric and kinematic similarity of LME to spacecraft, the LME Rossby number was similar to spacecraft values.
- ❑ **Centrifugal Bond number.** This ratio of *centrifugal* and *surface tension* forces determines when surface tension forces are important. It can be expressed as $\rho R d^2 (\Omega_0)^2 / \sigma$, where σ is the liquid surface tension. The centrifugal Bond number can be on the order of one for a slowly spinning spacecraft, and several thousand for a rapidly spinning spacecraft. The LME value of the centrifugal Bond number was varied from about one to a value large enough to make surface tension unimportant.
- ❑ **Galileo number.** This ratio of *viscous* and *gravity* forces determines the damping of gravity-induced free surface oscillations. It is extremely large for spacecraft and was also large for LME, as a result of the low residual effective gravity in space. Consequently, the similarity requirements imposed by the Galileo number are represented in LME.
- ❑ **Froude number.** This ratio of *inertia* and *gravity* forces is extremely large for spacecraft, indicating the unimportance of gravity forces in space. It also had a very large value for LME.

3.1.4 Response Parameters

The stated objectives of LME were realized by measuring the following response parameters:

- ❑ **Resonant conditions.** The most important characteristic of an oscillation is its natural frequency. The resonant condition was determined by measuring a parameter that obtained a maximum at the resonant frequency; in this case, the liquid torque exerted on the tank, as a function of the test variables.
- ❑ **Liquid force, torque, and energy dissipation.** The force and torques exerted on the tank by the oscillating liquid are important characteristics, not only in applications, but also in providing guidance and validation for analytical modeling. The resonant frequency was determined by noting the conditions at which the maximum torque occurs. Viscous energy dissipation could not be measured directly in LME tests, but it was computed from the measured torques and the known tank motion.

3.2 TECHNICAL REQUIREMENTS

3.2.1 Choice of Carrier

In Phase A, a trade study was made of the choices of Shuttle carrier. The study showed that middeck lockers were the best choice for LME, with the major advantage of this choice being the assistance it could provide the astronauts in conducting the tests and correcting any minor difficulties that might arise. LME was designed to meet all of the requirements of a middeck payload. After fabrication, during the early test phase, LME was reassigned to the SpaceHab on STS-84, whose lockers and constraints are practically identical to middeck lockers.

3.2.2 General Configuration and Middeck Constraints

The LME hardware was designed for a middeck locker double adapter plate attached to two payload mounting panels, with additional material stored in two single lockers. The general layout was shown previously on Figure 1-4.

Middeck power and lights. Middeck experiments can utilize up to 115 watts of electrical power (average) at 28 volt DC, and up to 200 watts peak for no more than ten seconds. A limited amount of lighting is also available, and more can be provided by temporary lights.

Middeck double adapter plate. A standard double adapter plate replaces two adjacent middeck lockers (one above the other). Its overall dimensions are 18.135 inches wide by 21.882 inches high. The payload cannot protrude more than 19.687 inches from the face of the double adapter plate, thus giving a usable volume of about 7800 in³ (4.5 ft³). The total weight of the experiment can be no more than 120 pounds, including the weight of the double adapter plate, and the experiment c.g. needs to satisfy certain other requirements [NSTS-21000-IDD-MDK, Rev. A, 1992].

Middeck lockers. A single locker has a usable volume of about 3500 in³ (17.312 inches wide by 9.950 inches high by 20.320 inches deep).

Overall LME Dimensions. As a result of the size, volume, and weight constraints, the maximum diameter of the LME spin table was chosen to be about 16.5 inches. The centrifugal acceleration at the center of the test tanks for the lowest spin rate needed to be small enough to allow surface tension effects to be investigated and still be at least ten times the background steady g-level (assumed to be about 10⁻⁴ g_o for design purposes [Dunbar, *et al.*, 1991]). The LME tank diameter was chosen to be 4.5 inches, and the center of each tank on the spin table was 5.9 inches from the spin axis. These choices permitted the minimum spin rate to be selected at a reasonable value of 4 rpm. The LME tanks were sufficiently large to simulate full-scale spacecraft tanks, and four such tanks could be mounted at a time around the periphery of the spin table.

3.2.3 LME Experiment Requirements and Rationale

The requirements described below are derived from the LME objectives and the choice of carrier. They are revisions of those described in the corresponding Phase A and Phase B documents [Dodge, 1989; Dodge and Deffenbaugh, 1993] to incorporate improvements made at PDR, NAR, and CDR.

3.2.3.1 Tanks

The tests tanks were unpressurized, sealed containers in the shape of spheres and circular cylinders ($L/d = 1$) having nominal diameters of 4.5 inches. LME employed a total of three sets of four tanks, with each set comprising two tanks of each shape. Two sets of four tanks were "bare" (i.e., contained no internal hardware), and the third set contained propellant management devices (PMD) of a design, such as central "vanes," that are used in some spinning spacecraft. All tanks were transparent to permit visual observation and recording.

Rationale. Flat-bottom cylindrical tanks were chosen as one of the LME tank shapes, not because they are widely used in spacecraft, but because they would (a) facilitate comparisons between test and theory, and (b) emphasize the effects of inertial oscillations, which are easily excited in cylindrical tanks. Spherical tanks were chosen as tanks representative of spacecraft usage. Data from the bare tanks were valuable in validating analytical models and in providing fundamental knowledge about fluid motions. Data from the tanks containing PMDs were valuable in determining the changes in energy dissipation resulting from their use. Model PMDs were designed with the aid of potential users of the LME data.

3.2.3.2 Tank Fill Levels

All tanks were pre-filled and sealed before flight. Each tank of the same shape was filled to a different level. The selected levels were one-third and two-thirds full.

Rationale. The selected fill levels covered a significant range of satellite operations and were sufficiently different to validate models parametrically. Although additional fill levels would have been desirable, Phase B trade studies concluded that this would require a capability to transfer liquids to the tanks from reservoirs, which would have substantially increased the mechanical complexity of the experiment and increased the probability of a mechanical malfunction during flight. Alternatively, the second set of bare tanks could have employed two other fill levels, but the Phase B trade study showed that using this set to investigate a different viscosity was more important parametrically than two additional fill levels. Adding more tanks of each shape would have also permitted more fill levels to be investigated, but twelve tanks appeared to be the maximum number that could be stored. Additional fill levels can be tested in a re-flight, if necessary.

3.2.3.3 Liquids

Two liquids with different viscosities were employed. The liquids "wetted" the tank material and were compatible with it, and the liquids were reasonably transparent to permit visual observations. One liquid had a low viscosity (e.g., 1 cp) to simulate typical spacecraft propellants. The second liquid had a viscosity about ten times greater than the first. The surface tension of the liquids was as large as possible, considering the other test requirements.

Rationale. The viscosity was varied in tests that were otherwise identical so as to discriminate clearly the influence of viscosity on liquid damping and energy dissipation. The need to use a wetting liquid and to minimize contact angle hysteresis were not critical for inertial oscillations, but hysteresis was minimized to diminish any influence it might have on the results. The choice of liquids was not critical and the selection was made on the basis of flight safety. Candidates included water, silicone oil, and immersion

(index of refraction matching) liquids. Water was the eventual choice. Glycerin was added to the water to obtain the second, higher viscosity liquid.

3.2.3.4 Spin Rates and Nutation Frequencies

Spin rates were low enough to maintain laminar flow in the tanks, permit visualization of the flow in the tanks (by a video camera mounted on the spin table), and satisfy the low and high centrifugal Bond number requirements. As discussed previously, the lowest allowed spin rate was about 4 rpm. The highest spin rate chosen was 20 rpm. An intermediate spin rate of 14 rpm was also used. For each spin rate, the nutation frequency could be varied from near zero to a value about equal to the spin rate or held constant at a selected value.

Rationale. A spin rate of 20 rpm was about as high as could be used for a 4.5-inch diameter tank and still be assured of laminar flow. Further, this spin rate yielded a centrifugal Bond number of about 30, which was large enough to make surface tension effects insignificant. The intermediate spin rate of 14 rpm yielded a centrifugal Bond number of about 15 (which was still large enough to make surface tension negligible) and allowed the tests to investigate the effect, if any, of spin rate on inertial oscillations.

The homogeneous vortex model predicts that the dominant inertial oscillations have a natural frequency in the range between zero and the spin rate, and the general theory indicated that other inertial resonances might occur in the range of zero to twice the spin rate. Hence, the spin table needed to be able to explore a nutation frequency range from zero to a value equal to the spin rate to locate all the dominant resonances.

3.2.3.5 Cone Angle

LME had to use a cone angle in the range of a few degrees, in order to simulate spacecraft. The value chosen was 5°.

Rationale. The design cone angle value of spinning spacecraft is typically 1° or so. For LME, the cone angle was, therefore, chosen to be small, but large enough to create liquid-induced torques that could be accurately measured using practical load cell instrumentation. Phase B design studies and laboratory investigations indicated that a value of 5° was adequate for both purposes.

3.2.4 Environmental Controls

3.2.4.1 Tank Pressure and Liquid Temperature

Tank liquid temperature did not have to be controlled specifically. The small power requirements of LME and the heat sink capability of the experiment kept the temperature near ambient (approximately 20 °C). The test tanks did not need to be pressurized since the liquids were non-volatile (i.e., "storable") and tank pressures remained near ambient. The temperature was measured periodically to ensure that the desired conditions had been achieved.

3.2.4.2 G-jitter

The lowest test spin rate (4 rpm) exerted a steady centrifugal acceleration of about $2.7 \times 10^{-3} g_0$ on the test liquids, which was more than ten times the ambient "effective" gravity of $2.4 \times 10^{-4} g_0$ during "normal" operations and was over fifty times the rms gravity level during "quiet" times [Dunbar, *et al.*, 1991]. The frequency content of the background g-level was also much higher than any LME spin rate.

The Shuttle environment also included thruster firings and random, sometimes large amplitude vibrations called "g-jitter." Because of the need to maintain the desired liquid orientation in the tanks, testing at the lowest spin rate could not be conducted during primary thruster firings, although the higher spin rate tests could be conducted, if necessary. Vernier engine burns would not cause problems because of their lower acceleration level and short duration. G-jitter would not normally cause problems for LME, because the frequency content of the jitter is considerably higher than the frequencies of inertial wave oscillations; that is, the liquid would "filter" out the g-jitter.

3.2.5 LME Instrumentation Requirements

All data acquisition instrumentation, except as noted below, was mounted on the spin table.

3.2.5.1 Electric Power

Electric power for instrumentation and electronics on the spin table was required to be supplied through slip rings from the SpaceHab power supply.

3.2.5.2 Data Transmission

To reduce electrical noise, an optical link was specified to transmit the test data from the rotating parts of the hardware to the experiment computer. The optical system was mounted on the spin table, with one "transmitter-receiver" mounted on the table and the other "transmitter-receiver" mounted on the experiment's stationary protective cover. Test commands were also transmitted to the spin table through the optical link.

3.2.5.3 Load Cells

The oscillatory torque exerted on the test tanks by the liquids was specified to be measured by an appropriate arrangement of load cells. Load cell sensitivity requirements were estimated from the homogeneous vortex model by computing the liquid torque exerted on a 4.5-inch diameter cylindrical tank with $L/d = 1$ when the tank was half full of liquid having a density of one gram per cm^3 . The predicted amplitude of the torque about a circumferential axis through the liquid c.g. was:

$$M = 1.2 \times 10^{-6} \lambda^2 \theta \left[\frac{(\lambda/\Omega_0)^2 - 0.83(\lambda/\Omega_0) + 0.73}{1 - (\lambda/0.67\Omega_0)^2} \right] - 1.7 \times 10^{-7} \Omega_0^2 \theta \quad (3-1)$$

where Ω_0 and λ are in rpm, θ is in degrees, and the torque is in in-lbs; the radial moment is comparable in magnitude. The natural frequency of the inertial oscillation is $0.67\Omega_0$ for this case. Equation (3-1) is plotted in Figure 3-1 for $\Omega_0 = 20$ rpm and $\theta = 5^\circ$, assuming a reasonable damping value such that the smallest value

LME Final Report

of the denominator in the resonance term in Eq. (3-1) is 0.1. With this assumption, the peak moment is about 0.01 in-lb; for a spin rate of 4 rpm, it would be about 0.0004 in-lb. To acquire adequate data at smaller and larger fill levels, the smallest torque that had to be discriminated was specified to be 0.0001 in-lb, and the largest torque was specified to be 0.04 in-lb. The resolution of the load cell was specified to be at least $\pm 5\%$ of the indicated signal to ensure that the data was accurate enough for model validation. In addition, the load cells had to be able to withstand launch loads and the steady centrifugal loads of flight testing. The load cells were designed to eliminate any centrifugal torque imposed on the sensing elements by the mass of the tanks.

These load cell requirements were severe, but previous ground testing [Dodge and Garza, 1967], LME Phase B design studies and laboratory investigations, as well as experience gained from the MODE middeck experiment [Van Schoor and Crawley, 1992], showed that load cells designed on the principle of using a "bending" sensing element and semiconductor strain gauges could meet the requirements.

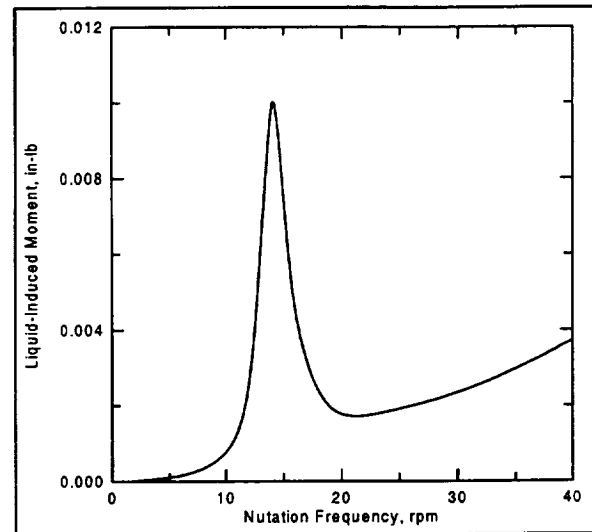


Figure 3-1. Estimated Moment for Half-Full LME Cylindrical Tank. $\Omega_0 = 20$ rpm.

The spike in the curve indicates a resonance.

3.2.5.4 Spin Rate and Nutation Frequency Counters

To obtain data on natural frequencies and to be able to compute energy dissipation rates from the test data, the resolution of the time history of the spin rate and nutation frequency was specified to be ± 0.1 rpm for each test. Calibrated controllers for the spin table drive motors were used for this purpose.

3.2.5.5 Spin Table Motion Instrumentation

The experiments were conducted for a fixed value of cone angle (5°). Consequently, there was no specific requirement for a spin table motion sensor, since the unsteady angular velocity and acceleration of the spin table at each tank location could be computed from the spin rate and nutation frequency. The motor controllers generated a reference signal from which the phase of the torque signals could be determined relative to the table motion.

3.2.5.6 Ambient Acceleration Instrumentation

Measurement of the background acceleration was specified to help interpret any anomalies that might be present in the test data. For this purpose, a three-axis accelerometer was mounted on the LME enclosure base. The required acceleration range of the accelerometers was $10^{-3}g_0$ to $0.1g_0$ over a range of frequencies from near zero to about ten Hertz.

3.2.5.7 Visual Recording and Lighting System

Visual recordings of the liquid motions in at least one tank per test were specified to aid in interpreting the measured moment data. A video camera was mounted on the spin table and focused on one

tank per test. A dilute suspension of small particles was added to the test liquid to aid in visualizing the bulk liquid motions. The lighting system and camera field of view were determined during Phase C.

3.2.5.8 Time

The data acquisition system was specified to supply time tags in the data records to correlate with test operations. In addition, a digital clock in the field of view of the camera was used to record elapsed test time.

3.2.6 Data Acquisition System

The experiment incorporated its own data acquisition and control system. Most measurements were measured in analog form (i.e., voltages) and transformed to digital form for storage. The analog-to-digital system (an electronic wiring board) was mounted on the spin table. The Shuttle Payload and General Support Computer (PGSC—a PC-compatible “briefcase” computer) was used to control the experiment and for temporary data storage.

The experiment computer largely controlled each test run, supplied signals to the electrical motors and instrumentation as needed, and temporarily stored the test data. Assistance from the mission specialists was required to change and verify system setups and to conduct other operations as needed.

3.2.7 Data Storage

The experiment generated approximately 4000K bytes of data that was stored permanently for later reduction and analysis. The results of each test series were stored temporarily in the PGSC’s disk drive, after which it was transferred to floppy disks for permanent storage. A single high density floppy disk had adequate capacity to store the results from all tests of each tank set in compressed form, which was estimated to be less than 1000K bytes.

3.2.8 Recorded Quantities

To summarize, the following quantities were measured and recorded for each test.

1. Spin rate (motor rpm).
2. Wobble rate (motor rpm).
3. Oscillatory liquid-torque amplitude time history (load cell).
4. Reference signal between angular position and coning motion (moment phasing).
5. Elapsed time from start of test.
6. Visual recordings of liquid motion.
7. Ambient acceleration (time history).
8. Enclosure temperature.
9. Load cell temperature.

All analog signals were acquired nearly continuously by sampling them at a high data rate.

3.2.9 Summary of Technical Requirements

<u>Parameter</u>	<u>Requirement</u>
Tank shapes	Circular cylinders ($L/d = 1$) and spheres
Number of tanks	Two of each shape per test set; three sets (changed in flight); one set to contain typical PMDs
Tank diameter	4.5 inches \pm 0.1 inches
Tank fill levels.....	Two per tank shape (1/3 and 2/3 full nominal; $\pm 0.5\%$ maximum difference between each tank of the same shape and fill level; volume measured to $\pm 0.25\%$)
Test liquid.....	Two liquids of different viscosity (nominal viscosities of 1 cp and 10 cp, measured to $\pm 5\%$); transparent; non-hazardous for use in the crew area
Spin rates	0 - 20 rpm, controlled and measured to ± 0.10 rpm
Nutation frequencies	0 - 40 rpm, controlled and measured to ± 0.10 rpm
Centrifugal Bond No	From about 1 to a value high enough to make surface tension effects negligible
Oscillatory moment measurement .	Load cells for each tank; ability to measure torque amplitudes as small as 0.0001 in-lb up to 0.04 in-lb; accuracy of $\pm 5\%$ of amplitude including temperature drift
Visual recording	Framing rate 30 to 60 pictures/sec; field of view to include one tank.
Time.....	Time tags in digital data recordings, and digital clock in field of view of visual recorder; ± 1 second.
Acceleration environment.....	No testing during primary thruster firings or during periods of g-jitter that exceed $10^{-3} g_0$ rms,
Ambient temperature.....	Between 18° C and 27° C; measured to $\pm 2^\circ$ C.
Power.....	28 volt DC, wattage within the capability of a middeck carrier
Data storage	Analog signals converted to 12 bit digital signals; total storage required is 4000K bytes
Drift of electronics	No more than $\pm 5\%$ from the calibration over the temperature range
Noise in data.....	No more than $\pm 0.5\%$ of minimum signal amplitude

3.3 LME DESIGN

3.3.1 Overview

The LME equipment consists of a mounting pedestal and drive unit which supports and rotates a circular table containing four tanks with liquid fill; a layout of the equipment was shown previously in Figure 1-4. The circular spin table is detachable from the pedestal for stowage during launch and landing. The tank supports on the spin table include strain gauge torque sensors to measure the torques exerted on the tanks by the moving liquid inside them. The pedestal contains two DC electric motors, one (the "spin" motor) to provide the controlled spinning of the spin table, the other (the "wobble" motor) to provide a nutation motion. The table contains an electronic data acquisition system (DAS) with which to amplify and digitize the strain gauge signals from the torque sensors. The DAS on the spin table is connected to an

operator console consisting of a standard NASA Payload and General Support Computer (PGSC) via an RS-422 serial link which is optically coupled from the table. Another RS-422 serial port on the PGSC is connected to the experiment interface unit (EIU) which functions to control the spin and wobble motor speeds and to switch power to the experiment modules. The experiment is under the control of the PGSC which sets the motor speeds according to the experiment operation profile selected by the operator, and stores the data transmitted to it by the DAS. Housekeeping data are also monitored by the DAS and the EIU and sent to the PGSC for storage.

3.3.2 LME Tanks

Figure 3-2 shows schematic drawings of the LME spherical and cylindrical tanks. The inside diameters of all tanks are nominally 4.5 inches and are constructed of a transparent polycarbonate plastic. The tanks were manufactured in two pieces and assembled with a special adhesive for polycarbonate plastic. Each tank has a fill port with a single o-ring seal. The fill port threads were locked in place with an adhesive thread locking compound after the tanks were filled to ensure a leak-tight port for all vibration environments.

Counterweights were attached to the top or bottom of each tank to make the geometric center of the tank coincide with the combined center-of-mass of the tank and the mounting structure that moved with the load cell. During flight, the centrifugal acceleration caused by the spinning forced the liquid to be symmetrically oriented along the outer wall of the tank. Thus, the axial location of the tank center and the center of mass of the tank-liquid-moving structure remained on a radial plane from the spin axis; this was important to minimize the "dead load" torque on the tank load cell. The weight of an empty cylindrical tank (with counterweights) was about 0.91 lb (415 grams), and the weight of an empty spherical tank (including counterweights) was about 0.68 lb (306 grams). The mass moments-of-inertia for an empty cylindrical tank are: $I_{spin} = 2.74 \text{ lb-in}^2$ (7930 gram-cm²) and $I_{trans} = 3.75 \text{ lb-in}^2$ (10850 gram-cm²). The corresponding values for an empty spherical tank are: $I_{spin} = 1.26 \text{ lb-in}^2$ (3690 gram-cm²) and $I_{trans} = 3.07 \text{ lb-in}^2$ (8990 gram-cm²).

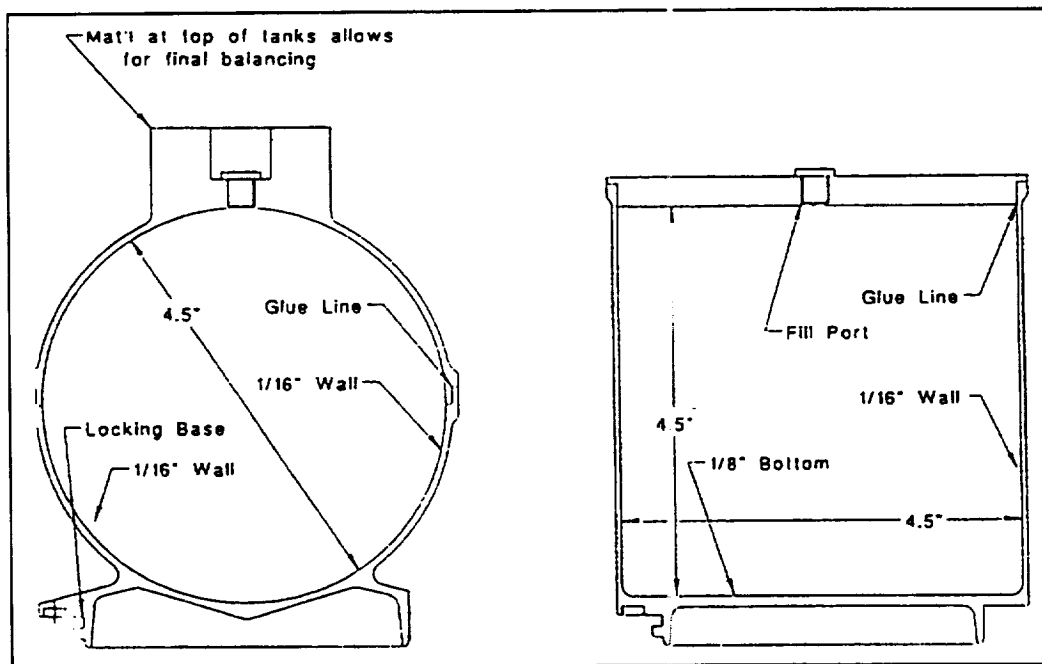


Figure 3-2. LME Liquid Test Tanks.

The tanks were transparent to permit flow visualization.

LME Final Report

None of the tanks was completely axisymmetric, and the cylindrical tanks had a slight axial taper (0.018 inch per inch of axial length) to allow them to be removed from the manufacturing mold.

The tanks were filled to either the 1/3 or 2/3 full level with a liquid consisting of pure water (nominal viscosity of 1.0 cp) or a mixture of pure water and glycerin (nominal viscosity of 10.0 cp). Cornauba wax particles were added to the water of one tank of each set to aid in flow visualization. The particles were approximately 100 micron diameter and had a density close to that of the water. The liquid/particle fill of the test tanks was selected for minimum toxicity and minimum hazard in case of leakage from the tanks. The liquid mixtures were selected as being compatible with the plastic, metallic, and adhesive materials of the test tanks. The liquid mixture specifications were submitted to the JSC toxicologist for review and approval.

The LME test tanks were filled at SwRI before LME delivery to KSC. A materials compatibility test was performed that confirmed that there was no degradation of structural strength due to any incompatibility between the fluid and sealed tank construction materials. Each tank was also proof pressure tested to 1.5 times its maximum design pressure (MDP) and leak tested to ensure that no unacceptable leakage of the contents could occur, either during or after ground, launch, or operational vibration and temperature environments are encountered.

A total of twelve tanks was required for the LME on-orbit operations. During launch and landing, all twelve tanks were stowed in a locker drawer. The tanks were removed from the locker only as needed and were immediately attached to the spin table. Each tank was stowed inside a resealable plastic bag when not in use so that the tank could be visually inspected for leaks before it was transferred to the LME spin table.

3.3.3 Tank Propellant Management Devices

In addition to two sets of "bare" spherical and cylindrical tanks, one set of two cylindrical tanks and two spherical tanks was fitted with generic propellant management devices (PMDs). PMDs are sometimes used in spinning spacecraft to position liquid over the tank outlets during non-spinning periods and sometimes to attempt to reduce large energy dissipation rates. Figure 3-3 shows the LME PMDs.

The cylindrical tank PMD was a circular plate containing a 2.23 inch (5.72 cm) diameter hole. It was located in the tank so as to bisect the tank into two equal halves. This kind of PMD has been found to damp liquid resonances [Pocha, 1984]. The PMD was made of 1 mm clear polycarbonate sheet material.

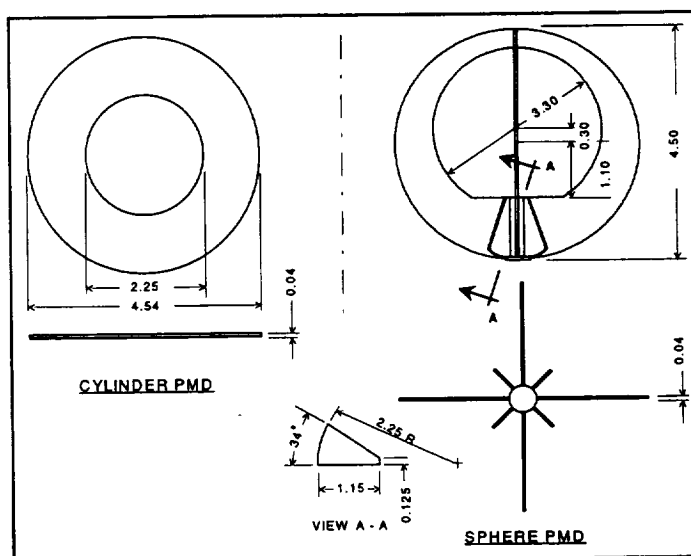


Figure 3-3. LME Propellant Management Devices.
The cylinder PMD bisects a cylindrical tank. The axis of the vaned sphere PMD is oriented along the radial axis of a spherical tank.

The spherical tank PMD was a typical vane design. It was composed of two large circular vanes that extended over the entire tank diameter and four small vanes. In a spacecraft, this kind of PMD captures a certain quantity of liquid between the large vanes during periods of weightlessness and directs it to the small vanes over the tank outlet. For LME, the axis of the vane system was oriented along a radial axis such that the small vanes were located at the outer diameter of the tank; this arrangement preserved the symmetry of the liquid orientation in the tank. The PMD was made of 1 mm clear polycarbonate sheet.

3.3.4 Load Cells and Tank Mounting Structures

The primary quantitative data obtained from the LME tests were the torques exerted on the test tanks by the contained liquid. These torques were measured by extremely sensitive load cells. As shown in Figure 1-4, two load cell structures were used for each tank to provide support for the test tank and a capability of sensing both radial and tangential torques. The load cells were attached to the tank mounting structures used to hold the tanks on the spin table.

Figure 3-4 schematically describes the parts of the tank mounting structure that move with the tanks, and thus exert a torque on the sensing elements of the load cells. Figure 3-5 shows the active parts of the load cell. (NOTE: All dimensions in these and succeeding figures are given in inches.) Other parts of the load cell needed to lock the load cell and tank mounting structure rigidly to the spin table when the hardware is stowed are not shown in Figure 3-4.

Tank mounting structure. The tank mounting ring structure shown in Figure 3-4 was made of aluminum and had a total weight of about 0.11 lb (50.6 gram). Its mass moments-of-inertia were: $I_{spin} = 0.66 \text{ lb-in}^2$ (1640 gram-cm²) about the tank symmetry axis, and $I_{trans} = 0.46 \text{ lb-in}^2$ (1350 gram-cm²) about a transverse axis through the center of mass of the tank. The entire weight of the ring structure, the test tank, and liquid was supported by the tensioned springs that connect the load cell (Figure 3-5) and the load cell holder brackets.

Load cells. As mentioned previously, each tank employed two load cells.

The load cells were made primarily of aluminum. The sensing element of each load cell was a set of semiconductor strain gauges mounted to very thin stainless steel beams, as shown in Figure 3-5. The plane of the sensing elements passes through the center of mass location of the tank and tank mounting structure. When a torque was exerted about the radial axis of the tank from the spin table axis to the tank center line,

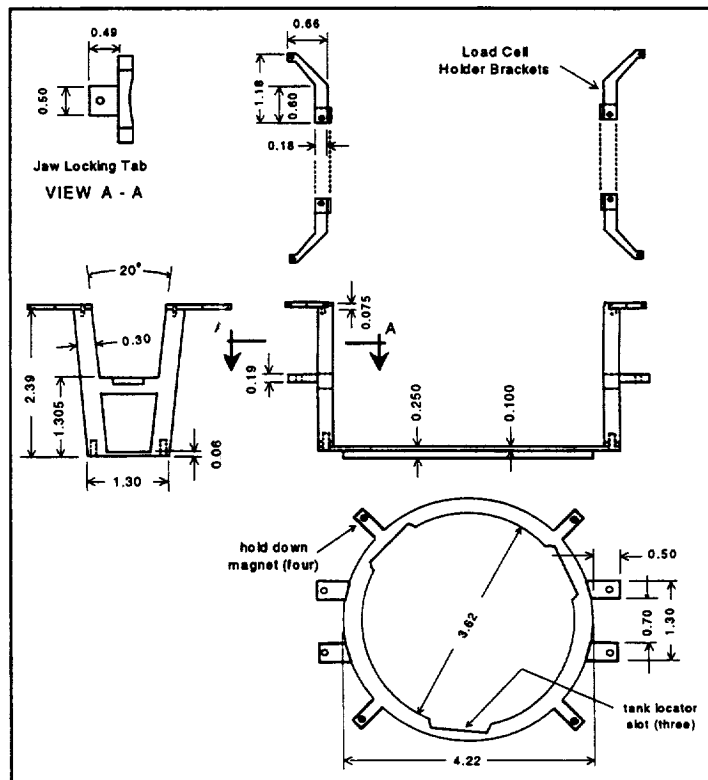


Figure 3-4. Tank Mounting Structure.

The mounting structure and tanks are supported entirely by the load cell springs connected to the load cell brackets; the support is effective only in a weightless environment.

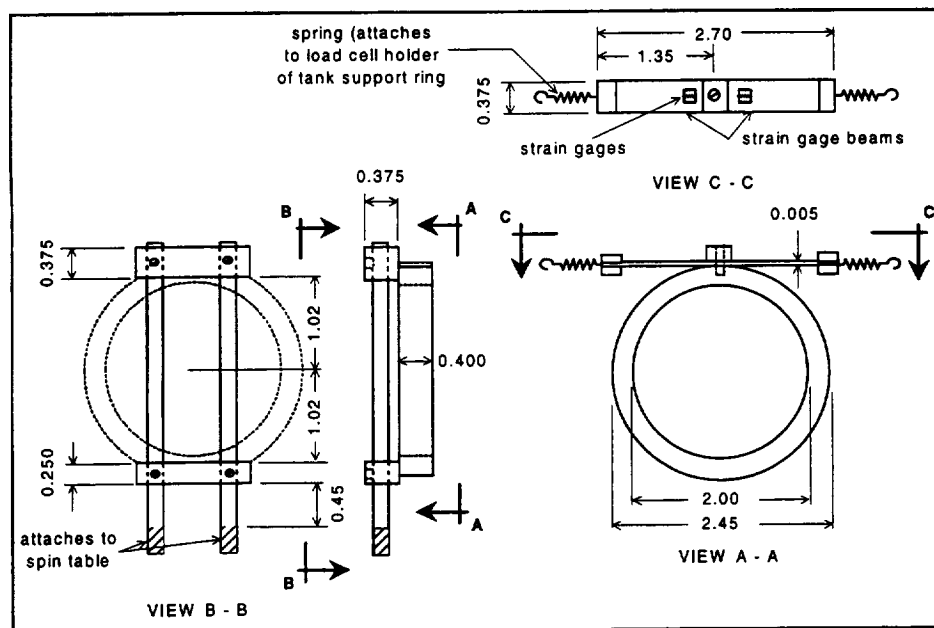


Figure 3-5. LME Load Cell Design.

Two load cells are used for each tank. The strain gauge sensing elements are connected electrically to measure the torque about a radial axis from the spin table center to the tank center and the torque about a tangential axis perpendicular to the radial axis, while being insensitive to radial and axial forces.

the beams of one of the two load cells deflected upward, and the beams of the other load cell deflected downward. Conversely, when a torque was exerted about the tangential axis of the tank (perpendicular to the radial axis), one end of each beam of a load cell deflected upward and the other end deflected downward, with an identical deflection pattern occurring for the beams of the other load cell. Thus, by using an appropriate electrical bridge, the load cells measured both radial and tangential torques simultaneously. (A radial torque also introduces a negligible twist to each beam.) For purely axial or radial motions of the tank without a change in the tilt of the tank, the strains imposed on the strain gauges effectively canceled out; thus, the load cells were insensitive to forces.

Load cell pre- and post-flight calibration. The strain gauge beams were connected to the tank support structure by tensioned springs. This arrangement provided adequate axial support of the tank in the weightless environment of flight but not in the 1-g environment of a laboratory, in which the tank and mounting structure would "sag" significantly. For that reason, the load cells could not be calibrated in the laboratory when they supported a tank. Instead, each load cell was calibrated by positioning it horizontally to eliminate the dead weight acting on the sensing elements, and a fixture was used to load the load cell statically over a range of torques. The sensitivities of a typical load cell as determined from this procedure were: 0.4 in-lb/volt (4.52×10^5 dyne-cm/volt) for radial torques and 0.09 in-lb/volt (1.02×10^5 dyne-cm/volt) for tangential torques. The difference between the two sensitivities was a result of the larger moment arm for radial torques compared to tangential torques. The smallest torque imposed on the load cells was 0.005 in-lb (5600 dyne-cm), although the minimum torque that could be sensed was somewhat smaller. The calibrations were repeated after the flight tests. The differences in pre- and post-flight calibration were small, so the pre-flight calibration factors were used to reduce the flight data.

Flight calibration. Just prior to a flight data test, the torque offset of each load cell was determined by rotating the spin table at the test spin rate without nutation. The measured torques (caused by slight

misalignments, etc.) were recorded so that they could be subtracted from the test measurements during in-flight data viewing and post-flight data analysis.

3.3.5 Spin Table

The LME spin table consisted of a 16.5-inch (41.9 cm) diameter aluminum disk measuring 0.375 inches (0.953 cm) thick. Figure 3-6 shows a drawing of the table and associated hardware, and Figure 3-7 shows a photograph of the spin table. The spin table carried the four tank mounting assemblies, which included a latching mechanism to lock the mounts to the table for protection of the strain measuring sensors when actual testing was not being done. The data acquisition system (DAS) was also mounted on the spin table. A small video camera was also mounted on the spin table to allow video data of the visualization particles to be recorded by an externally mounted video recorder. The lens of the camera was protected by a clear polycarbonate plastic cover.

The spin table was detachable from the pedestal rotational system (Section 3.3.6) for stowage during launch and landing. Two finger-retractable spring-mounted pins on the table fit into holes in the hub of the pedestal to latch the spin table to the pedestal. The orientation of the table on the pedestal was maintained in the correct orientation by an alignment pin on the pedestal hub. The design of the hub-pin latch was such that in the event of failure of one of the latch pins, the remaining pin was sufficient to hold the table to the pedestal for all rotational speeds up to and including the maximum runaway speed of 250 rpm. (An overspeed switch on the spin table actually limited the table speed to

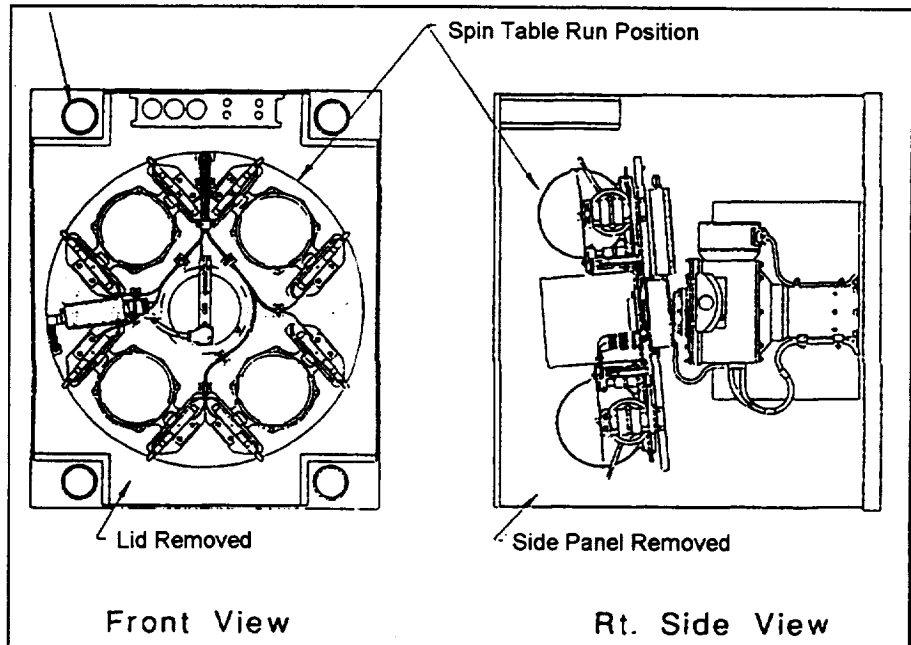


Figure 3-6. LME Spin Table.

The spin table is shown attached to the drive pedestal with spherical and cylindrical tanks mounted on it.



Figure 3-7. LME Spin Table.

Four tank mounting assemblies are shown with the assembled load cells and wiring.

40 rpm.) Centrifugal forces at the 250 rpm maximum runaway speed were not sufficient to overcome the spring forces of the pin springs and unlatch the pins from the pedestal hub. The spin table contained cutouts which allowed the position of the latching pins to be visually confirmed. The pin mechanisms contained alignment markers which allowed the pin positions to be seen through the table cutouts.

The tanks and tank mounting assemblies had a positive latching mechanism which were implemented by a bayonet twist and lock system on the bottom of each tank, as shown in Figure 3-8. Magnets on each tank and the mounting assembly lock together when the tank was rotated to the proper position, thus providing a force to prevent the tank from rotating free. Alignment marks on the tanks and the mounting assembly provided a visual check on the correct orientation of the tanks for assembly. The marks also provided visual confirmation that the tanks were in the locked orientation.

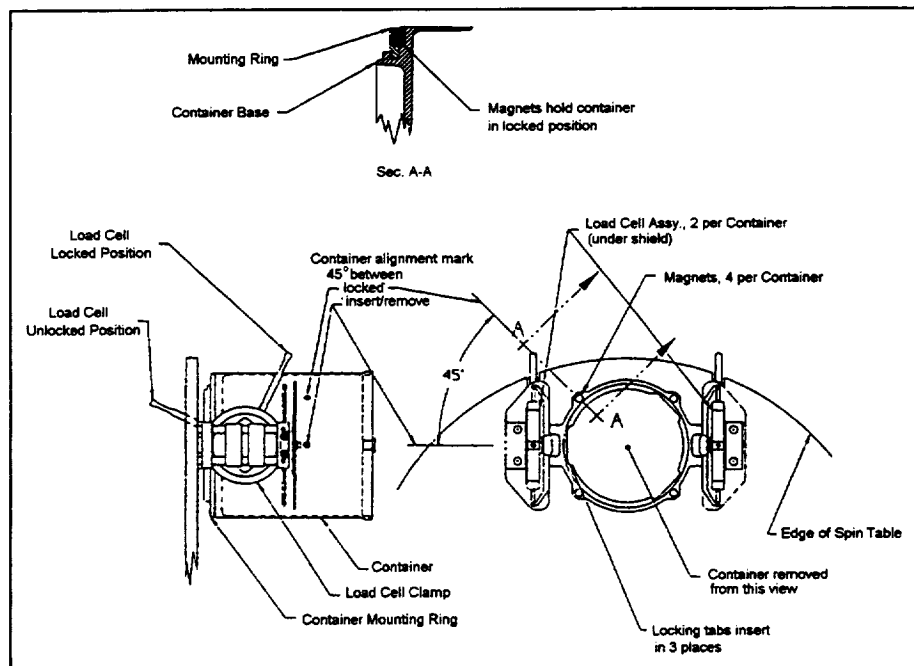


Figure 3-8. LME Tank/Load Cell Assembly.

The locking assembly prevents damage to the load cells during launch and re-entry.

Power to the electronic system on the spin table was provided through a set of slip rings at the top of the pedestal. A circular bayonet-type connector was provided on the pedestal hub with a matching plug on the spin table. The connector was disconnected when the spin table was separated from the pedestal and slip ring assembly. A dummy connector on the spin table provided a place to mount the electrical plug when the table was off the pedestal (stowed position). The spin table was mounted in a locker for launch and landing.

In order to prevent inadvertent malfunctions of the motor speed controllers and associated equipment from allowing the spin table to reach hazardous rotational speeds, a centrifugal switch was mounted to the spin table and connected via the slip rings to the power distribution circuitry. At rotational speeds greater than 40 rpm, the switch shut off power to the spin motor control circuits and consequently the spin motor. Spin table component mounting was designed to be able to withstand the 40 rpm speed without structural failure.

3.3.6 Pedestal System

The pedestal system for generating the spin and nutation motions to be imparted to the spin table and the mounted test tanks is shown in Figure 3-9. A 3D CAD drawing is shown as Figure 3-10. The pedestal contained a small electronically commutated DC (ECDC) motor (spin motor) to impart a spin motion directly to the mounted table, and another small ECDC motor (wobble motor) with an 80:1 gear reduction to impart a nutation motion via an eccentric arm on the bottom of the spin motor. The drive shaft at the top of the pedestal had a spherical bearing attachment to allow the shaft and spin motor to transmit to the spin table. Each of the two pedestal motors required an electronic driver circuit to commutate the motors and to regulate the speed of the motors. The motor speed controllers (MSC) are described in Section 3.2.12. The spin drive motor was a BEI Model DII38-20-006Z Brushless DC motor. Peak torque for the motor is 200 oz-in with a power dissipation of 343W at that torque. Actual torque requirements are lower so that power required was approximately 10.1W, steady state (motor plus speed control card).

The wobble motor was a Hathaway HT01001-B01-HE brushless DC motor with a peak torque of 7.5 oz-in and a maximum power requirement of 94W at that torque. The maximum speed was 3200 rpm, but the motor was geared down 80:1. The actual power required at steady LME speeds was approximately 3.0W.

Each ECDC motor had an associated optical encoder attached which provided an accurate feedback signal to the MSC to control the motor speed. The encoder also provided a single pulse per revolution to the computer measuring system to define the table rotational position and to provide a measurement of the wobble angle.

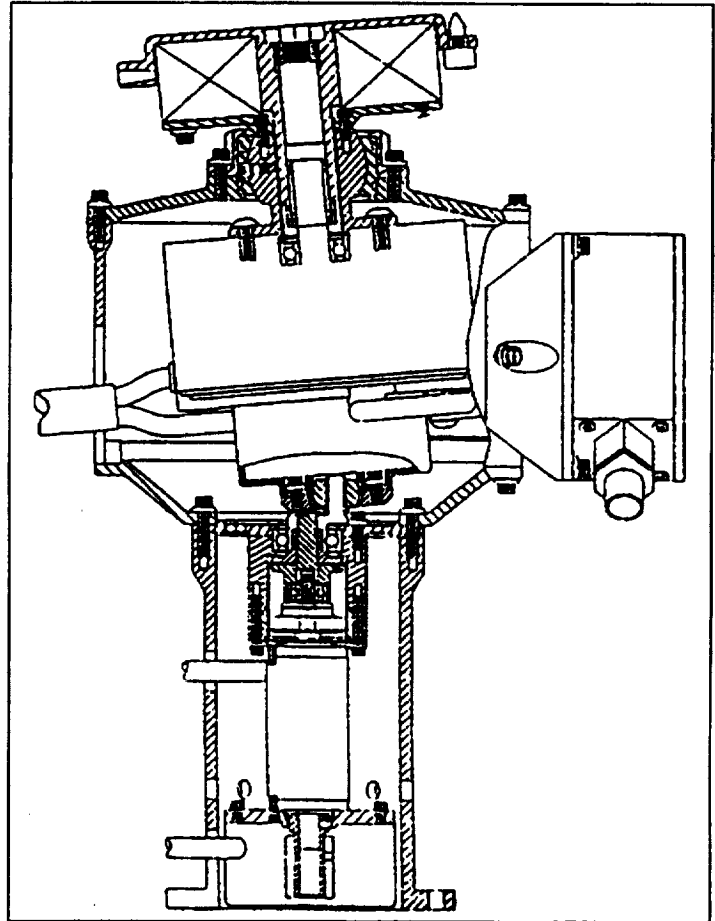


Figure 3-9. LME Pedestal Assembly.

Pedestal contains the two electric motors that drive the spin table.

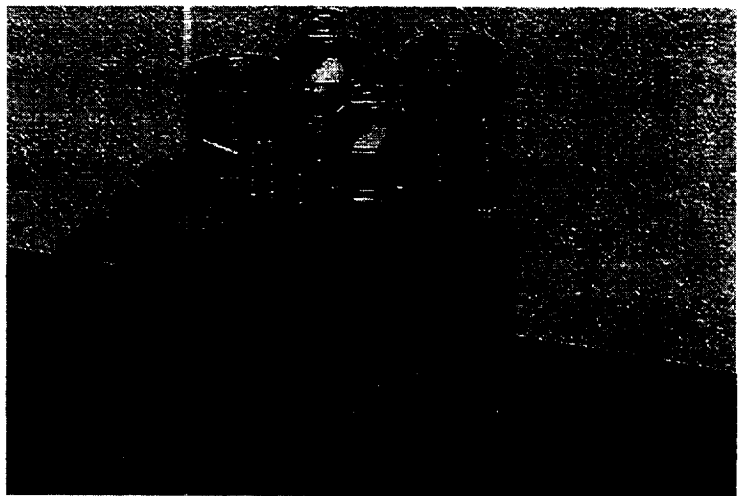


Figure 3-10. Pedestal Drive System.

Two spherical and two cylindrical tanks are shown mounted on the spin table, which is mounted on the drive pedestal. The drive pedestal is mounted on the double adapter baseplate.

LME Final Report

Each of the two drive motors had a bimetallic thermostat attached with heat conducting epoxy which interrupted the current flow to that motor if the motor case temperature exceeded 120° F. The pedestal fan was also protected by a low-speed detector module which shut off power to the drive motors and to the fan if the speed fell below 4000 rpm.

With a maximum 32VDC input to the payload, and with the spin table attached to the pedestal hub, the maximum rotational speed that could be attained by the system was 250 rpm. This runaway condition could occur as a result of a failure in the spin motor speed control board, by a failure in the PGSC software resulting in a normally disallowed high speed command, or a failure in the EIU circuits or firmware that misinterpreted an allowed PGSC speed command and sent the MSC circuits a high speed command. The spin motor was protected from this runaway condition by a centrifugally actuated switch located on the spin table.

3.3.7 Accelerometer

The spin rate of the tanks was chosen so that the steady centrifugal acceleration exerted on the liquids was at least ten times the ambient effective gravity at the middeck LME location. A three-axis accelerometer was rigidly attached to the LME baseplate to measure any small accelerations imposed on it during payload operation. The accelerometer data was digitized by the housekeeping measuring circuits in the Experiment Interface Unit (EIU).

3.3.8 Baseplate and Enclosure

The LME payload occupied the space of two SpaceHab lockers. LME was attached to a double adapter plate bolted to two payload mounting panels. Figure 3-11 shows a drawing of the LME enclosure attached to the payload mounting panel, and Figure 3-12 shows a photograph of it. The double adapter plate was shipped as an integral part of the payload. The LME enclosure provided support for mounting the PDM/EIU (Power Distribution Module/Experiment Interface Unit) for easy crew access to the electrical connectors for power and the PGSC and to the electrical breakers for power control, and support for the optical data

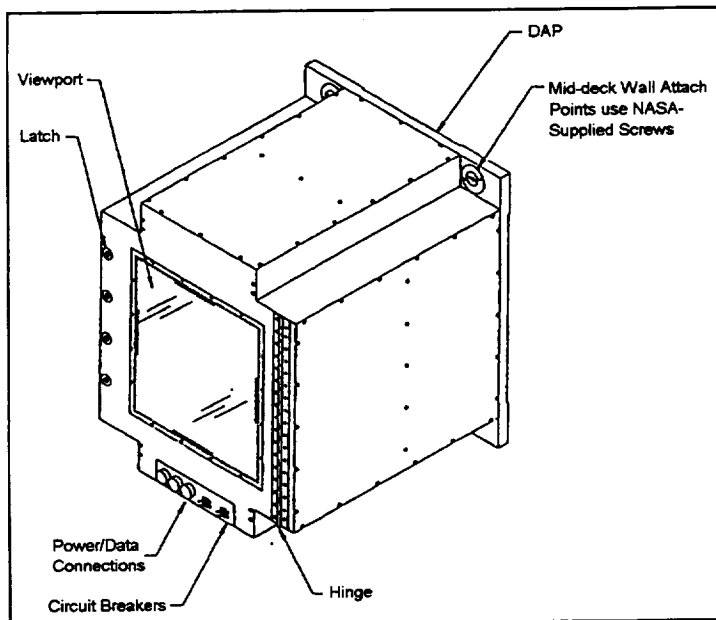


Figure 3-11. Schematic of LME Enclosure.
The viewport on the left of the figure provides visual access of LME operation.

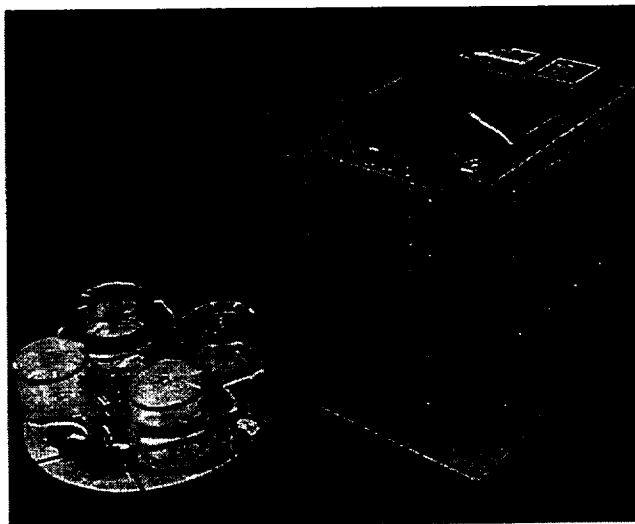


Figure 3-12. LME Enclosure.
The enclosure is shown on the right of the photograph. The spin table with tanks is shown at the left of the photograph.

link for data transmission from the DAS on the spin table to the PGSC. Access to the enclosure was provided by an access door on the front of the enclosure which was hinged along one side by a piano-type hinge to allow the door to be completely opened. The hinge was attached by flat-head screws which provide a zero interference for action of the hinge. The access door was latched at the side opposite the hinge with four 1/4-turn style latches. A clear polycarbonate window was provided in the access door to allow visual observation of the payload operations and to provide the opportunity to videotape the process from outside the experiment. The Optical Data Link (ODL) module for the enclosure was mounted at the center of the window on the inside.

3.3.9 Enclosure and Pedestal Cooling Systems

Since the LME payload was totally surrounded by the LME enclosure, dual electrically driven cooling fans were provided to allow air motion to dissipate the approximately 63 watts of power generated by the experiment during operation. One fan (enclosure fan) was mounted on the side of the LME enclosure and blew cabin air into the interior of the enclosure. The enclosure fan was capable of delivering 50 CFM at a rotational speed of 6400 rpm. The fan was an all-metal, cast aluminum, tube-axial design built to the requirements of MIL-B-23071. A low speed warning detector (LSWD) module was electrically connected to the fan to provide a signal to the PDM relay circuits to shut off all power to the LME experiment (including the enclosure fan) in case the speed of the fan decreased below 4000 rpm. Such a speed decrease would indicate a malfunction of the fan, either from electrical failure or from jamming of the blades from foreign material. The LME experiment could not be operated without proper operation of the enclosure fan since lack of cooling air would eventually result in overheating of the active electrical circuits and motors. The fan was protected from material outside the enclosure by the use of 1/8" diameter holes for air access from outside the enclosure, but was not protected from debris from inside the enclosure. Provisions for exhausting the enclosure cooling air was made by a set of 1/8" diameter holes in the plastic window of the enclosure access panel.

Because the two drive motors were also enclosed in the pedestal, a second fan (pedestal fan) was mounted on the side of the pedestal to drive enclosure air through the pedestal and exhaust it back into the enclosure. The pedestal fan was similar to the enclosure fan, capable of 50 CFM at a nominal speed of 6400 rpm. The pedestal fan was also protected by a LSWD module set to trip at 4000 rpm. In the event that the pedestal fan fell below the trip point of the LSWD, power to the experiment would be shut down, including power to both fans. The experiment could not operate without cooling air to the motors without damaging the motors. The drive motors also had bimetallic thermostats attached which shut off power to a motor if its case temperature exceeded 120°F. This protected the motors if the pedestal fan was operational, but something else in the motor drive system failed. Figure 3-13 shows the electrical block diagram of the enclosure cooling system and the low speed interlocks incorporated into the system.

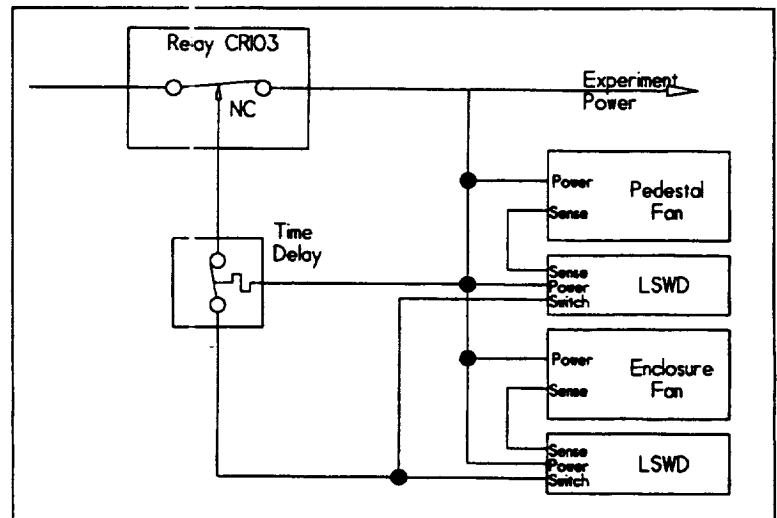


Figure 3-13. LME Cooling System Electrical Block Diagram.
This circuit shows the low speed warning detectors (LSWD) and the fan overtemperature sensors.

3.3.10 Enclosure Access Panel Electrical Interlock

To protect the crew from contact with rotating parts in the payload, an electrical interlock was installed on the PDM/EIU case to shut off power to the payload and the PGSC whenever the access door was open. If the access door was opened while the payload spin table was still rotating, about five minutes were required to spin down the payload.

3.3.11 LME Electrical System

The electrical system of LME consisted of two motor speed controllers, a data acquisition subsystem (DAS), an experiment interface unit (EIU), an operator interface computer (a NASA-supplied PGSC computer), and a power distribution module (PDM). A strain gauge amplifier (SGA) was co-located with each of the torque sensors. Two optical data link (ODL) modules allowed the RS-422 bi-directional serial data from the DAS to be transmitted to and received from the PGSC through the EIU across the rotating interface of the spin table. Figure 3-14 is a block diagram of the electronic system illustrating the interconnection of the various electronic components in LME.

3.3.12 Motor Speed Control

Each of the two drive motors was driven and controlled by an electronic speed control circuit, which in turn, was controlled by the EIU to turn the motors on and off and to set rotation speed and wobble frequency. The motor speed controllers, Eltrol Model 5-198-028-00, are designed to drive a wide range of permanent magnet DC brushless motors. Each of the controllers was identical except for differences in electrical gain and compensation settings. Figure 3-15 shows a block diagram of the MSC. The MSC accepted digital control signals from the EIU in the form of binary-coded decimal (BCD) digital signals, which set the speed at which the MSC will drive its particular motor. Other digital output lines from the EIU also commanded on/off and rotation direction functions. Digital lines from the MSC to the EIU provided data concerning different alarm conditions, and one analog line provided a voltage equivalent to motor speed. The MSC also accepted digital signals from an optical encoder attached to the motor shaft, and these signals were used as motor speed feedback signals for the MSC. Table 3-1 provides the nominal specifications for the MSC units. 28VDC power was supplied to each MSC from the PDM. Each power line to the MSC was routed through a high-temperature cutout switch, which was thermally attached to its respective motor. Overtemperature conditions in a motor [above 120° F (49° C)] resulted in the turn-off of power to that motor as a safety precaution. Part of verification testing of the motor assemblies verified that the thermal switch operated at its set point of 120° F (49° C) and that the motor did not generate toxic offgassing at that temperature.

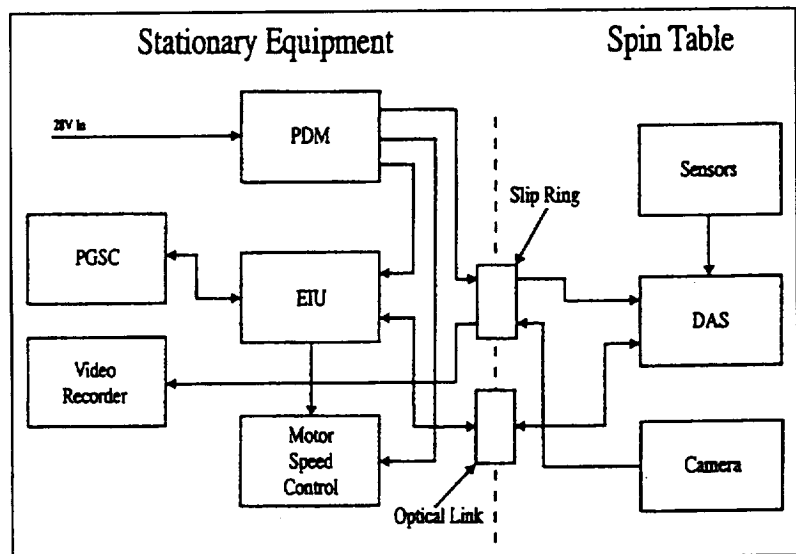


Figure 3-14. LME Electrical System Block Diagram.

This circuit illustrates the interconnection of the various electronic LME components.

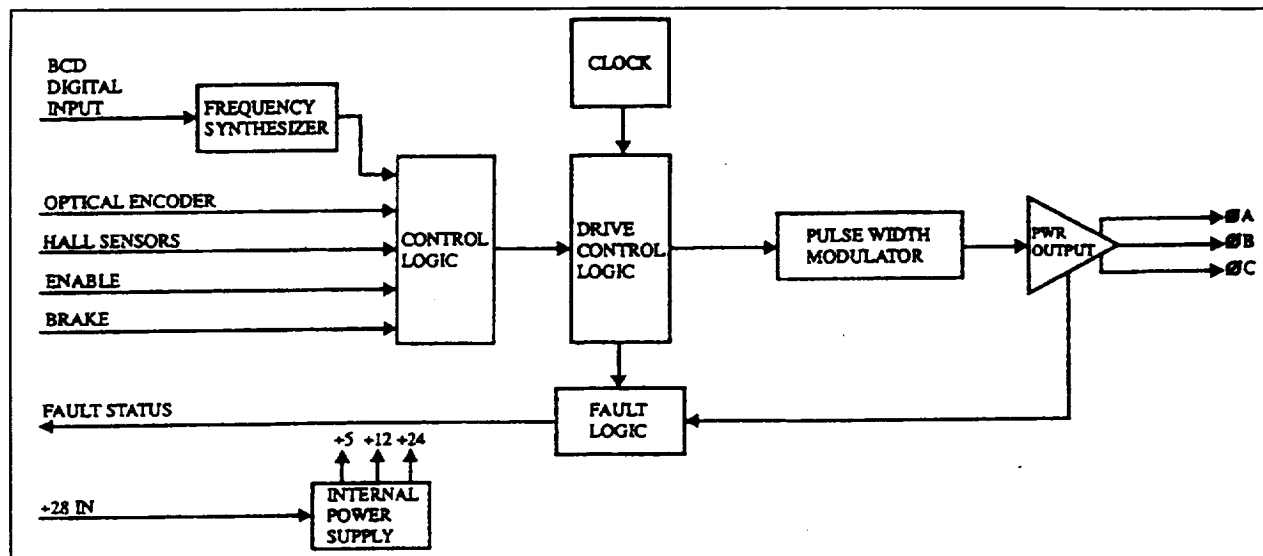


Figure 3-15. LME MSC Block Diagram.

This circuit shows the motor speed controller components.

Table 3-1. LME MSC Specifications

Input power bus:	26 TO 35VDC
Logic power Supply:	5VDC developed internally
Continuous output power:	144 watts (Note 1)
Continuous output current:	6 amps (Note 1)
Peak output current (3.0) sec.:	10 amps (Note 1)
Output voltage @ cont. output current and 28V nom bus:	24 volts
Efficiency:	92%
Operating temperature:	0 to 70 degrees C
Power amplifier:	switch mode drive
Power amp switching frequency:	24 kHz
Current loop bandwidth:	adjustable 2 - 4 kHz type
Phase lock loop bandwidth:	adjustable
Crystal Ref. oscillator:	2 MHz
Single Eurocard (VME Bus):	233.4 H X 160 D X31.8 W mm Size

Note 1: These values describe the maximum capability of the motor speed control circuit and do not reflect the actual power used.

3.3.13 Strain Gauge Amplifier (SGA)

The electrical output of the load cell strain gauges was in the low millivolt range. Since the tank sensors were located several inches from the analog input circuits of the Data Acquisition System (DAS), an amplifier to increase the voltage levels was located at the sensor positions. The Strain Gauge Amplifier consisted of a two-channel amplifier with a voltage gain of X50. Figure 3-16 shows a block diagram of the SGA circuit. Each SGA board serviced two strain gauge bridges, so one board was required for each side of a tank holder. The two outputs of the bridge were amplified by a X50 gain non-inverting differential amplifier implemented with half of a quad-amplifier integrated circuit on the board. Precision resistors were used to set the gain of the amplifier. The outputs from each differential amplifier were the differential inputs to the DAS for a single channel of strain gauge bridge data.

LME Final Report

Each of the SGA boards also included a solid-state temperature sensor using the Analog Devices AD590 Temperature Sensor IC.

3.3.14 Data Acquisition System (DAS)

The DAS circuits (Figure 3-17) were implemented on a printed wiring board contained in a small cabinet attached to the bottom of the spin table. The DAS amplified the low-level sensor signals, multiplexed between the various sensors on the spin table, digitized the amplified and multiplexed signals, and transmitted the digital data via an infrared optical link to the EIU. The controller provided serial I/O to the host EIU and controlled the multiplexer (MUX), the offset digital-to-analog converter (DAC), the analog-to-digital converter (ADC), and the programmable gain amplifier (PGA). A digital I/O section was also contained on the board design. In the DAS, the components were not populated for this section since the functions were not used. The Experiment Interface Unit (EIU) used the same board design as the DAS, and as such, required the digital I/O to interface with the motor speed controller (MSC) unit. The function of the digital I/O will be explained in the section covering the EIU.

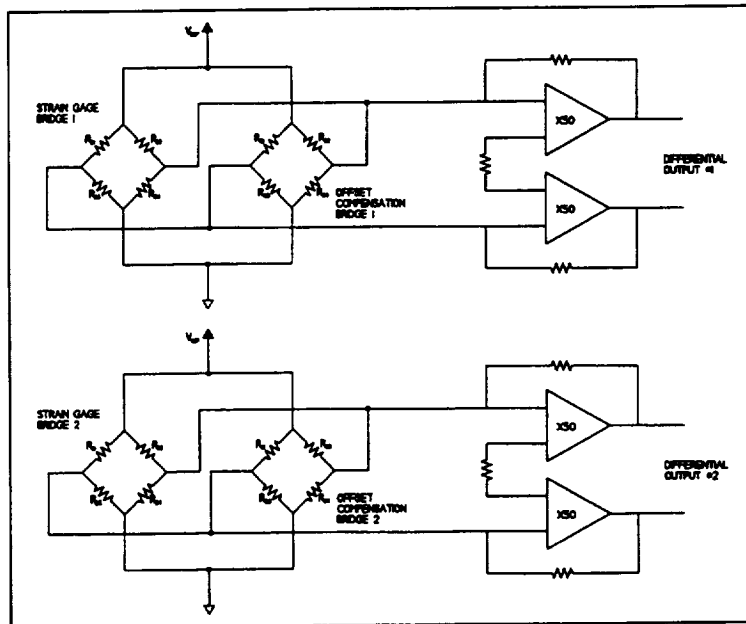


Figure 3-16. LME SGA Block Diagram.

This circuit shows the strain gauge bridges with the amplifiers.

The input section of the DAS consisted of differential sensor lines connected to the differential inputs of the MUX. The shields of the input lines were driven by a shield driver amplifier to reduce noise pickup in the lines. The input signal for the shield driver was obtained from the ground system of the DAS. The differential signals selected by the MUX were routed to a PGA for amplification. The PGA was under control of the microcontroller so that the gain could be programmed to the proper value for each of the input

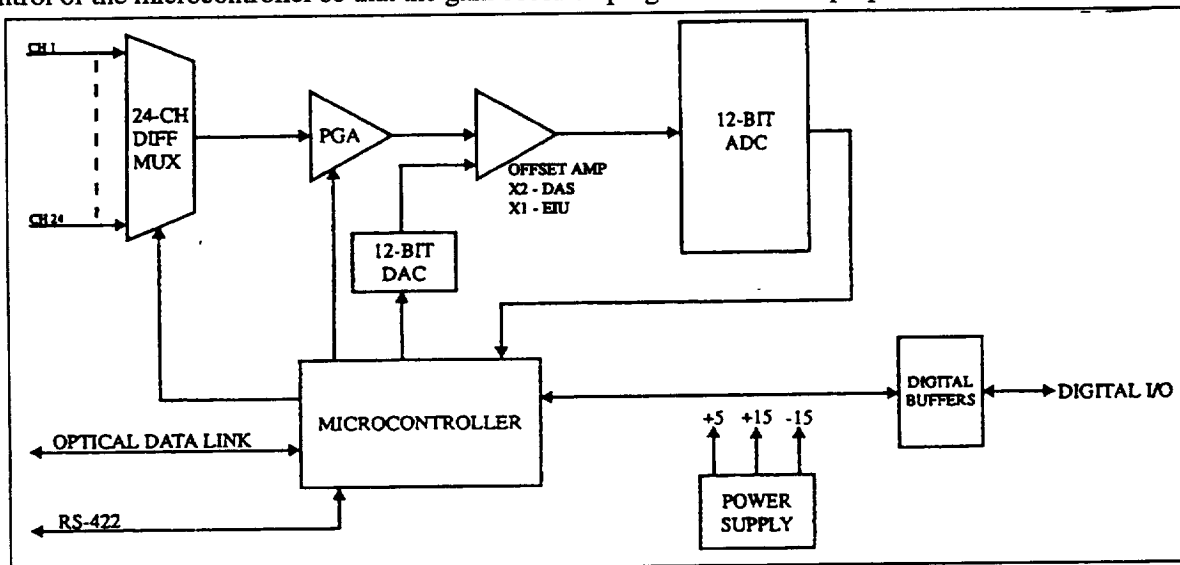


Figure 3-17. LME DAS/EIU Block Diagram.

This circuit shows the DAS/EIU components.

lines as it is selected. The output of the PGA was an amplified replicate of the input signal but at a level appropriate for digitizing.

The amplified signal was then offset to remove nominal steady signals from the strain gauge signal. The DAS offset amplifier is X2 and the EIU has a X1 offset amplifier.

Once the input signals were amplified and offset, they were applied to the ADC circuits. The ADC was a 12-bit unit capable of digitizing the signals at a 100 kHz rate. The ADC was under control of the microcontroller for timing and also supplied the output digital data to the microcontroller in 8-bit blocks. The reference voltage from the ADC was buffered by a unity gain op amp and supplied the strain gauge bridges for excitation current.

The microcontroller unit generated the timing of the digitizing sequence and set the gain and offset for each of the input channels and also selected the channel to be digitized.

Power to operate the DAS/EIU circuitry was supplied by two switching power supply modules mounted on the DAS/EIU printed wiring assembly (PWA). 28VDC was supplied to the module through the slip rings on the spin table for the DAS or directly from the PDM in the case of the EIU and was converted to the required +5V and ± 15 V levels by the supply modules.

3.3.15 Optical Data Link

The Optical Data Link (ODL) consisted of two identical modules. One was mounted to the center of the spin table, and the other was mounted directly opposite the spin table on the inside surface of the enclosure viewport. The ODL was simply a line to connect the DAS CPU RS-422 interface with one of the RS-422 ports on the PGSC across the open space (gap) between the spin table and the enclosure lid.

Each module consisted of a transmitting electro-optical driver and a receiving opto-electrical driver. The transmitting circuit converted the RS-422 electrical pulses to light pulses emitted from a single infrared LED. The receiving circuit used three infrared photo detectors to sense the optical pulses of the opposing module and converted those optical pulses to RS-422 electrical pulses. Three detectors were required to ensure that the detected signal was well over the input threshold of the opto-electrical driver.

3.3.16 Experiment Interface Unit (EIU)

Operation of the experiment was always under control of the PGSC, which in turn had an operator interface through a serial RS-422 port to the EIU to provide the commands to the experiment and to receive the measured data for display on the PGSC screen and for storage on hard/floppy disk by the PGSC. The EIU had interfaces which included a parallel digital interface with each of the two motor speed controllers, a serial optical link with the DAS on the spin table, and a digital control interface to the PDM. The analog circuits on the EIU were identical to those on the DAS and were used to monitor housekeeping data from the PDM and temperature sensors on the two drive motors and the motor speed controllers.

3.3.17 Power Distribution Module (PDM)

The main power input to the LME system was the Shuttle 28VDC supply for the SpaceHab. The power to the system was routed through the Power Distribution Module (PDM) for the appropriate

switching, filtering, and overcurrent protection to comply with payload safety and EMI requirements. Figure 3-18 is a block diagram of the PDM showing the functionality and interconnection of the unit. The PDM was under the control of the EIU insofar as switching of power to the subunits of the electronic system. A safety feature was included on the PDM by the inclusion of a low speed warning switch for each of the enclosure and pedestal fans which connect to a solid state relay on the PDM. If for some reason the enclosure or pedestal fan did not operate at the proper speed, the PDM relay removed power from the EIU, the spin table, and the two motor speed controllers as well as both fans. Thus, excessive temperatures above the specified touch temperature limit of 113° F were prevented. If a fan speed shutdown occurred, the PGSC software detected the loss of communication with the DAS and the EIU and signaled the operator that the shutdown condition exists.

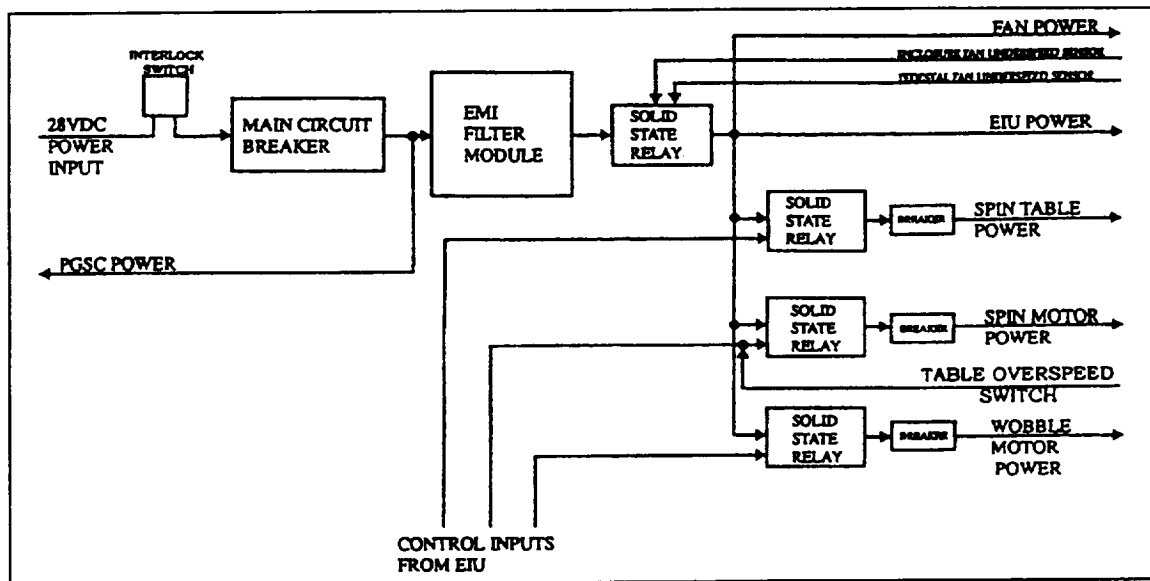


Figure 3-18. LME PDM Block Diagram.

This circuit shows the power distribution module components.

The 28VDC input line to the PDM was routed through the input circuit breaker, the door interlock switch, and the input EMI filter. The filter provided both protection of the LME system from susceptibility to external EMI and protection of the Shuttle environment from EMI radiated and conducted from the LME system. The filter was designed to allow the LME system to comply with the requirements of NSTS 21000-IDD-MDK.

The PDM contained solid state relays which control power to the various subunits of the system. The relays are controlled by electrical signals from the EIU which enable power application.

3.3.18 LME 28VDC Power Interconnection

28VDC power was distributed throughout the experiment package using interconnect cabling. The wire used for interconnect power cabling was selected to conform to the MIL-W-22759 specification. The wire was a Teflon-insulated, nickel-plated copper wire with a minimum size of #26 AWG for any current carrying function. Where possible, #24 AWG twisted shielded pair was used for all 28VDC power runs. All cables were bundled, with an EMI gauze wrap and a final Teflon tape wrap. The cables were anchored

to the support structure to minimize vibration of the cables. Figure 3-19 shows a power wiring and fusing diagram for the LME payload. All power carrying wires were protected by either the main breaker, which had a rating of three amps, or by one of the three one amp breakers. The derated current handling capacity of #24 AWG wire was 7.5 amps, according to TA-92-038 and TM 102179, which was well above the maximum protection of three amps supplied by the main circuit breaker. Some of the LME cable bundles also contained signal wires and wires carrying less than 500 mA of secondary power current. Protection of these wires was through the current output limiting of the switching power supply modules.

3.4 FABRICATION AND ASSEMBLY

Flight hardware was fabricated and assembled using a drawing control system already established at SwRI for other NASA and military programs. Each component, subassembly, and assembly had a fabrication or assembly drawing, which detailed all fabrication and assembly requirements for that assembly. Associated with each assembly drawing was a Manufacturing Planning Sheet (MPS), which listed in detail the steps to be used to assemble or fabricate the part. Materials, process documents, and parts lists were listed on the MPS. Each step of the MPS was initialed by the person performing the operation and, if an inspection step was required, it was stamped by the QA inspector or Government inspector. Each drawing was reviewed by cognizant engineering, Project Management, and by QA for conformance to all project requirements. MPS's were reviewed by the same people as well as by the Government representative, if so delegated.

Parts and materials purchasing for the program used a system of Materials Requisitions and Purchase Orders, which were reviewed by the QA inspector for completeness and adherence to project part requirements. Incoming materials and supplies were inspected by the QA inspector for adherence to specifications in accordance with internal SwRI procedures.

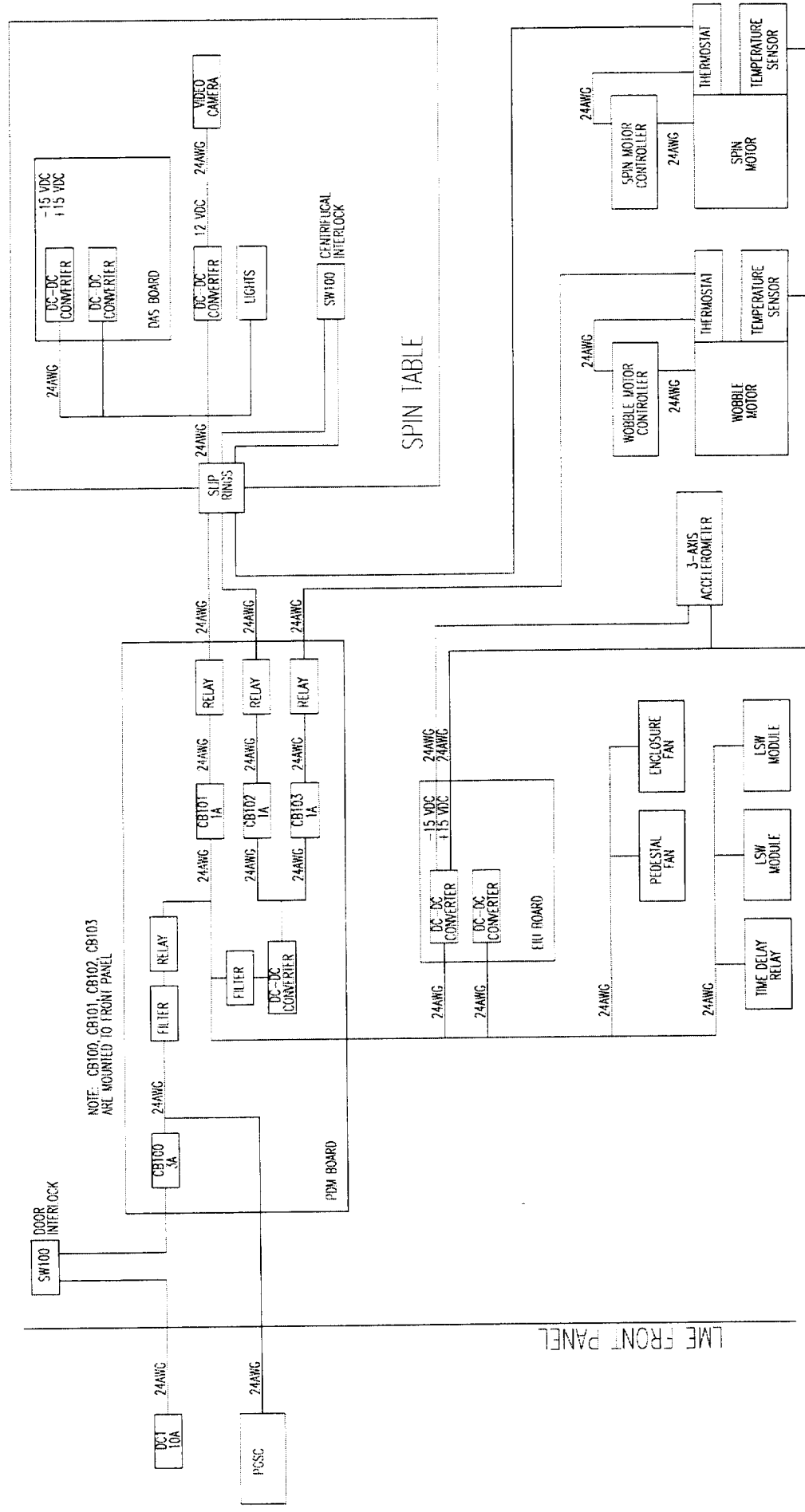


Figure 3-19. LME Power Wiring and Fusing Diagram.
This figure shows the wire sizing and fusing for LME.

This page left intentionally blank.

4. VERIFICATION TESTING

The objective of the verification test program was to confirm that all of the flight hardware fabricated and assembled for the LME conformed to all project requirements. The test program was performed in accordance with the Verification Plan (6322-VP-01, Rev 2, dated February 22, 1996). Each test was performed using an approved test procedure and was monitored by the SwRI or LeRC QA inspector. The Verification testing was divided into four categories based on the source of the particular requirement being verified. These categories were: Science Requirements, Integration, Safety, and Project Acceptance Tests.

4.1 SCIENCE REQUIREMENTS VERIFICATION

The Science Requirements Verification Test was to verify that LME meets all of the Science Requirements set forth in the Experiment Requirements Document (6322-ERD-01). The item numbers, verification requirements, method of verification (Inspection, Test, or Analysis), origin of the requirement (page number from 6322-ERD-01), and whether it passed or failed the test, is shown in Table 4-1 below. The specific test procedure, which also served as the official datasheet and permanent record for the outcome, was the Science Verification Test Procedure (6322-SVTP-01, dated 11-11-96).

Table 4-1. Science Requirement Verification.

ITEM NO.	VERIFICATION REQUIREMENT	METHOD	ORIGIN (pg)	PASS/ FAIL
3.1	Number of Tanks: The number of test tanks shall be twelve.	I	19	Pass
3.2	Tank Shape: There shall be six tanks that are right circular cylinders and six tanks that are spherical.	I	19	Pass
3.3	Tank Diameter: The nominal diameter of each test tank shall be 4.5 ± 0.1 in. ID measured to a resolution of 0.05 in.	I	19	Pass
3.4	Tank Fill Level: The volume of the six cylindrical tanks is nominally 1173 ml. Three of the cylindrical tanks shall be filled 1/3 full, 391 ± 5 ml, the other three shall be filled 2/3 full, 782 ± 5 ml. The volume of each of the spherical tanks is nominally 782 ml. Three of the spherical tanks shall be filled 1/3 full, 261 ± 5 ml, the other three shall be filled 2/3 full, 521 ± 5 ml.	T	19	Pass
3.5	Fill Liquid Viscosity Measurement: The fill liquid viscosities shall be nominally 1 and 10 cp measured to ± 0.5 cp.	T	19	Pass
3.6	Spin Motor Speed Range: The spin motor shall be capable of being commanded to operate over the range of 0 - 20 rpm.	T	19	Pass
3.7	Wobble Motor Speed Range: The wobble motor shall be capable of being commanded to operate over the range of 0 - 40 rpm.	T	19	Pass
3.8	Spin Motor Speed Accuracy: The spin rate shall be measured to an accuracy of ± 0.10 rpm.	T	19	Pass
3.9	Wobble Motor Speed Accuracy: The wobble rate shall be measured to an accuracy of ± 0.10 rpm.	T	19	Pass
3.10	Load Cell Range: The measurement range of the tank load cells shall be from 0.0001 to 0.04 in-lb.	T	19	Pass
3.11	Load Cell Temperature Drift: The calibration of the load cells shall drift less than 0.05% per °C.	T	19	Pass
3.12	Load Cell Accuracy: The accuracy of the tank load cell measurements shall be $\pm 5\%$ of maximum amplitude.	T	19	Pass

Table 4-1 Continued.

ITEM NO.	VERIFICATION REQUIREMENT	METHOD	ORIGIN (pg)	PASS/ FAIL
3.13	Video Framing Rate: The framing rate of the video system shall be 30 or 60 frames/sec.	I	19	Pass
3.14	Video Imaging: The video system shall be able to visualize the bulk fluid flow within the monitored tank.	A or T	19	Pass
3.15	Video Light Level: The light level available on the spin table when installed in the middeck area shall be sufficient for good video coverage.	A or T	19	Pass
3.16	Spin Table Digital Clock Accuracy: The accuracy of the spin table digital clock shall be ± 1 second/24 hours.	T	19	Pass
3.17	Temperature Environment: The LME cooling system shall maintain the electronics, motors and load cells within a temperature of less than 49°C with an ambient temperature of 18 to 27°C.	T	19	Pass
3.18	Load Cell Temperature: The temperature of each load cell shall be monitored near the strain gauges and recorded at the start and end of an experiment run.	I	19	Pass
3.19	Load Cell Temperature Accuracy: The accuracy of the load cell temperature measurement shall be $\pm 2.0^\circ\text{C}$.	T	19	Pass
3.20	DAS Analog Input Resolution: The digitized resolution of the analog inputs to the DAS shall be 12-bits.	I	19	Pass
3.21	DAS Analog Input Drift: The drift of the calibration of the DAS analog inputs shall be less than 0.05% per °C.	T	19	Pass
3.22	Measurement Noise Level: The noise level of the digitized strain gauge signal shall be less than 0.5% of the maximum signal amplitude.	T	19	Pass
3.23	Data Storage: The PGSC shall store 8.3 Mbytes of the digitized raw data on the PGSC fixed disk and on floppy diskettes per Software Requirements Specification, 6322-SRS-01.	I	19	Pass
3.24	Acceleration Environment: No testing during primary thruster firing or during periods of g-jitter that exceeds 10^{-3} g rms. Confirm requirement is in Flight Data file.	I	19	Pass

4.2 INTEGRATION VERIFICATION

The Integration Requirements Verification Test was to verify that LME met all of the Integration Requirements set forth in the SpaceHab Experiment Interface Definition Document (MDC91W5023F). The original Verification Plan was written based on the initial indication that LME would be flown in the Orbiter Middeck. The Interface Requirements were specified in the "Shuttle/Payload Interface Definition Document for Middeck Accommodations (NSTS 21000-IDD-MDK). Three months prior to delivery, LME was re-assigned to SpaceHab, so the Interface Requirements were changed. A comparison of these two interface documents revealed that the interfaces were almost identical. In the event of a difference, LME was tested to the most severe of the two requirements, so in the event of a re-flight it would be qualified for both locations. The item numbers, verification requirements, method of verification (Inspection, Test, or Analysis), origin of the Orbiter requirements (page number from NSTS 21000-IDD-MDK), origin of the SpaceHab requirements (page number from MDC91W5023F), and whether it passed or failed the test, is shown in Table 4-2. The specific test procedure, which also served as the official datasheet and permanent record for the outcome, was Integration Verification Test Procedure (6322-IVTP-01, dated 2-4-97).

LME Final Report

Table 4-2. Integration Verification.

ITEM NO.	VERIFICATION REQUIREMENT	METHOD	ORBITER ORIGIN (pg)	SPACEHAB ORIGIN (pg)	PASS/ FAIL
4.1	Experiment Envelope: The experiment assembly including safety shroud shall not exceed the user envelope of 21.882 inches in height by 18.135 inches in width by 20.562 inches in depth (does not include thickness of payload mounting panels).	T	3-4	3-19	Pass
4.2	Experiment Weight and CG: The experiment weight and CG shall not exceed the values specified in Figure 4.8.2-2 of Pages 4-10.	T	4-7	4-15	Pass
4.3	Locker-Stowed Accessories Weight: The weight of locker-stowed accessories shall not exceed 54 lb.	T	4-7	4-12	Pass
4.4	Locker-Stowed Accessories CG: The CG of a fully packed locker shall be no more than 14 inches from the locker wire tray attachment face.	T	4-7	4-12	Pass
4.5	Experiment Mounting: The LME double adapter plate shall mount to two single payload mounting panels and shall meet the same attachment and envelope requirements as an SSP-supplied double adapter plate.	I	3-14	4-15	Pass
4.6	Kick/Push-Off Loads: The experiment shall be designed to withstand a 125 pound load distributed over a 4 in X 4 in area.	A	4-3	4-6	Pass
4.7	Random Vibration: The experiment shall be designed to withstand launch and landing random vibration loads.	T	4-3	4-2	Pass
4.8	Acoustic Loading: The LME shall be designed to meet the specified acoustic loads generated during lift-off and caused by aero noise.	I	4-4	4-7	Pass
4.9	Acoustic Noise Generation: Experiment shall meet acoustic noise generation levels for middeck environments.	T	4-4	4-8	Pass
4.10	Power Requirement: The experiment shall require less than 130 watts of electrical power over the Orbiter DC supply voltage range.	T	7-1	7-2	Pass
4.11	Voltage Range: The experiment shall operate over the Orbiter DC voltage range of 22.5 to 32.0VDC.	T	7-1	7-2	Pass
4.12	Grounding and Bonding: The experiment package shall adhere to bonding and grounding requirements of NSTS 21000-IDD-MDK Section 8.4.1 and 8.5.1.	T	8-11 8-13	8-13	Pass
4.13	Depressurization: All vented enclosures shall be capable of withstanding depressurization from 15.2 psia to 3.95 psia at a rate of 24.0 psi/min	A	6-2	N/A	Pass

4.3 SAFETY VERIFICATION

The Safety Requirements Verification Test was to verify that LME met all of the Safety Requirements set forth in the Phase II Flight Safety Data Package (6322-SP-01, Revision 2). The results of these tests were used to close all Hazard Reports in the Phase III Flight Safety Data Package (6322-SP-01, Revision 3). The item numbers, verification requirements, method of verification (Inspection, Test, or Analysis), origin of the requirement (Hazard Report Number in 6322-SP-01, Revision 2), and whether it passed or failed the test, is shown in Table 4-3. The specific test procedure, which also served as the official datasheet and permanent record for the outcome, was Flight Safety Test Procedure (6322-FTSP, 01 through 16).

Table 4-3. Flight Safety Verification.

ITEM NO.	VERIFICATION REQUIREMENT	METHOD	ORIGIN	PASS/ FAIL
5.1	Flammability of materials: a) Materials shall be selected from MFSC-HDBK-527F/JSC 09604 for a flammability rating of "A". b) Materials not meeting MFSC-HDBK-527F/JSC 09604 shall be assessed for flammability.	a) I b) T	LME-HR-01	Pass
5.2	Offgassing of materials: a) Materials shall be selected from MFSC-HDBK-527F/JSC 09604 for acceptable toxic offgassing. b) Materials not listed in MFSC-HDBK-527F/JSC 09604 shall be assessed at White Sands for acceptable toxic offgassing.	a) I b) T	LME-HR-02	Pass
5.3	Adequate structural design for launch, landing and on-orbit environment: a) The LME structure shall be designed to withstand the worst case launch, landing and on-orbit/emergency loading with safety factors of 1.4 minimum for load capacity and 1.0 minimum for fracture control. b) A random vibration test shall be performed at 3 dB greater than the expected flight vibration spectrum as specified in NSTS 21000-IDD-MDK. c) Fasteners will be selected from applicable MS or NAS standard fasteners and acquired and tested per SwRI Fastener Integrity Plan, 6322-FIP-01. d) A sine sweep vibration test shall be performed to ensure that the first mode of vibration for the LME is greater than 30 Hz. e) Analysis of LME enclosure to demonstrate containment of debris with positive margins. Analysis and testing of latches and analysis of hinge to demonstrate that inadvertent operation will not occur. Review crew procedures to incorporate instruction to stow tanks within 30 minutes. f) Materials shall be selected in accordance MSFC-SPEC-522B Table I for resistance to stress corrosion. g) LME hardware will be fabricated and assembled in accordance with approved drawings, parts lists, and procedures to prevent defective manufacture. h) Hardware shall be designed in accordance with NHB 8071.1 and LME Fracture Status Report, 6322-FSR-01, to minimize potential failures due to fracture. i) Hardware shall be designed with redundant load paths and appropriate containment to prevent release of hardware from rotating equipment.	a) A b) T c) I, T d) T e) A, T, I f) I g) I h) I i) I, A	LME-HR-03	Pass

Table 4-3 Continued.

ITEM NO.	VERIFICATION REQUIREMENT	METHOD	ORIGIN	PASS/ FAIL
5.3 (cont'd)	j) LME hardware will be fabricated and assembled in accordance with approved drawings, parts lists, and procedures to ensure redundant load paths. k) LME threaded fasteners shall be self-locking type or shall be locked with a thread locking adhesive. Fasteners required to maintain enclosure integrity shall be tested in accordance with Fastener Integrity Plan, 6322-FIP-01.	j) I k) I	LME-HR-03	Pass
5.4	Proper fabrication/assembly to prevent injury to crew members: a) LME hardware will be designed to comply with the intent of NASA STD-3000 to remove sharp edges and corners. b) LME hardware shall be fabricated to comply with approved design drawings, parts lists, and procedures to prevent sharp edges and corners. c) The use of purchased parts shall conform to the intent of NASA STD 3000 in that no sharp edges and corners shall be accessible. d) LME hardware shall be fabricated to comply with approved design drawings, parts lists, and procedures to prevent defective manufacture and assembly. e) LME design will be designed to comply with the intent of NASA STD-3000 to provide sufficient clearance for on-orbit procedures without trapping hands or fingers. f) LME hardware will be assembled to comply with the intent of NASA STD-3000 to provide sufficient clearance for on-orbit procedures without trapping hands or fingers. g) Alignment marks will be provided to position spin table mounting flanges to drive pedestal to avoid hand entrapment during installation.	a) I b) I c) I d) I e) I f) I g) I	LME-HR-04	Pass
5.5	Proper EMI/EMC design: a) Design shall require cables using twisted shielded pairs with shields carried through connectors to separate pins. b) Cables shall be designed per NSTS 21000-IDD-MDK requirements for bonding and EMI. c) Avionics shall be designed per NSTS 21000-IDD-MDK requirements for bonding and EMI. d) LME will use an EMI filter to reduce conducted and radiated emissions to reduce susceptibility to external interference.	a) I b) I c) T d) I	LME-HR-07	Pass
5.6	Adequate design to prevent structural failure of fluid tanks: a) Tanks shall be designed with a minimum safety margin of 1.5 for internal pressure, and proof tested at 1.5 MDP. (Test Pressure = 11.1 psig) b) Tanks shall be leak tested subsequent to 1.5 MDP with subsequent inspection for cracks and flaws. c) Fluid in tanks shall be a non-hazardous material such as water or water/glycerin mixture or other such material. d) Fluid tank fill port will be leak tested to 7.4 psid in accordance with LME Tank Seal Leak Test. e) Fluid tanks will have alignment marks to ensure proper assembly during on-orbit operations. f) Tank materials and adhesives shall be compatible with filling fluid in accordance with manufacturer's recommendations and specifications.	a) A, I, T b) I c) I d) T e) I f) I	LME-HR-09	Pass

Table 4-3 Continued.

ITEM NO.	VERIFICATION REQUIREMENT	METHOD	ORIGIN	PASS/ FAIL
5.6 (cont'd)	g) Tank materials will be tested to ensure compatibility with the test fluids in accordance with LME Fluid Tank Material Compatibility Test Plan (Phase II Safety Action Item #3). h) The threaded fill port plug will be locked with adhesive thread locking compound to prevent backout.	g) T h) I	LME-HR-09	Pass
5.7	Over-heated equipment: a) Motors and electrical assemblies shall have adequate conductive and forced-air cooling with mechanical thermostats for protection. b) Cooling fans will have low speed detection modules that inhibit power to LME in the event of a fan failure to prevent excessive temperatures.	a) I, T b) I, T	LME-HR-10	Pass
5.8	Adequate design of electrical system to eliminate fire hazard: a) Electrical power distribution circuitry shall be designed in accordance with NSTS 18798 (Letter TA-92-038) and GSFC PPL-19. b) LME hardware will be fabricated in accordance with approved drawings, parts lists, and procedures to ensure proper wire sizes and fusing.	a) I b) I	LME-HR-11	Pass
5.9	Adequate design of thermal control system to eliminate high touch temperature: a) Cooling fans will have low speed detection modules that inhibit power to LME in the event of a fan failure to prevent excessive temperatures. b) Thermal analysis shall show acceptable touch temperature during normal operations.	a) T b) A	LME-HR-12	Pass
5.10	LME design prevents crew contact with rotating LME components: a) The LME access door contains an electrical interlock that inhibits power when the door is open. Functional test of interlock switch. b) Test procedures call for power to be disconnected from the LME before the access door is opened.	a) I, T b) I	LME-HR-13	Pass
5.11	LME design is adequate to withstand loads during on-orbit operations: a) A motor speed controller will control spin table speed to a safe speed. b) A centrifugally operated switch shall be attached to the spin table to inhibit motor power if the spin table reaches an overspeed condition of 40 rpm. c) The LME enclosure will provide containment of debris if the spin table reaches a runaway speed condition of 250 rpm. d) The LME enclosure will provide containment of debris if the latch pins fail. e) Tanks and holders have alignment marks to ensure proper assembly during on-orbit operations. f) The tank support system shall be designed to withstand centrifugal loads at the overspeed condition of 40 rpm. g) The tank support system will be tested at the overspeed condition of 40 rpm to ensure structural integrity. h) The tanks shall be designed to withstand puncture at the overspeed condition of 40 rpm.	a) I, T b) I, T c) A d) A e) I f) A g) T h) T	LME-HR-14	Pass

Table 4-3 Continued.

ITEM NO.	VERIFICATION REQUIREMENT	METHOD	ORIGIN	PASS/ FAIL
5.12	Shatterable materials shall be contained to prevent crew injury: a) LME glass bulbs, LEDS, and diodes will have clear polycarbonate covers. b) LME video camera lens shall have a clear polycarbonate cover permanently attached.	a) I b) I	LME-HR-15	Pass

4.4 GROUND SAFETY TESTS

The Ground Safety Requirements Verification Test was to verify that LME met all of the Ground Safety Requirements set forth in the Phase 0/I/II Ground Safety Data Package (6322-SP-02). The results of these tests were used to close all Hazard Reports for Ground Safety. The item numbers, verification requirements, method of verification (Inspection, Test, or Analysis), origin of the requirement (Hazard Report Number in 6322-SP-02), and whether it passed or failed the test, is shown in Table 4-4. The specific test procedure, which also served as the official datasheet and permanent record for the outcome, was Ground Safety Verification Test Procedure (6322-GSP-01).

Table 4-4. Ground Safety Verification.

ITEM NO.	VERIFICATION REQUIREMENT	METHOD	ORIGIN	PASS/ FAIL
6.1	Adequate structural design for ground handling loads: a) Handling fixture designed to withstand handling loads with safety factor of 3.0. b) Packing case support structure designed to withstand shipping loads with safety factor of 3.0. c) Handling fixture threaded fasteners will have safety factor of 3.0 for anticipated loads. d) Handling fixture assembly procedure shall specify proper torque.	a) A b) A c) A d) I	LME-GHR-01	Pass
6.2	Elimination of hazards due to sharp edges, corners, and rotating equipment: a) Ground handling equipment will meet the intent of MIL-STD-1472 with respect to sharp edges, corners, and pinch points. b) Front panel will have interlock to prohibit power to rotating equipment if cover is open. c) Ground handling hardware will be assembled in accordance with approved drawings, parts lists, and procedures.	a) I b) I c) I	LME-GHR-02	Pass
6.3	Elimination of hazards due to electrical shock: a) LME hardware will have safety shield over all electrical connectors. b) LME connectors cannot be mismatched. c) LME cabinets and enclosures will be designed to have proper grounding. d) All exposed parts of LME payloads will be a ground potential when power is applied.	a) I b) A c) A d) T	LME-GHR-03	Pass

4.5 ACCEPTANCE TESTS

The Project Requirements Verification Test was to verify that LME met all of the Project Requirements set forth in the SOW NAS3-27252, Exhibit B, Product Assurance Requirement. These Project Requirements imposed by the contract included Reliability, Cleanliness and three Acceptance Tests. The Acceptance Tests were Vibration, Acoustic and Thermal. The item numbers, verification requirements, method of verification (Inspection, Test, or Analysis), origin of the requirement (SOW NAS3-27252), and whether it passed or failed the test, is shown in Table 4-5. The specific test procedure, which also served as the official datasheet and permanent record for the outcome, was Project Requirements Test Procedure (6322-PRVP, dated 02-17-97).

Table 4-5. Project Requirement Verification.

ITEM NO.	VERIFICATION REQUIREMENT	METHOD	ORIGIN (pg)	PASS/ FAIL
7.1	Reliability: Parts selection and application shall support a reliability of 0.90 for 168 hours of operation in space.	A	3	Pass
7.2	Cleanliness: The experiment shall conform to cleanliness requirements of NSTS 21000-IDD-MDK.	I	3	Pass
7.3	Vibration Environment: The experiment shall be capable of withstanding the vibration environment of launch and landing as detailed in NSTS 21000-IDD-MDK. This item is identical to 5.3 b) and 5.3 d), and the testing and witnessing for 5.3 b) and 5.3 d) will apply here.	T	3	Pass
7.4	Acoustic Environment: The experiment shall be capable of withstanding the acoustic environment of launch and landing as detailed in NSTS 21000-IDD-MDK. This item is identical to 4.9, and the testing and witnessing for 4.9 will apply here.	T	5/3	Pass
7.5	Thermal Environment: The experiment shall be capable of withstanding and operating in the thermal environment of the Shuttle Middeck. This item is identical to 5.2 b), and the testing and witnessing for 5.2 b) will apply here.	T	5/3	Pass

5. FLIGHT OPERATIONS

5.1 OVERVIEW

Once in orbit, the mission specialists unstowed and assembled the LME experimental apparatus and verified its operation. A series of tests was then conducted in accordance with the test matrix. Using software installed on the PGSC, the mission specialists selected when each specific test series was conducted. If needed, the mission specialists were able to change the parameters of the tests to reflect experience gained from previous tests. The mission specialists changed cassettes in the video cassette recorder when needed and performed other housekeeping duties. At the conclusion of the tests, the mission specialists disassembled and restowed the apparatus.

All flight operations performed by the mission specialists were described in a loose-leaf manual that also contained checklists for unstowing, assembling, verifying, disassembling, and stowing procedures. The LME Principal Investigator and other LME principals were available on the ground for consultation and troubleshooting. Astronauts Carlos Noriega and Edward Lu were the mission specialists assigned to perform the on-orbit operations for LME. A photograph of LME on-orbit mission specialist, Dr. Edward Lu, is shown in Figure 5-1.

5.2 EXPERIMENT ASSEMBLY AND CHECKOUT

The LME experiment hardware was housed in a double locker, while the spin table, fluid tanks, cables, manuals, and other auxiliary equipment were stowed in standard storage lockers. The launch and landing configuration of the LME hardware is depicted in Figures 5-2 and 5-3. To conduct the LME tests, the spin table was removed from the storage locker and mounted to the drive pedestal, and then the fluid tanks were removed from the storage locker and mounted on the spin table. The final assembly is shown in Figure 5-4. The items stowed in storage drawers were:

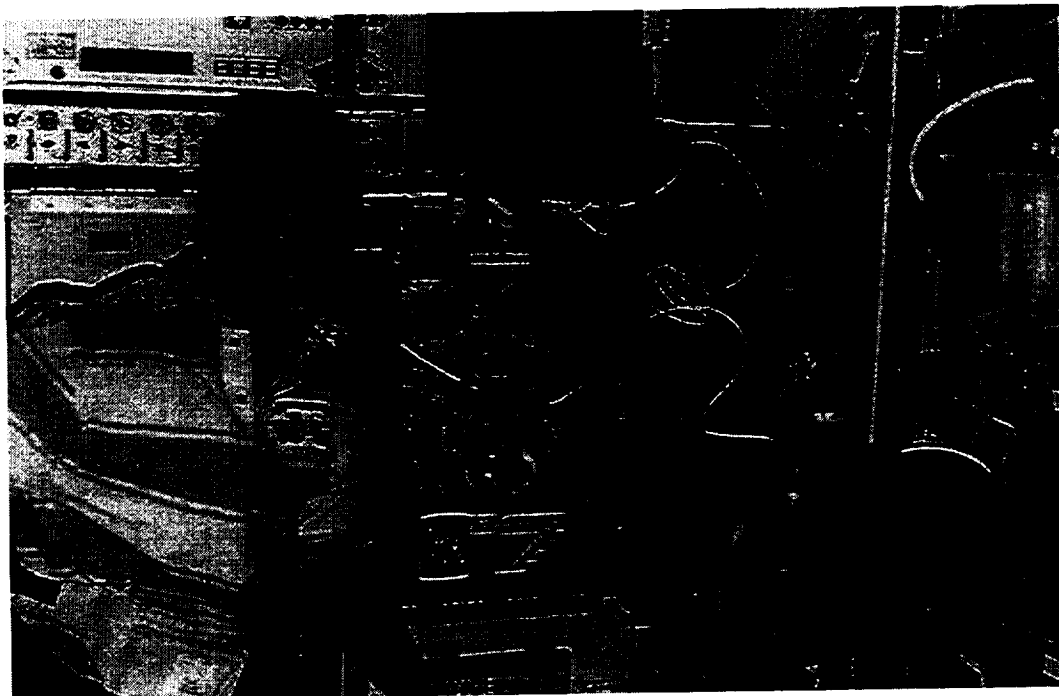


Figure 5-1. LME On-Orbit in SpaceHab Aboard STS-84.
Mission Specialist, Dr. Edward Lu, is shown next to LME.

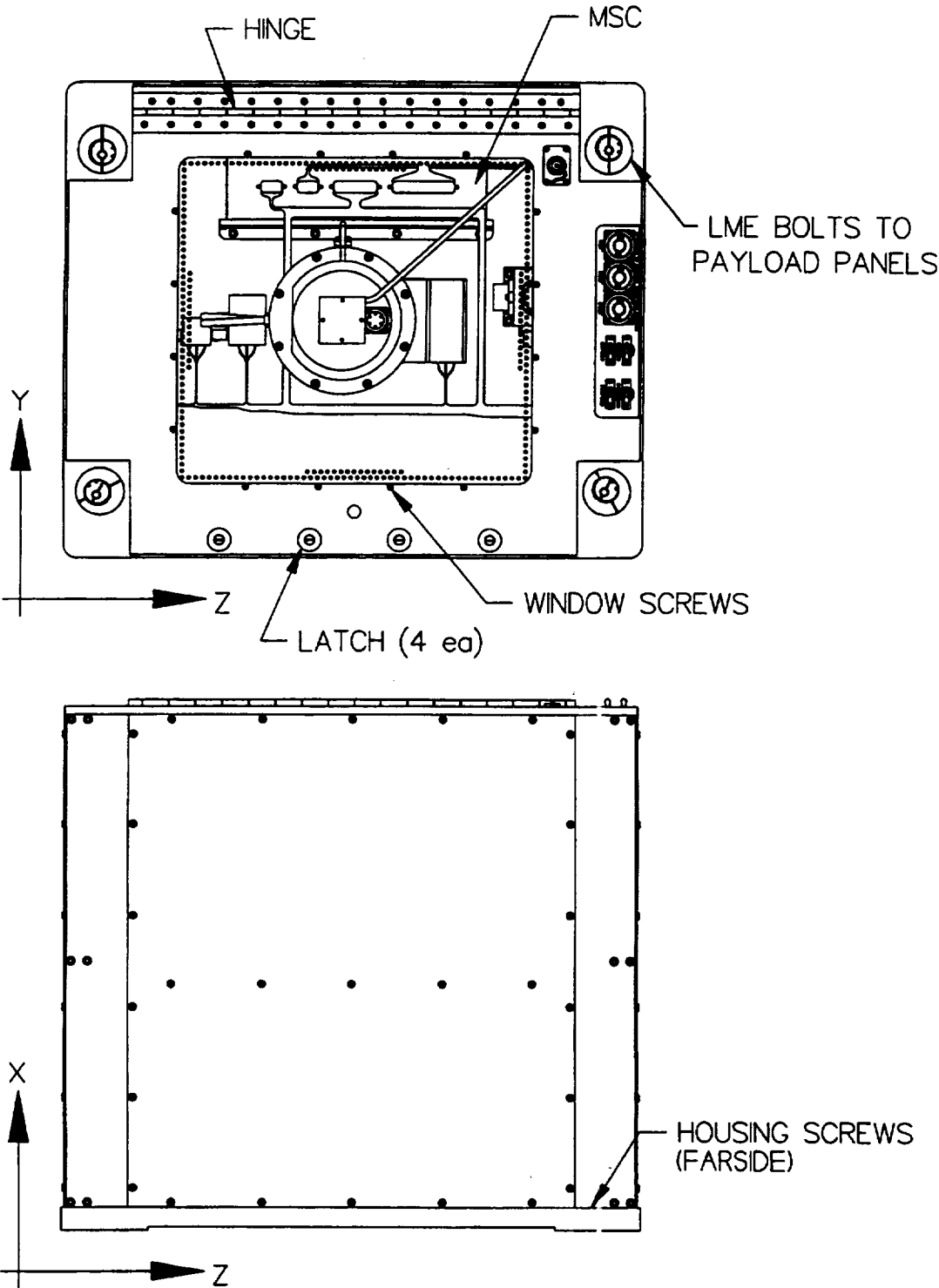


Figure 5-2. LME Enclosure Assembly.

The top view shows the enclosure as the crew member saw LME in the stow configuration.

LME Final Report

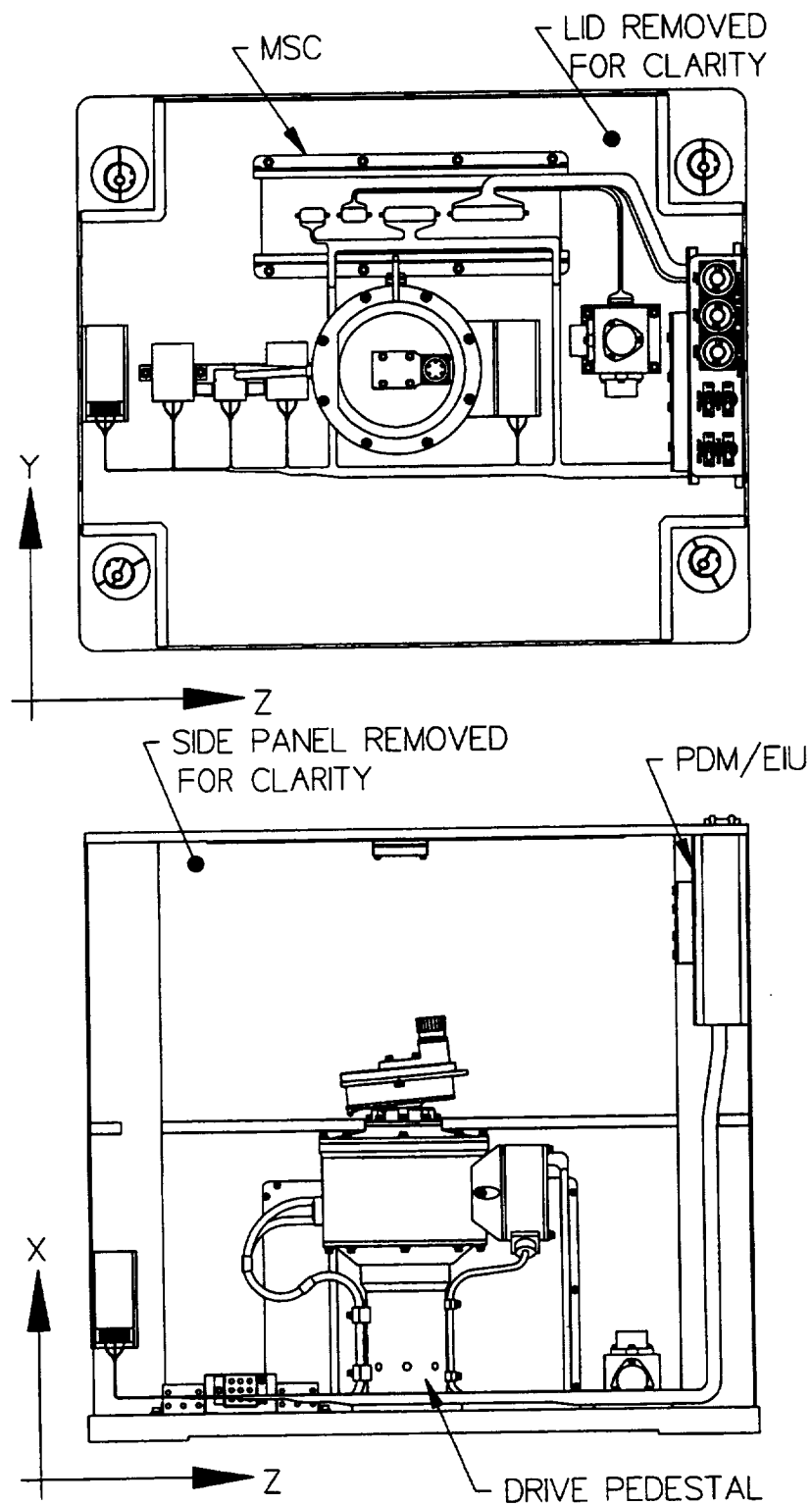


Figure 5-3. LME Stow Configuration.

This view shows the top and side view without the cover or side plates.

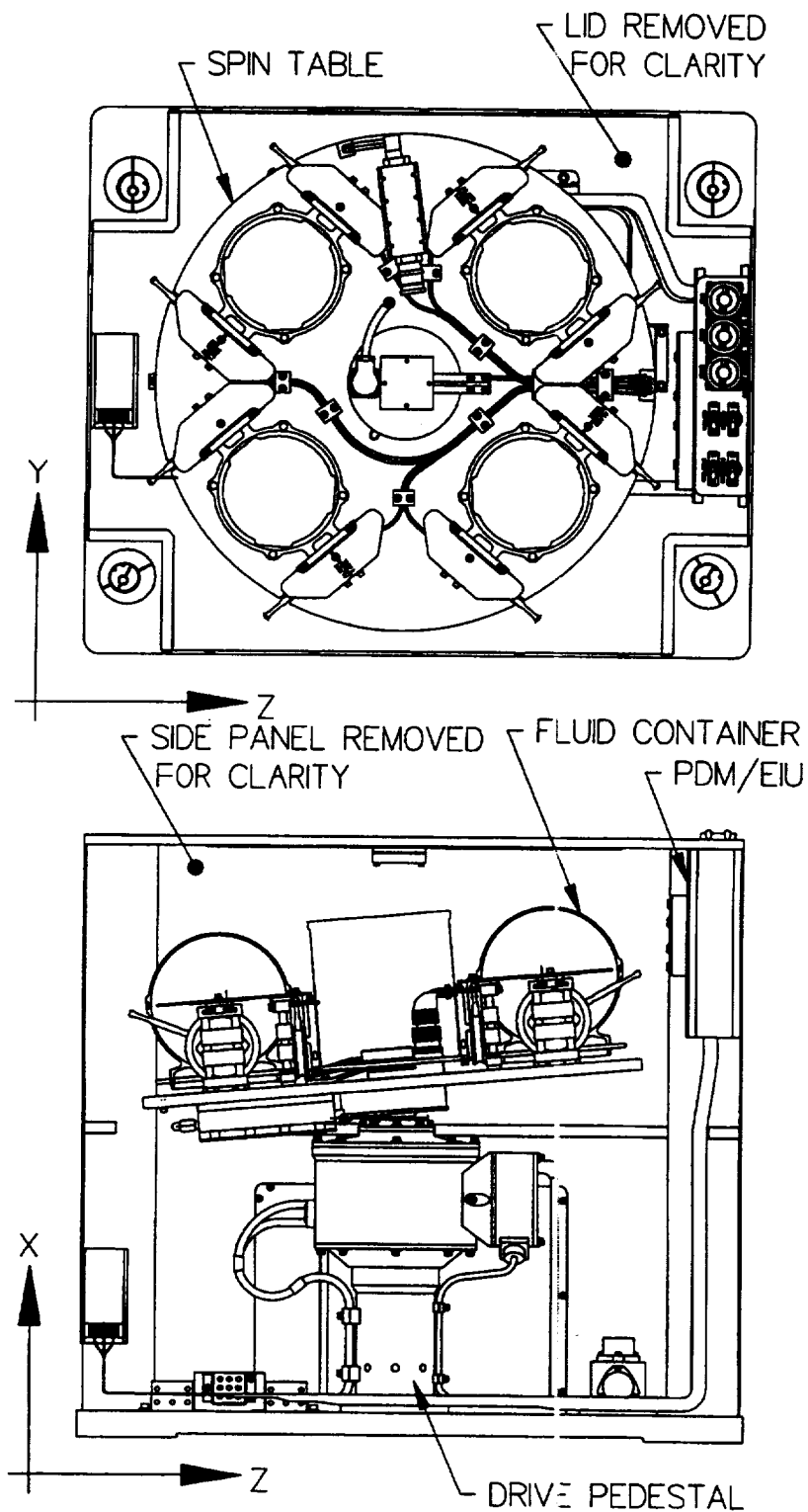


Figure 5-4. LME Run Configuration.

This figure shows the top view without tanks, and the side view with tanks and without the cover or side panel.

- Spin Table: This assembly included the load cells with mounting fixtures for the fluid tanks. The DAS, camera, and communications optical data link were also mounted to this assembly.
- Fluid Tanks: Twelve sealed tanks, six spherical and six cylindrical, were the test items. There were combinations of fill levels, fluid viscosity, and propellant management device models in the tanks.
- PGSC: A NASA-supplied computer was dedicated to this payload for communicating the control commands to the MSC, EIU, and DAS and for storing the DAS and EIU data on diskettes.
- Camcorder: A NASA-supplied camcorder was used to record the video taken by the LME-supplied camera mounted on the spin table and for documenting the operations as seen through the shield.
- Cabling: The necessary cabling between the PGSC and EIU, the camcorder and the spin table camera, and the main power cable were stored in the drawer.
- Diskettes: A sufficient quantity of diskettes for storing LME data and the control program were stowed in the storage drawer.
- Videotape: A sufficient quantity of videotapes for recording the spin table camera sequences and the overall documentary video were supplied.
- Manuals: LME operating manuals and operating procedure checklists were supplied.

Assembly and checkout of the LME apparatus included the following operations.

1. Unlatch the ¼-turn fasteners and open the transparent lid of the enclosure, as shown in Figure 5-5.
2. Align the hub, as shown in Figure 5-6, then transfer the spin table from its storage locker to its operational position and latch in place, as shown in Figures 5-7 and 5-8.
3. Remove the first set of fluid tanks from the storage locker, per Table 5-1, and mount to the load cell fixtures on the spin table.
4. Unlatch the load cells from their rigidized, launch configuration.
5. Close and latch the lid **after visually confirming that all load cells are unlatched**.
6. Connect the LME PDM on the front panel of the enclosure to the SpaceHab power supply, using the cable stowed in the storage locker.
7. Connect the EIU data terminal on the front panel of the enclosure to the PGSC, using the cables stowed in the storage locker.
8. Connect the camcorder to the video outlet terminal on the front panel of the enclosure to the camcorder; the camcorder and the cable are stowed in the storage locker.
9. Attach the camcorder to a nearby and convenient location using Velcro™ fasteners.
10. Verify set-ups using the checklists from the LME flight operations manual.
11. Turn on power to LME and activate the PGSC software to verify the communications between the PGSC and the DAS and EIU.
12. Using the PGSC software, run the series of tests for the installed fluid tank set.

13. Switch fluid tanks and repeat the tests for remaining two tank sets.
14. Deactivate the LME package and return all items to their original stowed position.

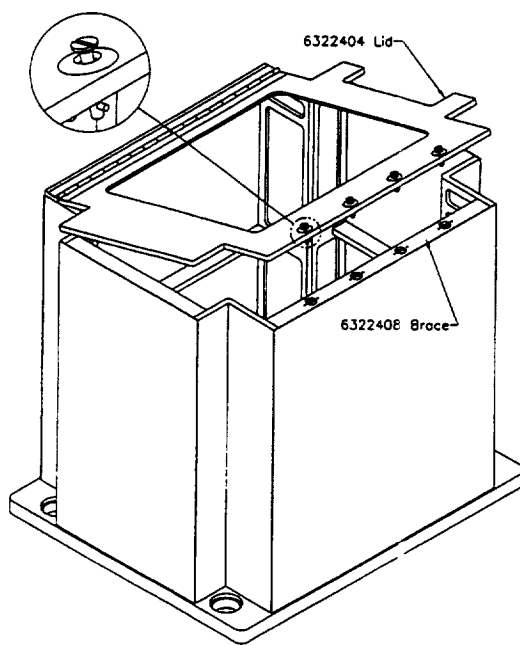


Figure 5-5. View of Enclosure and Lid Showing Locations of 1/4-Turn Fasteners.

Using a flathead screwdriver, the crew member rotated the 4 fasteners counterclockwise a 1/4-turn until each popped open.

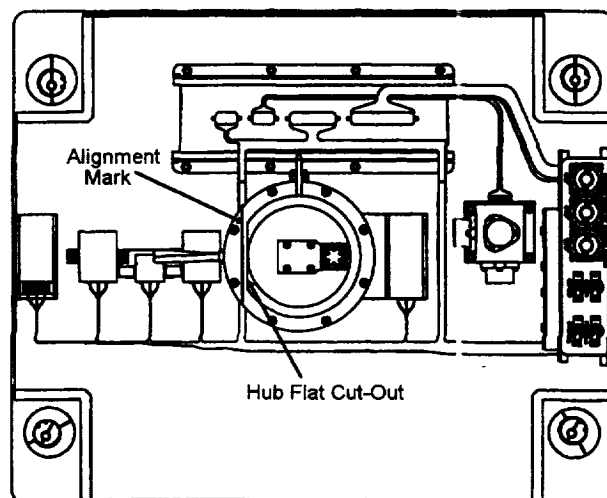


Figure 5-6. Hub Alignment Mark.

To align the drive pedestal, the hub was moved by hand, so the hub flat cutout was parallel with the alignment mark on the stationary pedestal.

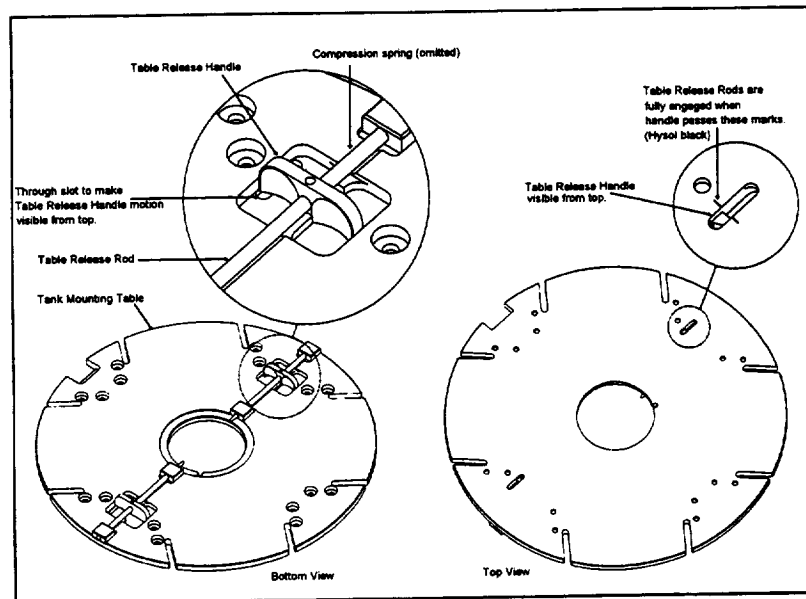


Figure 5-7. Spin Table Latch Pin with Alignment Marks.

The crew member was to locate the table release finger handles and with these finger handles facing away from the operator, reach around the outer edge of the table and with the middle two fingers pull the handles to the full outboard position overcoming the spring force.

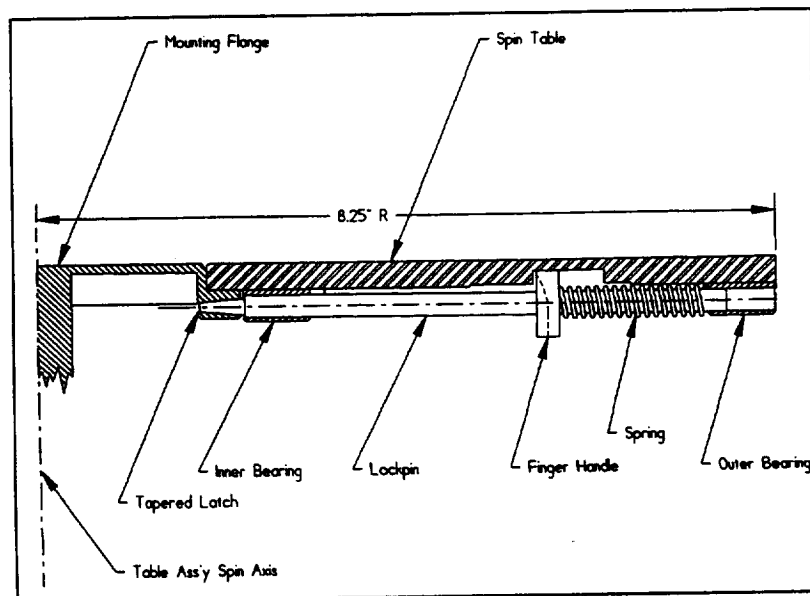


Figure 5-8. Spin Table Latch Pin, Cross-Section View.

Once the table was firmly seated against the hub flange, the crew member gradually released the finger handles until the tapered table latch pins seat in the access holes provided on the side of the hub.

**Table 5-1. Fluid Tank Identification List
(by Test Set and Position)**

Label	Shape	Viscosity	Fill Level	PMD	Position	Test Set
CL2A1A	Cylinder	Low (1 cp)	2/3 (780 ml)	No	1	A
SL2A2A	Sphere	Low (1 cp)	2/3 (520 ml)	No	2	A
CH2A3A	Cylinder	High (10 cp)	2/3 (780 ml)	No	3	A
SH2A4A	Sphere	High (10 cp)	2/3 (260 ml)	No	4	A
CL1A1B	Cylinder	Low (1 cp)	1/3 (390 ml)	No	1	B
SL1A2B	Sphere	Low (1 cp)	1/3 (520 ml)	No	2	B
CH1A3B	Cylinder	High (10 cp)	1/3 (390 ml)	No	3	B
SH1A4B	Sphere	High (10 cp)	1/3 (260 ml)	No	4	B
CL1B1C	Cylinder	Low (1 cp)	1/3 (390 ml)	Yes	1	C
CL2B2C	Cylinder	Low (1 cp)	2/3 (780 ml)	Yes	2	C
SL1B3C	Sphere	Low (1 cp)	1/3 (260 ml)	Yes	3	C
SL2B4C	Sphere	Low (1 cp)	2/3 (520 ml)	Yes	4	C

5.3 OPERATIONS DURING TESTING

5.3.1 Loading Software

After the LME apparatus was assembled and checked, the mission specialists activated the software on the PGSC as shown in the photograph in Figure 5-9. The screens displayed on the PGSC monitor displayed instructions and commands to conduct the LME test matrix. The software also verified the operation of the data acquisition system following test run completion. The mission specialists then inserted the first data floppy disk (from the storage pouch) into Drive B of the PGSC, and archived the data on the labeled floppy disks. This was repeated for all three test series.

5.3.2 Test Selection

The crew member activated the LME "Wobble" software and selected "Run Test." The PGSC monitor displayed the LME fluid tank set at the top of this data screen. The conditions for each pre-programmed test were presented, and the display indicated which tests of the matrix were completed satisfactorily and which tests remained to be conducted. The display was updated after each test. A user's guide to the interface screen is included in Appendix B.

The test matrix for each fluid tank set was identical. The test matrix is also described below in Section 5.3.6. After each tank change, a new fluid tank set series was selected at the top of the "Run Test" screen.

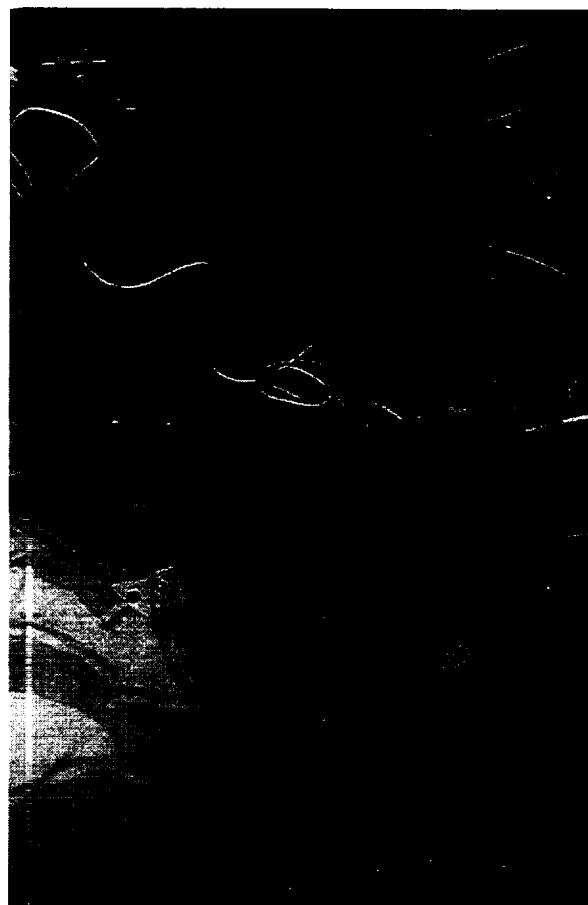


Figure 5-9. LME During Operation.
Mission Specialist, Edward Lu, is shown using checklist to activate the PGSC software.

LME Final Report

The mission specialist selected the next test series to be conducted, using the "Run Test" screens and commands displayed on the PGSC monitor. As stated above, the test sequence was organized to provide the most useful test data early in the test sequence. So, the specified testing order was followed by selecting the "Multiple Tests" button at the top center of the "Run Test" screen. The specialist, however, had the option of changing the time duration, spin rate, and nutation frequencies of each test series, based upon previous test results and consultation with the LME ground personnel. The PGSC screen displays indicated the status of the tests included in the test matrix and also presented an option to repeat any test series.

5.3.3 Instrumentation Verification and Observation

During the conduct of each test series, the PGSC monitor displayed the following information:

1. Component and test status (cooling fan operation, motor temperatures, test status) was displayed on the "Run Test" screen.
2. Data graphs (spin motor speed: actual and planned; nutation motor speed: actual and planned; updated torque time-history of each load cell) were selected from the "View Data" screen.

The mission specialist cycled through the various screens as the test proceeded to verify the progress of the test series. At any time during a test, the mission specialist could have aborted the test by clicking on an "Abort" button; such actions might have been needed in case of malfunctions or a large g-jitter disturbance occurred during the test. All test activities were coordinated with the PI via voice communication with the ground.

At various times during the tests, data diskettes and videotapes had to be changed or downlinked directly. Convenient times for changing these items were noted in the test schedule described in Section 5.3.6. The PGSC software kept track of running time and data diskette capacity in the event that either of these had to be changed at times other than those noted.

5.3.4 Fluid Tank Set Change

At the conclusion of all the tests for a given fluid tank set, the mission specialist changed the fluid tanks to the next fluid tank set. The mission specialist first had to exit the PGSC software so that the LME power could be disconnected. After the spin table had come to a complete stop, the transparent lid could be opened to gain access to the spin table. The mission specialist then had to lock the load cell frames and rigidize the load cells to prevent damage during the fluid tank change. The fluid tanks could then be removed safely from the load cell fixtures by opening the release clamps. The fluid tanks were then stowed in the storage locker. The next set of fluid tanks (stowed in the storage locker) were inserted in the load cells by reversing the process just described. Closing and latching the transparent lid completed the fluid tank change operation. The mission specialist then re-entered the PGSC software to continue the LME tests. After returning to the "Run Test" screen, the mission specialist then selected the next fluid tank series described in the upper left corner of the screen.

5.3.5 Ground Communications

The LME Principal Investigator and other key LME design personnel were at JSC mission center throughout the LME flight. These personnel were available to relay special instructions to the mission specialists, answer questions, and troubleshoot difficulties in conducting the test matrix.

5.3.6 Test Matrix

Table 5-2 shows the test matrix used in the flight experiment to accomplish LME's objectives. As discussed earlier, two general types of tests were conducted: *sine sweep tests* to investigate liquid resonances, and *sine dwell tests* to investigate steady state energy dissipation. The two higher spin rate sweep tests (20 and 14 rpm) were meant to verify that inertial wave resonances scale with the spin rate when surface tension effects are negligible. The lowest spin rate sweep tests (4 rpm, Bond No. = 1.2) were meant to investigate the effects of surface tension on inertial wave resonances when these effects are comparable to the effects of centrifugal acceleration. The rate at which the wobble motor rotation was increased for the sine sweep tests was chosen (on the basis of analysis and previous ground slosh tests) to ensure that the dominant resonance would be excited into a nearly steady state condition as the nutation frequency passed through the resonance frequency. This sweep rate was 1/20th of the total frequency search range per minute. For the sine dwell tests, the wobble motor rotation rates were selected for each spin rate such that the liquid in the spherical tanks would be excited into near-resonance conditions for the higher wobble motor spin rate, and the liquid in the cylindrical tanks would be excited into near-resonance conditions for the lower wobble motor spin rate, based on the predictions of the homogeneous vortex model described earlier. Each set of tests was preceded by a period of steady spinning without nutation to settle the liquids into their equilibrium configuration and to calibrate the load cells.

Table 5-2. LME Sweep Test Matrix.

Test Type	Spin Rate, rpm	Wobble Rate, rpm	Duration, min	Centrifugal Acc., g	Bond No.
Calibrate	20	0	5	0.067	30
Sweep	20	2 → 40	20	0.067	30
Calibrate	14	0	5	0.033	15
Sweep	14	2 → 28	20	0.033	15
Calibrate	4	0	5	0.0027	1.2
Sweep	4	1 → 8	30	0.0027	1.2
Calibrate	20	0	5	0.067	30
Dwell	20	12	4	0.067	30
Dwell	20	18	4	0.067	30
Calibrate	14	0	5	0.033	15
Dwell	14	8.5	5	0.033	15
Dwell	14	12	5	0.033	15
Calibrate	4	0	5	0.0027	1.2
Dwell	4	2.5	10	0.0027	1.2
Dwell	4	2.5	10	0.0027	1.2

The same test matrix was repeated for each set of tanks to investigate the effects of fill level and PMD design on resonance frequencies and energy dissipation. The two tanks of each shape in a tank set

LME Final Report

contained liquid of different viscosities to investigate the effects of liquid viscosity on these same liquid oscillation characteristics.

The timeline to accomplish all the tests for all the tank sets is shown in Table 5-3. The tests for a single set of tanks could be completed in about 160 minutes. All the runs for a single tank set could be executed continuously; however, there was a break between tank sets to allow the tanks to be changed, which could be extended to several hours to accommodate other mission operations. In flight, the LME tests were conducted in fact over several days. The total time requirement was approximately ten hours, including the time needed for unstowing, assembly, disassembly, and restowing.

5.4 RAPID SAFING

In the event that the test operations had to be shut down rapidly, a "rapid safing" procedure was developed. The timeline for these procedures is shown as Table 5-4.

5.5 DEVIATIONS DURING FLIGHT OPERATIONS

During the flight tests, several deviations occurred from the planned operations and test matrix. These are described below.

Latching the enclosure access door. The enclosure access door had to be closed and latched (using four ¼-turn style latches, as described in Figure 5-5) to enable power to the experiment. After assembling the hardware and inserting the first tank set, the mission specialists encountered considerable difficulties pushing in and turning the ¼-turn style latches, using the available screwdriver. Eventually, they abandoned these attempts. Since no tests could be conducted until the access door was closed and the interlock switch engaged, the mission specialists suggested using strips of "NASA gray tape" (known commercially as duct tape) around the edges of the door to hold the door in the closed position, and the LME team, as well as the NASA safety officer, approved this decision. SpaceHab technical personnel stress analyzed the requirements for the needed length of tape strips to ensure that the access door would not open accidentally during re-entry. This modification of the planned operations caused no further problems.

High random acceleration level. The level of random accelerations at the spin table was considerably higher than anticipated (as a result of the 80 to 1 speed reducer on the wobble motor). Initially, these accelerations tripped the accelerometer switch that was designed to prevent testing during high levels of g-jitter. Since the random accelerations were continuous, it was necessary to disable the accelerometer switch (a software modification) to enable the test matrix to be conducted. The result of this action was that the test data contained a significant level of random noise superimposed on the true data signals. The effect of the noise and the methods used to eliminate it during the data analysis are described in Section 6. The noise did, however, prevent the LME personnel from identifying resonance frequencies in real time from the downlinked data.

Incomplete test matrix. The delays encountered because of the difficulty in latching the access door and because the tests for the first tank set had to be re-started after disabling the accelerometer cut-off switch stretched out the test time to the point that the 4 rpm sine dwell tests for the third tank set could not be conducted. In addition, the 20 rpm sine sweep test for the third tank set was conducted, but the test data was inadvertently not recorded on floppy disks; thus, this data set was also not available. With these two exceptions, all the other tests were completed successfully.

Table 5-3. Timeline of Test Runs.

Container Set #1	Spin (rpm)	Wobble (rpm)	Dur'm (min)	Test Time (hours)							
				1	2	3	4	5	6	7	8
Cal	20	0	5								
High Sweep	20	2-40	20								
Sweep Disks&Tape	off	off	5								
Cal	14	0	5								
Med Sweep	14	2-28	20								
Sweep Disks&Tape	off	off	5								
Cal	4	0	5								
Low Sweep	4	1-8	30								
Sweep Disks&Tape	off	off	5								
Cal	20	0	5								
High Wobble1	20	12	4								
High Wobble2	20	18	4								
Cal	14	0	5								
Med Wobble1	14	8.5	5								
Med Wobble2	14	12	5								
Cal	4	0	5								
Low Wobble1	4	2.5	10								
Low Wobble2	4	3.5	10								
Sweep Containers	off	off	10								
Container Set #2											
Cal	20	0	5								
High Sweep	20	2-40	20								
Sweep Disks&Tape	off	off	5								
Cal	14	0	5								
Med Sweep	14	2-28	20								
Sweep Disks&Tape	off	off	5								
Cal	4	0	5								
Low Sweep	4	1-8	30								
Sweep Disks&Tape	off	off	5								
Cal	20	0	5								
High Wobble1	20	12	4								
High Wobble2	20	18	4								
Cal	14	0	5								
Med Wobble1	14	8.5	5								
Med Wobble2	14	12	5								
Cal	4	0	5								
Low Wobble1	4	2.5	10								
Low Wobble2	4	3.5	10								
Sweep Containers	off	off	10								
Tank Set #3											
Cal	20	0	5								
High Sweep	20	2-40	20								
Sweep Disks&Tape	off	off	5								
Cal	14	0	5								
Med Sweep	14	2-28	20								
Sweep Disks&Tape	off	off	5								
Cal	4	0	5								
Low Sweep	4	1-8	30								
Sweep Disks&Tape	off	off	5								
Cal	20	0	5								
High Wobble1	20	12	4								
High Wobble2	20	18	4								
Cal	14	0	5								
Med Wobble1	14	8.5	5								
Med Wobble2	14	12	5								
Cal	4	0	5								
Low Wobble1	4	2.5	10								
Low Wobble2	4	3.5	10								
Sweep Containers	off	off	10								

LME Final Report

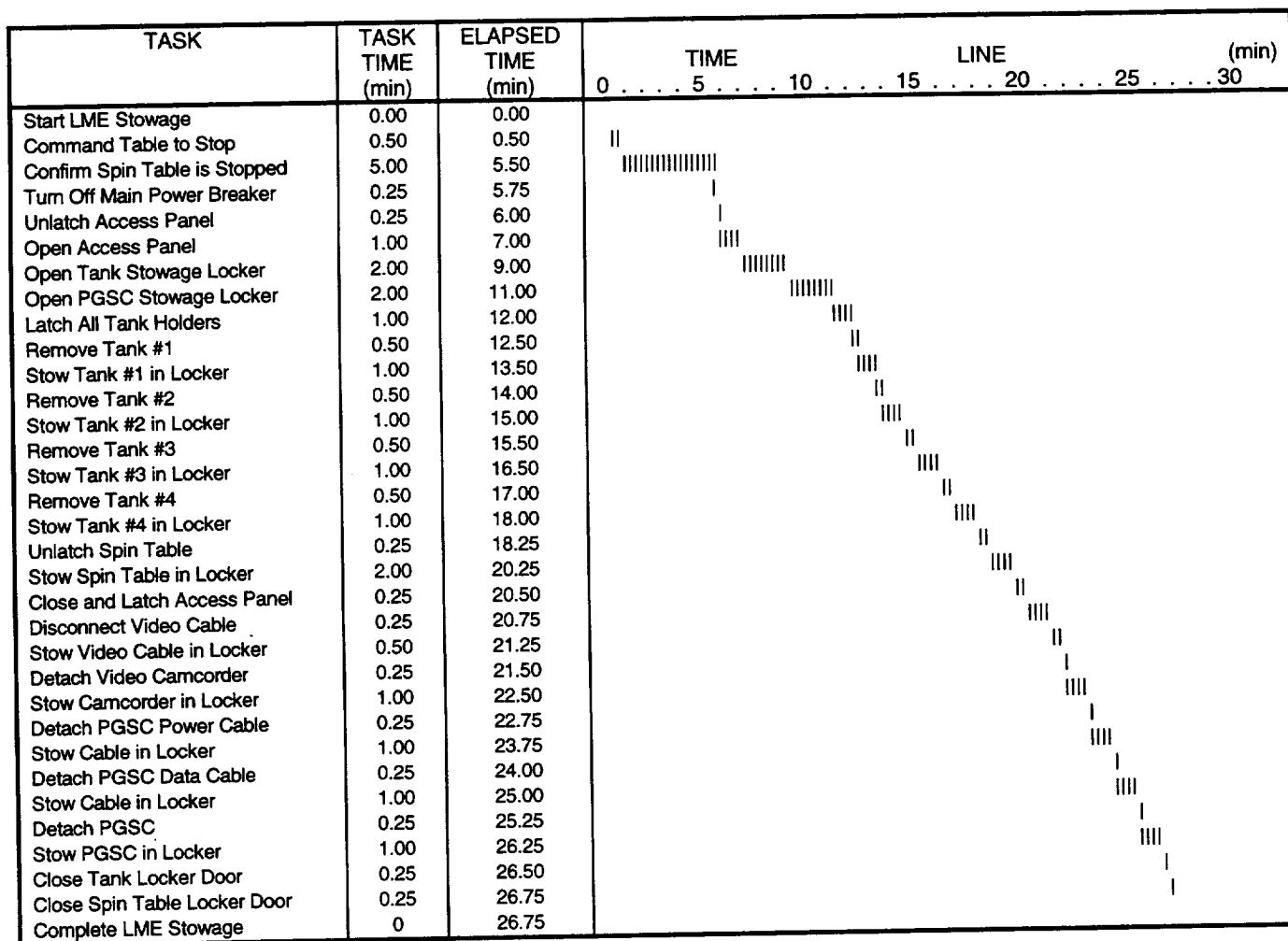


Figure 5-10. LME Rapid Safing Timeline.
Shuttle safety required rapid safing within 30 minutes.

This page left intentionally blank.

6. FLIGHT DATA ANALYSIS

6.1 INTRODUCTION

For the reasons discussed in previous sections of this report, LME employed two general types of tests, each having a specific objective. For the *sine sweep tests*, the spin rate was held constant and the nutation frequency was varied over a range. For the *sine dwell tests*, the spin rate and nutation frequency were held constant for an extended period of time.

6.1.1 Sine Sweep Tests Characteristics

The objectives of the sine sweep tests were to determine the resonant frequencies and apparent viscous damping of the liquid oscillations.

Resonant frequency. At a resonance, the liquid-induced torque sensed by the load cells had a local maximum. Thus, the resonant frequencies were determined by examining the torque time histories for maxima. The rate of change of the nutation frequency was small enough to allow the amplitudes of the resonant torques to obtain their steady-state values; the sweep rate was small initially and increased logarithmically in time, so that most of the test time was devoted to the range $\lambda < \Omega_0$ where theory indicated that prominent resonances occurred [Dodge, *et al.*, 1996].

Sine sweep tests for each tank set were conducted for three different spin rates, two of which (nominally 20 rpm and 14 rpm) produced centrifugal accelerations sufficiently high to make the effects of surface tension negligible. These spin rate tests investigated how liquid resonant frequencies varied with spin rate; theory indicates that the resonant frequency is proportional to the spin rate. The third spin rate (nominally 4 rpm) was sufficiently small such that the Bond number, defined as $Bo = \rho R \Omega_0^2 d / \sigma$, was of order unity, where ρ is the liquid density and σ is the liquid surface tension. For Bond numbers of unity or less, the liquid is effectively in a low-gravity environment and the interface is highly curved. Thus, the 4 rpm spin rate tests simulated a slowly-spinning spacecraft and quantified the influence of surface tension on the resonances.

Figures 6-1 and 6-2 show how the predicted resonant frequency (the nutation frequency λ that excites the resonance) of the most prominent resonance varies with the liquid fill rate for cylindrical and spherical tanks [Dodge, *et al.*, 1996]. (For computational reasons, the predictions for $Bo = 1$ for the cylindrical tank assume the cylinder is infinitely long in the axial direction.) In general, the resonance ratio λ/Ω_0 is predicted to increase somewhat as the liquid fill level increases and to be independent of the spin rate Ω_0 for $Bo \gg 1$.

Damping. The apparent damping γ (fraction of critical damping) was determined by the "width" $\Delta\lambda$ on the nutation frequency axis at which the torque amplitude was $1/\sqrt{2}$ times the resonant peak amplitude, as shown in Figure 6-3 [Abramson, 1966]. This damping coefficient is useful for equivalent mechanical models of an inertial wave oscillation, such as a single degree of freedom rotating, nutating disk [Dodge, *et al.*, 1994].

LME Final Report

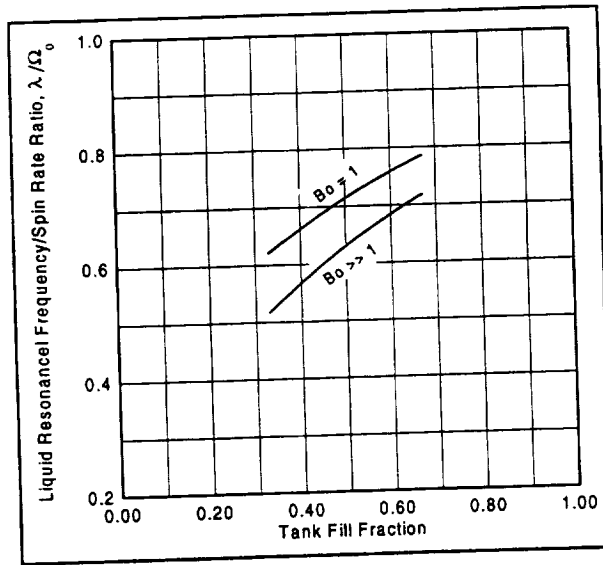


Figure 6-1. Predicted Resonant Frequency for a Spinning, Nutating Cylindrical Tank.
For $Bo \gg 1$, the resonant frequency increases in direct proportion to the spin rate.

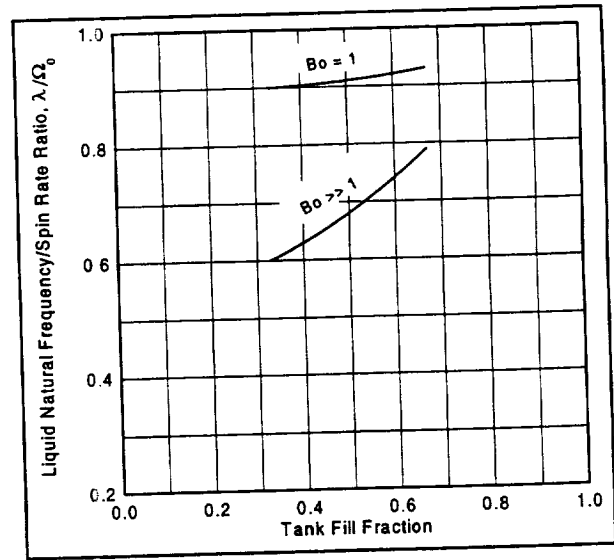


Figure 6-2. Predicted Resonant Frequency for a Spinning, Nutating Spherical Tank.
For $Bo \gg 1$, the resonant frequency increases in direct proportion to the spin rate.

6.1.2 Sine Dwell Test Characteristics

The objective of the sine dwell tests was to quantify the energy dissipation rates of the liquid oscillations under steady state conditions. The spin rate and the nutation frequency were held constant for up to 20 minutes, to ensure that the liquid oscillations reached a steady state condition. Since each tank set consisted of cylindrical and spherical tanks, two sine dwell tests were conducted for each tank set, with the rotation frequency of one test selected to excite resonant oscillations in the cylindrical tanks, and the nutation frequency of the other test selected to excite resonant oscillations in the spherical tanks.

Energy dissipation rates. The energy dissipation rate for each tank was computed from the measured torque amplitude and the angular velocity of the spin table at the tank location by:

$$E_i = 0.5(T_{total} - T_{rigid})\omega_i \cos \phi_i$$

(6-1)

Here T_{total} was the amplitude of the measured sinusoidal torque, T_{rigid} was the computed torque for the empty tank and tank structure, ω was the sinusoidal angular velocity of the spin table and ϕ was the phase angle between the torque and the angular velocity sine waves; the phase angle ϕ was computed from the timing marks recorded in the data stream after compensating for the rigid body torque. The subscript i

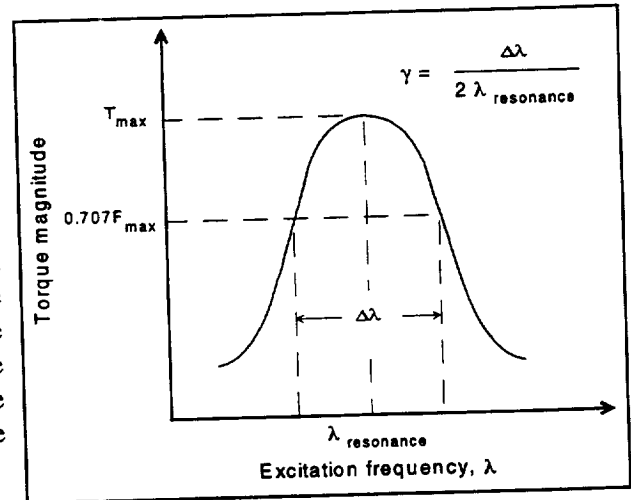


Figure 6-3. Half Power Damping Computation.
Rigid body torques must be subtracted from the torque amplitudes before determining the half-power points.

indicates a radial or tangential component of the parameter. The total energy dissipation rate is the sum of the radial and tangential dissipation rates.

When the phase angle ϕ is between -90° and $+90^\circ$, the energy dissipation rate is positive, according to Eq. (6-1). This means that the liquid extracts energy from the nutation, which is eventually transformed into heat by viscous stresses (for a spacecraft, the energy is extracted from the spin kinetic energy). Conversely, when the phase angle is between 90° and 270° , the energy dissipation rate is negative, and the liquid contributes energy to the nutation; this is unrealistic, since the liquid oscillations would then decay rather than continue in a steady state.

The rigid body torques needed for Eq. (6-1) were computed from the relation:

$$T_{rigid,i} = I_{trans}\alpha_i \pm (I_{spin} - I_{trans})\Omega_0\omega_i \quad (6-2)$$

where the + sign was used if i corresponded to the radial component and the - sign was used for the tangential component.

The energy dissipation rate obtained from the sine dwell tests is related theoretically to the damping coefficient γ determined from the sine sweep tests. The form of the relation depends on the inertial wave analytical model; detailed comparisons with the analytical models are given in a companion SwRI IR&D final report [Dodge, *et al.*, 1998].

6.1.3 Spin and Nutation Rates

The spin rate and nutation frequency of the spin table were provided by the "spin" motor and the "wobble" motor. In the conceptual design [Dodge, 1989], the wobble motor axis was tilted at $\theta \approx 5^\circ$ to the spin motor axis to simulate a spacecraft cone angle, and the spin motor itself (which was attached to the spin table) was rotated by the wobble motor. Thus, the rotation rate Ω_0 of the table was the sum of the rotation rates of the two motors, $\Omega_0 = \Omega_{spin}\cos\theta + \Omega_{wobble} \approx \Omega_{spin} + \Omega_{wobble}$ (since $\cos\theta \approx 1$), and the nutation frequency of the table was Ω_{wobble} . This design required slip ring or similar device to transmit electric power to the rotating spin motor. To eliminate this requirement and to provide a more compact package, the spin motor housing in the final design was mounted on a swash-plate-like arrangement tilted at 5° to the wobble motor shaft axis as was described in Section 4. The swash plate did not rotate (and so the spin motor housing did not rotate), but it was connected to the wobble motor by a coupling that caused the tilt angle of the swash plate to rotate around the wobble motor shaft axis. Since the spin motor was directly connected to the spin table, the spin table rotation rate was the spin motor rotation rate $\Omega_0 = \Omega_{spin}$, and the tilt angle vector of the spin table rotated at the wobble motor rotation rate. This arrangement rotated the angle between the wobble motor shaft axis and the spin table axis around a vector through the wobble motor shaft at a rate equal to the wobble motor spin rate. Therefore, the spin table performed a coning motion.

For the final design, the unsteady angular velocity ω and unsteady angular acceleration α of a point on the spin table, such as one of the LME tanks, is given in a coordinate system rotating with the table by:

$$\omega = \Omega_{wobble}\theta\sin(\lambda t + \beta) \quad (6-3a)$$

$$\alpha = \lambda\Omega_{wobble}\theta\cos(\lambda t + B) \quad (6-3b)$$

LME Final Report

where β is a phase angle that depends on the angular location of the table point in question. For comparison, the angular velocity and acceleration of an off-axis tank in a spinning spacecraft are given by: $\omega = \lambda\theta\sin(\lambda t + \beta)$ and $\alpha = \lambda^2\theta\cos(\lambda t + \beta)$. The kinematics of the spin table motion was not analyzed in detail until after the hardware had been fabricated, at which point it was found that the nutation frequency of the spin table was given by:

$$\lambda = \Omega_{spin} - \Omega_{wobble} \quad (6-4)$$

instead of $\lambda = \Omega_{wobble}$ as in the conceptual design. Thus, the amplitude of ω for LME was not equal to $\lambda\theta$, as it is for a spacecraft. These differences between Eqs. (6-3) and (6-4) and the analogous spacecraft relations were not critical because the liquids in the LME tanks were still subjected to a spinning, nutating motion.

The LME test matrix was formulated on the assumption that $\lambda = \Omega_{wobble}$. Thus, the actual range of nutation frequencies investigated in the tests was different than the range proposed in the LME Experiment Requirements Document. Other implications of Eq. (6-4) will be discussed during the later discussion of the test results.

6.1.4 Liquid Properties

The surface tension of the water in the LME tanks was about 4×10^{-4} lb/in (70 dyne/cm), and the surface tension of the water-glycerin mixture was slightly less. The density of the water was 0.036 lb/in³ (1.0 gram/cm³), and that of the water-glycerin mixture was 0.041 lb/in³ (1.14 gram/cm³). The viscosity of the water was 0.86 cp, and the viscosity of the water-glycerin mixture was 9.5 cp. All liquid property measurements were made at 75° F (23.9°).

6.1.5 Flight Test Matrix Descriptors

Each test conducted in the flight program was assigned a unique identification descriptor (the data disk file name) based on the following scheme:

Test Descriptor: I XX YY

where:

- I = A or B or C to describe the tank set
- XX = 00 for a sine sweep test for $\Omega_{spin} = 20$ rpm
 = 01 for a sine sweep test for $\Omega_{spin} = 14$ rpm
 = 02 for a sine sweep test at $\Omega_{spin} = 4$ rpm
 = 03 for a sine dwell test for $\Omega_{wobble} = 13$ rpm and $\Omega_{spin} = 20$ rpm
 = 04 for a sine dwell test for $\Omega_{wobble} = 16.8$ rpm and $\Omega_{spin} = 20$ rpm
 = 05 for a sine dwell test for $\Omega_{wobble} = 5.4$ rpm and $\Omega_{spin} = 14$ rpm
 = 06 for a sine dwell test for $\Omega_{wobble} = 11.7$ rpm and $\Omega_{spin} = 14$ rpm
 = 07 for a sine dwell test for $\Omega_{wobble} = 2.8$ rpm and $\Omega_{spin} = 4$ rpm
 = 08 for a sine dwell test for $\Omega_{wobble} = 3.4$ rpm and $\Omega_{spin} = 4$ rpm
- YY = run number (=1 for the first test, 2 for a first repetition, 3 for a second repetition, etc.)

6.2 DATA ANALYSIS

6.2.1 Data Reduction

Torque data were acquired in the form of time histories of strain gauge voltages. The data were sampled 40 times during each spin rate period, which was more than adequate to resolve the details of the highest frequencies used in the tests.

All the strain gauge voltages were severely contaminated by high and low frequency noise from a variety of sources including the wobble motor speed reducer. The true data signal was not readily evident in the raw data. Figure 6-4 shows a typical voltage time history sample from one of the strain gauge bridges, in this case acquired near the start of a sine sweep test conducted at a 20 rpm spin rate. This raw signal was dominated by random noise, although the true sinusoidal response at the nutation frequency can be seen imbedded in the data. Consequently, it was necessary in the post-flight data processing to extract the true signal from each strain gauge time history by digital filtering using filtering routines in LabView software. After filtering, the strain gauge signals were combined to compute the appropriate torques. For sine sweep tests, all data components at frequencies that were somewhat higher than the highest nutation frequency and somewhat lower than the lowest nutation frequency used in the test were filtered. For sine dwell tests, for which the frequency of the true signal did not vary with time, the filtering closely bounded the test nutation frequency. The filtering yielded good results except for the 4 rpm spin rate tests; for these low spin rate tests, all the low frequency noise could not be completely filtered without affecting the true signal.

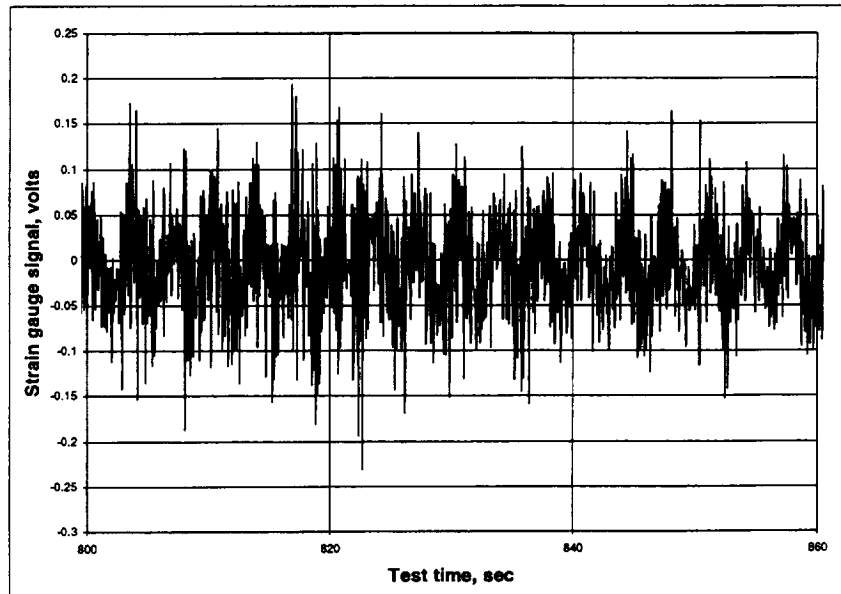


Figure 6-4. Sample Data Time History for a Sine Sweep Test.
Torque signal at the nutation frequency is masked by higher frequency, higher amplitude noise from a variety of sources.

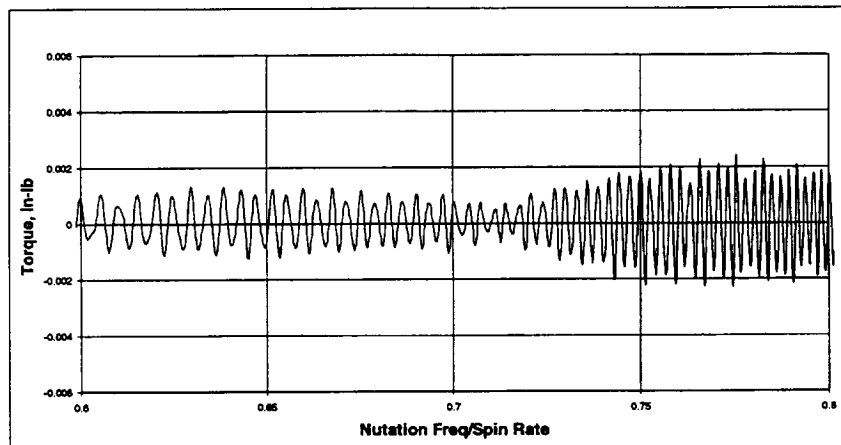


Figure 6-5. Sample Filtered Torque Data for a Sine Sweep Test.
Time history has been converted to nutation frequency and normalized by spin rate.

Figure 6-5 shows a typical sine sweep torque history after the strain gauge signals have been filtered and combined, in this case for the same 20 rpm spin rate test shown in Figure 6-4. In Figure 6-5, the test time shown in Figure 6-4 on the abscissa axis has been converted to nutation frequency corresponding to the

test time, and the nutation frequency has been normalized by dividing it by the spin rate to make it easier to compare the occurrence of resonances in the test results to the predictions shown in Figures 6-1 and 6-2. There is still some noise in the torque response history, but in general the filtered response is about as clean as might be expected for a vibration test.

6.2.2 Sine Sweep Test Results

For a sine sweep test, the nutation frequency was varied over a prescribed range by increasing the rotation rate of the wobble motor exponentially in time from a starting value of near zero to a final value of about twice the spin motor rotation rate. As an example, Figure 6-6 shows the wobble motor rotation rate history for Test A0002, for which the wobble motor rotation increased from 0.2 rad/sec (1.9 rpm) to 3.9 rad/sec (37.6 rpm). Since the nutation frequency was the difference between the spin motor and wobble motor rotation rates, the actual nutation frequency of this test decreased from an initial value of 18.1 rpm to zero (when the wobble motor spin rate was 20 rpm after about 900 sec), and then increased to 17.6 rpm in the retrograde direction at the end of the test. The prograde motion occupied 900 of the 1200 test seconds, and the retrograde motion occupied 300 seconds. Consequently, the sweep rate through the retrograde motion was probably too fast to excite liquid resonances.

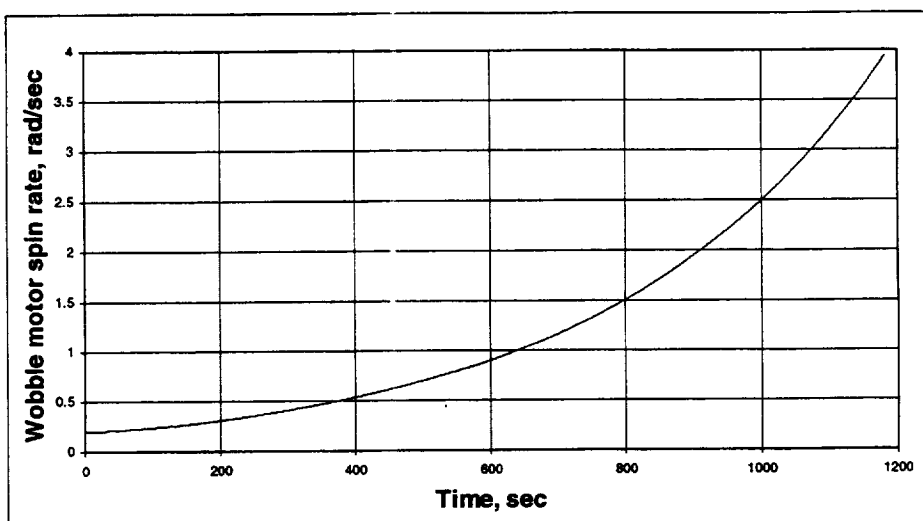


Figure 6-6. Wobble Motor Rotation Rate for Test A0002 (20 rpm spin rate).
Nutation frequency varies from 18.1 rpm to 0 rpm to -17.6 rpm.

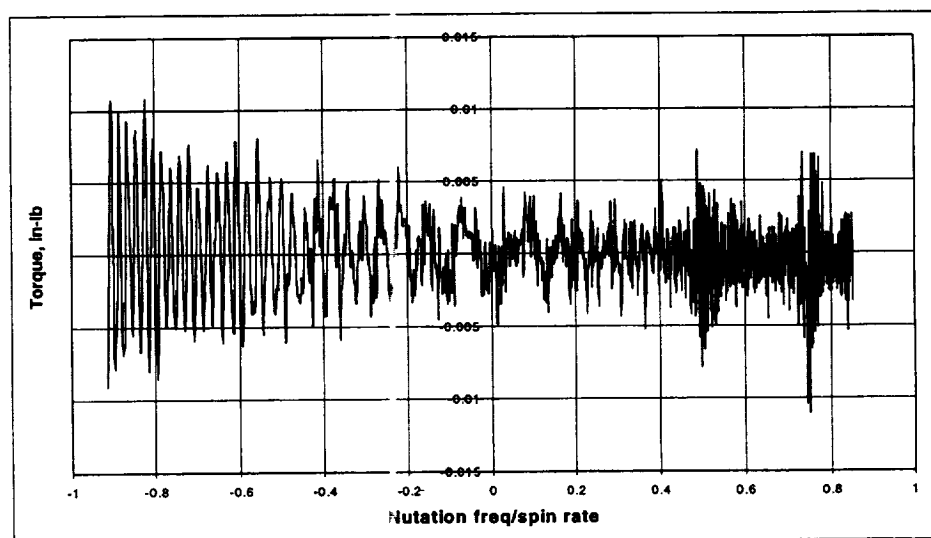


Figure 6-7. Radial Torque for Tank 1 (2/3 full cylinder) in Test A0101.
Torque amplitude depends on magnitude of the spin table motion.

Typical results. Figure 6-7 shows a typical sine sweep test result; in this case, the radial torque amplitude history for Tank 3 of Test A0101 (2/3 full cylinder, viscosity = 1 cp, spin rate = 14.1 spin rate) as a function of λ/Ω_0 . In terms of the actual test time, the start of the test corresponds to the highest value of

λ/Ω_0 (i.e., the right hand side of the graph) and the end of the test to the lowest (negative) value. The slight "jaggedness" of this plot is the result of several factors, including some residual noise in the data, but the primary causes are: (1) the large number of nutation cycles compressed into the graph, (2) the finite data sampling rate of the tests, which sometimes missed the peak of a cycle, and (3) the plotting software, which draws a straight line from one data point to the next without any "smoothing."

This plot indicates that there are two liquid resonances, one near $\lambda/\Omega_0 \approx 0.5$ and a second near $\lambda/\Omega_0 \approx 0.76$. (The torque peak near $\lambda/\Omega_0 \approx 0.85$ is the transient associated with the start of the test and does not indicate a liquid resonance). The relative magnitude of these two peaks is deceiving, however, because the amplitude of the excitation creating the liquid motion is considerably different for each peak. It is not a straightforward matter to determine a method to normalize the torques to account for the different excitation amplitudes. For a rigid body, the excitation would depend on three rotation rates: (1) the angular acceleration α of the body, (2) the angular velocity ω of the body, and (3) the steady spin rate Ω_0 ; the appropriate combination of these factors is given by the right hand side of Eq. (6-2). For a liquid, however, the relevant equivalent rigid-body inertias I_{trans} and I_{spin} are not known. (In fact, the analytical models predict the equivalent inertias, but for consistency in the comparisons, the analytical models are not used to reduce the test data.) In the absence of better information, the normalizing factor for the test torques is assumed to be the sum $\alpha + \Omega_0\omega$, which is based on an analogy with Eq. (6-2). The ratio of a test torque to this normalizing factor has dimensions of moment of inertia, so in effect, the equivalent inertias of the liquid

as a function of λ/Ω_0 are given by this normalization method. Figure 6-8 shows the result of normalizing the data of Figure 6-7. The normalized resonance at $\lambda/\Omega_0 \approx 0.5$ is much reduced compared to the one at $\lambda/\Omega_0 \approx 0.76$. The higher-frequency resonance $\lambda/\Omega_0 \approx 0.76$ is concluded to be the most prominent resonance. In fact, the frequency of this resonance agrees well with the predicted resonance frequency shown previously in Figure 6-1. Figure 6-9 shows an expansion of the torque response in the vicinity of this resonance.

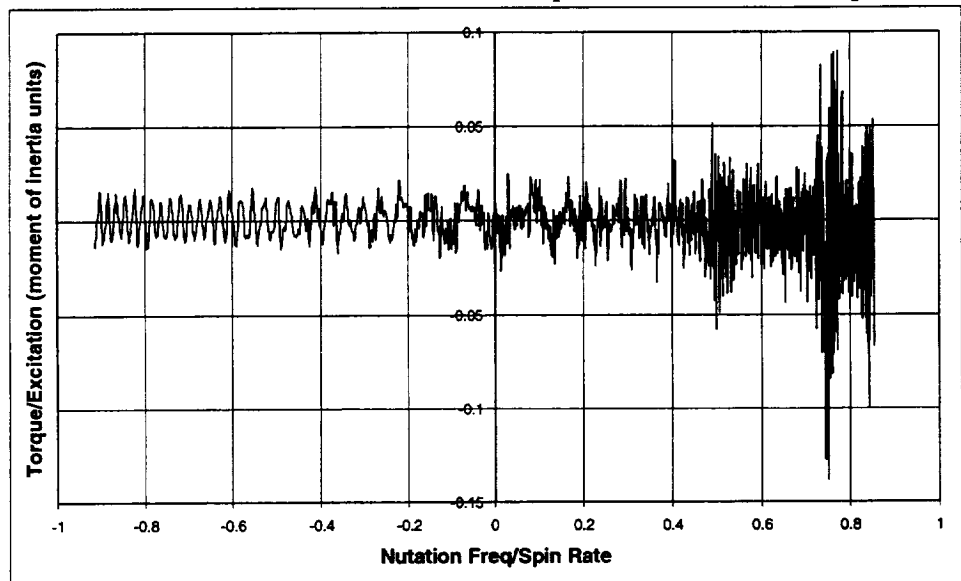


**Figure 6-8. Normalized Radial Torque for Tank 1
2/3 full cylinder) in Test A0101.**

Most prominent resonance occurs for $\lambda/\Omega_0 \approx 0.76$.

The damping was computed from Figure 6-9 by the half-power method described in Section 6.1.1. The component of the torque due to the rigid body response of the tank and support structure is about 0.0003 in-lb, which is negligible compared to the total radial torque. The peak torque amplitude from Figure 6-8 or 6-9 is about 0.09 moment-of-inertia units. The half-power amplitude is thus $0.707 \times 0.09 = 0.0064$ moment-of-inertia units. The resonant frequency occurs at $\lambda = 0.76\Omega_0$, and the half-power frequency width from Figures 6-8 or 6-9 is $\Delta\lambda = 0.03\Omega_0$. Thus, the viscous damping coefficient is computed to be $\gamma = \Delta\lambda/2\lambda = 0.03/(2 \times 0.76) = 0.02$, or 2% of critical damping. This level of damping is about the same as the

free-surface slosh damping for a tank of similar size and liquid, which is reasonable since most of the energy dissipation occurs at the tank walls for both free surface sloshing and inertial wave oscillations.

Figure 6-10 shows a summary of the damping coefficients γ determined from the radial torque responses for the high spin rate tests. The damping coefficients appeared to depend little, if at all, on the spin rate, so the average γ for $\Omega_0 = 14$ rpm and $\Omega_0 = 20$ rpm is plotted in the figure. In general, the resonant damping coefficient increased with fill level and liquid viscosity.

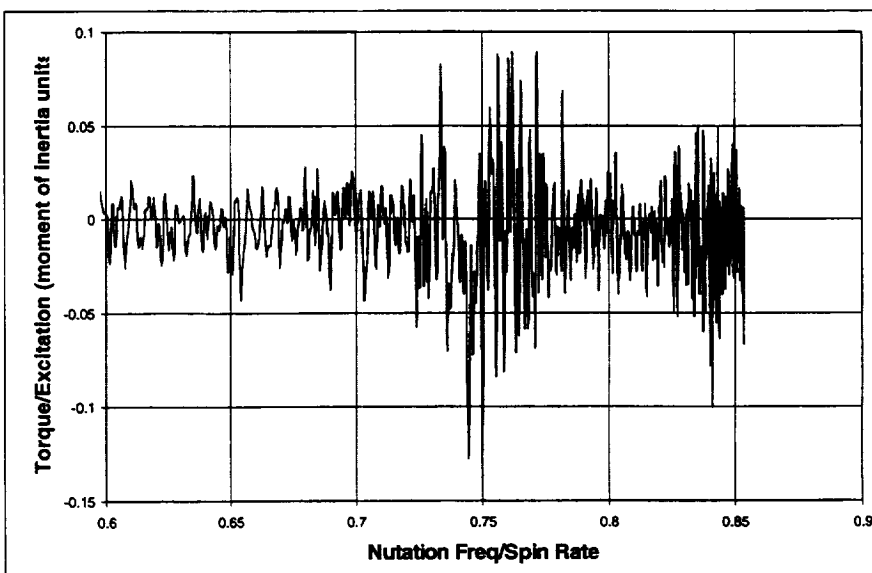


Figure 6-9. Expansion of Radial Torque for Tank 1 (2/3 full cylinder) in the Region of the Most Prominent Resonance.

The half power frequency width $\Delta\lambda \approx 0.03 \Omega_0$

Tangential torque responses. The torques measured about the tangential axis also displayed resonant liquid oscillations. For example, Figure 6-11 shows the tangential torque response for the same Test A0101, for which the radial torque was shown previously in Figure 6-7. The resonance at $\lambda/\Omega_0 \approx 0.76$ is apparent in Figure 6-11. However, the general shape of the resonance curve is significantly different from the radial torque response. This difference was caused by the radial offset of the center-of-mass of the liquid from the center of the tank (as a result of the liquid orientation against the outer wall of the tank); the radial offset introduced a non-resonant rigid-body-like tangential torque that was superimposed on the resonant tangential torque, which tended to hide the resonant peak. Because the resonant peak was partially obscured in the tangential torque responses, it was generally not possible to determine damping values from the tangential torque data.

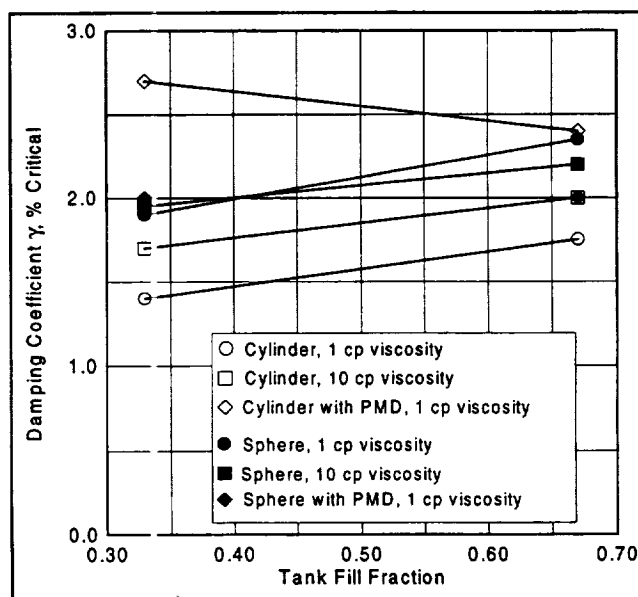


Figure 6-10. Damping of Liquid Resonances for Both Cylinders and Spheres.

Damping tends to increase with fill fraction and liquid viscosity.

There were also some tests in which the resonant frequency determined from the tangential torque responses was slightly less than the resonant frequency determined from the radial torque responses. The homogeneous vortex model is not capable of predicting these differences in resonant frequency, since only

one resonance is predicted for a given fill level [Dodge, *et al.*, 1996]. The "length" of the liquid volume for the 1/3 full tank, for which the difference in resonant frequencies is the greatest, is considerably longer in the tangential direction than it is the radial direction, whereas for the 2/3 full tank, for which the length and depth are about equal, there was little difference in the radial and tangential resonant frequencies. It is not clear, however, why the different liquid radial and tangential lengths would result in slightly different resonances for the two axes.

An explanation of these observations will need a more complete analytical model or a reliable CFD simulation.

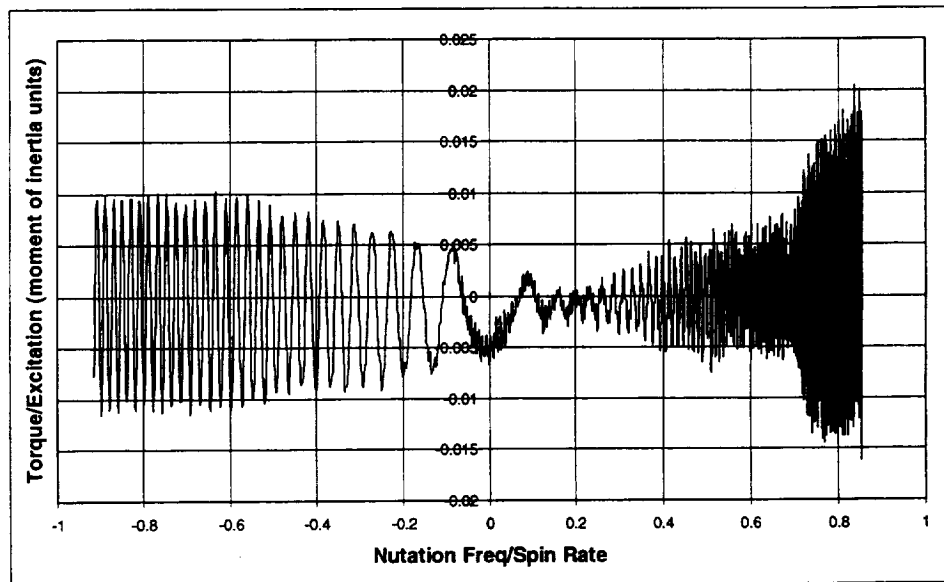


Figure 6-11. Radial Torque for Tank 1 (2/3 full cylinder) in Test A0101.

Torque amplitude depends on magnitude of the spin table motion.

D.C. offset. Many of the measured sinusoidal torque responses showed a d.c. offset. The steady spin period that preceded each sweep test was designed to eliminate such offsets in the recorded sweep responses (by compensating for the offset in the software), but apparently nutation introduced an additional uncompensated offset.

Summary of cylindrical tank results.

Table 6-1 summarizes the resonant frequency and damping results for all the $Bo \gg 1$ cylinder tank tests conducted at 14 rpm and 20 rpm. In some cases, the tangential torque resonances were not distinct enough to allow either the resonant frequency or the damping to be ascertained. These cases are indicated by "—" in Table 6-1.

The radial torque resonances for the 1/3 and 2/3 full tanks occurred for nutation frequencies in the range between $\lambda = 0.73\Omega_0$ and $0.78\Omega_0$, although the tangential torque resonances covered a wider range between $\lambda = 0.55\Omega_0$ and $0.75\Omega_0$. These results are compared to the predictions of the homogeneous vortex model in Figure 6-12. As can be seen, the analytical predictions compare better to the observed tangential torque resonances

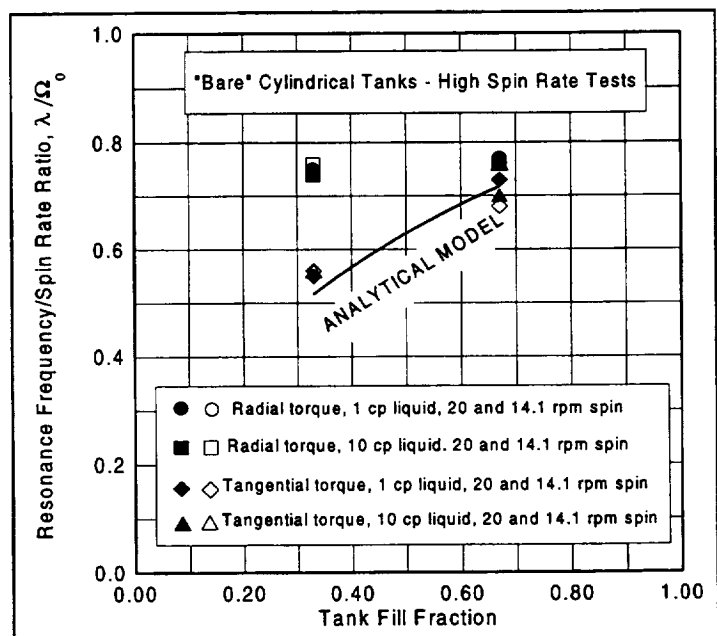


Figure 6-12. Comparison of Predicted Resonant Frequencies to Test Results for Cylindrical Tanks.

Homogeneous vortex model generally underpredicted the tests.

Table 6-1. Summary of Resonant Frequency λ_{res} and Damping λ Data for Cylindrical Tanks

			Tank 1 ($\mu = 1$ cp)				Tank 3 ($\mu= 10$ cp)			
			Radial Torque		Tangential Torque		Radial Torque		Tangential Torque	
TEST	Spin Rate rpm	λ_{res} , rpm	γ , %	λ_{res} , rpm	γ , %	λ_{res} , rpm	γ , %	λ_{res} , rpm	γ , %	COMMENTS resonances are not as prominent as for 14.1 rpm spin rate second smaller resonance at $\lambda = 7.0$ rpm (radial and tangential) resonances amplitudes are small several smaller resonances in radial axis
A0002	20.0	15.4	1.8	14.6	---	15.2	2.0	14.0	---	
A0101	14.1	10.7	1.7	10.1	---	10.7	2.0	10.7	---	
B0001	20.0	15.4	---	11.0	---	14.8	---	---	---	
B0101	14.1	10.6	1.4	8.0	---	10.7	1.7	8.0	---	
			Tank 1 ($\mu = 1$ cp)				Tank 2 ($\mu = 1$ cp)			
			λ_{res} , rpm	γ , %	λ_{res} , rpm	γ , %	λ_{res} , rpm	γ , %	λ_{res} , rpm	γ , %
C0101	14.1	10.3 and 10.9	2.7	10.7	---	10.4	2.4	10.6	---	tanks contain a PMD

resonances are not as prominent as for 14.1 rpm spin rate

second smaller resonance at $\lambda = 7.0$ rpm (radial and tangential)

resonances amplitudes are small

several smaller resonances in radial axis

than to the observed radial torque resonances. For both sets of resonances, however, the ratio λ/Ω_0 at resonance remained nearly constant when Ω_0 was changed from 14 rpm to 20 rpm; this is in agreement with the predictions. [It should be noted that even though the radial torque resonances occurred over a small range of λ/Ω_0 ratios, the wobble motor and spin motor rotation rates and the actual nutation frequencies were quite different for each resonance. Hence, these resonances were not an artifact of the physical setup that occurred at some definite wobble motor or spin motor speed.]

The video recordings confirmed the existence of liquid resonances. The video camera focused primarily along the tangential axis of a cylindrical tank, and during the time when the nutation frequency was sweeping through a resonance, the amplitude of the vortex-like oscillation in the liquid volume about the tangential axis increased dramatically and then decreased. There was also some motion evident at the free surface when the wobble motor speed was greater than the spin motor speed.

None of the test results for $Bo = 1$ (i.e., the "low gravity" tests) showed any resonances. In fact, the actual nutation frequencies used in these tests did not exceed about $\lambda = 0.6\Omega_0$, so the resonances, which are predicted to occur at $\lambda = 0.65\Omega_0$ and higher (as shown by Figure 6-1) would not have been excited in the tests. The video recordings did show, however, that the liquid interface was highly curved for $Bo = 1$, as expected.

The damping ratio γ computed from the resonant torque curves was of the order of 1% to 2%. The damping increased with liquid viscosity and fill level, as expected.

For the cylindrical tanks containing a PMD, the damping was considerably larger than for the "bare" tanks. This result agrees with previous findings for a similar PMD in a cylindrical tank with hemispherical ends [Pocha, 1987] in which resonant liquid oscillations found from drop tower tests were damped by the PMD. Furthermore, at least for the 2/3 full tank, the PMD, which bisected the tank into almost equal halves, appeared to split the radial-axis resonance into two smaller resonances with frequencies slightly larger and slightly smaller than for the "bare" tank.

Graphs of the liquid torque responses for all the tests are given in Appendix C.

Summary of spherical tank results. Liquid resonant oscillations were not expected to be prominent in the spherical tank sweep tests torques, since such oscillations are excited for a spherical tank primarily by viscous stresses at the tank walls. Nonetheless, some resonances were observed. The resonances tended to be more highly damped than for the cylindrical tank, and thus smaller in amplitude. The observed resonances again tended to be clustered near $\lambda = 0.75\Omega_0$, which in this case were generally higher than the predicted values, as shown in Figure 6-13.

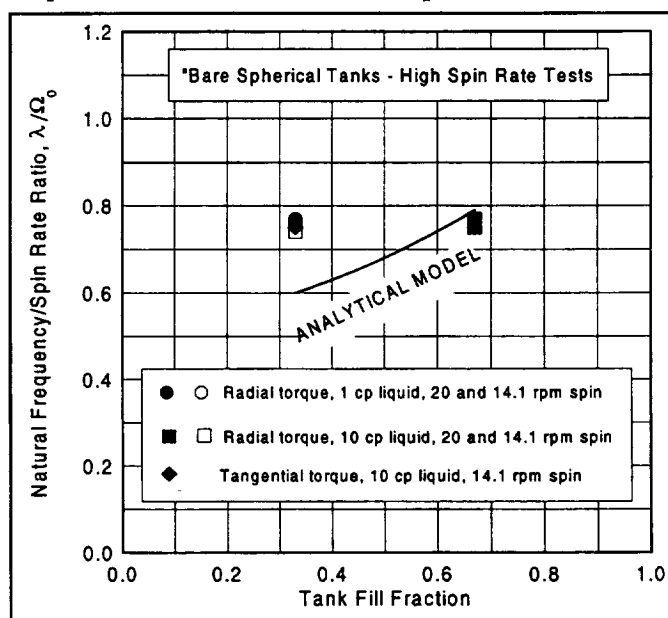


Figure 6-13. Comparison of Predicted Resonant Frequencies to Test Results for Spherical Tanks.
Homogeneous vortex model generally underpredicted the tests slightly.

Evidently, the large viscous coupling of the liquid to the tank walls (or perhaps small non-axisymmetric imperfections in the tanks) was sufficient to excite resonances.

There was little or no difference in the radial and tangential resonant frequencies, perhaps because the "length" and "depth" of the liquid volume for the 1/3 and 2/3 full spherical tanks were not greatly different.

As shown by Figure 6-10, varied PMDs of the spherical tanks of Set C tended to increase the radial-axis liquid resonance amplitudes slightly but not the tangential axis resonances. This increased resonant amplitude was accompanied by a tendency for the damping to be decreased.

Just as for the cylindrical tanks, the tests at $Bo = 1$ did not reveal any resonances, again for the same reasons discussed for the cylindrical tanks. The liquid interface was highly curved, as was expected.

Table 6-2 summarizes all the resonant frequency and damping results for the spherical tank sweep tests conducted at 14.1 and 20 rpm. Graphs for all the liquid torque responses are given in Appendix D.

6.2.3 Sine Dwell Test Data

For a sine dwell test, the filtered torque responses were all clean sine waves of constant amplitude. For that reason, typical torque plots are not shown. The rotation rates of the spin motor and the wobble motor were held constant during a sine dwell test for a period long enough for the liquid oscillations to achieve a steady state condition.

Cylindrical tanks. Table 6-3 summarizes the torque and energy dissipation results for all cylindrical tanks, for spin rates of 20 rpm and 14 rpm. Figure 6-14 shows a plot of all the valid computed energy dissipation rates. Results for the "low gravity" tests $\Omega_0 \approx 4$ rpm are not shown because the phase angle of the torque responses with respect to the tank angular velocity could not be determined reliably.

The torque amplitude results were reasonably consistent (e.g., they increased with spin rate). The computed energy dissipation rates for Tank 1 of Tank Sets A, B, and C were also reasonably consistent and in most cases positive, especially for the radial axis torques. However, the computed energy dissipation rates for Tank 3 of Tank Sets A and B were generally negative (phase angles greater than 90°), which as was discussed previously is physically unrealistic. Since the energy dissipation rates were small, the phase angle between the torque and the angular

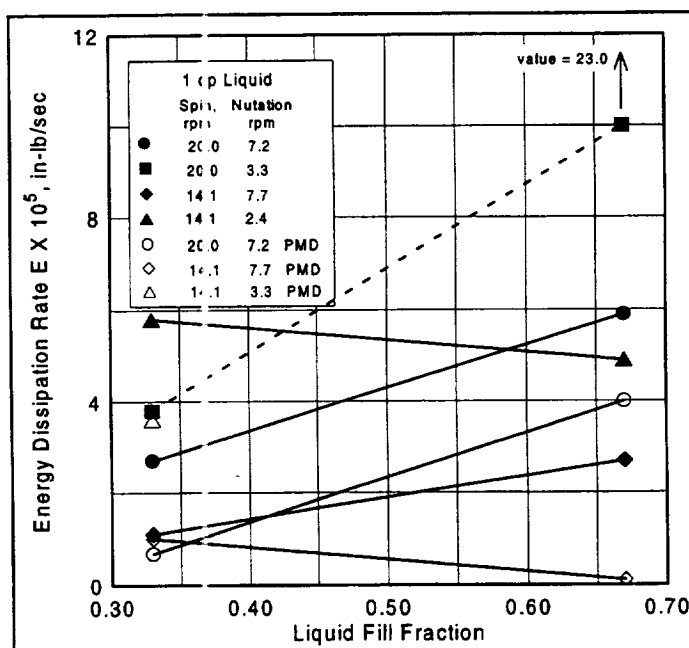


Figure 6-14. Energy Dissipation Rates for Cylindrical Tanks.

Dissipation rates increase with fill fraction and spin rate.

Table 6-2. Summary of Resonant Frequency λ_{res} and Damping γ Data for Spherical Tanks

		Tank 2 (μ = 1 cp)				Tank 4 (μ= 10 cp)				
TEST	Spin Rate rpm	Radial Torque		Tangential Torque		Radial Torque		Tangential Torque		COMMENTS
		λ _{res} , rpm	γ, %	λ _{res} , rpm	γ, %	λ _{res} , rpm	γ, %	λ _{res} , rpm	γ, %	
A0002	20.0	15.4	3.2	---	---	15.4	2.3	---	---	radial resonances only
A0101	14.1	10.6	1.5	---	---	10.7	2.0	10.6	---	second smaller resonance at λ = 7.0 rpm in radial axis
B0001	20.0	15.4	---	---	---	15.2	2.0	---	---	Tank 4 radial resonance is much more prominent
B0101	14.1	10.7	1.9	---	---	10.6	1.9	10.6	---	Smaller resonances at 7.3 rpm in radial axis
		Tank 3 (μ = 1 cp)				Tank 4 (μ = 1 cp)				
TEST	Spin Rate rpm	λ _{res} , rpm	γ, %	λ _{res} , rpm	γ, %	λ _{res} , rpm	γ, %	λ _{res} , rpm	γ, %	COMMENTS
		10.6	2.0	---	---	10.7	2.0	10.6	2.0	
C0101	14.1									tanks contain a PMD

Table 6-3. Summary of Energy Dissipation Rate Data for Cylindrical Tanks.

 ω = tank angular velocity; T = net torque; ϕ = phase angle between T and ϕ ; E = energy dissipation rate

TEST	Spin Rate, rpm	ω , rad/sec	T_{radial} , in-lb	ϕ_{radial} , degree	E_{radial} , in-lb/sec	$T_{tangential}$, in-lb	$\phi_{tangential}$, degree	$E_{tangential}$, in-lb/sec
A0301, Tank 1	20	0.114	0.00155	48.3	5.9×10^{-5}	0.00903	86.9	2.7×10^{-6}
A0301, Tank 3	20	0.114	0.00166	102.2	-2.0×10^{-5}	0.00213	52.1	7.5×10^{-5}
A0401, Tank 1	20	0.149	0.00333	24.8	2.3×10^{-4}	0.00106	106.9	-2.3×10^{-5}
A0401, Tank 3	20	0.149	0.00216	128.2	-1.0×10^{-4}	0.00628	133.1	-3.2×10^{-5}
A0501, Tank 1	14.1	0.056	0.00136	45.5	2.7×10^{-5}	0.00089	95.8	-2.5×10^{-6}
A0501, Tank 3	14.1	0.056	0.00117	98.4	-4.8×10^{-6}	0.00168	95.7	-4.7×10^{-6}
A0601, Tank 1	14.1	0.103	0.00112	32.0	4.9×10^{-5}	0.00019	139.3	-7.5×10^{-6}
A0601, Tank 3	14.1	0.103	0.00095	153.0	-4.3×10^{-5}	0.00083	95.1	-3.8×10^{-6}
B0301, Tank 1	20	0.114	0.00133	69.5	2.7×10^{-5}	0.00212	98.1	-1.7×10^{-5}
B0301, Tank 3	20	0.114	0.00256	159.9	-1.4×10^{-4}	0.00254	100.5	-2.6×10^{-5}
B0401, Tank 1	20	0.149	0.00302	80.9	3.8×10^{-5}	0.00085	95.1	-5.6×10^{-5}
B0401, Tank 3	20	0.149	0.00197	139.8	-1.1×10^{-4}	0.00101	115.2	-3.2×10^{-5}
B0501, Tank 1	14.1	0.056	0.00073	58.0	1.1×10^{-5}	0.00271	95.5	-7.3×10^{-6}
B0501, Tank 3	14.1	0.056	0.00053	109.3	-4.9×10^{-6}	0.00260	103.5	-1.7×10^{-5}
B0601, Tank 1	14.1	0.103	0.00113	6.27	5.8×10^{-5}	0.00090	106.4	-1.3×10^{-5}
B0601, Tank 3	14.1	0.103	0.00046	111.4	-8.6×10^{-6}	0.00106	106.4	-1.6×10^{-5}
C0301, Tank 1	20	0.114	0.00027	63.5	6.8×10^{-6}	0.00228	56.2	7.3×10^{-5}
C0301, Tank 2	20	0.114	0.00101	45.6	4.0×10^{-5}	0.00275	16.2	1.5×10^{-4}
C0401, Tank 1	20	0.149	0.00002	118.3	-7.4×10^{-7}	0.00094	102.8	-1.5×10^{-5}
C0401, Tank 2	20	0.149	0.00075	107.5	-1.7×10^{-5}	0.00009	174.5	-6.4×10^{-6}
C0501, Tank 1	14.1	0.056	0.00048	38.7	1.0×10^{-5}	0.00298	90.5	-7.9×10^{-7}
C0501, Tank 2	14.1	0.056	0.00048	85.5	1.1×10^{-6}	0.00197	85.7	4.2×10^{-6}
C0601, Tank 1	14.1	0.103	0.00071	9.01	3.6×10^{-5}	0.00089	74.7	1.2×10^{-5}
C0601, Tank 2	14.1	0.103	0.00042	165.6	-2.1×10^{-6}	0.00031	79.5	2.9×10^{-6}

velocity of the tank tended to cluster around 90° , so slight errors in determining the phase angle were probably responsible for the computed negative energy dissipation rates in many cases. However, in other cases, the phase angle was considerably larger than 90° . The load cell calibrations and the sign of the torque response of the load cells for Tank 3 were checked after the flight and found to be correct, so the reasons why the computed phase angle for this tank tended to be greater than 90° are not apparent. The computed negative energy dissipation rates also tended to occur more often for torque responses about the tangential axis than for the radial axis.

As shown in Figure 6-14, the energy dissipation rates tended to increase with fill fraction and spin rate. They also tended to increase with a decrease in nutation frequency, although this tendency is confounded somewhat by the fact that the unsteady angular acceleration increased when the nutation frequency decreased in the range $0 \leq \lambda \leq \Omega_0$, which, therefore, increased the excitation amplitude imposed on the liquid.

Positive and negative energy dissipation rates also occurred for tanks containing PMDs, but the PMDs tended to reduce the energy dissipation rate compared to the bare cylindrical tanks. This same trend was observed for the damping coefficient γ computed from the sine sweep test results.

Spherical tanks. Table 6-4 summarizes the results for the spherical tanks, for $\Omega_0 = 20$ and 14 rpm; again, the low gravity 4 rpm test results are not shown.

For the spherical tanks, the energy dissipation rates computed for the radial torques were nearly all positive. However, just as for the cylindrical tanks, some of the computed energy dissipation rates for the tangential axis torques were negative.

Figure 6-15 shows the computed (positive) energy dissipation rates for the spherical tanks, for all the high spin rate tests. The dissipation rates for bare tanks tended to increase with fill level and spin rate. For the tanks with PMDs, however, the dissipation tended to decrease with an increase in fill level. This result is probably the result of the design of the vaned PMD; the PMD blocked much of the vortex motion for small fill levels, whereas it was more open with less blockage for higher fill levels. The absolute level of the dissipation rate for the PMD tanks was sometimes larger and sometimes smaller than for the comparable bare tank.

6.2.4 Comparison of Energy Dissipation Rates to Ground and Spacecraft Flight Results

Many ground-test studies of energy dissipation in rotating, nutating tanks have been

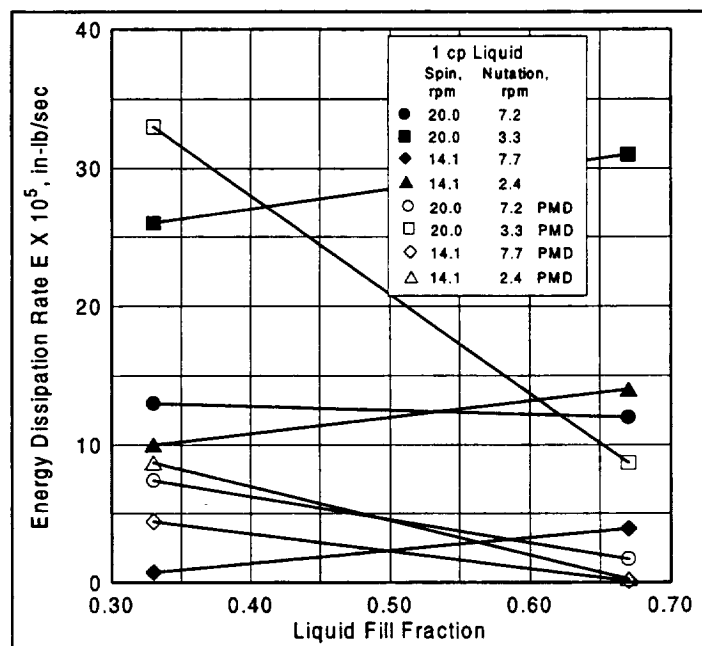


Figure 6-15. Energy Dissipation Rates for Spherical Tanks.

Dissipation rates tended to increase with fill fraction and spin rate.

Table 6-4. Summary of Energy Dissipation Rate Data for Spherical Tanks.

 ω = tank angular velocity; T = net torque; ϕ = phase angle between T and ϕ ; E = energy dissipation rate

TEST	Spin Rate, rpm	ω , rad/sec	T_{radial} , in-lb	ϕ_{radial} , degree	E_{radial} , in-lb/sec	$T_{\text{tangential}}$, in-lb	$\phi_{\text{tangential}}$, degree	$E_{\text{tangential}}$, in-lb/sec
A0301, Tank 2	20	0.114	0.00426	60.8	1.2×10^{-4}	0.00209	138.7	-9.0×10^{-5}
A0301, Tank 4	20	0.114	0.00047	95.5	-2.6×10^{-6}	0.00117	135.3	-4.7×10^{-5}
A0401, Tank 2	20	0.149	0.00414	6.00	3.1×10^{-4}	0.00237	89.8	5.9×10^{-7}
A0401, Tank 4	20	0.149	0.00080	174.7	-5.9×10^{-5}	0.00121	85.8	6.6×10^{-6}
A0501, Tank 2	14.1	0.056	0.00151	20.9	3.9×10^{-5}	0.00101	89.6	2.1×10^{-7}
A0501, Tank 4	14.1	0.056	0.00041	9.40	1.1×10^{-5}	0.00081	77.2	5.1×10^{-8}
A0601, Tank 2	14.1	0.103	0.00287	15.7	1.4×10^{-4}	0.00132	96.9	-8.2×10^{-6}
A0601, Tank 4	14.1	0.103	0.00090	22.0	4.3×10^{-5}	0.00090	93.2	-2.6×10^{-6}
B0301, Tank 2	20	0.114	0.00246	25.5	1.3×10^{-4}	0.00202	97.5	-1.5×10^{-5}
B0301, Tank 4	20	0.114	0.00061	63.9	1.5×10^{-5}	0.00151	82.6	1.1×10^{-5}
B0401, Tank 2	20	0.149	0.00356	12.2	2.6×10^{-4}	0.00217	90.8	-2.8×10^{-6}
B0401, Tank 4	20	0.149	0.00086	50.6	4.1×10^{-5}	0.00149	79.3	2.1×10^{-5}
B0501, Tank 2	14.1	0.056	0.00033	37.5	7.4×10^{-6}	0.00149	75.9	1.0×10^{-5}
B0501, Tank 4	14.1	0.056	0.00310	39.1	6.8×10^{-5}	0.00105	91.9	-9.9×10^{-7}
B0601, Tank 2	14.1	0.103	0.00198	5.08	1.0×10^{-4}	0.00132	88.2	2.1×10^{-6}
B0601, Tank 4	14.1	0.103	0.00060	15.5	3.0×10^{-5}	0.00105	86.9	2.9×10^{-6}
C0301, Tank 3	20	0.114	0.00458	73.5	7.4×10^{-5}	0.00103	131.9	-3.9×10^{-5}
C0301, Tank 4	20	0.114	0.00118	75.2	1.7×10^{-5}	0.00089	119.7	-2.5×10^{-5}
C0401, Tank 3	20	0.149	0.00560	37.6	3.3×10^{-4}	0.00236	101.7	-3.6×10^{-5}
C0401, Tank 4	20	0.149	0.00144	35.7	8.7×10^{-5}	0.00084	81.1	9.6×10^{-6}
C0501, Tank 3	14.1	0.056	0.00201	38.9	4.4×10^{-5}	0.00169	97.3	-6.0×10^{-6}
C0501, Tank 4	14.1	0.056	0.00042	84.2	1.2×10^{-6}	0.00064	85.5	1.4×10^{-6}
C0601, Tank 3	14.1	0.103	0.00187	25.3	8.7×10^{-5}	0.00145	91.1	-1.5×10^{-6}
C0601, Tank 4	14.1	0.103	0.00022	77.1	2.5×10^{-6}	0.00050	98.6	-3.9×10^{-6}

conducted previously at very high spin rates to minimize the effects of gravity on the liquid orientation. Most of these studies resulted in energy dissipation correlations of the form:

$$E = Km_{liquid}\Omega_0^3d^2\left(\frac{\Omega_0}{\lambda}\right)\theta^2\sqrt{\frac{\mu}{\rho\Omega_0d^2}} \quad (6-5)$$

where K is proportionality constant of order unity that depends on the spacecraft-tank geometry, μ is the liquid viscosity, ρ is the liquid density, d is the tank diameter, and θ is the cone angle [Vanyo, 1973]. The dependency of E on θ^2 follows from Eq. (1-2). For comparison to this ground-test correlation, a typical LME case is: 2/3 full spherical tank $m_{liquid} = 1.15$ lbs (521 grams); $d = 4.492$ in (11.4 cm); $\Omega_0 = 20$ rpm (2.09 rad/sec); $\lambda = 3.3$ rpm (0.345 rad/sec); $\mu = 5.6 \times 10^{-5}$ lb/sec-in (1 cp); $\rho = 0.037$ lb/in³ (1 gram/cm³); and $\theta = 4.8^\circ$. Assuming that $K \approx 1$, Eq. (6-5) predicts that the LME energy dissipation rate is $E = 0.00014$ in-lb/sec. The LME parameters correspond to Test A0401, Tank 2, for which the measured energy dissipation rate, as shown in Table 6-4, is about 0.00031 in-lb/sec. The predicted and measured values of E are reasonably close considering that the value of K in Eq. (6-5) is not known for the LME geometry and that the correlation is based on data that contains a large amount of scatter. The comparisons for other fill levels, spin rates, and nutation frequencies are equally close.

Both Eq. (6-5) and the LME data plotted in Figures 6-14 and 6-15 agree in the trend that the energy dissipation rate increased with an increase in spin rate or fill level and decreased with an increase in nutation frequency.

Non-proprietary data from flight tests of actual spinning spacecraft are difficult to find. However, comparisons of Eq. (6-5) to a considerable number of flight tests for "anonymous" spacecraft have been made previously [Dodge, 1982]. It was found that the ratio of the dissipation rate measured in flight to that predicted from Eq. (6-5) varied from about 0.3 to about 6. The ratios of the various LME test data to Eq. (6-5) vary in the range of 0.3 to 0.5. Consequently, it can be concluded that the LME test results compare with and predict the available flight test data reasonably well.

Other ground test data acquired from drop tests of small model tanks are available for specific spacecraft. Generally, only the rate of growth of the cone angle is given, so direct comparisons with LME test results are not easily made. However, the cylindrical tank PMD used in LME was based on one such drop test, and, as mentioned previously, the LME results for damping and liquid resonances were comparable to the drop tower results.

This page left intentionally blank.

7. CONCLUSIONS AND RECOMMENDATIONS

The Liquid Motion Experiment, which flew on STS 84 in May 1997, was an investigation of the characteristics of liquid motions in spinning, nutating tanks. The LME test results should aid in determining the effects of such motions on the stability of spinning spacecraft.

The flight program included:

- ☐ sine sweep tests to determine the frequency of inertial wave liquid resonances and the damping of such resonances; and
- ☐ sine dwell tests meant to determine the rate at which energy is dissipated by the liquid oscillations.

The test tanks were cylinders and spheres. Two different high spin rates were used to simulate high gravity conditions and to permit the scaling of resonances with spin rate. A low spin rate was also used to simulate low gravity conditions. Two different sets of "bare" tanks were tested, with each set containing two cylindrical tanks and two spherical tanks. The fill level of the tanks in each set was held constant ($2/3$ or $1/3$ full) and the liquid viscosity was varied. A third set of two cylindrical and two spherical tanks that contained generic propellant management devices was also tested. The primary quantitative data obtained from the flight tests were the radial-axis and tangential-axis torques exerted on the tanks by the liquid oscillations. Qualitative video recordings of the oscillations in one cylindrical tank were also acquired.

Although the torque data acquired from the tests was contaminated by low and high frequency noise, post-flight digital filtering allowed the true data signals to be recovered for the high spin rate tests. The filtering was not entirely successful for the lowest spin rate tests, so consequently the differences in liquid oscillations between high and low gravity conditions could not be determined from the test results.

To assess the success of LME, the minimum success criteria as presented in the introduction is compared to the results.

Minimum success criteria:

- ☐ Reducible torque time histories are required for both tanks of a given shape with a single fluid for the two highest spin rates.

As shown by Table 7-1, good reducible torque time histories were acquired for:

- ☐ Cylinders with low viscosity liquid for both fill levels, and high and medium spin rates.
- ☐ Spheres with low viscosity liquid for both fill levels, and high and medium spin rates.
- ☐ Spheres with high viscosity liquid for both fill levels, and high and medium spin rates.

Table 7-1. Data Quality Test Matrix
40 Data Sets out of 72 Provided Good Data, 56% Success Rate

Label	Shape	Viscosity	Fill Level	PMD	Sine Sweep Tests			Sine Dwell Tests		
					High	Medium	Low	High	Medium	Low
CL2A1A	Cylinder	Low (1 cp)	2/3 (780 ml)	No	Good	Good	Bad	Good	Good	Bad
SL2A2A	Sphere	Low (1 cp)	2/3 (520 ml)	No	Good	Good	Bad	Good	Good	Bad
CH2A3A	Cylinder	High (10 cp)	2/3 (780 ml)	No	Good	Good	Bad	Bad	Bad	Bad
SH2A4A	Sphere	High (10 cp)	2/3 (260 ml)	No	Good	Good	Bad	Good	Good	Bad
CL1A1B	Cylinder	Low (1 cp)	1/3 (390 ml)	No	Good	Good	Bad	Good	Good	Bad
SL1A2B	Sphere	Low (1 cp)	1/3 (520 ml)	No	Good	Good	Bad	Good	Good	Bad
CH1A3B	Cylinder	High (10 cp)	1/3 (390 ml)	No	Good	Good	Bad	Bad	Bad	Bad
SH1A4B	Sphere	High (10 cp)	1/3 (260 ml)	No	Good	Good	Bad	Good	Good	Bad
CL1B1C	Cylinder	Low (1 cp)	1/3 (390 ml)	Yes	No*	Good	Bad	Good	Good	No**
CL2B2C	Cylinder	Low (1 cp)	2/3 (780 ml)	Yes	No*	Good	Bad	Good	Good	No**
SL1B3C	Sphere	Low (1 cp)	1/3 (260 ml)	Yes	No*	Good	Bad	Good	Good	No**
SL2B4C	Sphere	Low (1 cp)	2/3 (520 ml)	Yes	No*	Good	Bad	Good	Good	No**
Tests with Good Data/Total Tests					8/12	12/12	0/12	10/12	10/12	0/12

* Test Run, But Data Not Recorded

** Test Not Run

The data acquired from the **sine sweep tests** showed that the liquids in the cylindrical tanks exhibit prominent resonances. The data allowed the following observations:

- ☐ the resonances for the radial axis occurred in a nutation frequency range between $0.74\Omega_0$ and $0.78\Omega_0$, where Ω_0 is the steady spin rate, and for the tangential axis in a nutation frequency range between $0.56\Omega_0$ and $0.78\Omega_0$;
- ☐ the observed tangential axis resonant frequencies agreed well with analytical predictions, but the predictions were 25% too low compared to the radial axis resonances for the 1/3 full tank; and
- ☐ the damping coefficients determined from the torque response curves by the half-power method were about 1% to 2% of critical, increased with liquid viscosity and fill level, and were nearly independent of spin rate.

The liquids in the spherical tanks also exhibited resonances, although the amplitudes of the resonant torques were not as large as for the cylindrical tanks. These resonances were not anticipated since the liquid in a spherical tank is excited primarily by small viscous stresses exerted on the tank walls or by non-axisymmetric imperfections of the tank shape. The following observations were made from the test data:

- ☐ the resonances tended to cluster in a nutation frequency range between $0.74\Omega_0$ and $0.78\Omega_0$;
- ☐ the resonant frequencies for the 2/3 full tank were closely predicted by the analytical models, but the predictions were 20% too low for the 1/3 full tank; and
- ☐ the damping was somewhat larger than the damping computed for the cylindrical tanks.

Propellant management devices tended to damp the cylindrical tank resonances and increase the amplitude of the resonances for the spherical tanks.

The **sine dwell tests** allowed the energy dissipation rate of the liquids to be computed from the steady state torques measured in the sine dwell tests, in conjunction with the phase angle between the torque sinusoidal response and the angular velocity of the spin table. The following observations can be made from these data and computations:

- ❑ torque amplitudes were reasonably consistent and increased with spin rate and fill level;
- ❑ the energy dissipation rates were small since the liquid oscillations were non-resonant;
- ❑ the phase angles were near 90° , so small errors in determining the angles sometimes led to the computation of negative energy dissipation rates, and there appeared to be a consistent error in the phase angle for one cylindrical tank of both bare tank sets (in location three on the spin table); and
- ❑ energy dissipation rates for the cylindrical tanks containing PMDs were reduced compared to the bare tanks, and the energy dissipation rates for the spherical tanks containing PMDs sometimes, but not always, increased, depending on fill level and other parameters; these trends generally agreed with the trends found from the damping coefficients computed from the sine sweep tests.

The computed energy dissipation rates agreed well with previous ground test data for similar geometries and spin rates. Although comparisons with flight data from actual spacecraft were limited, the LME results appeared to agree with and predict the flight data reasonably closely.

On the basis of these tests, the following recommendations are offered.

- ❑ Improved analytical models and CFD simulations using a viscous liquid are needed to predict more exactly the resonant frequencies, torques, damping, and energy dissipation rates in tanks similar to the ones used in the LME tests for liquid oscillations in both the radial and tangential axes.
- ❑ Further flight tests are needed to help resolve the questions raised by the first flight tests.
 - The tests should employ an improved flow visualization technique, and the vibration isolation technique for the torque load cells should be improved to eliminate the noise in the data to a very low level; the improvements should especially allow data from low spin rate (low gravity) tests to be more completely analyzed.
 - Additional tank geometries and tank locations should be investigated. For example, some spacecraft designs position their tanks on the spin axis rather than offsetting them as in the first LME flight.
 - From the first flight results, it is clear that the effects of PMDs on the liquid responses depend on tank shape and PMD design in a complicated way, sometimes enhancing the oscillations and sometimes damping them. Future flights of LME are needed to investigate specific PMD designs proposed for current spacecraft to eliminate unexpected interactions between the PMD and the liquid motions.

This page left intentionally blank.

8. REFERENCES

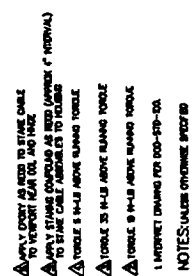
- Abramson, H. N., 1966, **The Dynamic Behavior of Liquids in Moving Containers**, NASA SP-106.
- Agrawal, B. N., 1984, *An Overview of INTELSAT Activities on Liquid Slosh, Dynamic Behavior of Liquids on Spacecraft Attitude Control*, Proc. 1st INTELSAT/ESA Symposium, Washington, D.C.
- Agrawal, B. N., 1990, *Attitude Stability of Asymmetric Dual-Spin Spacecraft with Large Liquid Fraction*, **AIAA Paper 90-3491-CP**.
- Agrawal, B. N., 1993, *Dynamic Characteristics of Liquid Motion in Partially Filled Tanks of a Spinning Spacecraft*, **AIAA J. Guidance and Control**, **16**, pp. 636-640.
- Baker, W. E., Westine, P. S., and Dodge, F. T., 1991, *Similarity Methods in Engineering Dynamics - Theory and Practice of Scale Modeling*, **Fundamental Studies in Engineering**, Vol. 2, Elsevier, Amsterdam.
- Chen, K. and Pletcher, R., 1991, *Simulation of Three-Dimensional Liquid Sloshing Flows Using a Strongly Implicit Calculation Procedure*, **AIAA Paper 91-1661**.
- Chobotov, M. V. and Purohit, G. P., 1993, *Low-Gravity Propellant Gauging System for Accurate Predictions of Spacecraft End-Of-Life*, **AIAA J. Spacecraft and Rockets**, **30**, pp. 92-101.
- Dodge, F. T. and Garza, 1967, *Experimental and Theoretical Studies of Liquid Sloshing at Simulated Low Gravity*, **ASME J. Applied Mechanics**, **34**, pp. 555-561.
- Dodge, F. T., 1982, *Energy Dissipation in GSTAR/Spacenet Liquid Propellant Tanks*, Final Report, SwRI Project 04-6771-111.
- Dodge, F. T., 1989, *Outreach Definition Study: Liquid Motion in a Rotating Tank. 1. Technical Requirements Document*, Final Report, Contract NAS3-25358, Southwest Research Institute.
- Dodge, F. T., and Deffenbaugh, D., 1993, *Experiment Requirements Document for the Liquid Motion in Rotating Tanks Experiment*, Document 4792-ERD-01, Revision 2, Mod 1, SwRI Project 04-4792.
- Dodge, F. T., Unruh, J. F., Green, S. T., and Cruse, M. W., 1994, *A Mechanical Model of Liquid Inertial Waves for Use with Spinning Spacecraft*, **Fluid Transients 1994**, ASME, New York.
- Dodge, F. T., Cutshall, W. K., Green, S. T., and Unruh, J. F., 1996, *Modeling Low-G Motions in Spacecraft Tanks*, Final Report, Southwest Research Institute IR&D Project 04-9769.
- Dodge, F. T., Green, S. T., and Unruh, J. F., 1998, *Modeling Liquid Motions in Spinning Spacecraft Tanks*, Final Report (in preparation), Southwest Research Institute IR&D Project 04-9946.
- Dunbar, B. J., Thomas, D. A., and Schoess, J. N., 1991, *The Microgravity Environment of the Space Shuttle Columbia During STS-32*, NASA Tech Paper 340.
- Ebert, K., 1984a, *Analysis of Propellant Sloshing Effect, Dynamic Effects of Liquids on Spacecraft Attitude Control*, Proc. First INTELSAT/ESA Symposium, Washington, D.C., pp. 228-246.
- Ebert, K., 1984b, *Liquid Sloshing on Slowly Spinning Spacecraft, Dynamic Effects on Liquids on Spacecraft Attitude Control*, Proc. First INTELSAT/ESA Symposium, Washington, D.C., pp. 247-270.
- El-Rahab, M., and Wagner, P., 1974, *Vibration of a Liquid with a Free Surface in a Spinning Spherical Tank*, **J. Sound and Vibration**, **76**, pp. 83-93.
- Everstine, G. C., 1981, *Structural Analogies for Scalar Field Problems*, **Int. J. Numerical Methods in Engineering**, **17**, pp. 471-476.

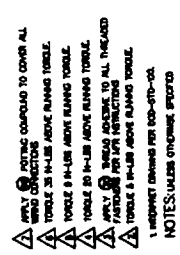
- Greenspan, H. P., 1969, **The Theory of Rotating Fluids**, Cambridge University Press.
- Guibert, J., 1984, *An Approximate Solution for Propellant Slosh in a Spinning Tank*, **Dynamic Effects of Liquids on Spacecraft Attitude Control**, Proc. First INTELSAT/ESA Symposium, Washington, D.C., pp. 179-198.
- Guibert, J., 1986, *Forced Motion on Spinning Test for Slosh-Moment Investigations*, ONERA Report T.P. No. 1986-82.
- Harrison, J., 1984, *A Review of the Scale Model Method for Predicting Spacecraft Nutation Divergence*, **Dynamic Effects of Liquids on Spacecraft Attitude Control**, Proc. First INTELSAT/ESA Symposium, Washington, D.C., pp. 295-305.
- Hubert, C. and Goodzeit, N., 1984, *The Effects of Propellant Motion on a Spinning Spacecraft with Vented Tanks*, **Dynamic Effects of Liquids on Spacecraft Attitude Control**, First INTELSAT/ESA Symposium, Washington, D.C., pp. 329-336.
- McIntyre, J., Sicilian, J., and Giezen, J., 1990, *A Benchmark for Inviscid Incompressible Flow in Spinning Containers*, **Proc. Forum on Benchmark Test Cases for Computational Fluid Dynamics**, preprint, ASME Spring FED Conference, Toronto, Canada.
- NSTS-21000-IDD-MDK, Rev. A, April 1992.
- Pederson, L., 1984, *The Homogeneous Vortex Approximation to the Dynamics of Spinning Spacecraft with Partially Filled Liquid Containers*, Term Paper, Fluid Mechanics, II, M.I.T., Dept. of Aeronautical and Astronautical Engineering.
- Pfeiffer, F., 1974, *Ein Näherungsverfahren für Flüssigkeitgefüllte Kreisel*, **Ingenieur-Arkiv**, 43, pp. 306-316.
- Pfeiffer, F., 1984, *On Contained Rotating Fluids in Satellite Dynamics*, **Dynamic Effects of Liquids on Spacecraft Attitude Control**, Proc. First INTELSAT/ESA Symposium, Washington, D.C., pp. 149-178.
- Pocha, J. J., 1987, *An Experimental Investigation of Spacecraft Sloshing*, **Space Communication and Broadcasting**, 5, pp. 323-332.
- Selmi, M., Li, R., and Herbert, T., 1992, *Eigenfunction Expansion of the Flow in a Spinning and Nutating Cylinder*, **Phys. Fluids A**, 4, pp. 1998-2007.
- SpaceHab Experiment Interface Definition Document**, MDC91W5023F, September 1996.
- Thomson, W. T., 1961, **Introduction to Space Dynamics**, John Wiley & Sons, New York
- Van Schoor, M. C. and Crawley, E. F., 1992, *The Nonlinear Forced Response Characteristics of Contained Fluids in Microgravity*, ASME Symposium Volume AMD-154/FED-142, pp. 145-160.
- Vanyo, J. P., 1973, *An Energy Assessment for Liquids in a Filled Precessing Cavity*, **ASME J. Applied Mechanics**, 40, pp. 851-856.
- Weihs, D., and Dodge, F. T., 1991, *Liquid Motions in Nonaxisymmetric, Partially Filled Tanks Rotating at Zero Gravity*, **AIAA J. Spacecraft and Rockets**, 28, pp. 425-432.
- Wilson, J., Maas, D., and Magers, R., 1972, *Three Axis Air Bearing Test Results of a Dual-Spin Spacecraft*, **AIAA Paper 72-860**.
- Zedd, M. F. and Dodge, F. T., 1985, *Energy Dissipation of Liquids in Nutating Spherical Tanks Measured by a Forced Motion-Spin Table*, Naval Research Laboratory Report NRL 8932, Washington, DC.

APPENDIX A

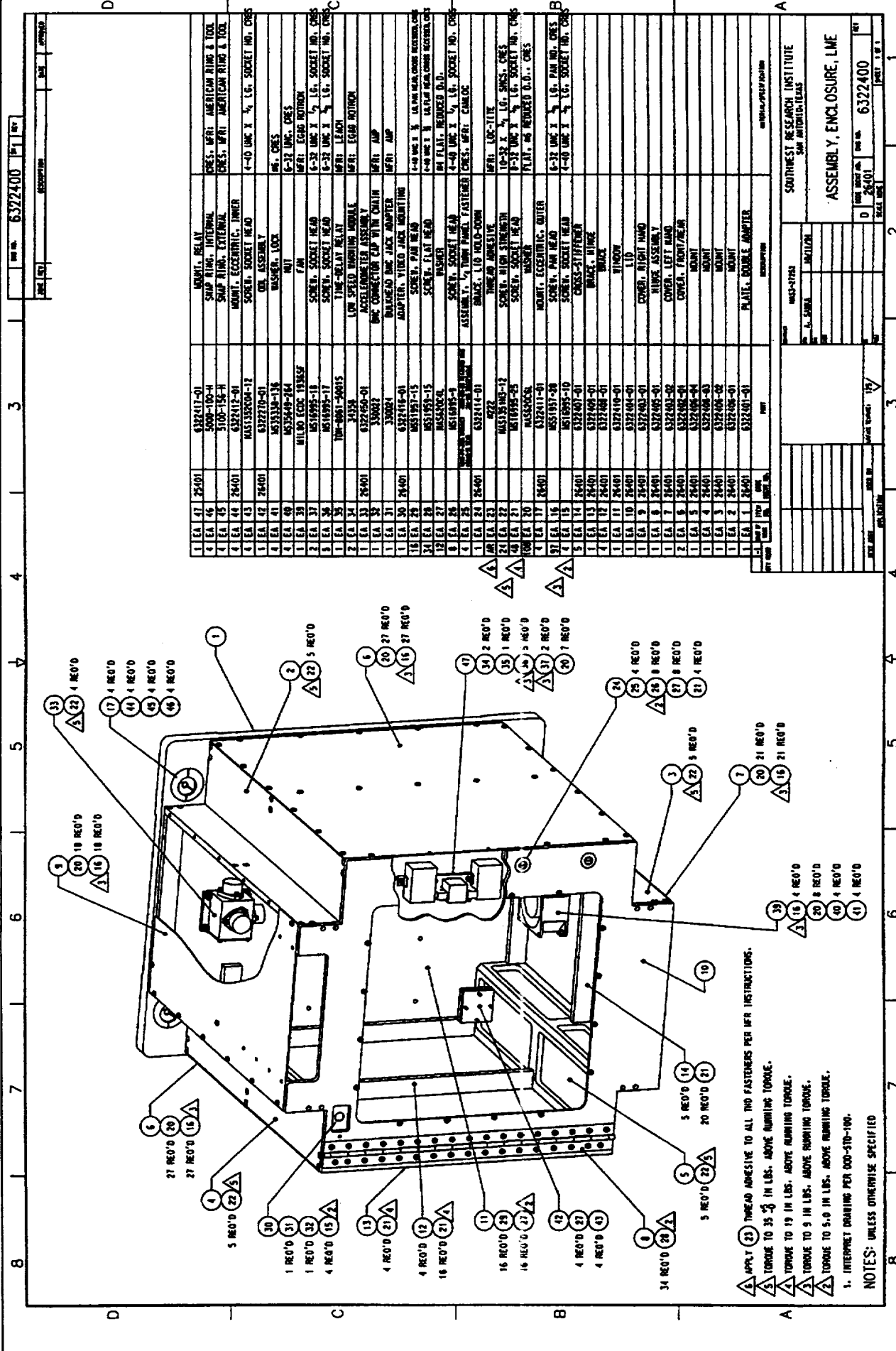
Mechanical Assembly Drawings

This page left intentionally blank.





LME Final Report



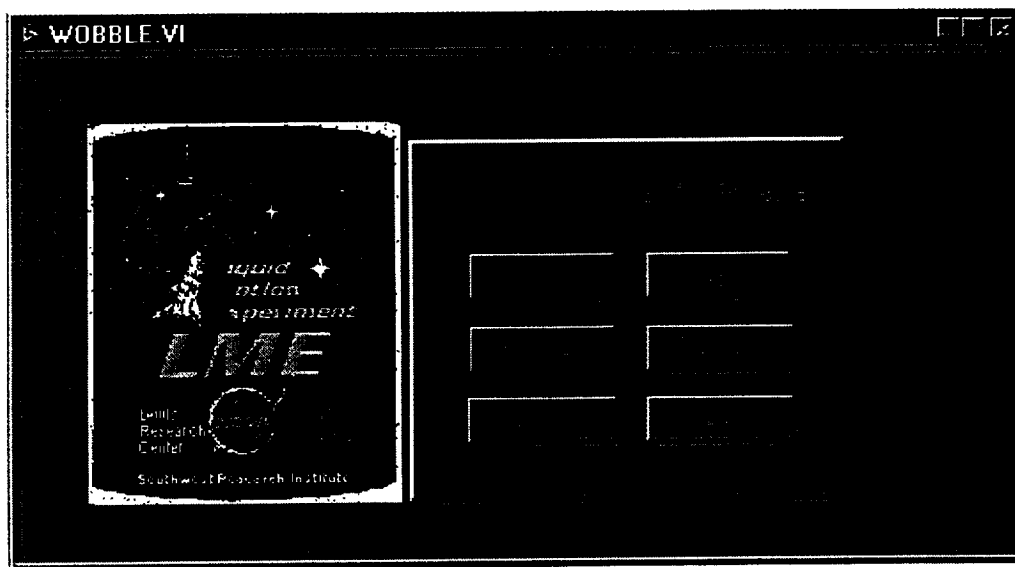
APPENDIX B

Software User's Guide

This page left intentionally blank.

SOFTWARE USER'S GUIDE**"Wobble" Screen**

When the PGSC is activated, one of the software icons will be "Wobble." The user should click on this icon. The initial LME interface screen will appear.

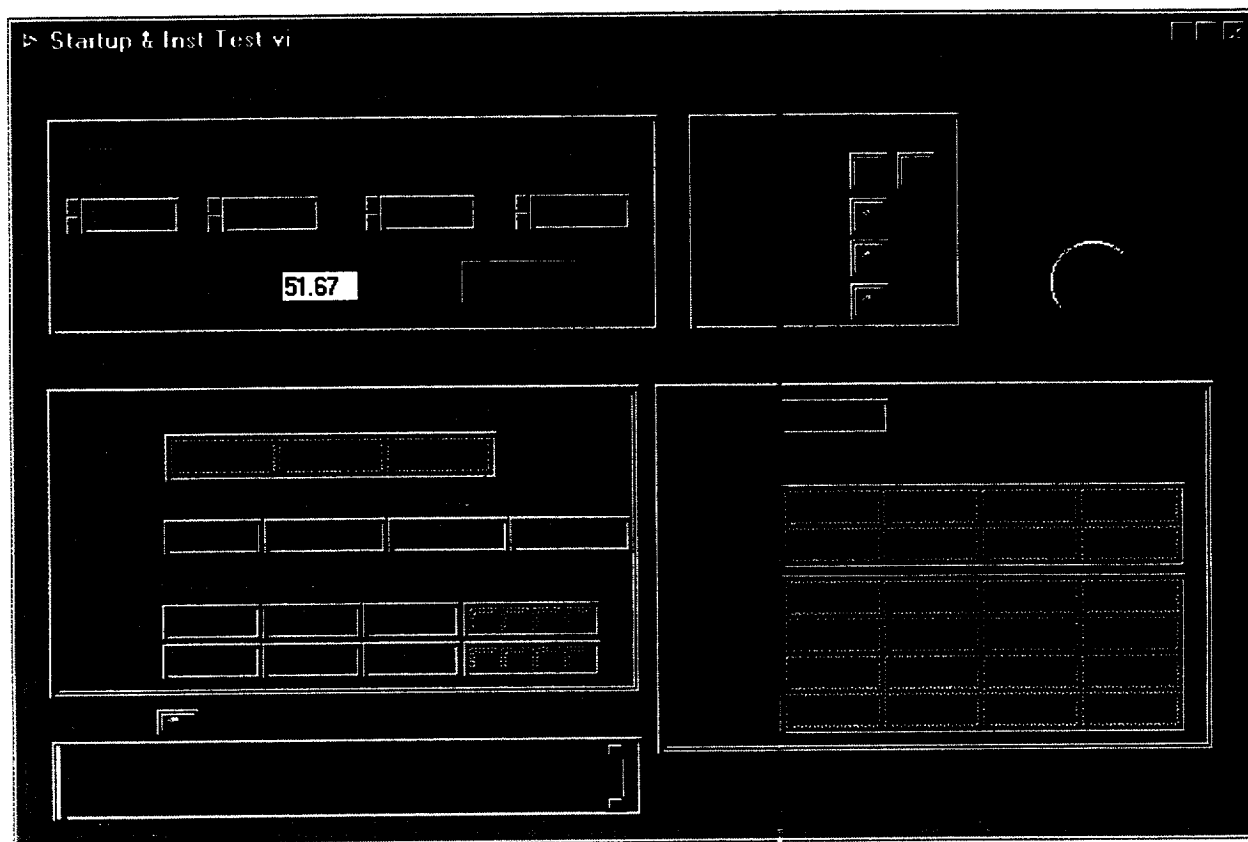


A checksum calculation will be done in the background and a "CRC Calculated for File" screen will appear. The CRC of the proper software version will be listed in the Flight Data File. If these agree, the user should click "OK." If these do not agree, the user should get instructions from the PI on the ground before proceeding.

Normal operation is to accept the default test set-up configuration parameters. If the set-up parameters need to be altered, instructions for alternate values will be supplied by the PI. In the event these need to be changed, the process would be to click on the "Configure" button and a screen will appear that allows the user to input different configuration parameters. To run a test, click on the "Run Test" button.

"Startup & Instrumentation Test" Screen

To start a test sequence, the user should click on the "Run Test" button on the previous "Wobble" screen. The "Startup & Instrumentation Test" screen will appear.



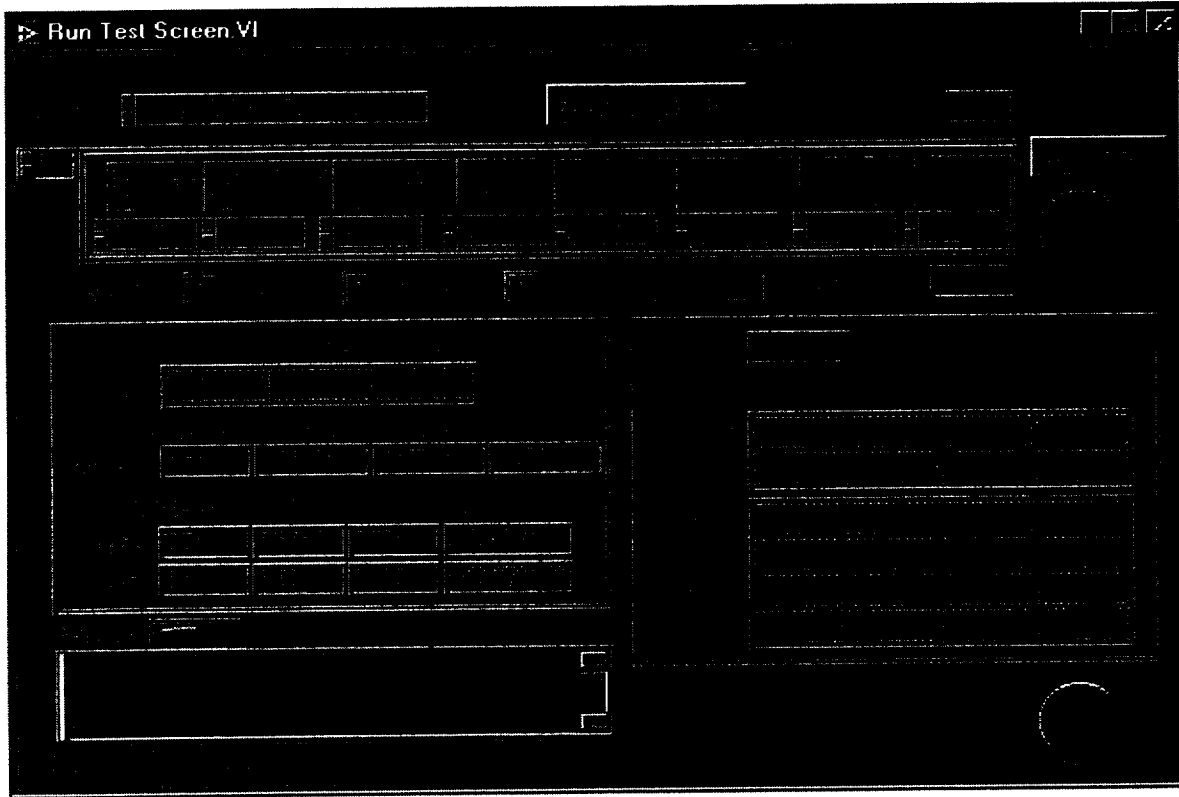
This screen describes the system functional test that is being conducted prior to the actual test sequence. In this panel, the command and data communications are verified and the LME spin and wobble motors are activated at nominal speeds.

The initialization process is two minutes. During the first minute of this period, the spin motor will activate and the table should spin at the specified spin speed of 20 rpm. During the second minute, the wobble motor will also activate and the table should continue to spin at 20 rpm and wobble at 10 rpm. The lights in the upper right hand box will indicate activation of the spin and wobble motor. Visually confirm that both functions occurred. If the table spins and wobbles are indicated and no fault screen appears, then the system passed the initialization test. After this initialization period, a "Pass/Fail" question box will automatically appear.

The user will accept the initialization by clicking on "Pass" and the "Run Test Screen" will appear.

"Run Test" Screen

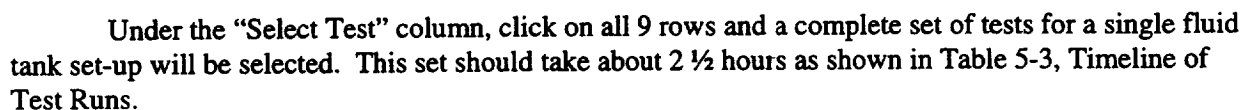
The LME tests are conducted in the "Run Test Screen."



Observe the test conditions in the top row of numbers under "Spin Rate." These are the default values for each pre-programmed test. If the default values need to be changed per instructions from the PI on the ground, just click on the field and type in the new value. Under normal operations, click on "Select Multiple Tests" button. A list appears as shown on the following page. Select all of the pre-programmed tests as a series and click on "Return." This will return you to this "Run Test Screen." Once acceptable conditions are shown, the user should click on the "Start Test" button in the upper right hand corner. The test will then begin and run automatically. If a problem occurs, the user should click on the "Abort" button and notify the PI for instructions. The "Run Test" screen will automatically close and return to the initial "Wobble" screen.

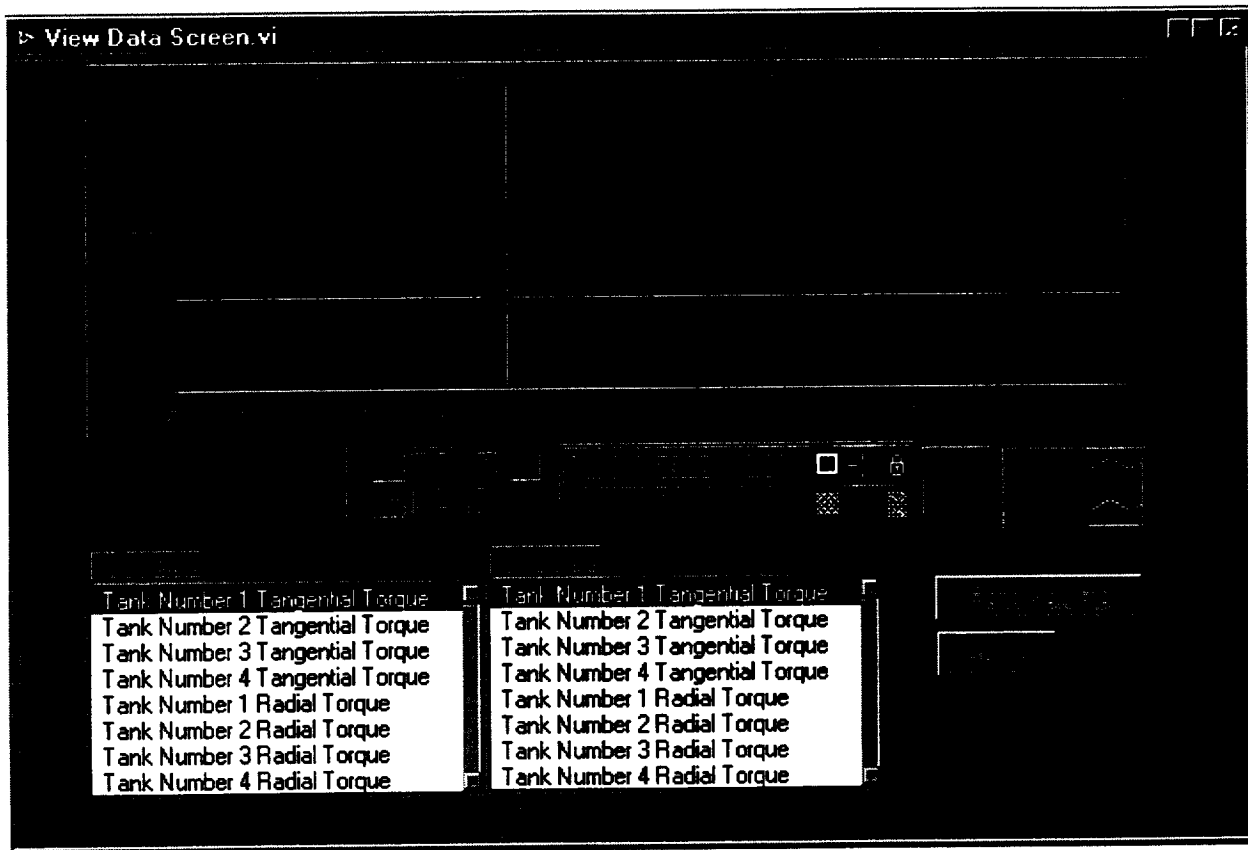
Once the test is successfully completed, the user can either select the next test by clicking on the number in the upper left hand corner, below the test tank designation, or another multiple test series from the "Select Multiple Tests" screen. If the user wants to view data after a test, the user should click on the "Stop" button. The initial "Wobble" screen will appear. The only reason for changing any of these default values will be if the results from one set of tests justify an unplanned set of test conditions for a new test run.

For each new tank set, increment the "tank set" window by clicking on the active area and selecting the next set number.



“View Data Screen”

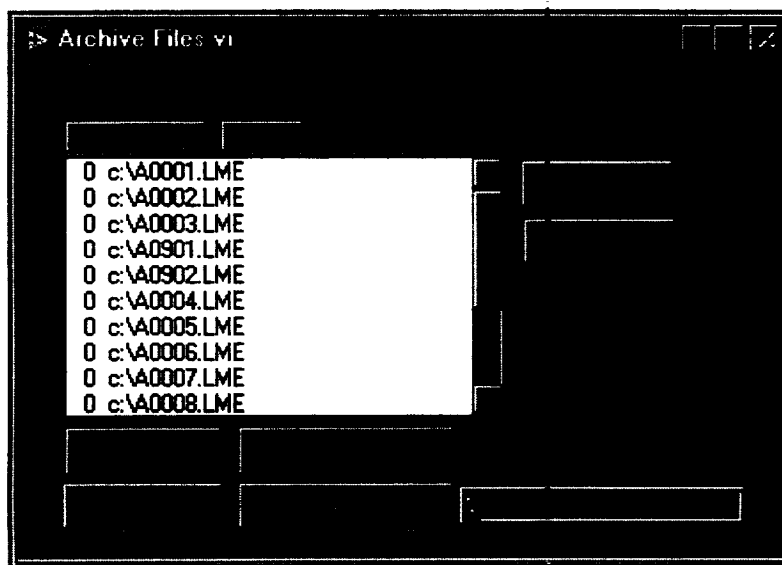
Click on the “View Data” button and select a data file from the data file list and click on “Open.” A plot screen appears and a X-Y plot will appear as shown below.



After reviewing the data, the user should click on “Return.” This will return to the initial “Wobble” screen. The next test can be selected by clicking on “Run Test” again; or, if all tests are complete, click on “Exit.”

"Archive Files" Screen

The PGSC will automatically store data on the hard disk for each test. After each full tank test series is complete, install one of the floppy disks provided and labeled for that fluid tank test series. The data should be archived and, if possible, downlinked to the PI. The user can select multiple files by clicking on them, select all the files which have not been archived yet, or select all the files. A path where the files will be zipped to should be selected by clicking on the "set archive path" button (the box on the screen will show the path). When they click on the "archive" button, the files will be zipped to the directory previously selected and the log file will be updated to reflect the files have been archived.



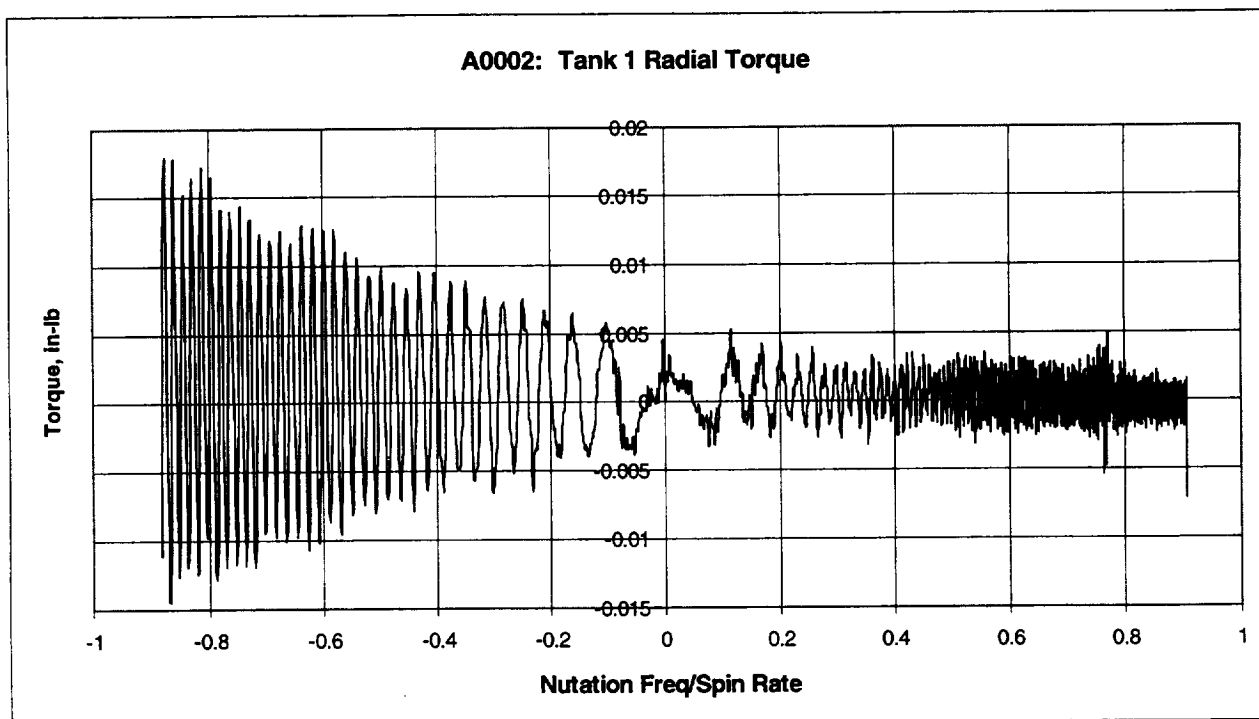
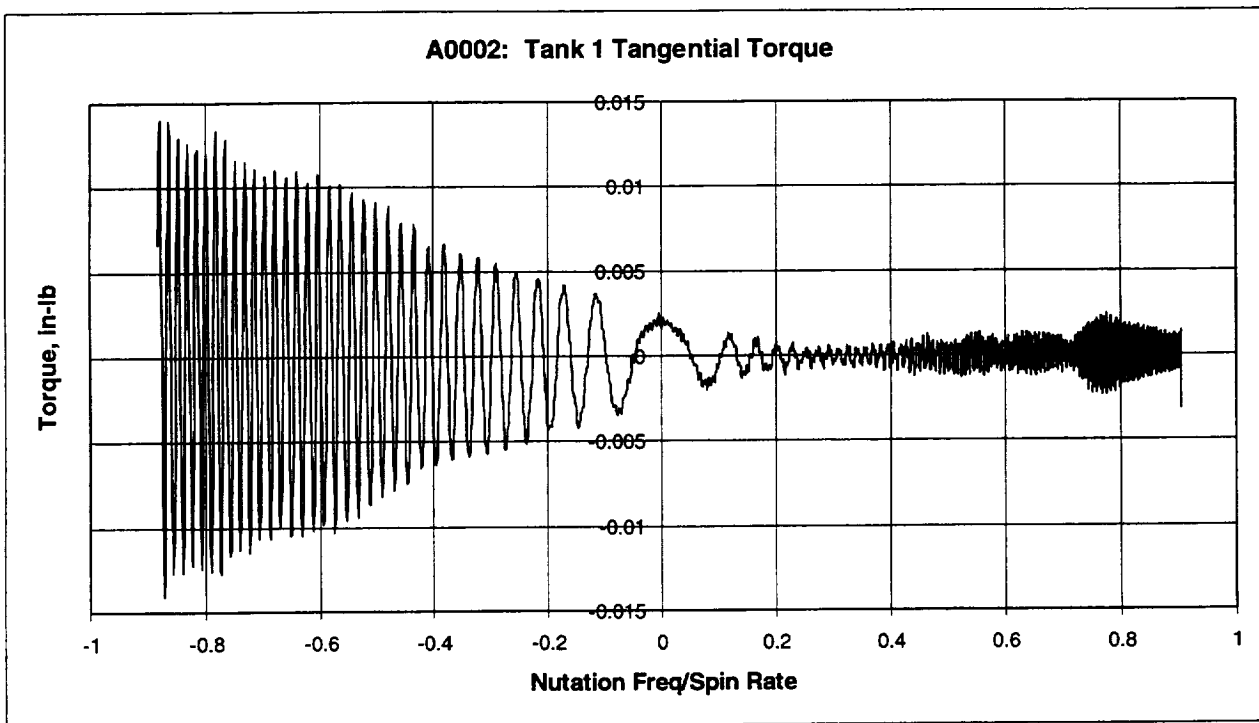
APPENDIX C

Summary of Radial and Tangential Torque Histories for Cylindrical Tanks

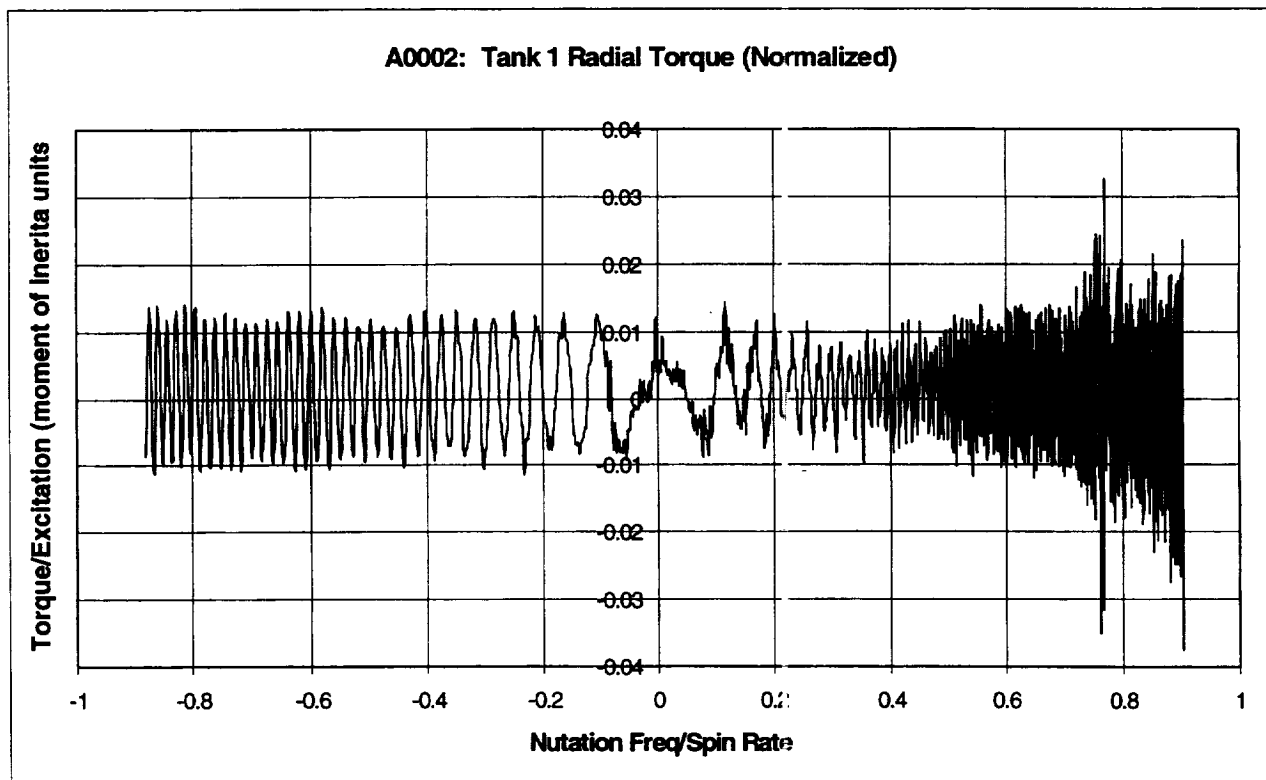
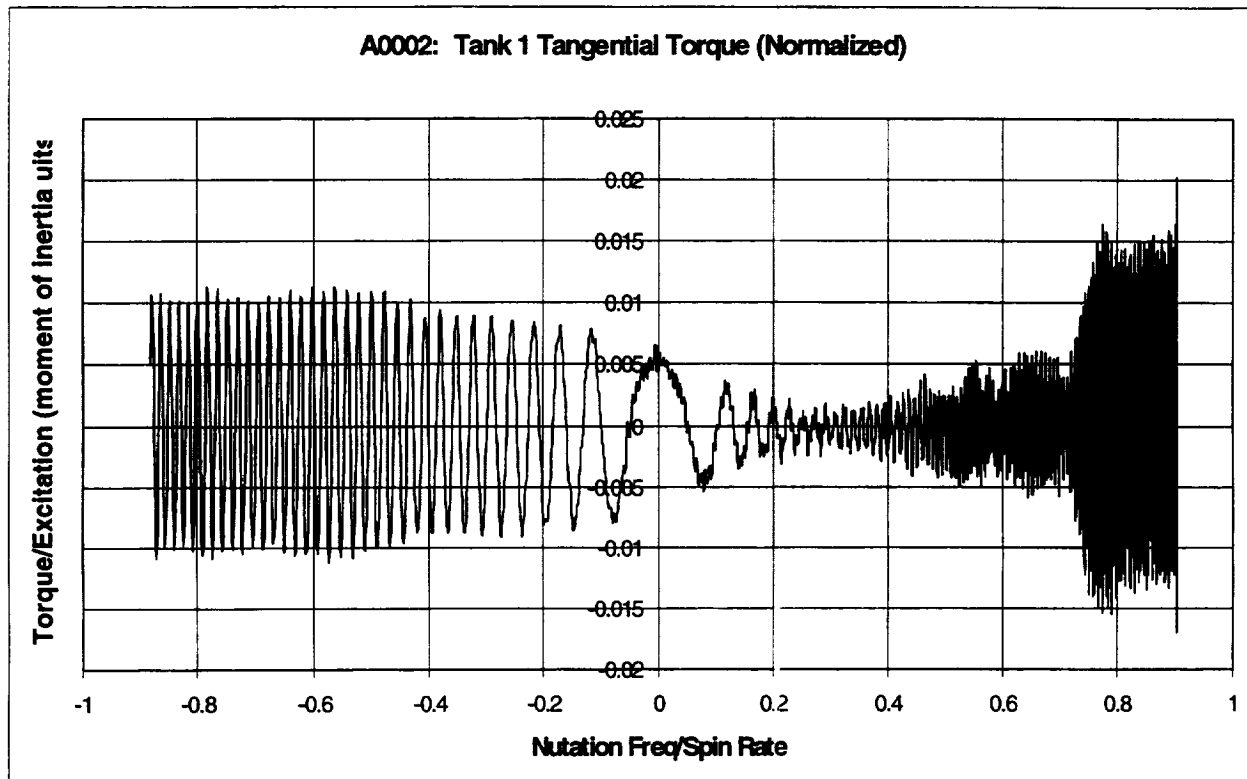
This page left intentionally blank.

A0002: 20 RPM SWEEP TESTS - TANK SET A, CYLINDRICAL TANKS 1 AND 3Nutation Sweep Range: 18.1 rpm \rightarrow 0 \rightarrow 17.6 rpm

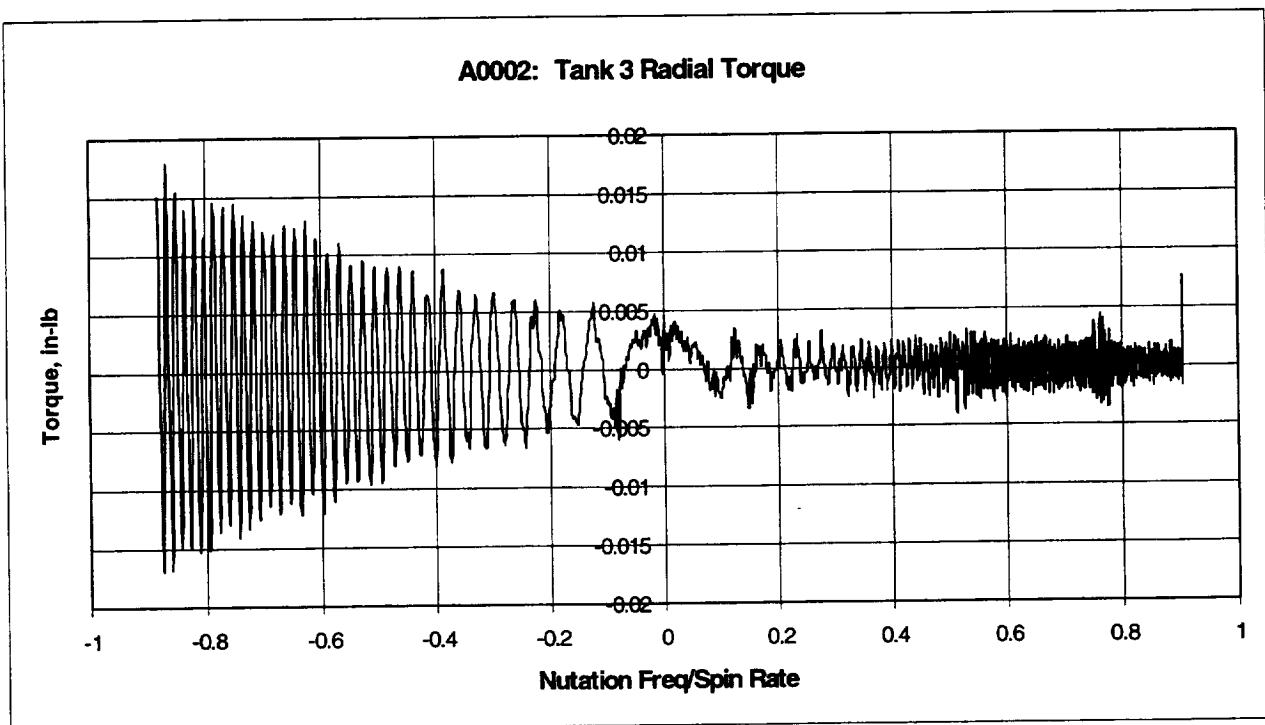
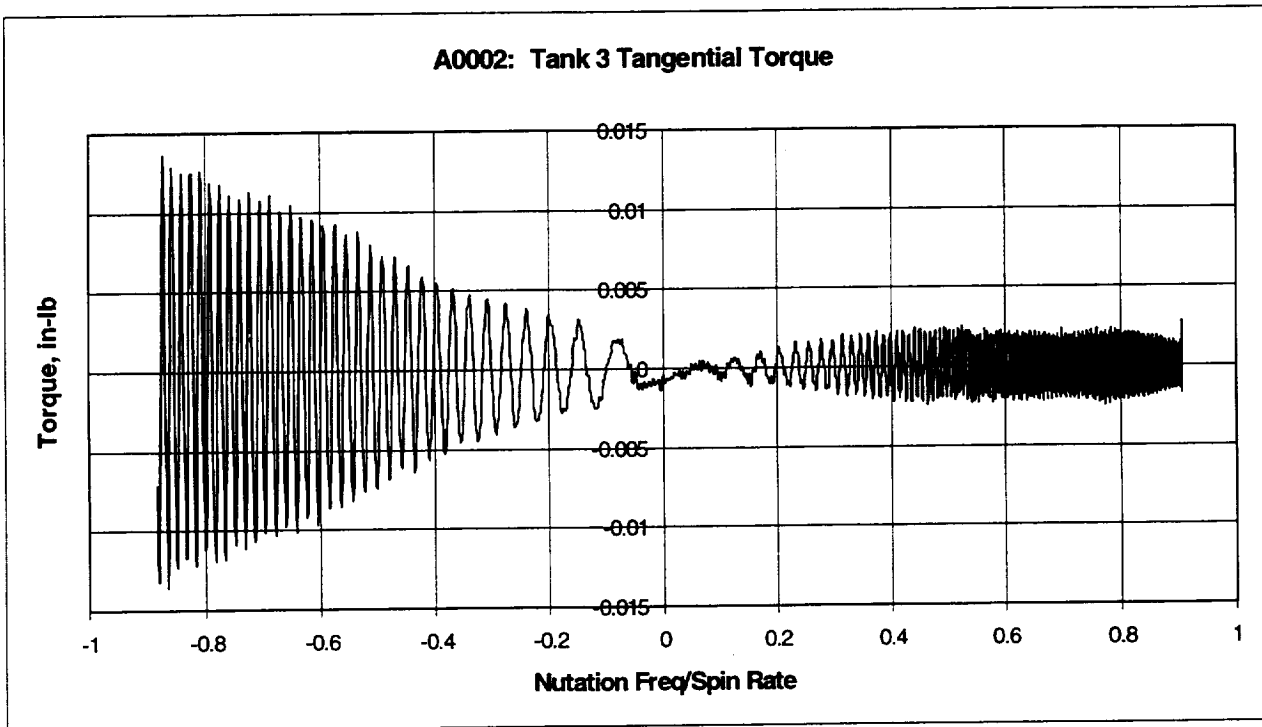
Tank 1: 2/3 Full - Liquid Viscosity = 1 cp



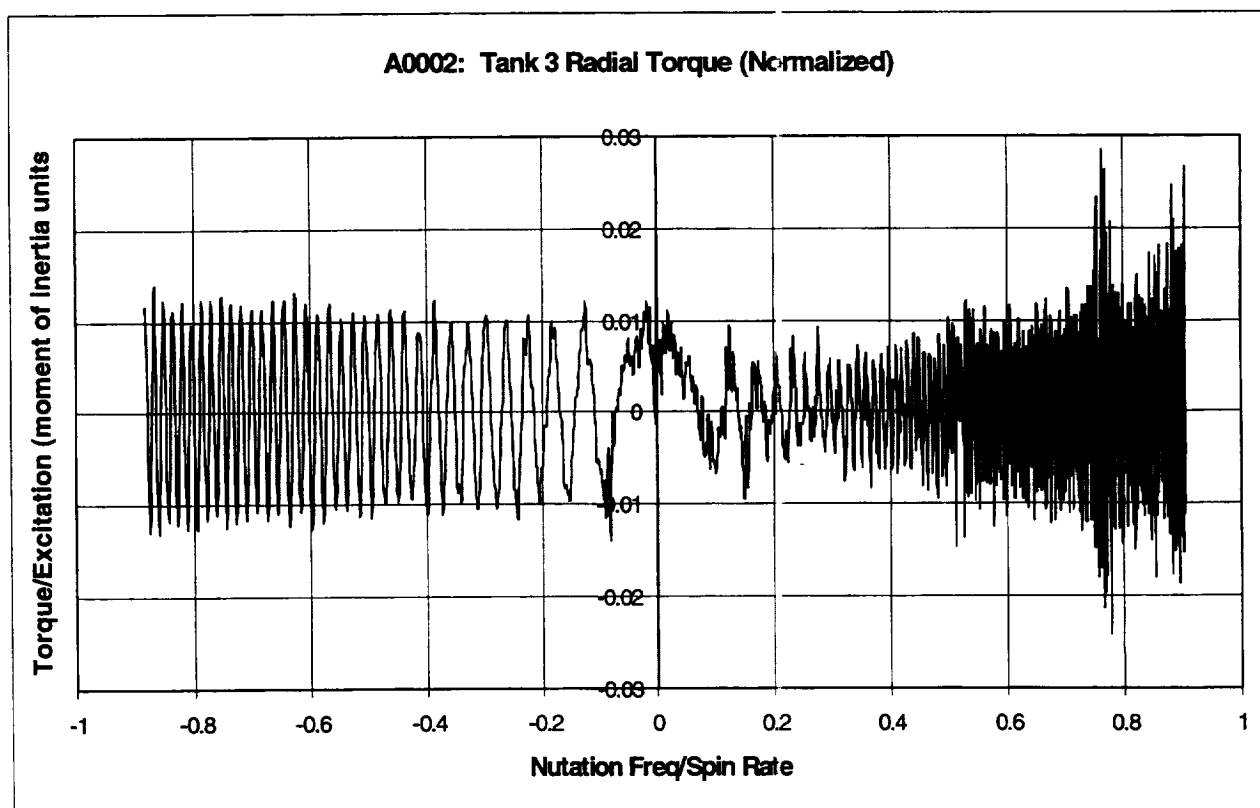
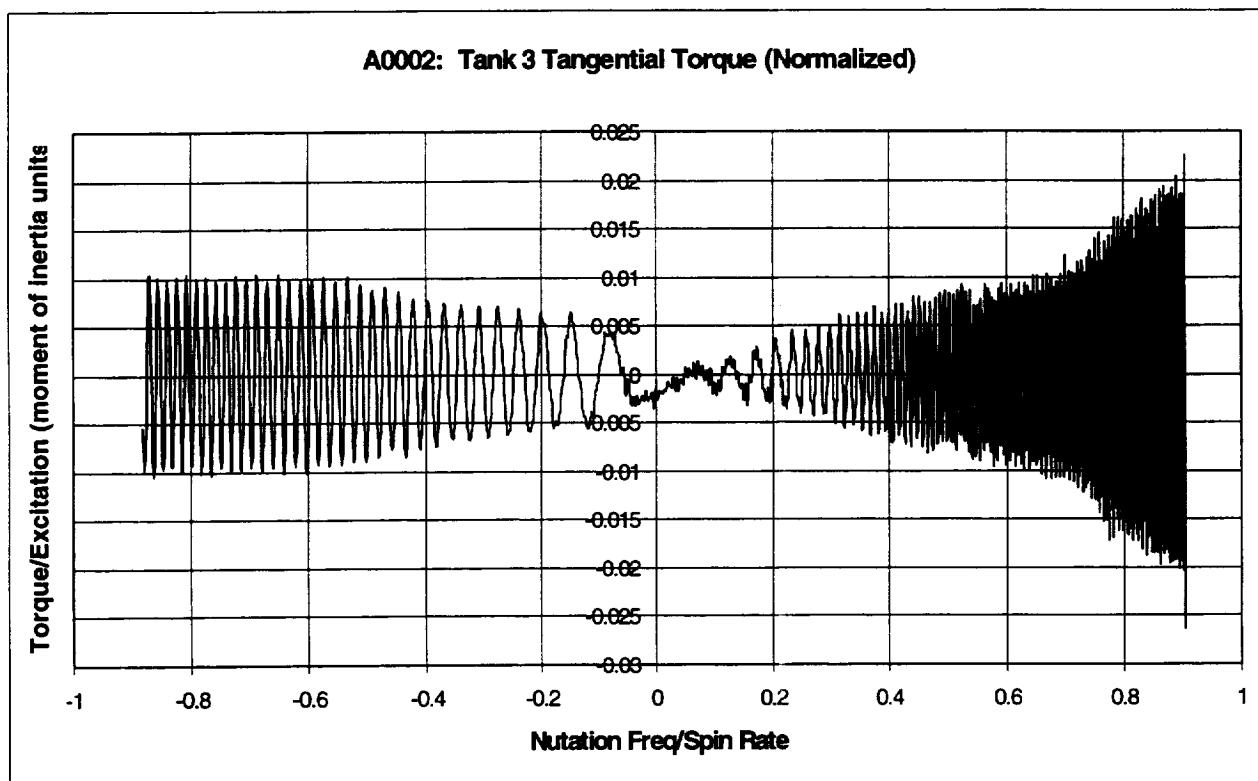
Tank 1 (A0002): concluded

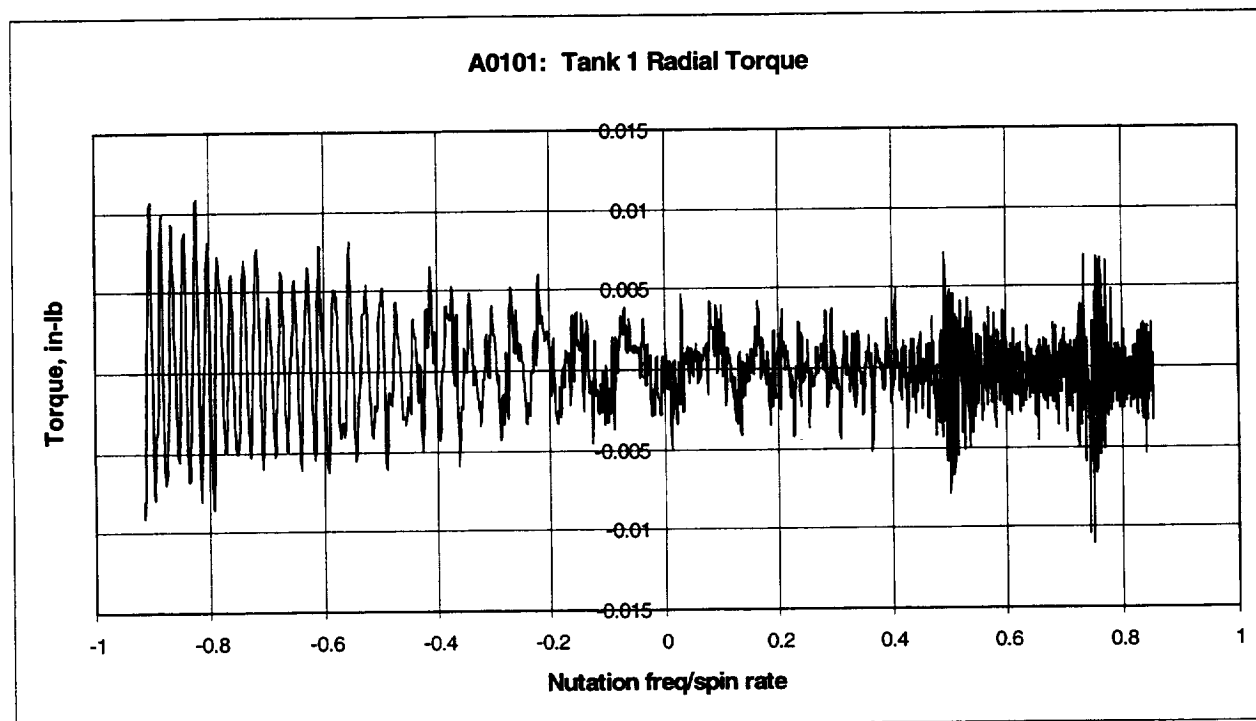
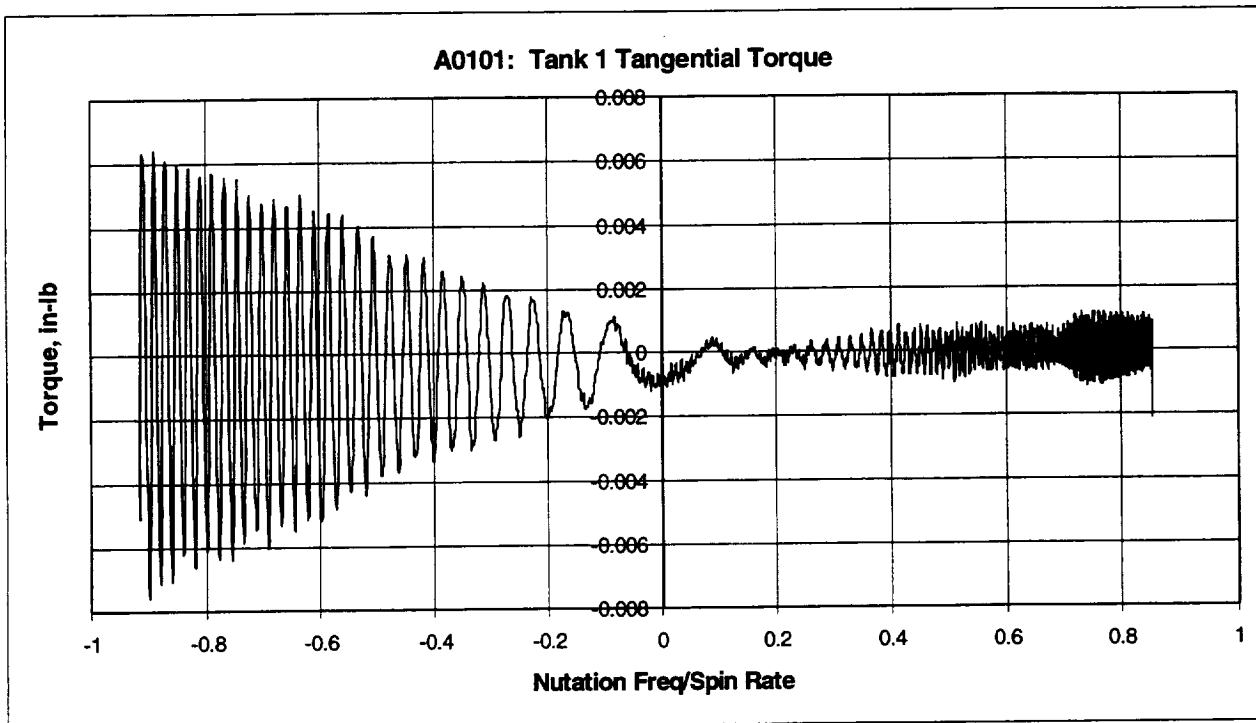


Tank 3 (A0002): 2/3 Full - Liquid Viscosity = 10 cp

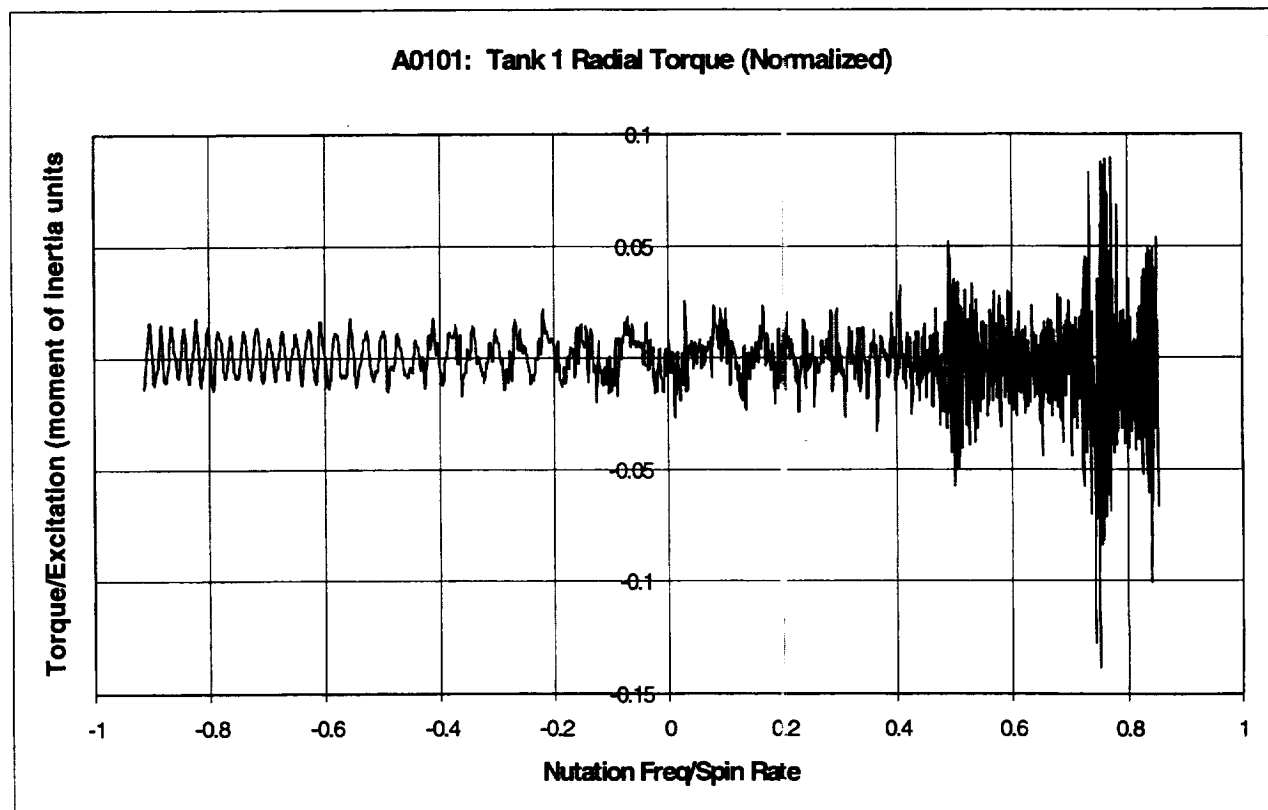
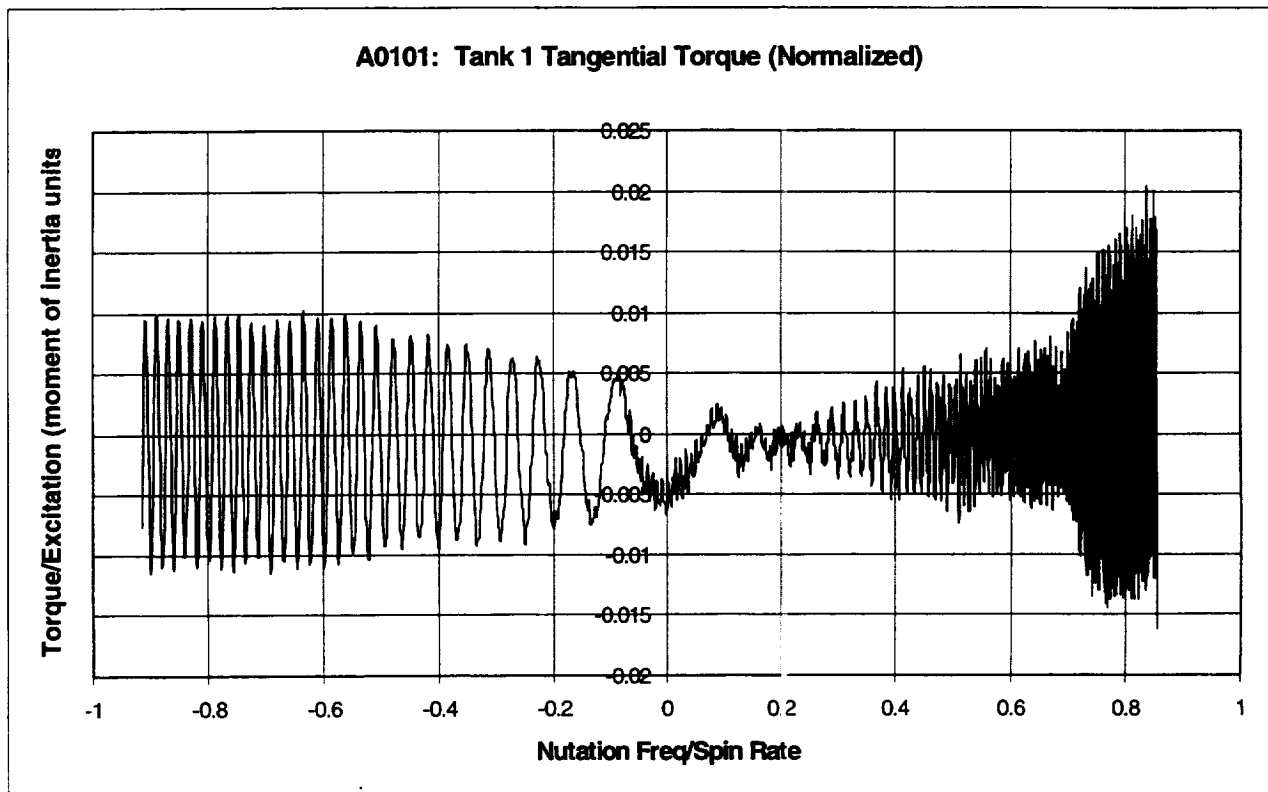


Tank 3 (A0002): concluded

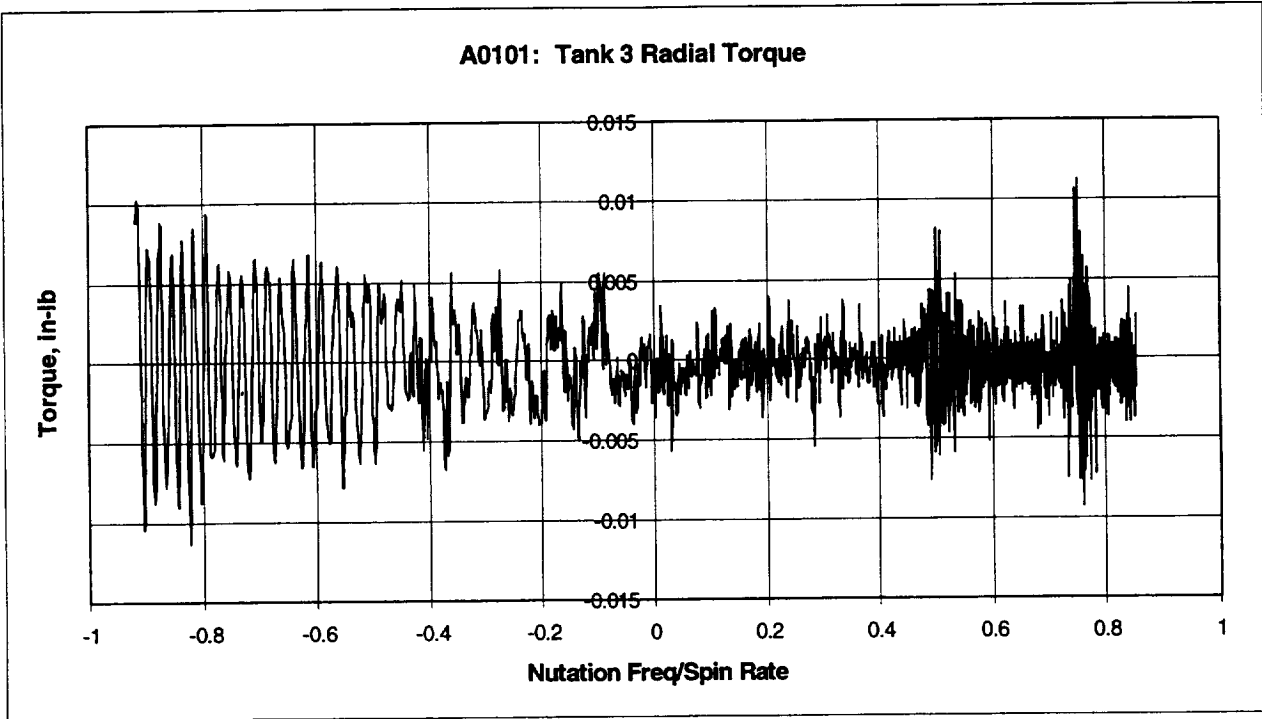
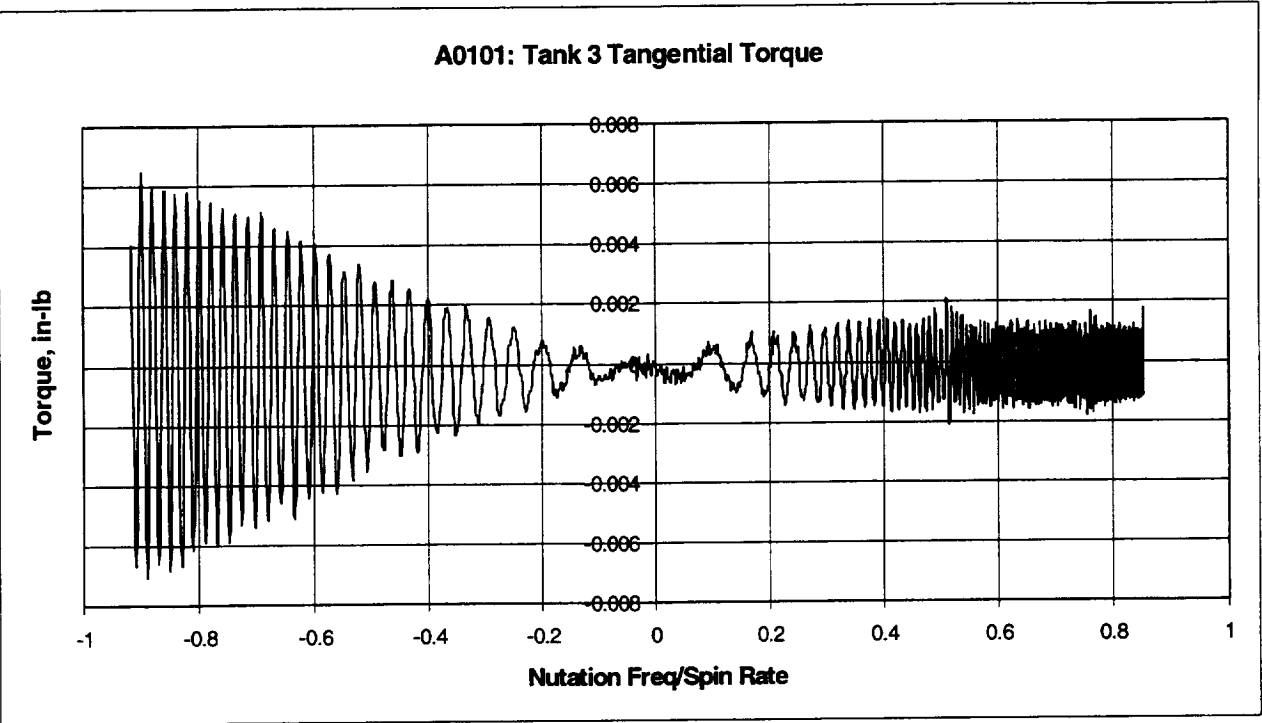


A0101: 14.1 RPM SWEEP TESTS AT - TANK SET A, CYLINDRICAL TANKS 1 AND 3**Nutation Sweep Range: 12.0 rpm \rightarrow 0 \rightarrow 12.8 rpm****Tank 1: 2/3 Full - Liquid Viscosity = 1 cp**

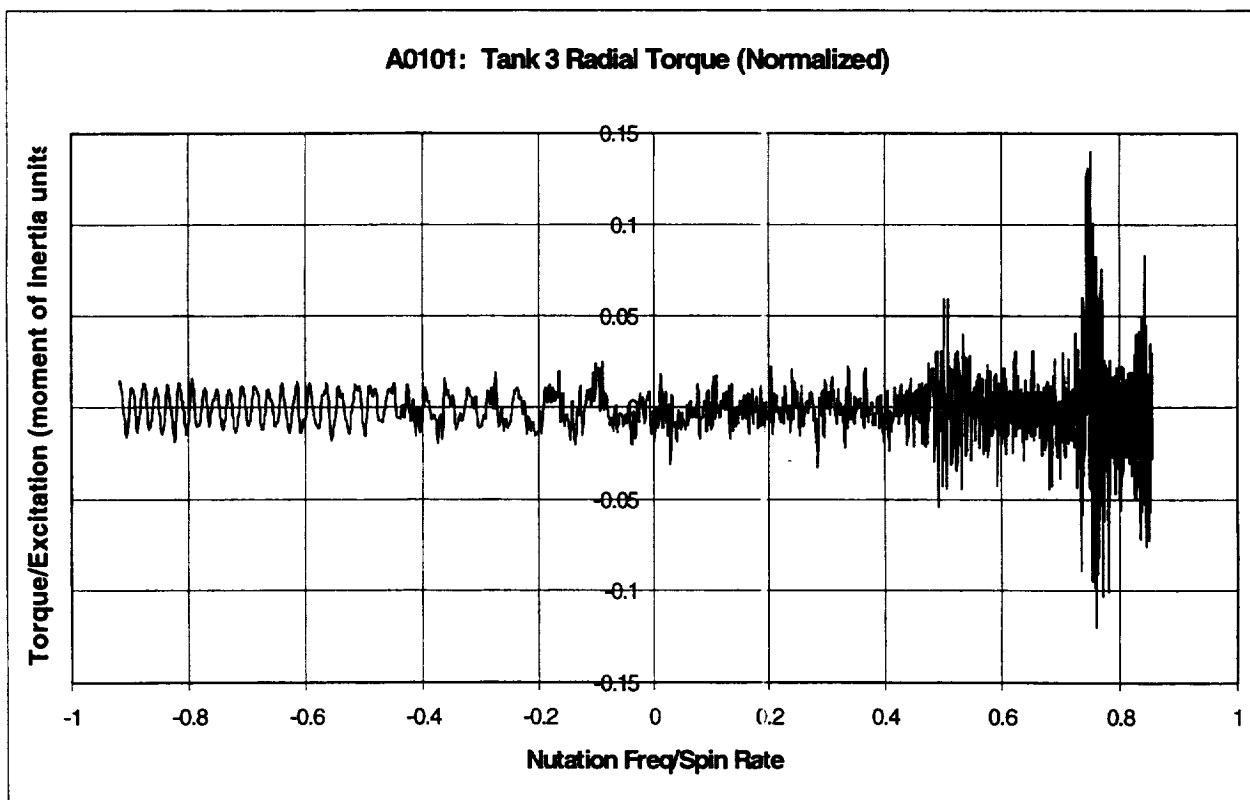
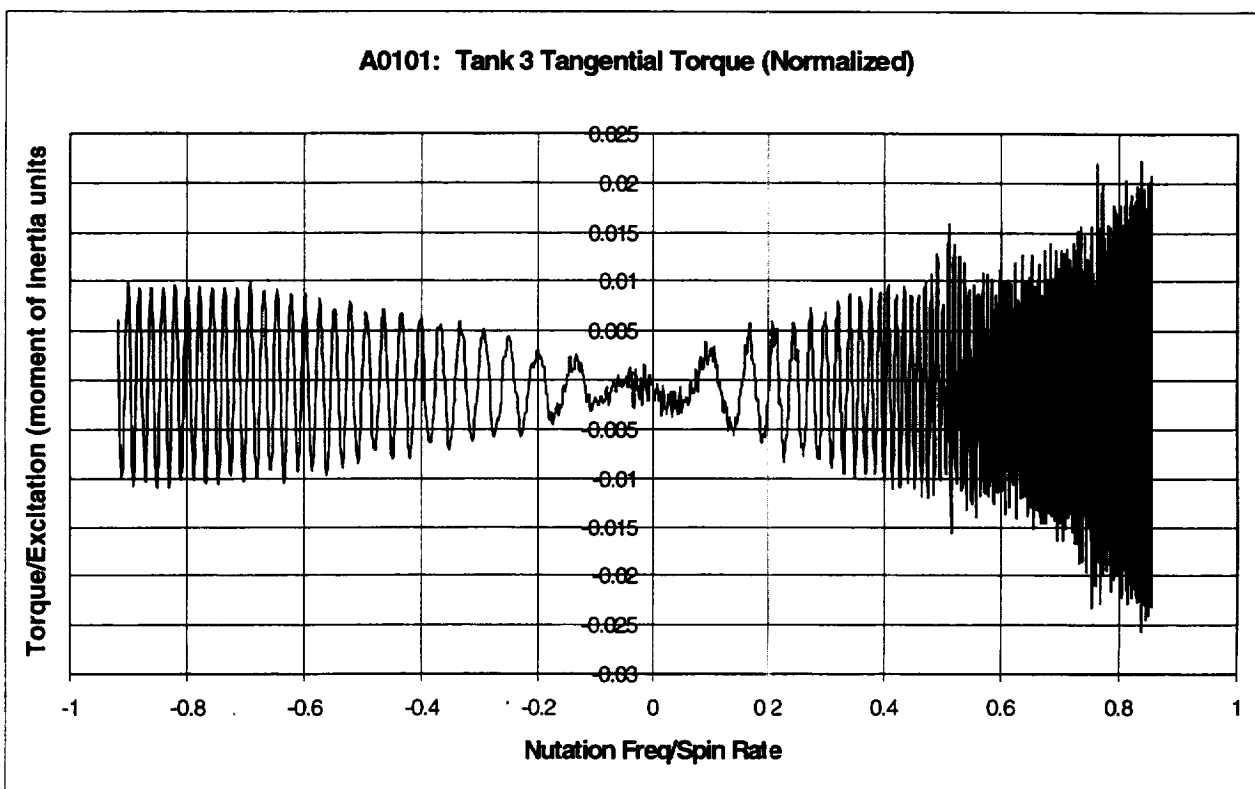
Tank 1 (A0101): concluded



Tank 3 (A0101): 2/3 Full - Liquid Viscosity = 10 cp

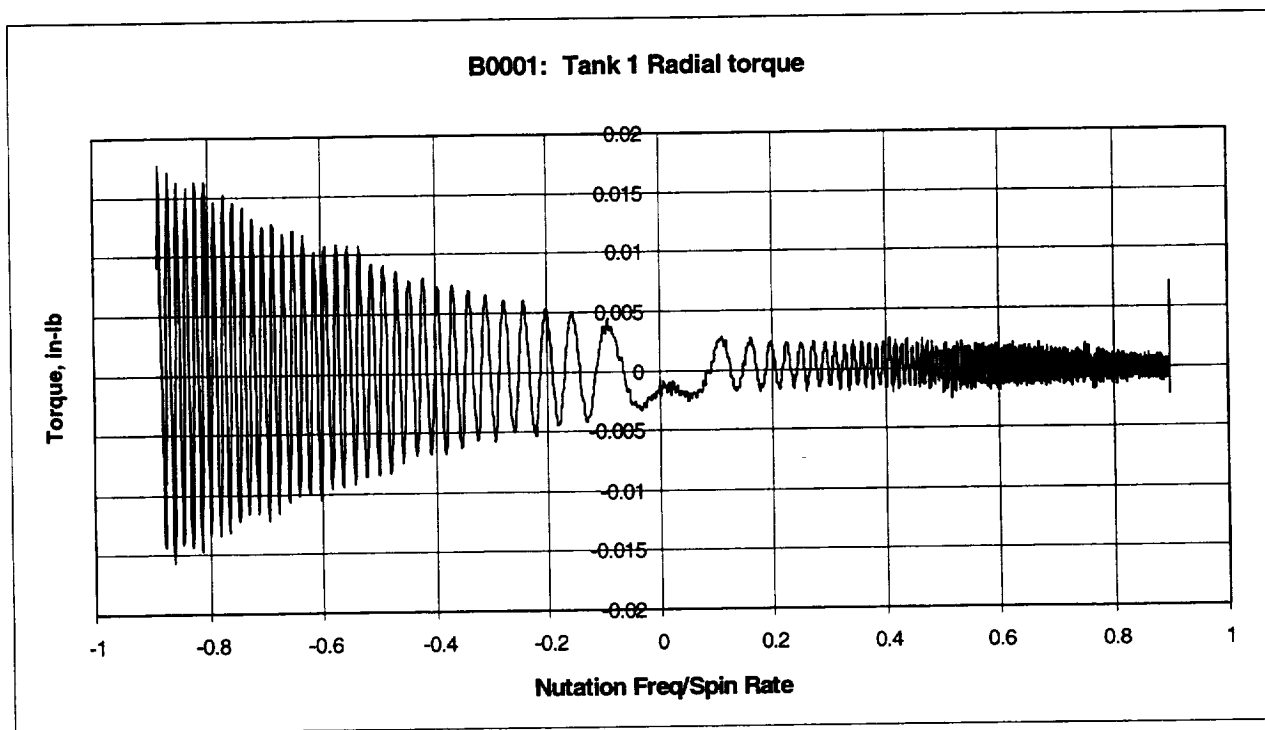
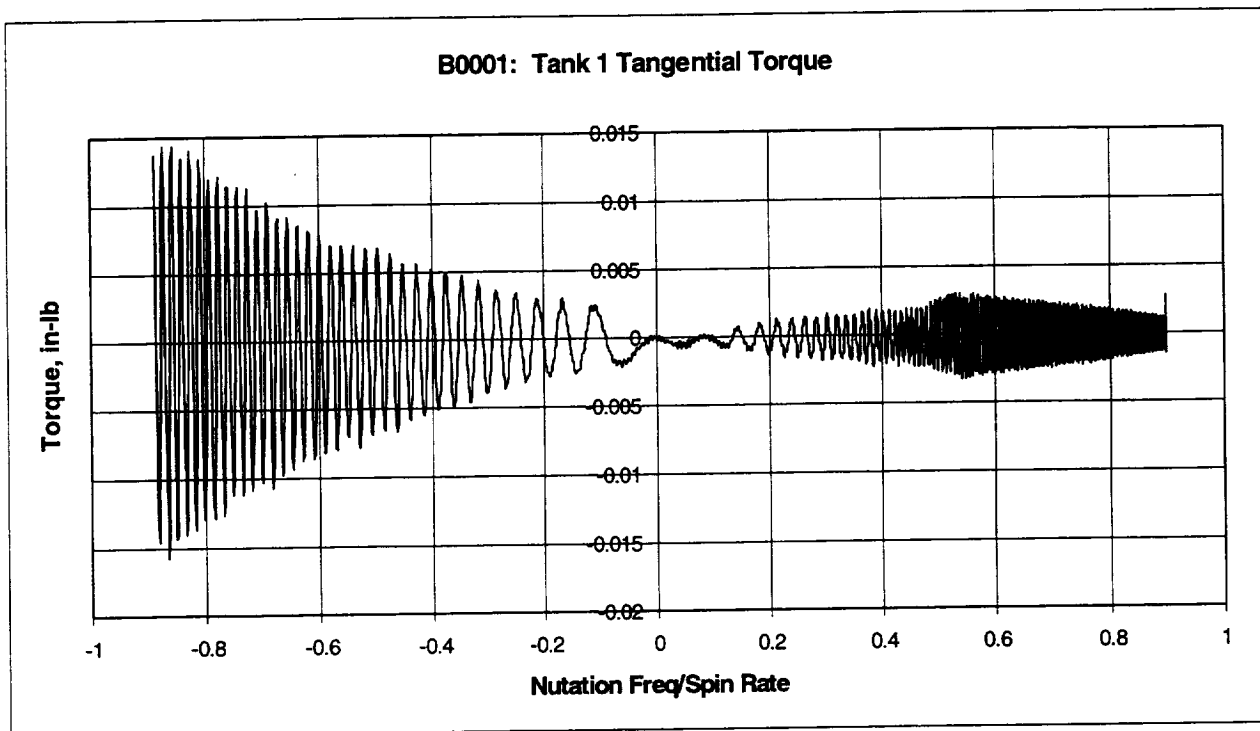


Tank 3 (A0101): concluded

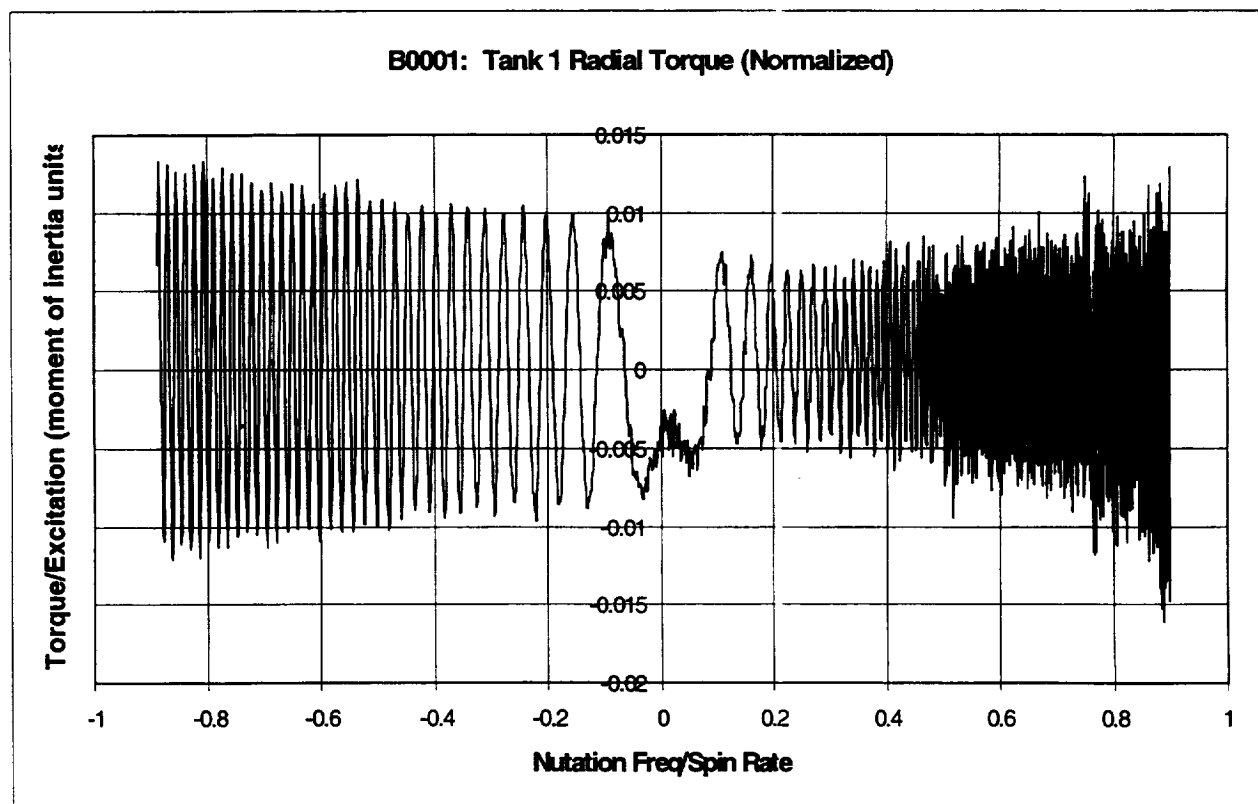
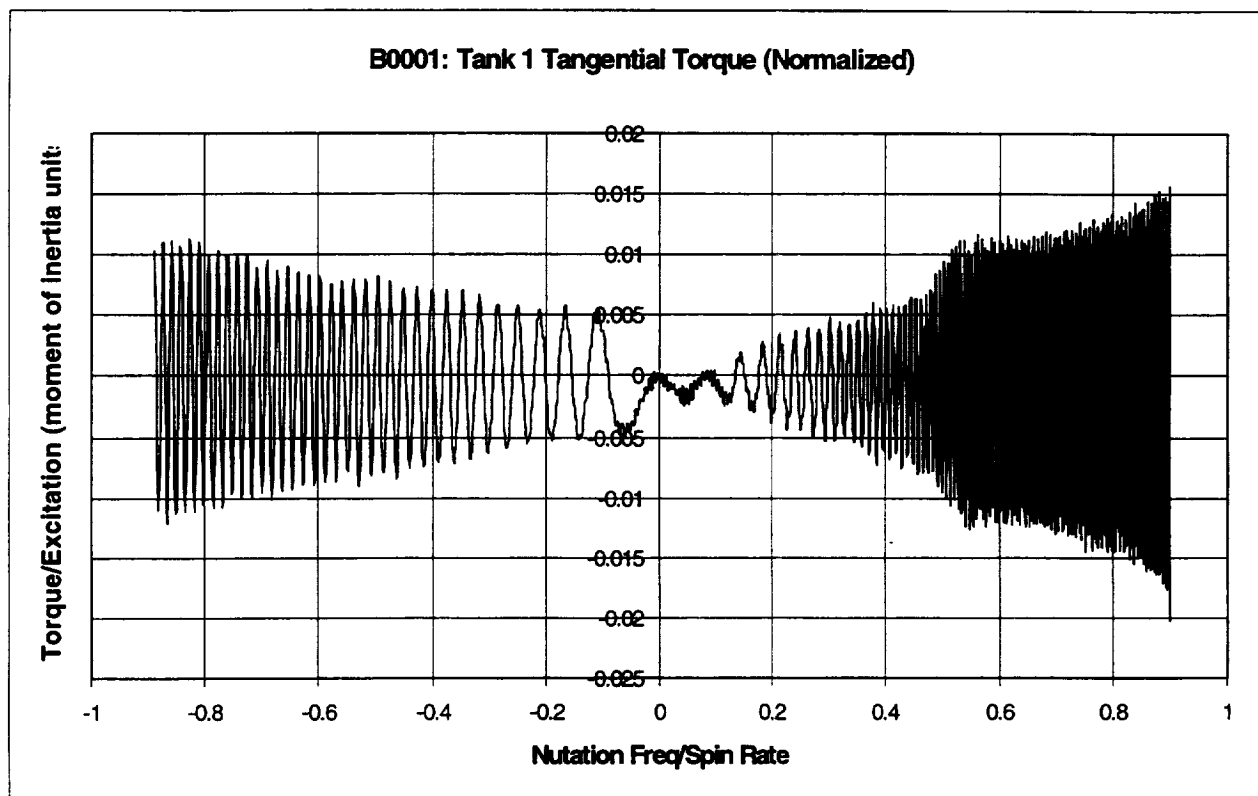


B0001: 20 RPM SWEEP TESTS - TANK SET B, CYLINDRICAL TANKS 1 AND 3Nutation Sweep Range: 18.1 rpm \rightarrow 0 \rightarrow 17.6 rpm

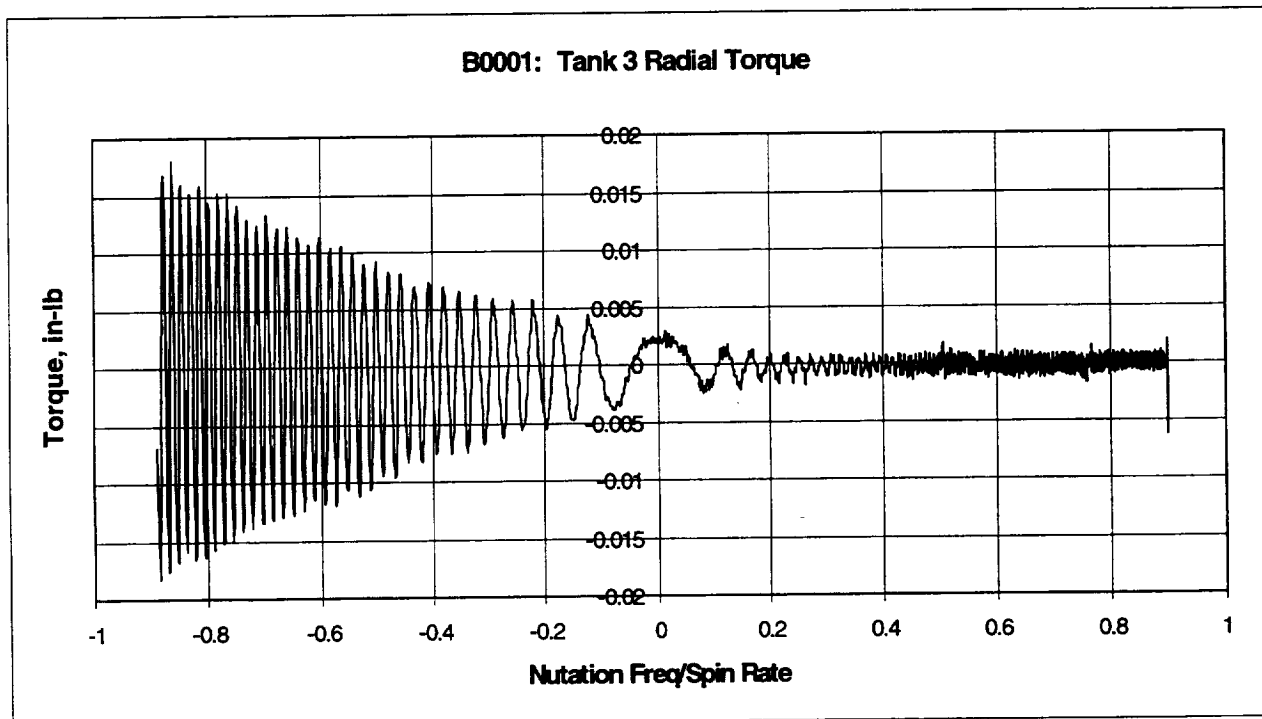
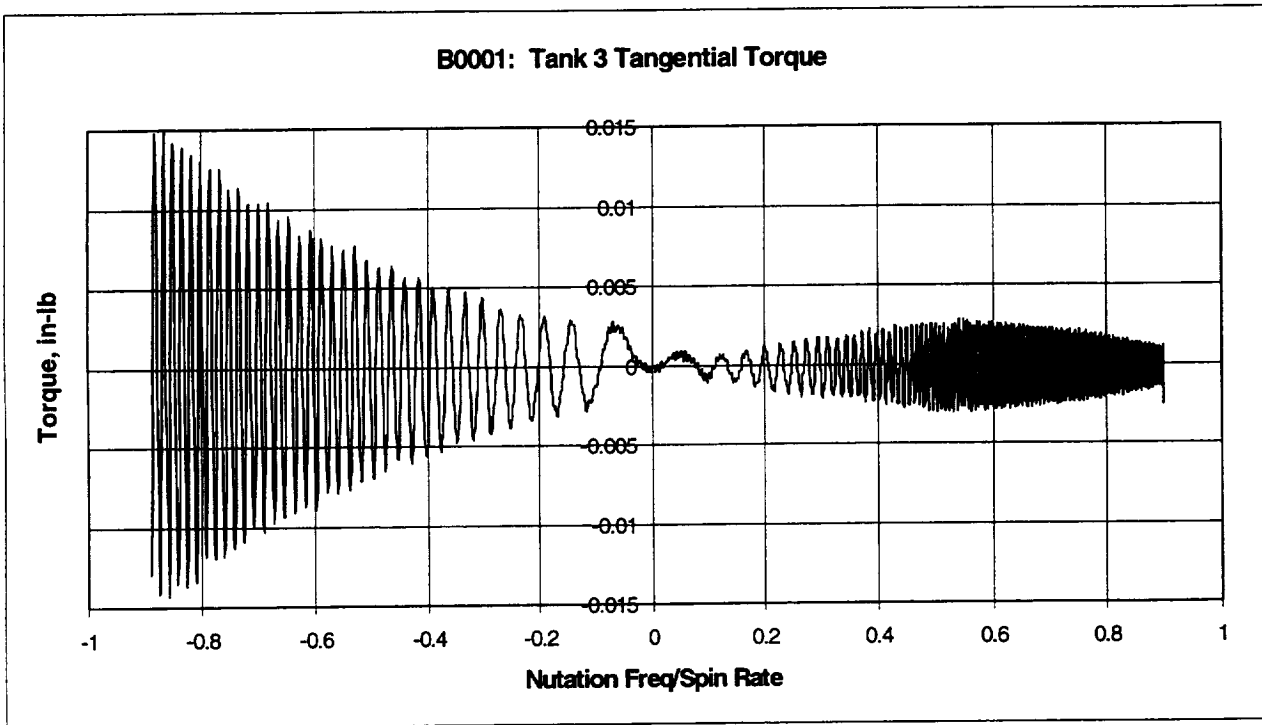
Tank 1: 1/3 Full - Liquid Viscosity = 1 cp



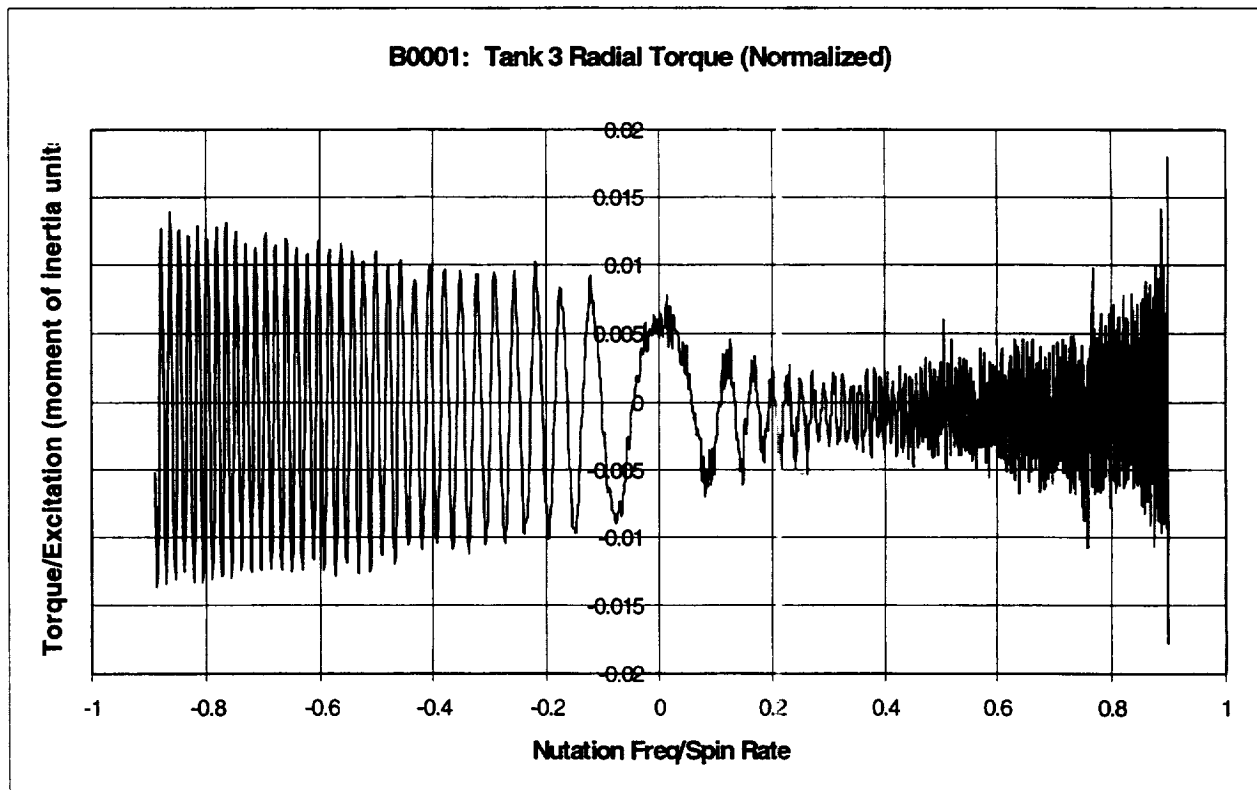
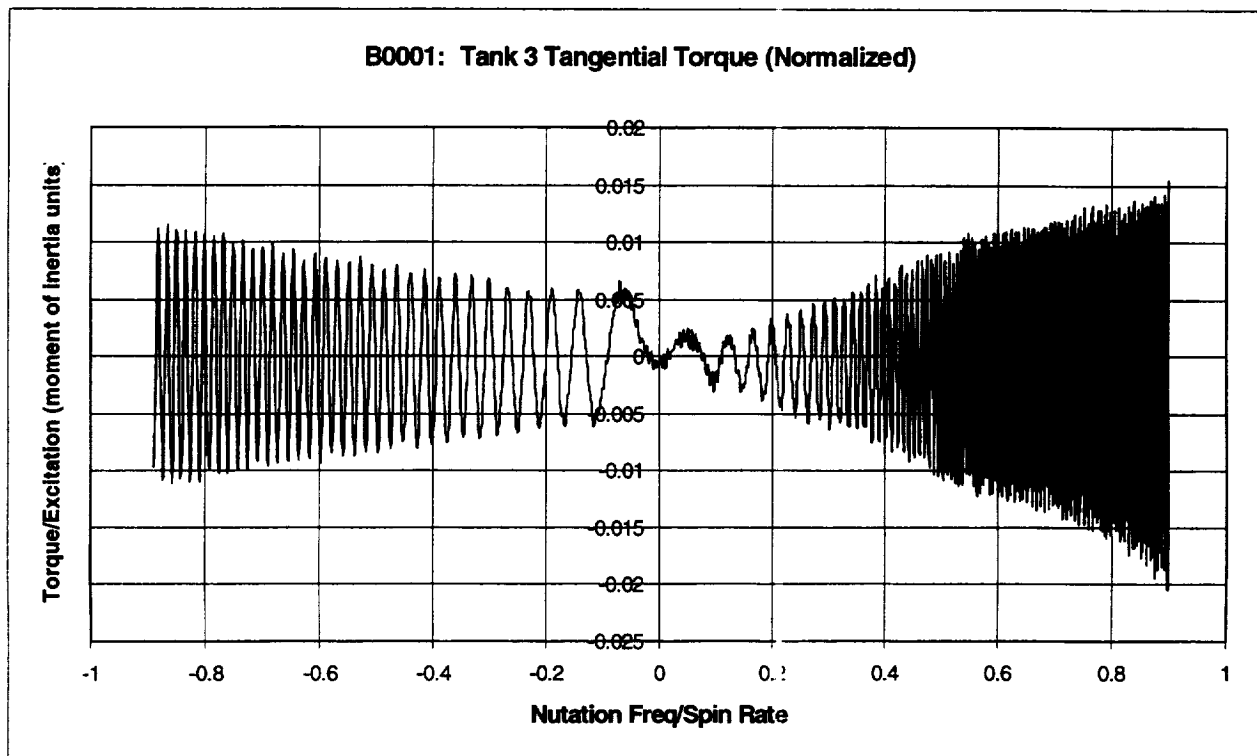
Tank 1 (B0001): concluded



Tank 3 (B0001): 1/3 Full - Liquid Viscosity = 10 cp



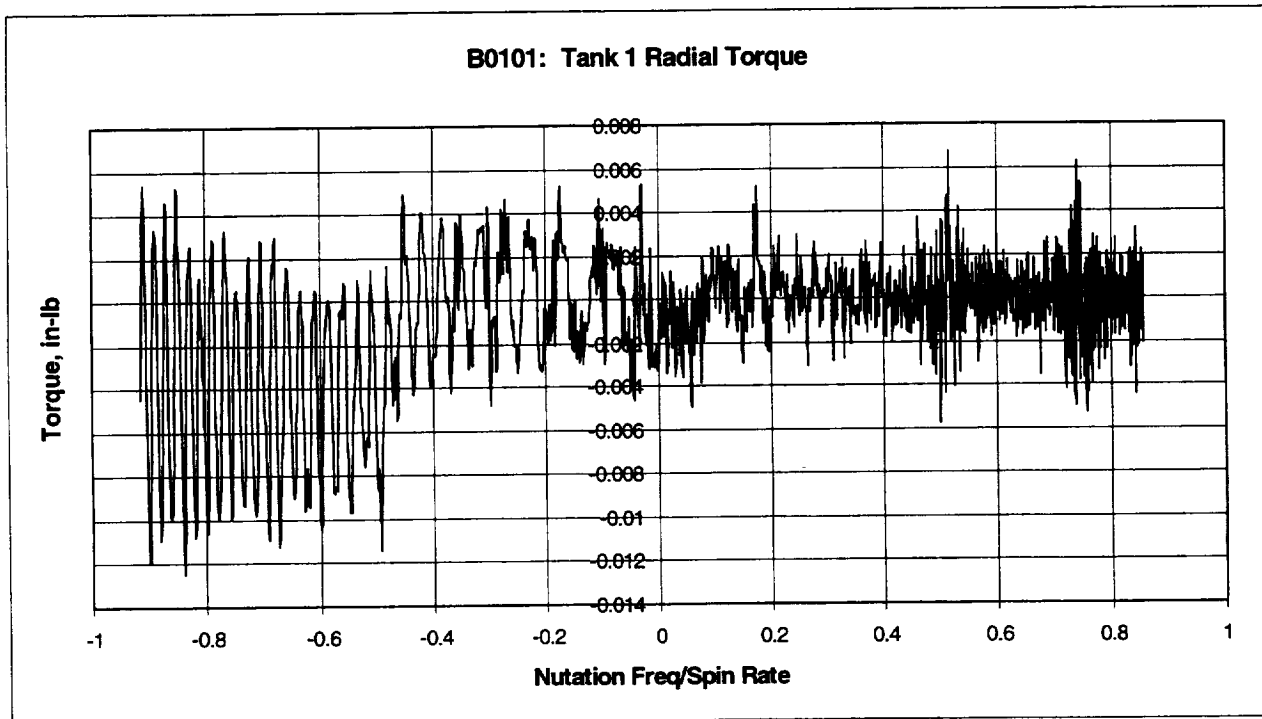
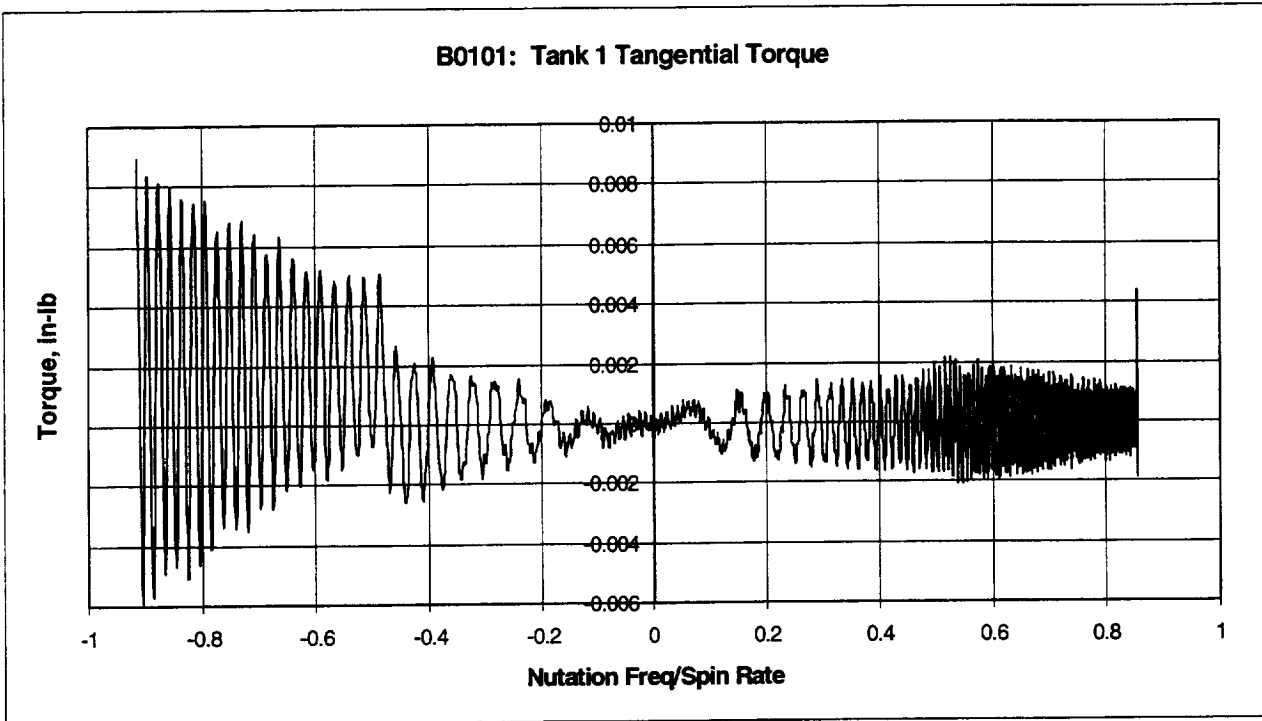
Tank 3 (B0001): concluded



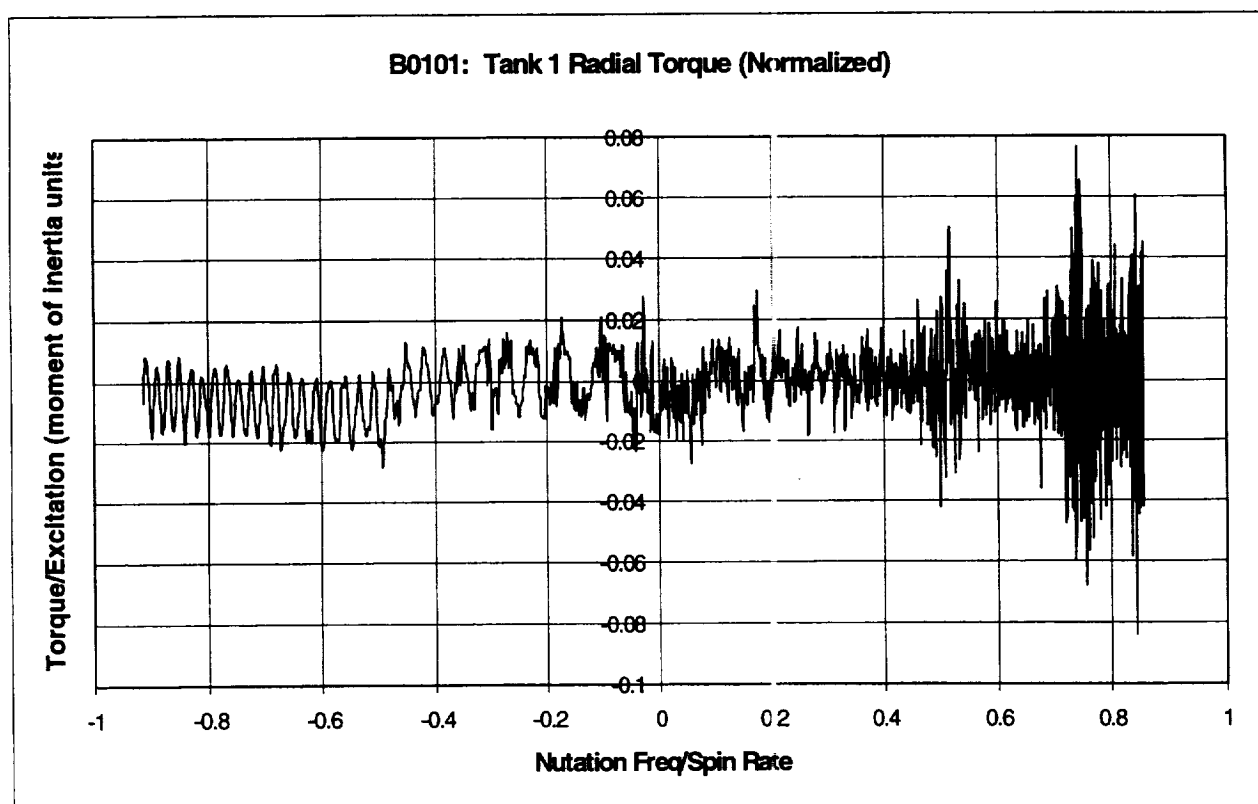
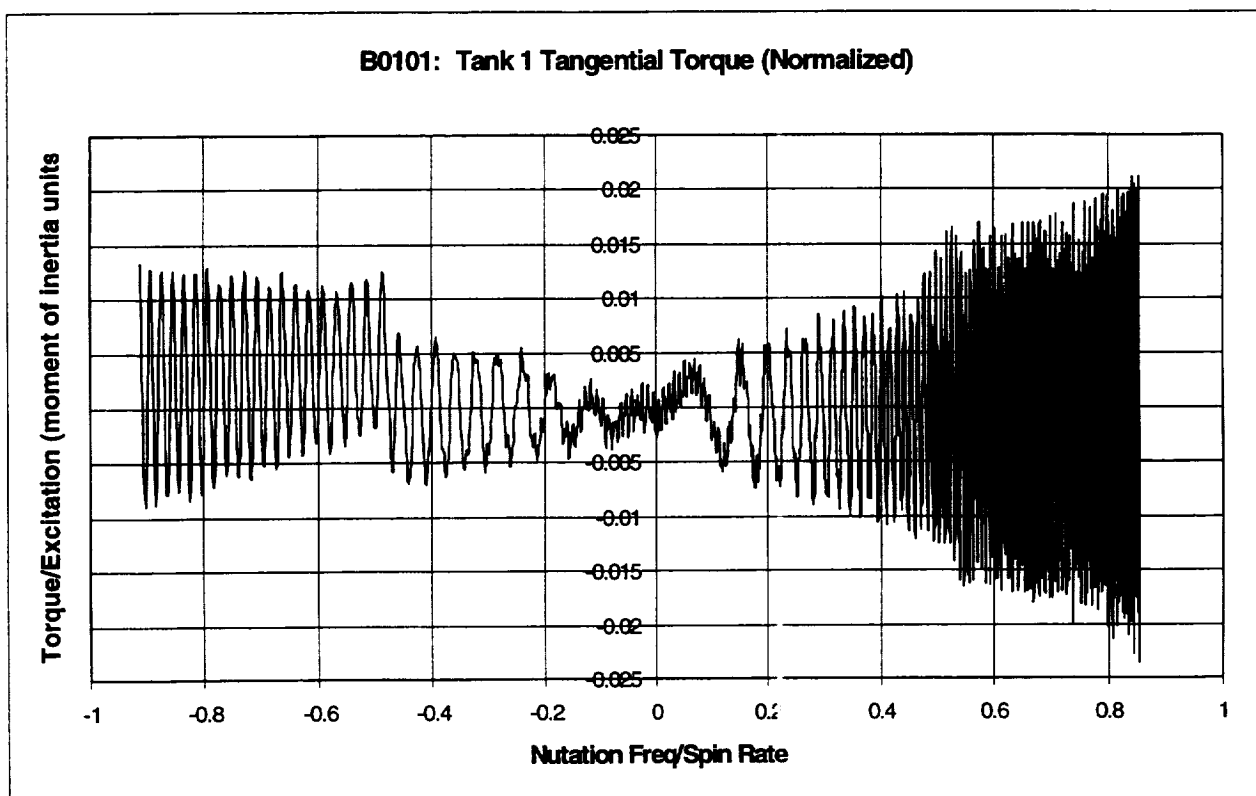
B0101: 14.1 RPM SWEEP TESTS - TANK SET B, CYLINDRICAL TANKS 1 AND 3

Nutation Sweep Range: 12.0 rpm \rightarrow 0 \rightarrow 12.8 rpm

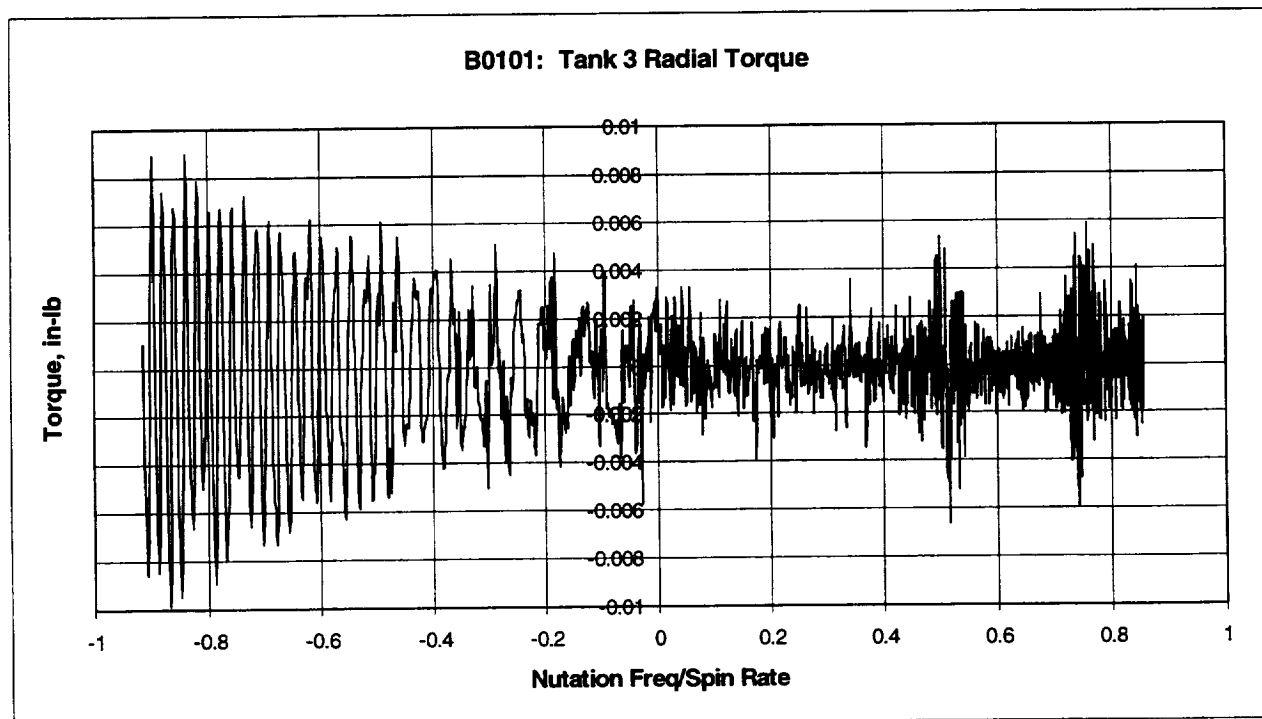
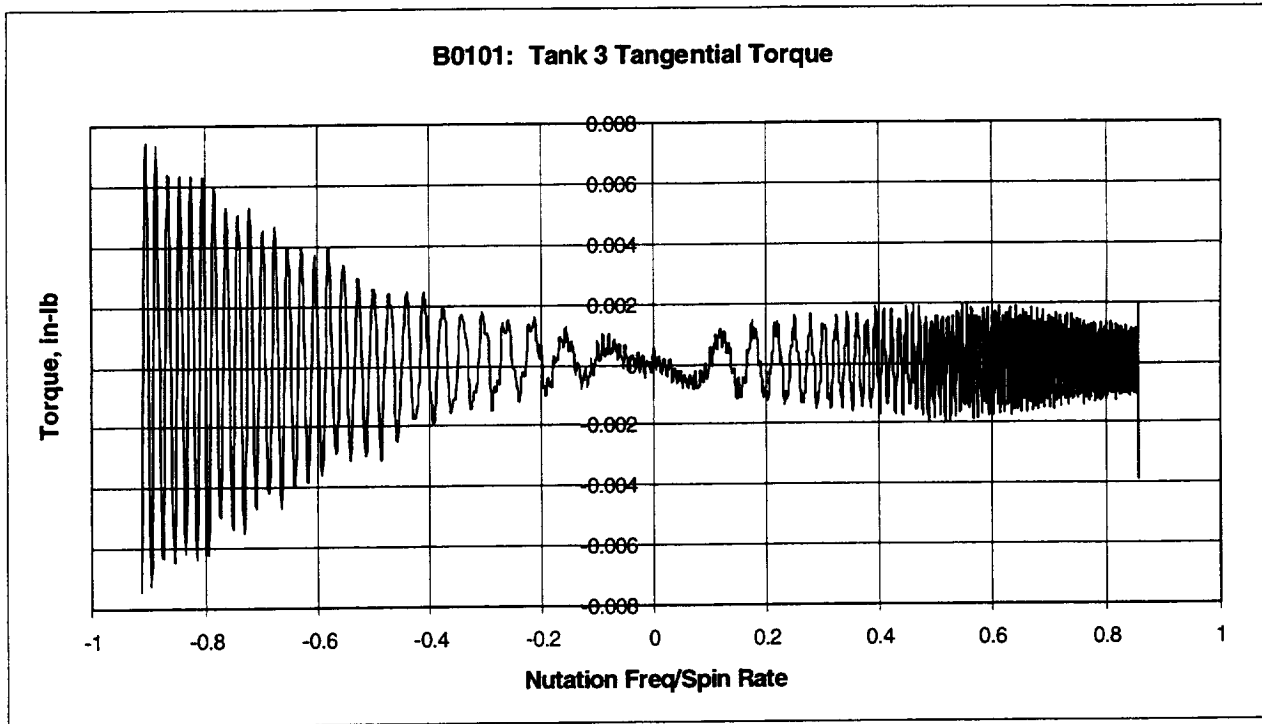
Tank 1: 1/3 Full - Liquid Viscosity = 1 cp



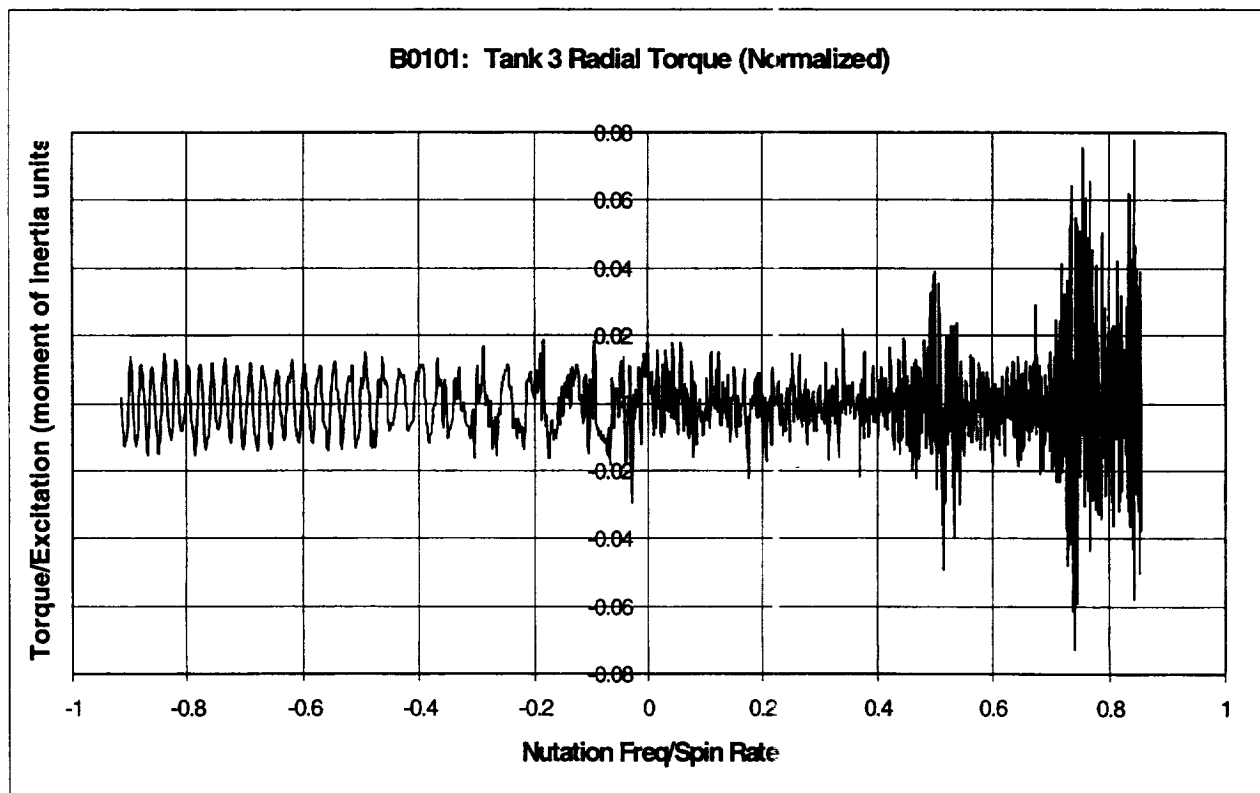
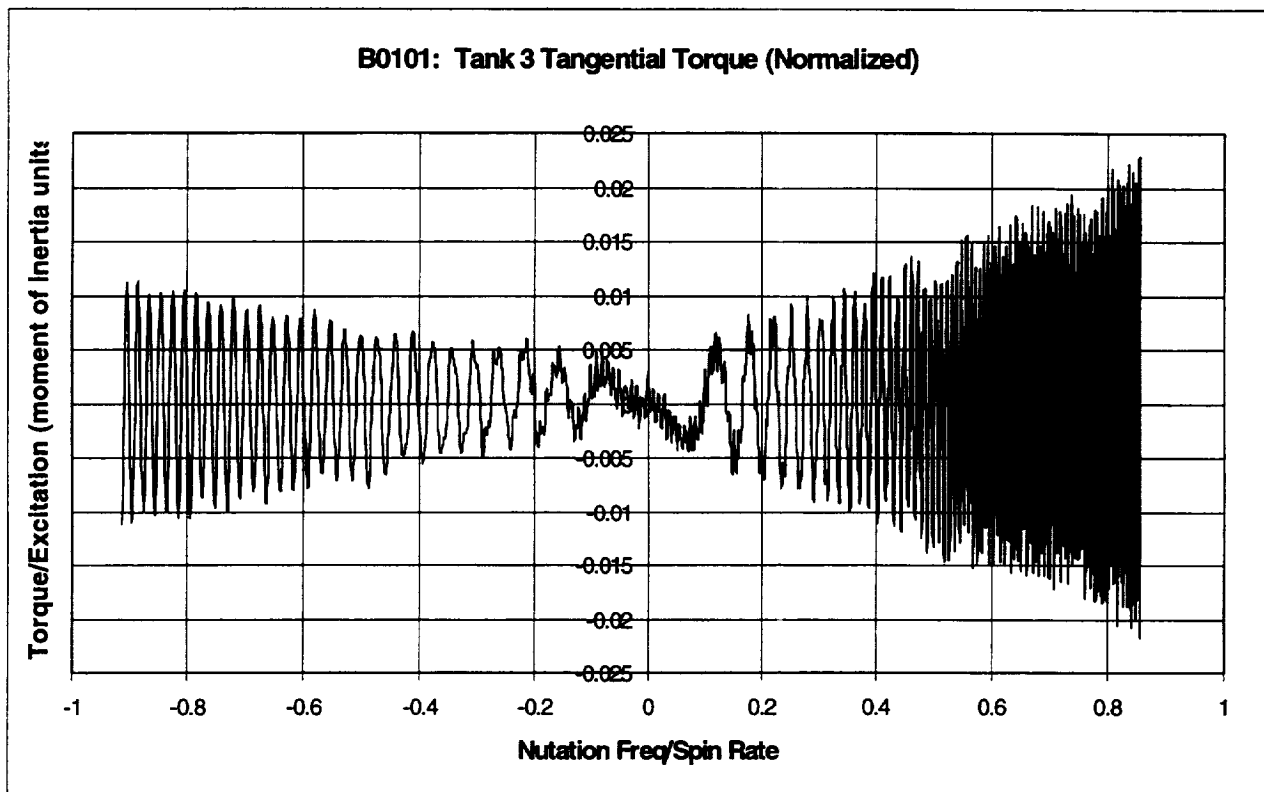
Tank 1 (B0101): concluded

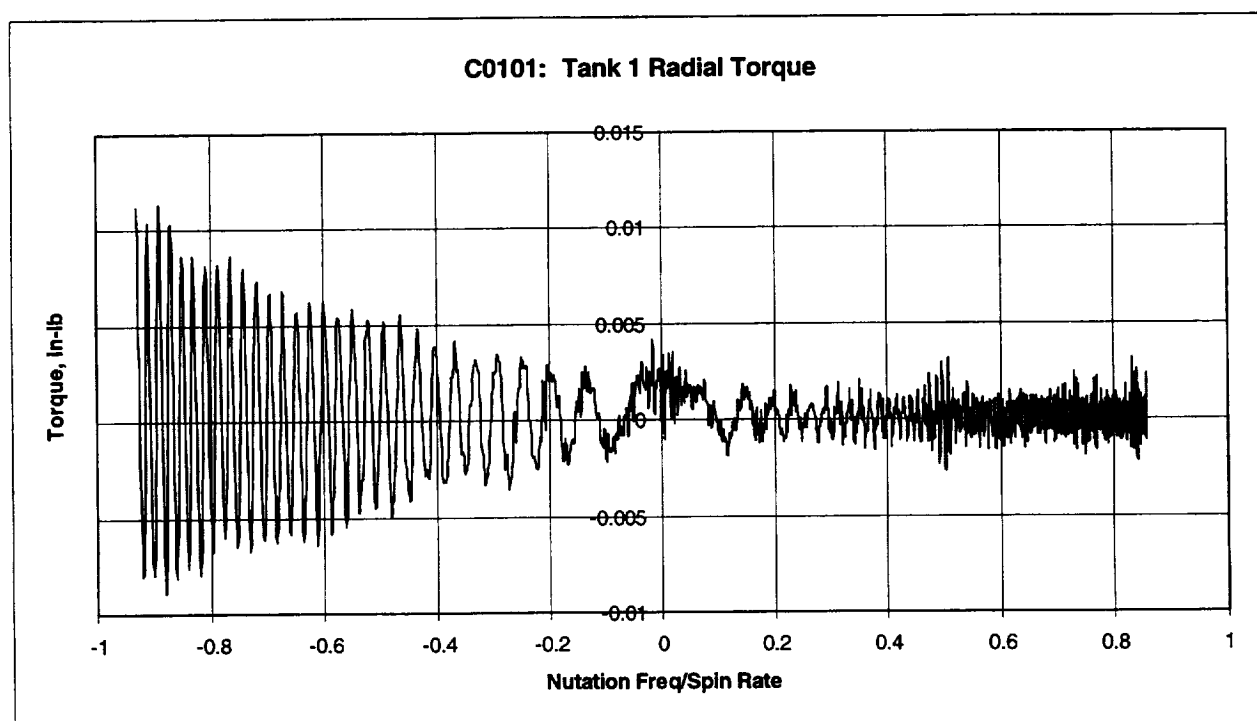
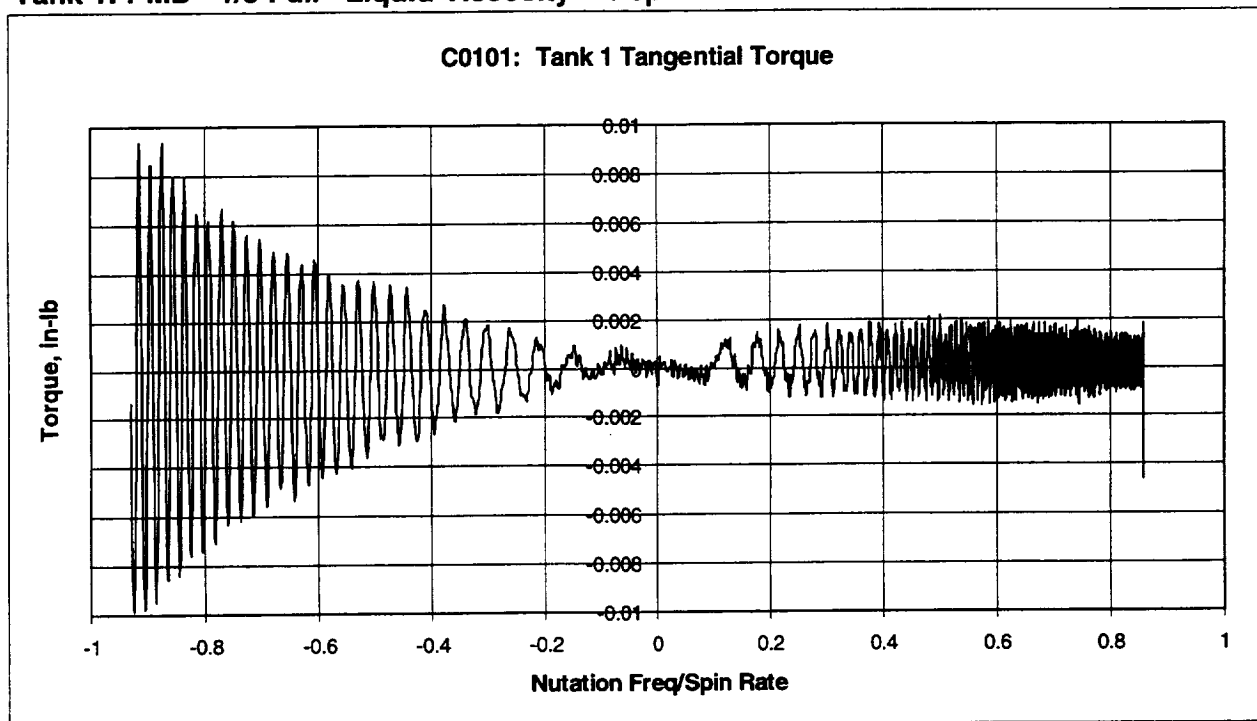


Tank 3 (B0101): 1/3 Full - Liquid Viscosity = 10 cp

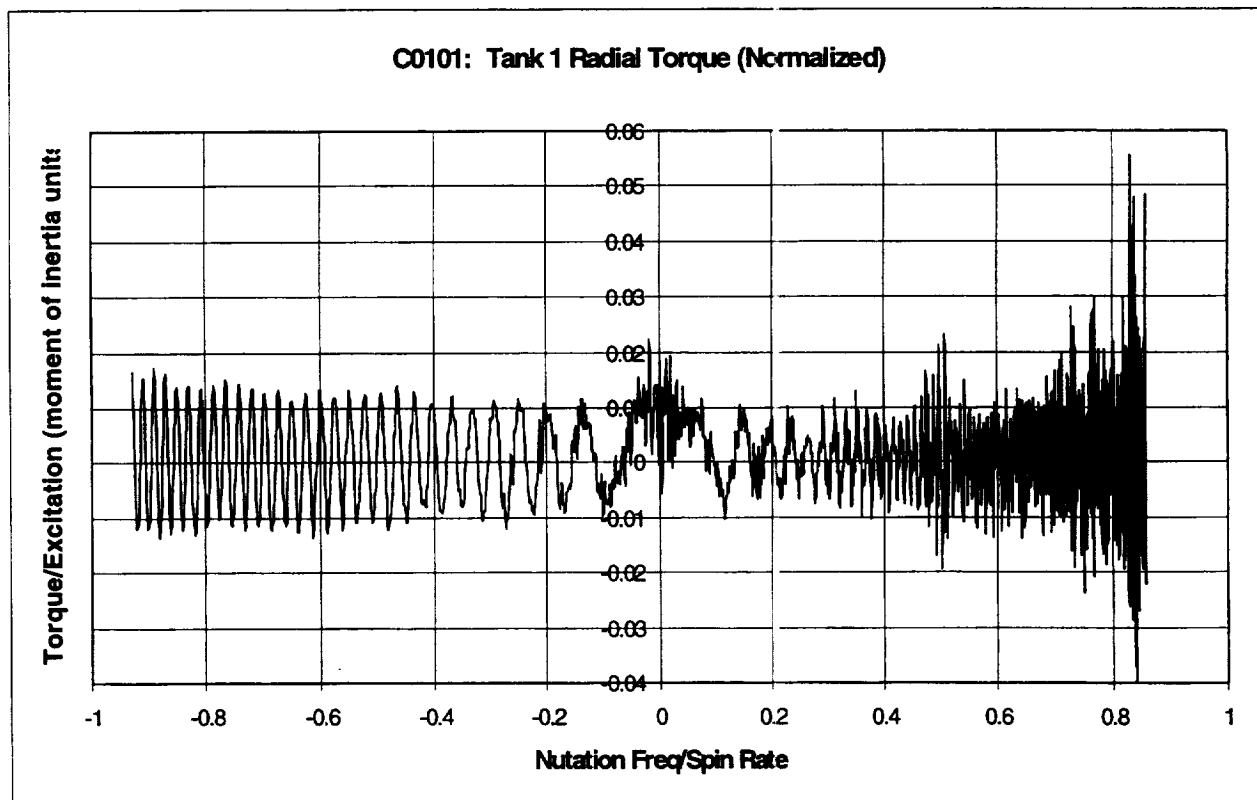
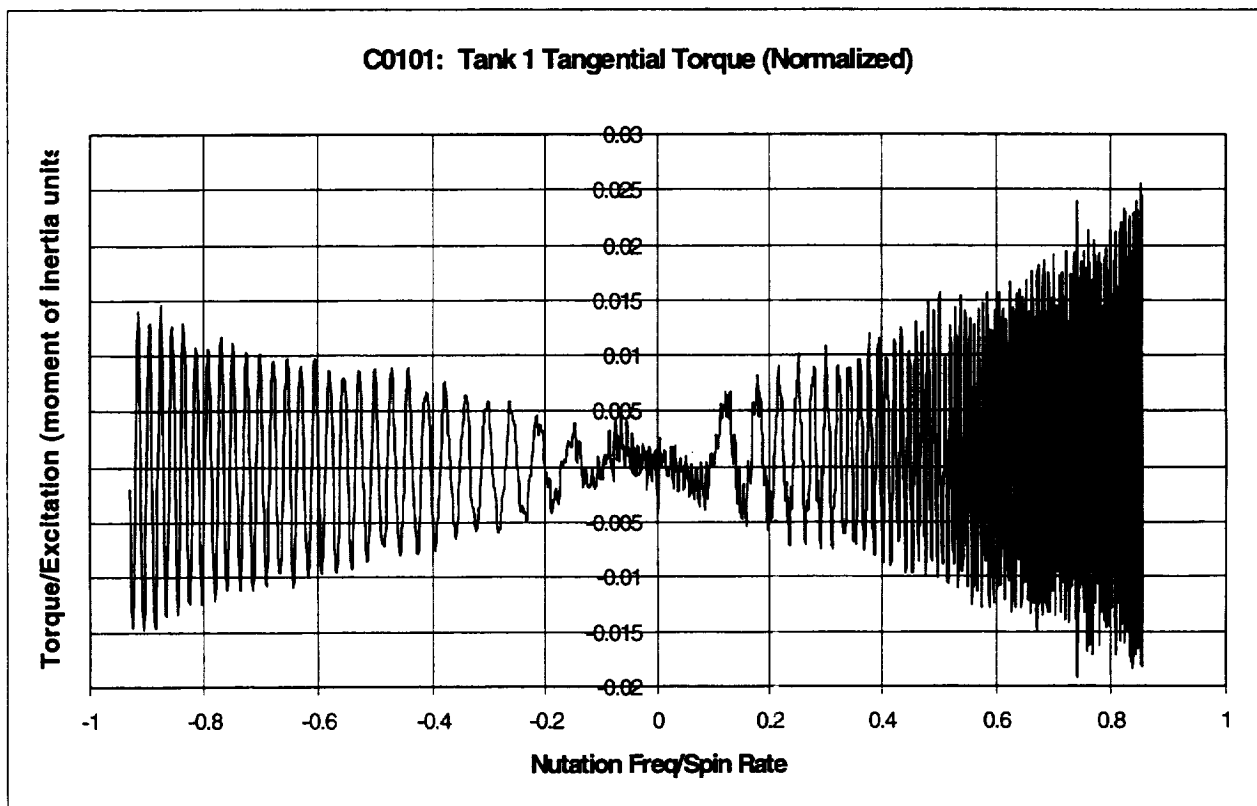


Tank 3 (B0101): concluded

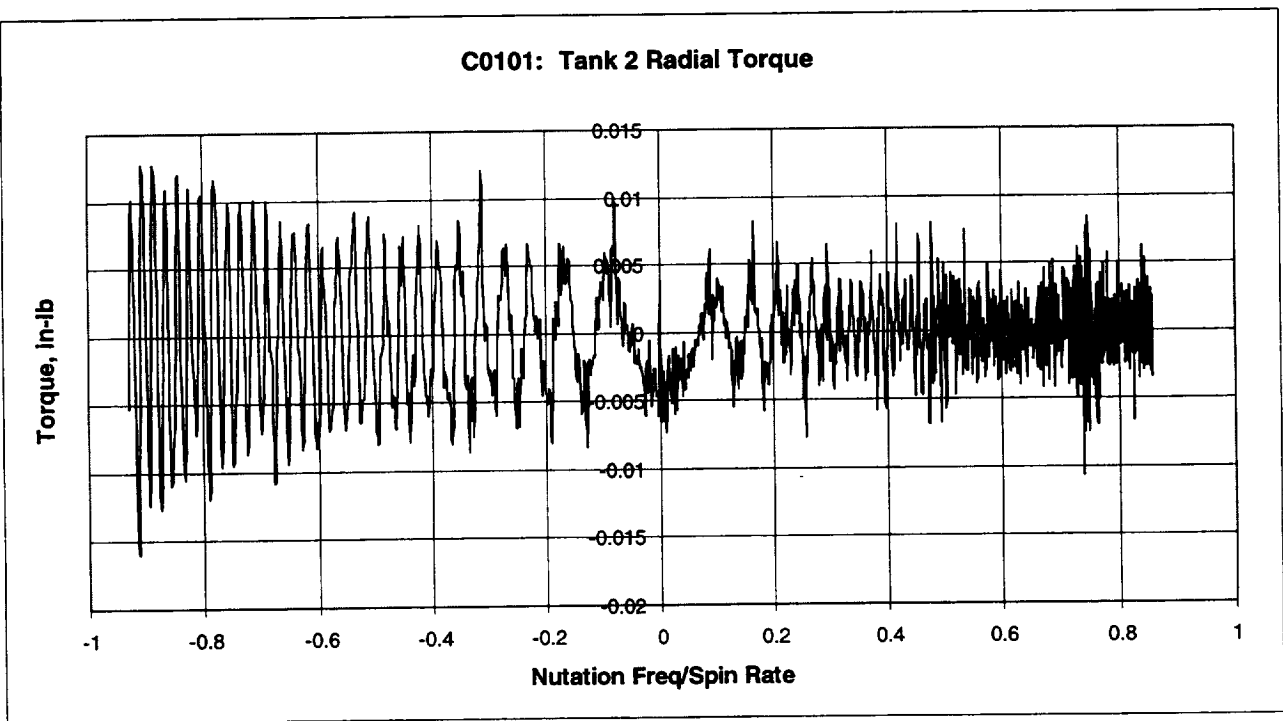
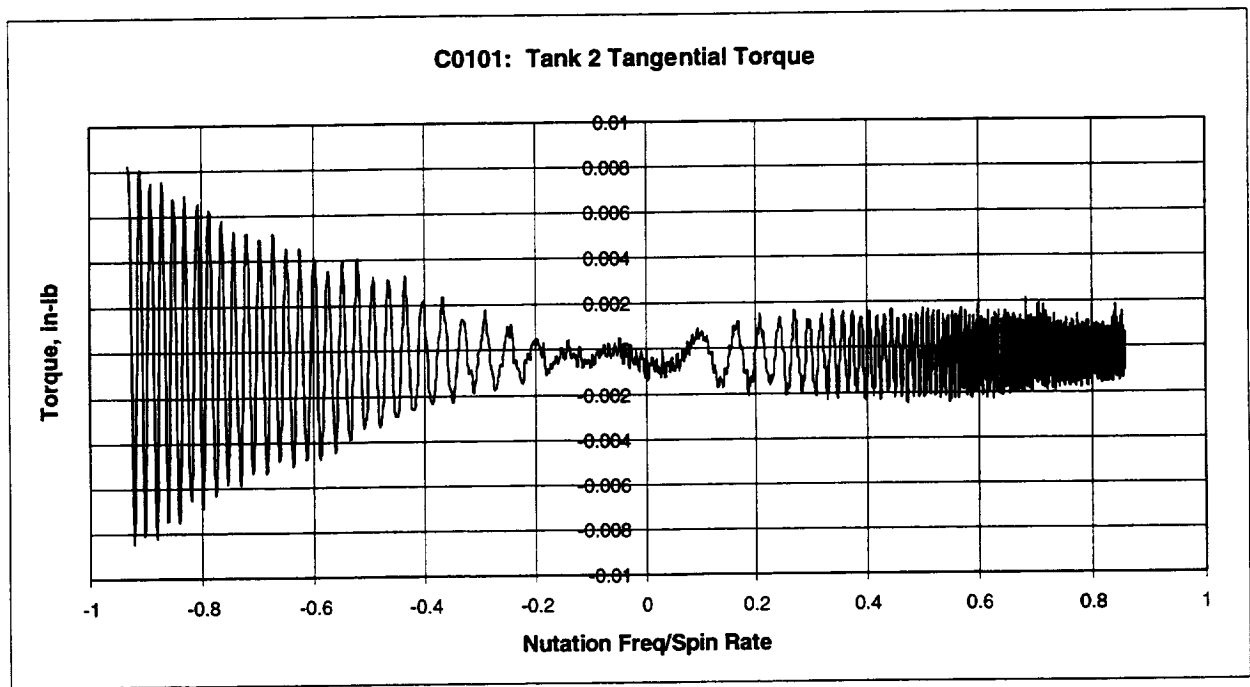


C0101: 14.1 RPM SWEEP TESTS - TANK SET C, CYLINDRICAL TANKS 1 AND 2**Nutation Sweep Range: 12.0 rpm \rightarrow 0 \rightarrow 12.8 rpm****Tank 1: PMD - 1/3 Full - Liquid Viscosity = 1 cp**

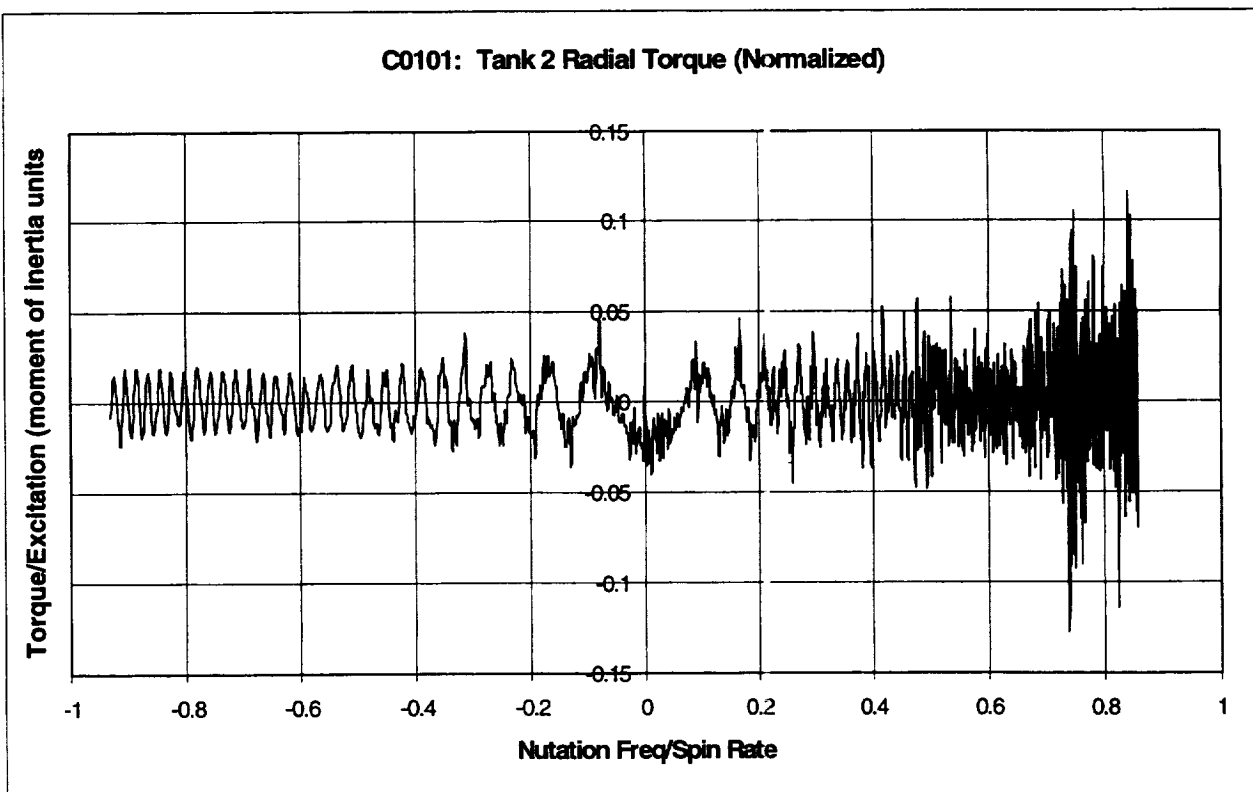
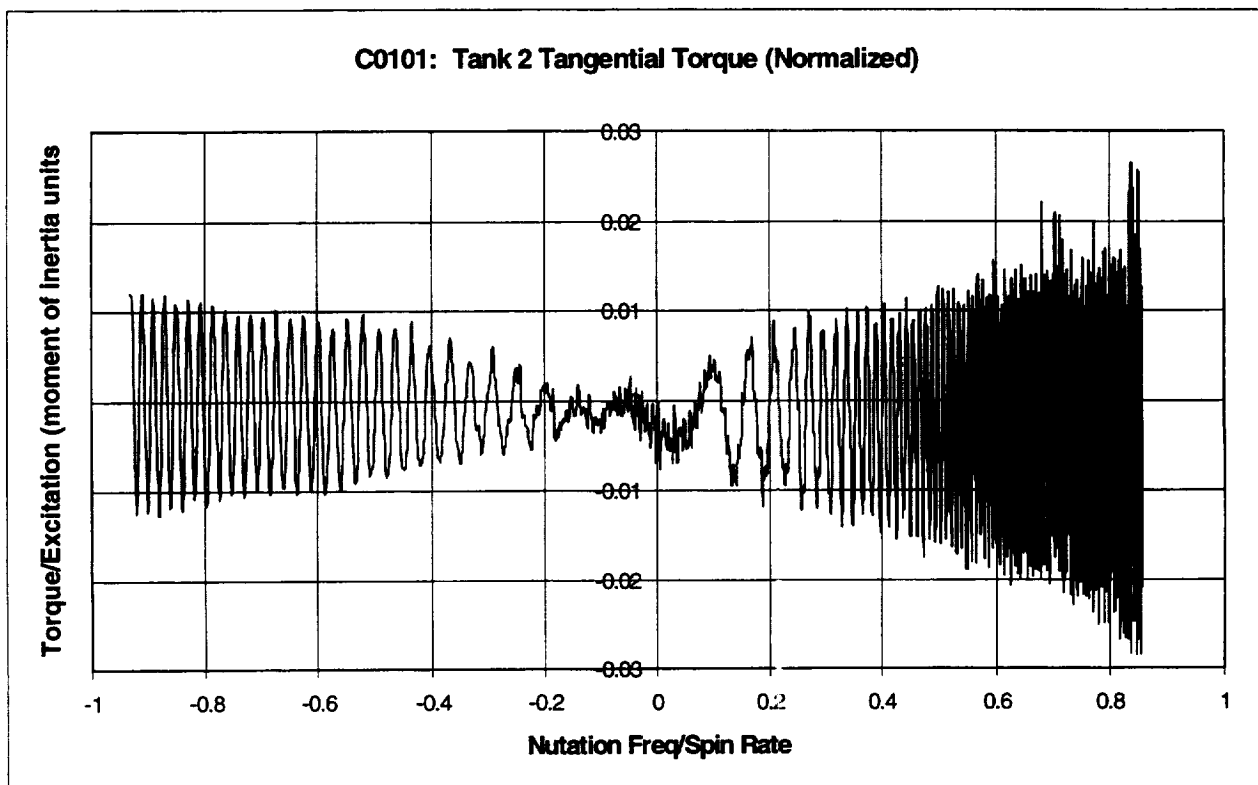
Tank 1 (C0101): concluded

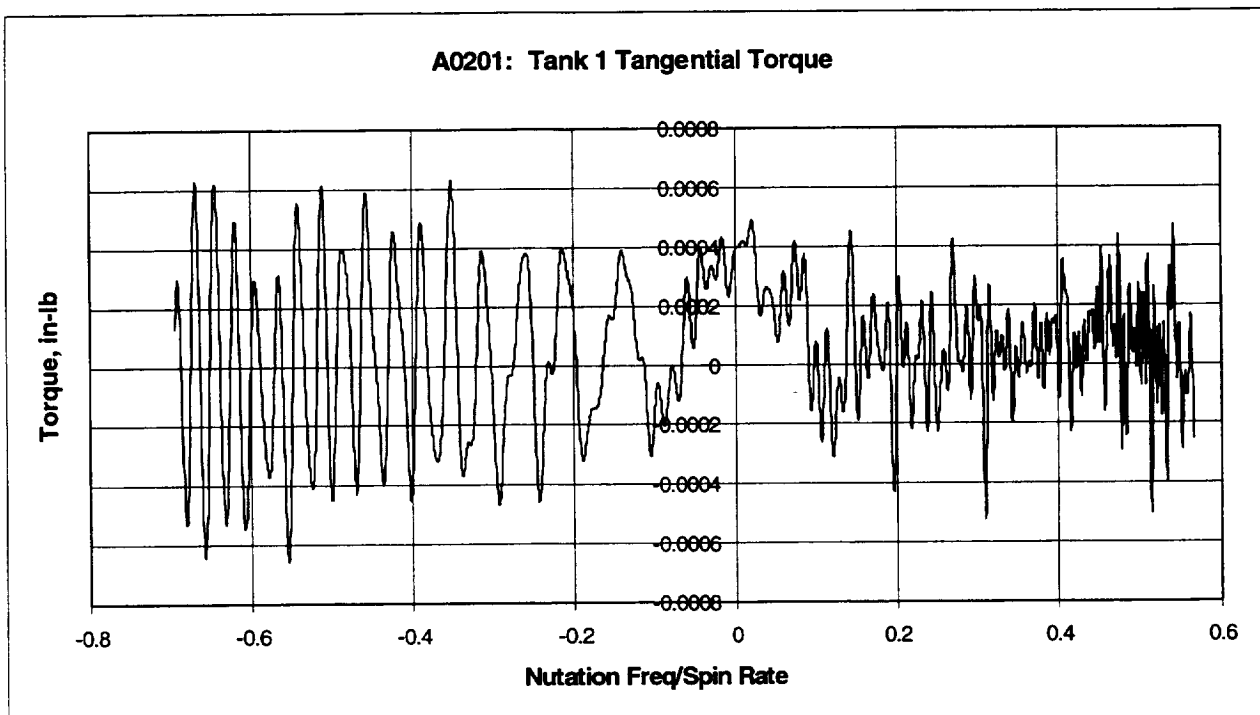
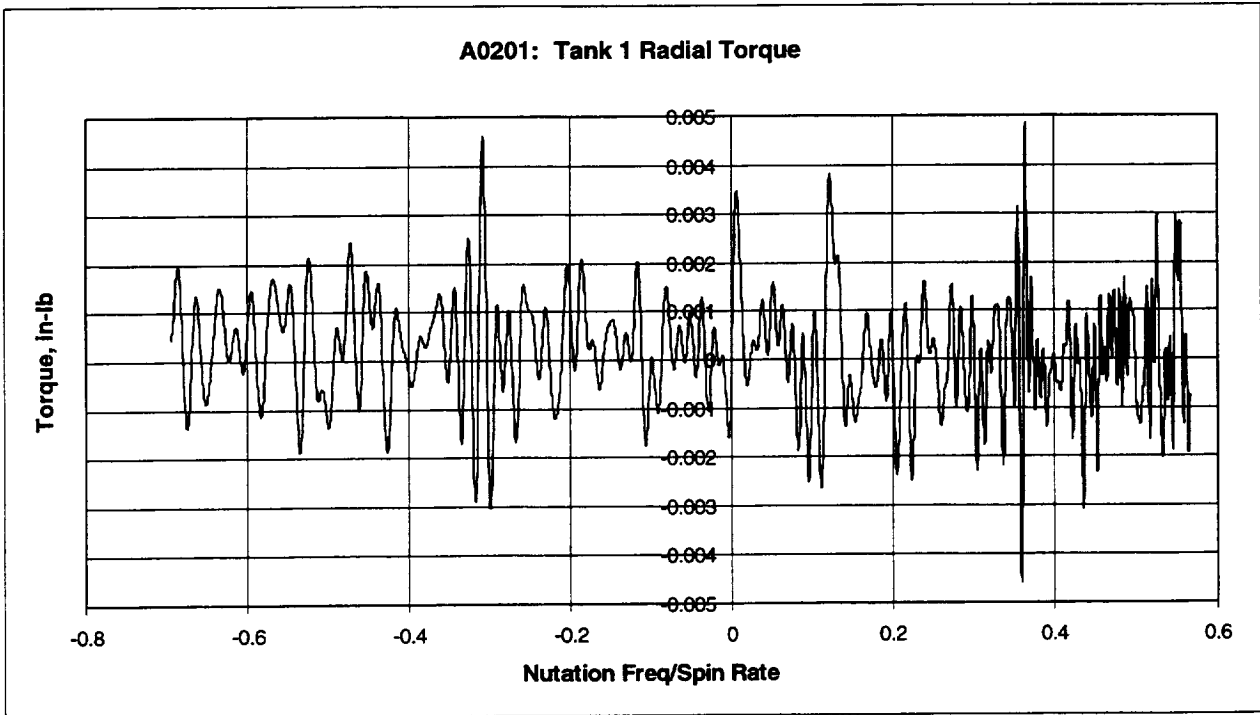


Tank 2 (C0101): PMD - 2/3 Full - Liquid Viscosity = 1 cp

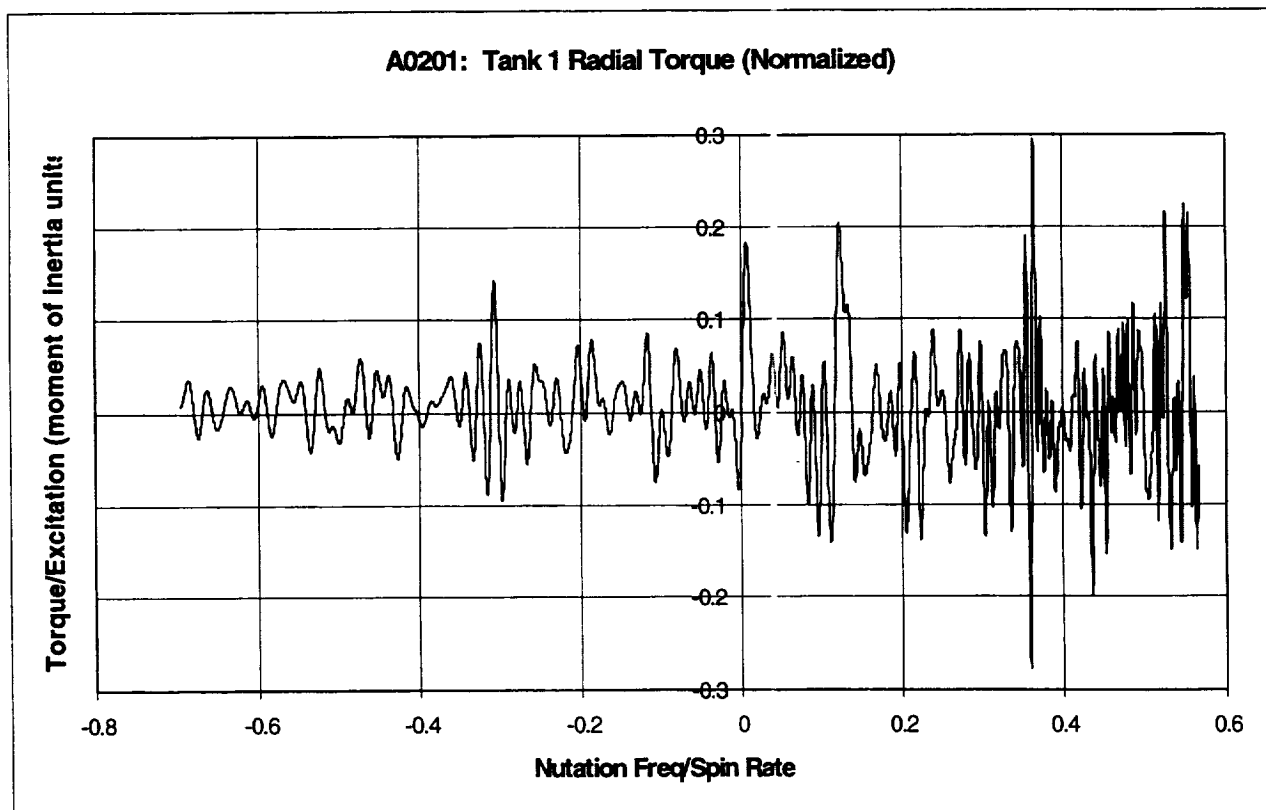
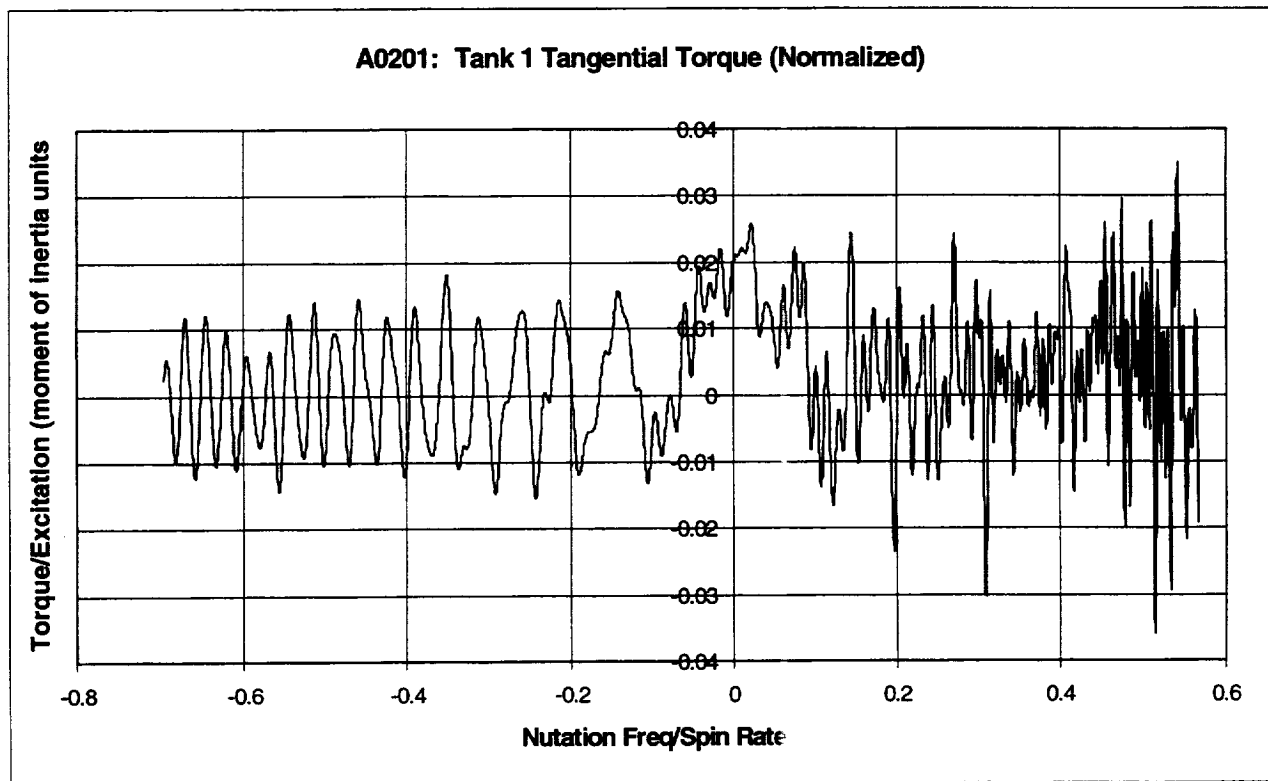


Tank 2 (C0101): concluded



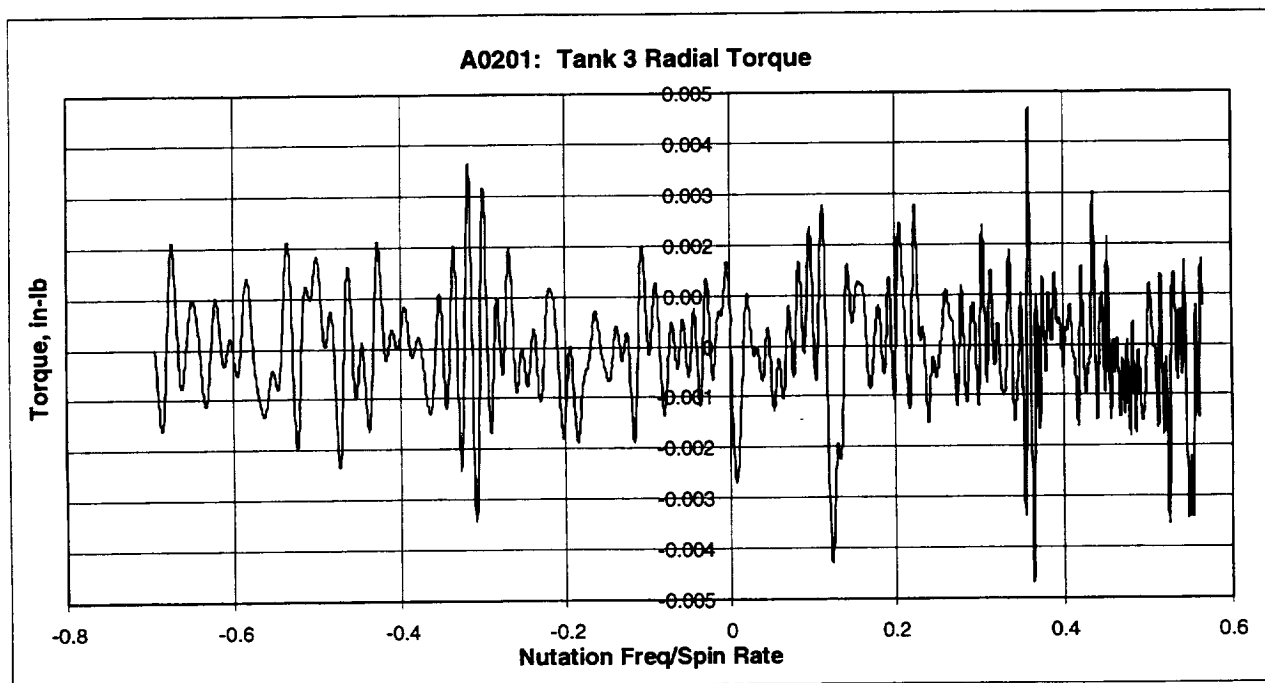
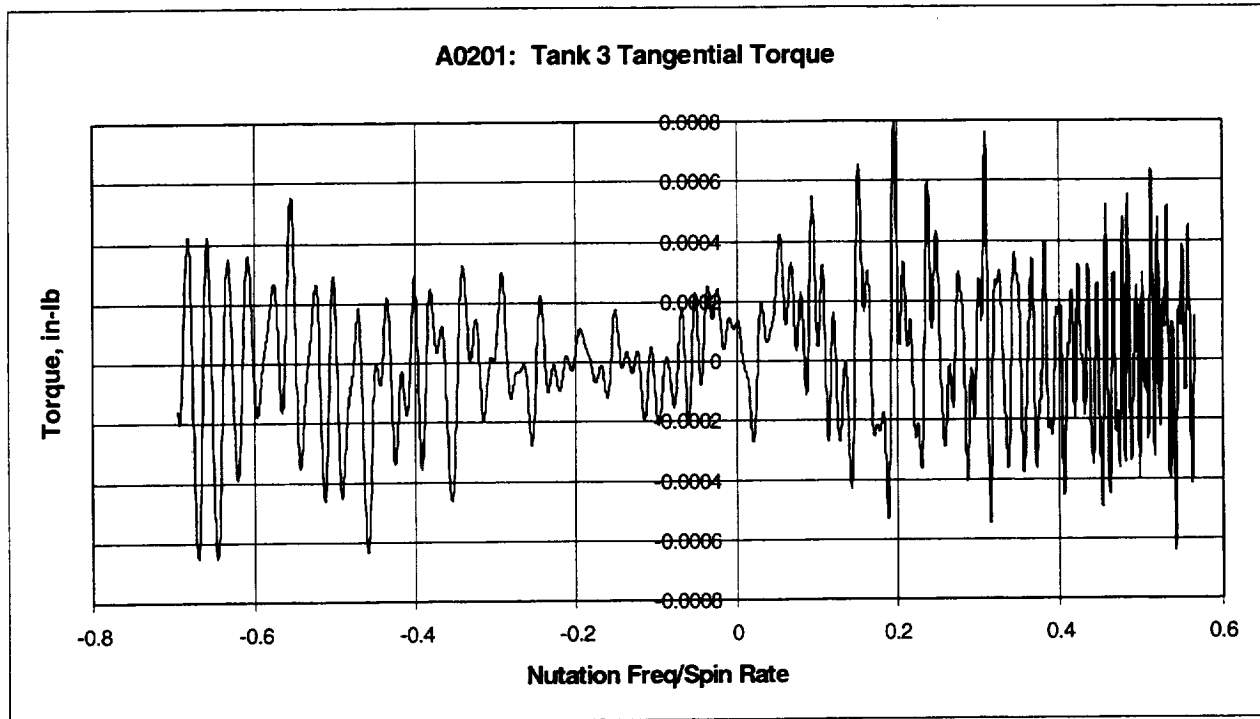
A0201: 4.5 RPM SWEEP TESTS - TANK SET A, CYLINDRICAL TANKS 1 AND 3**Nutation Sweep Range : 2.6 rpm \rightarrow 0 \rightarrow 3.1 rpm****Tank 1: 2/3 Full - Liquid Viscosity = 1 cp**

Tank 1 (A0201): concluded

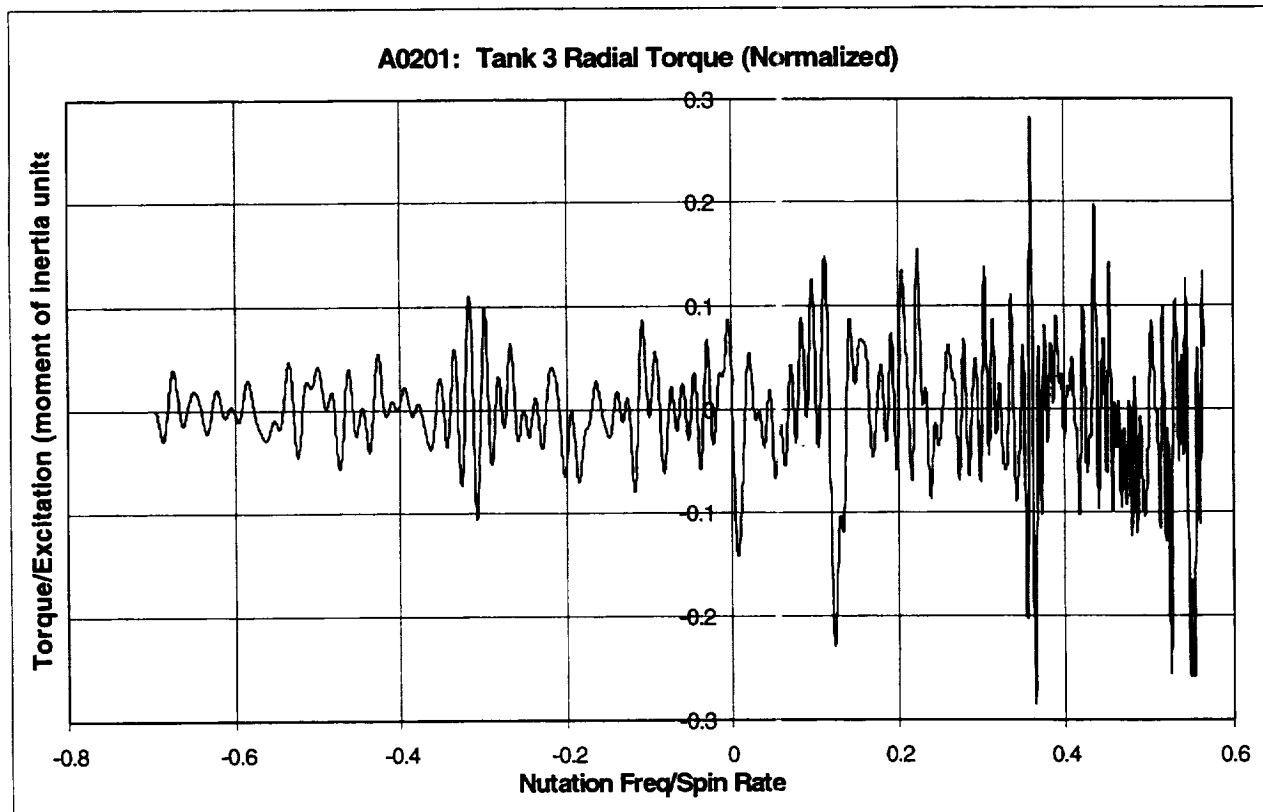
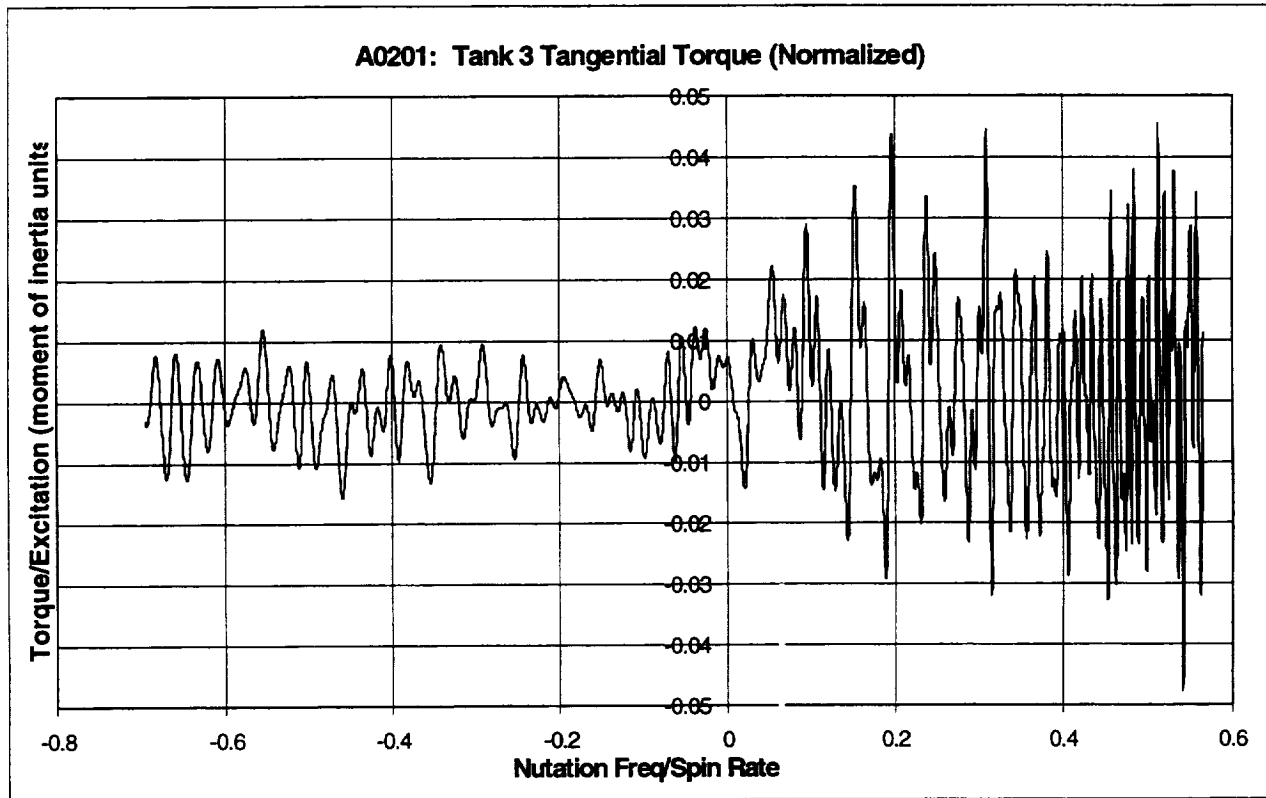


A0201: SWEEP TESTS AT 4.5 RPM - TANK SET A, CYLINDRICAL TANKS 1 AND 3Nutation Sweep Range: 2.6 rpm \rightarrow 0 \rightarrow 3.1 rpm

Tank 3: 2/3 Full - Liquid Viscosity = 10 cp

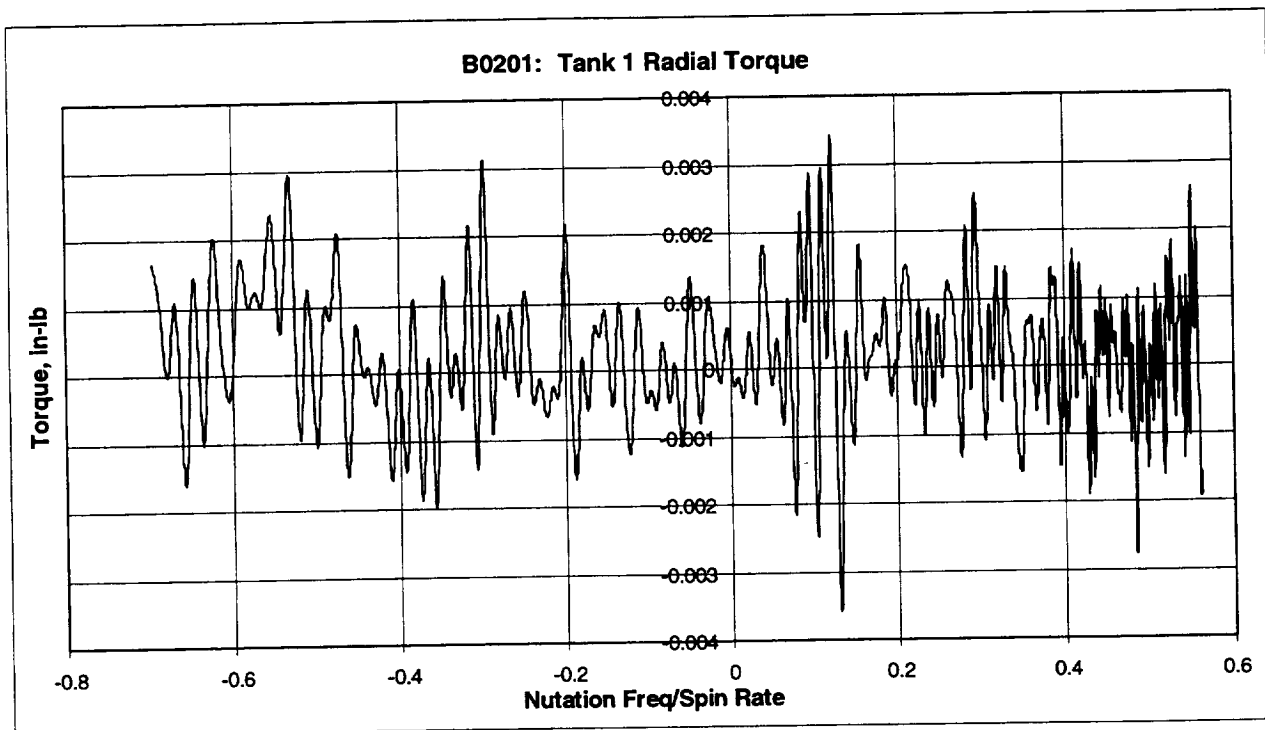
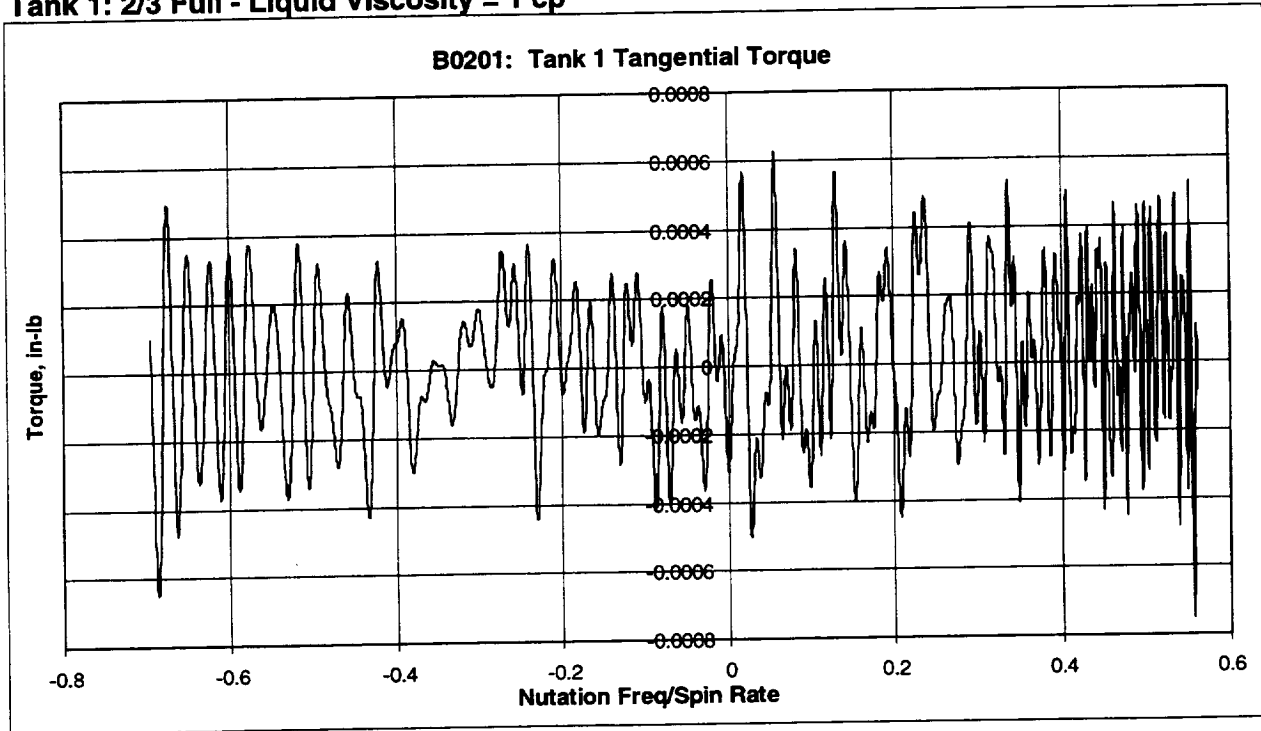


Tank 3 (A0201): concluded

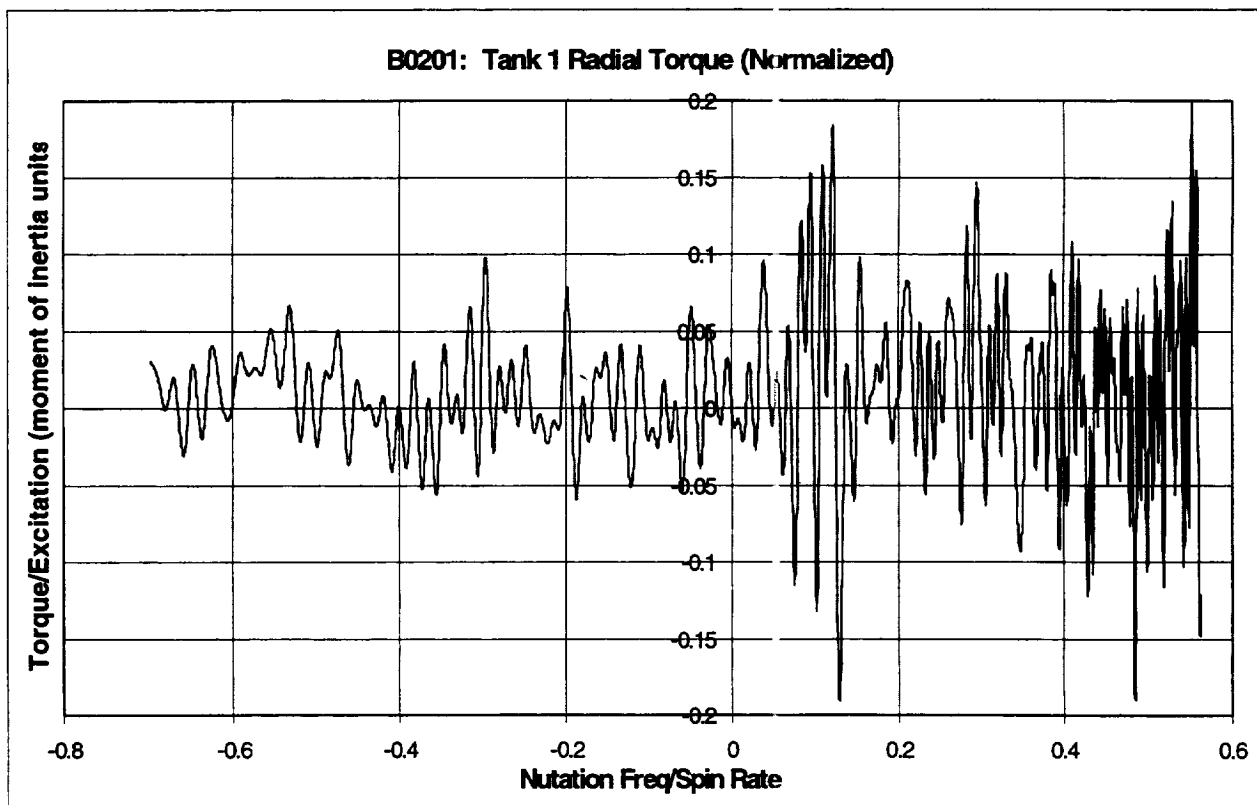
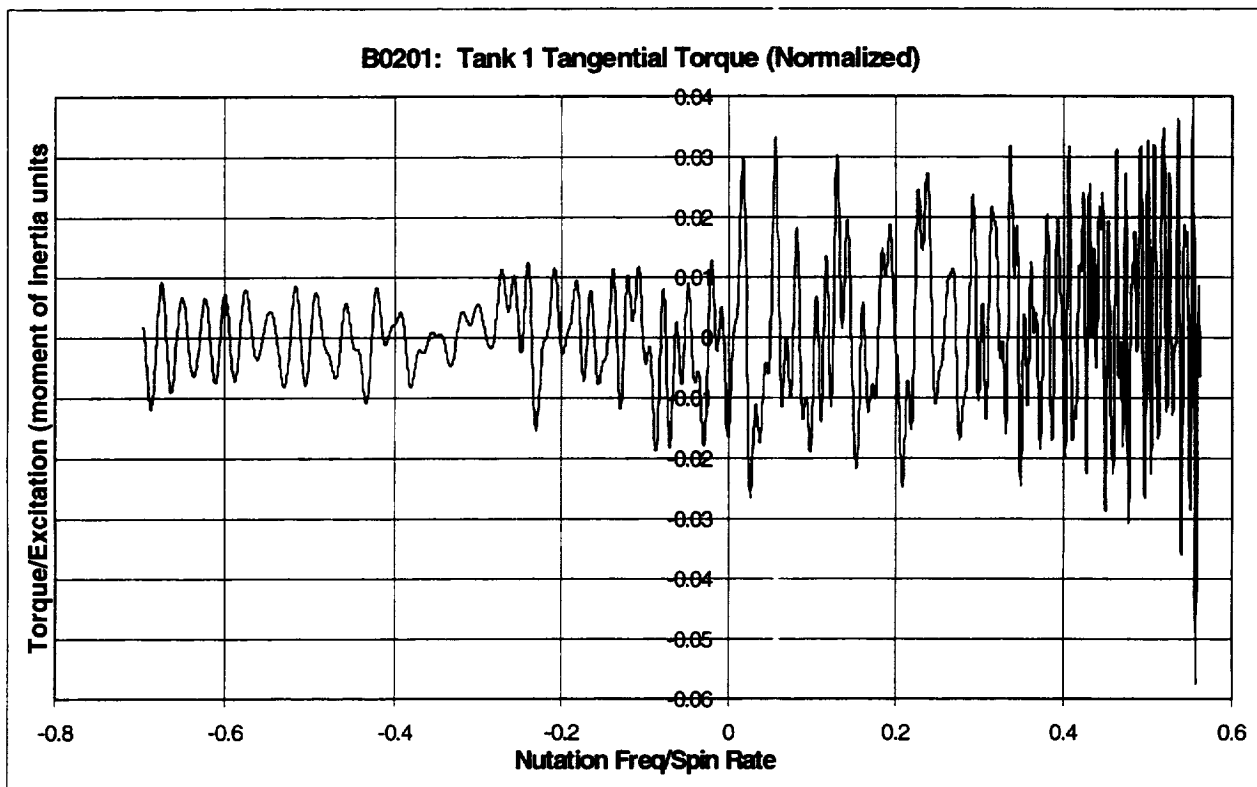


B0201: 4.5 RPM SWEEP TESTS - TANK SET B, CYLINDRICAL TANKS 1 AND 3Nutation Sweep Range: 2.6 rpm \rightarrow 0 \rightarrow 3.1 rpm

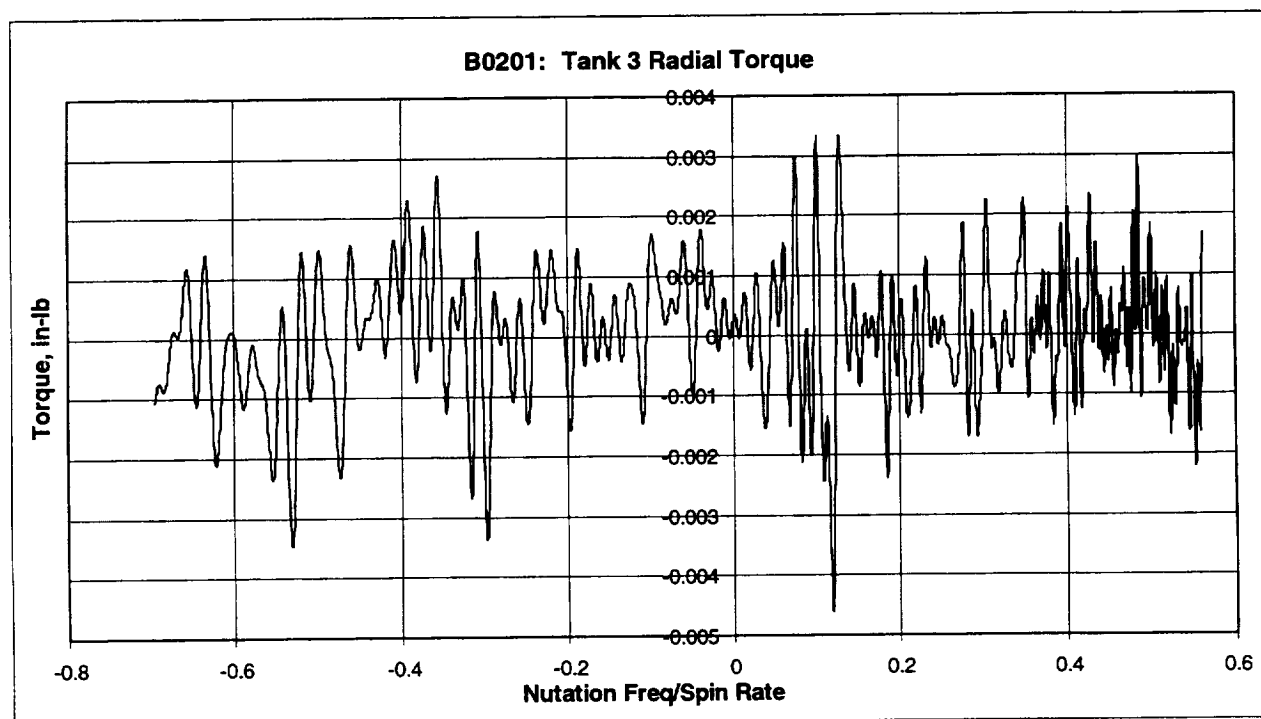
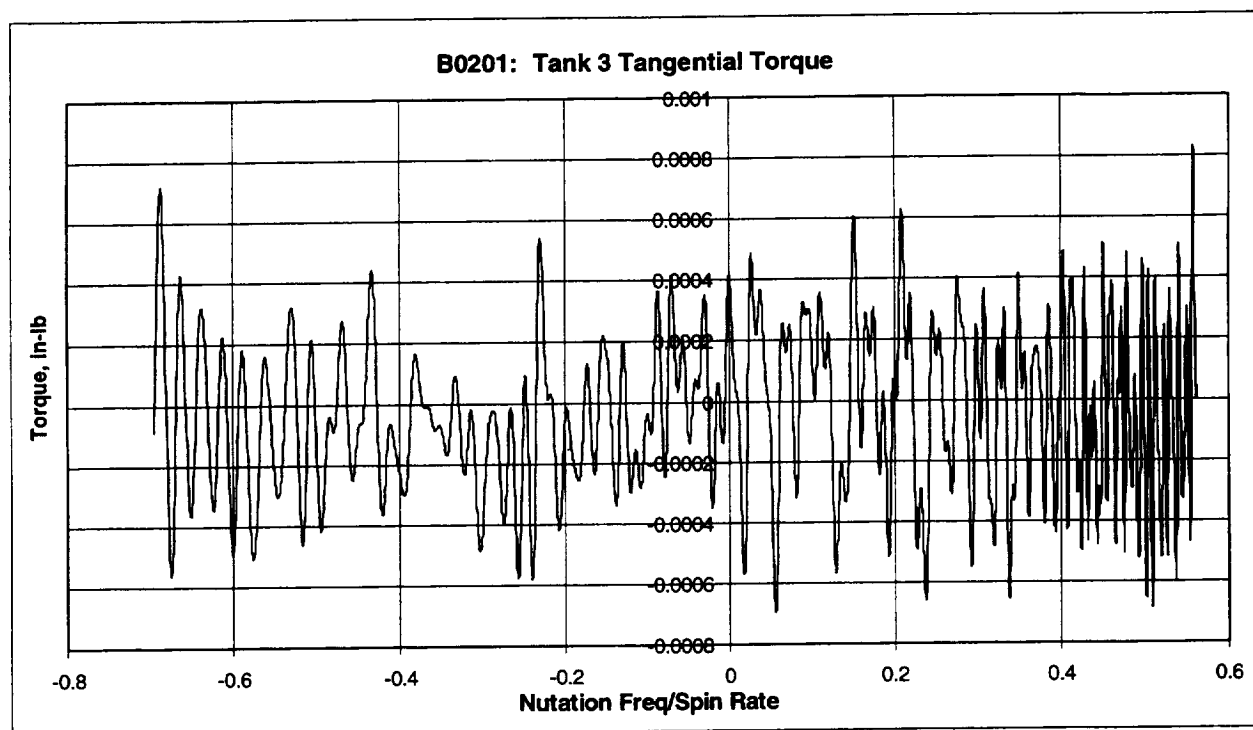
Tank 1: 2/3 Full - Liquid Viscosity = 1 cp



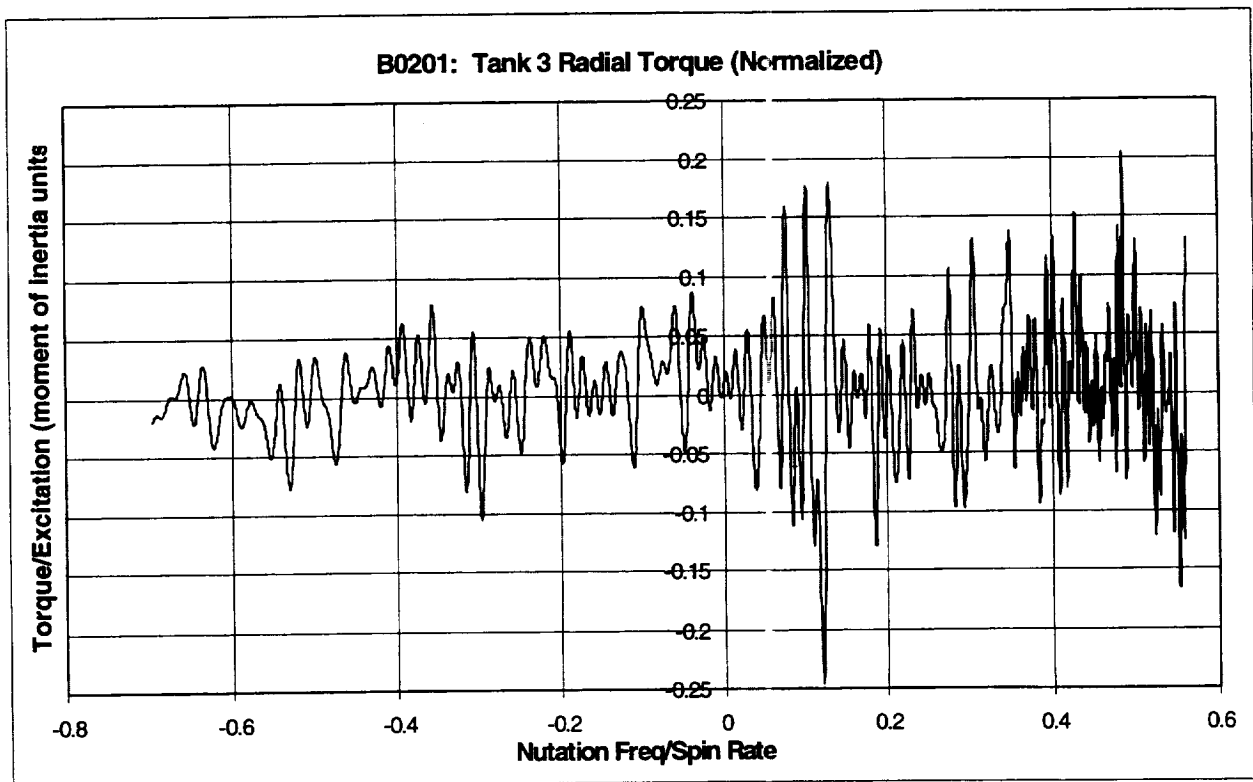
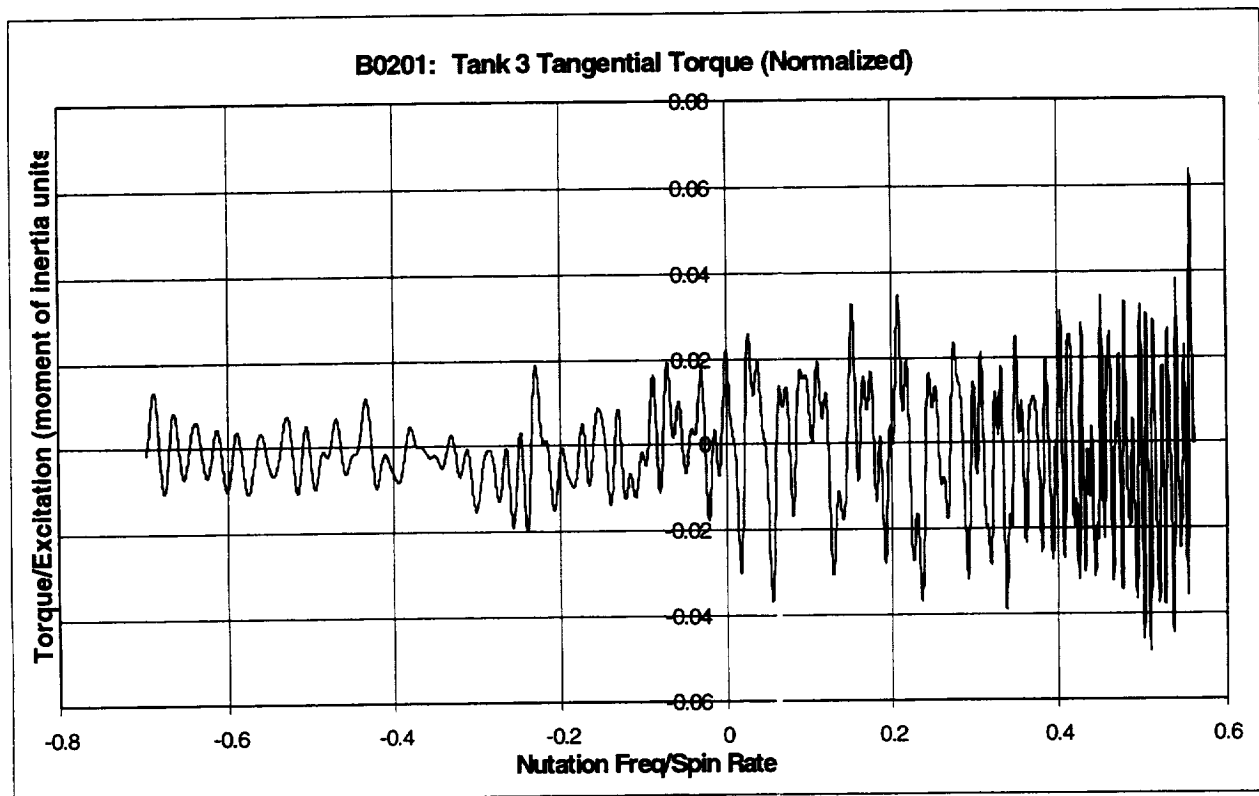
Tank 1 (B0201): concluded

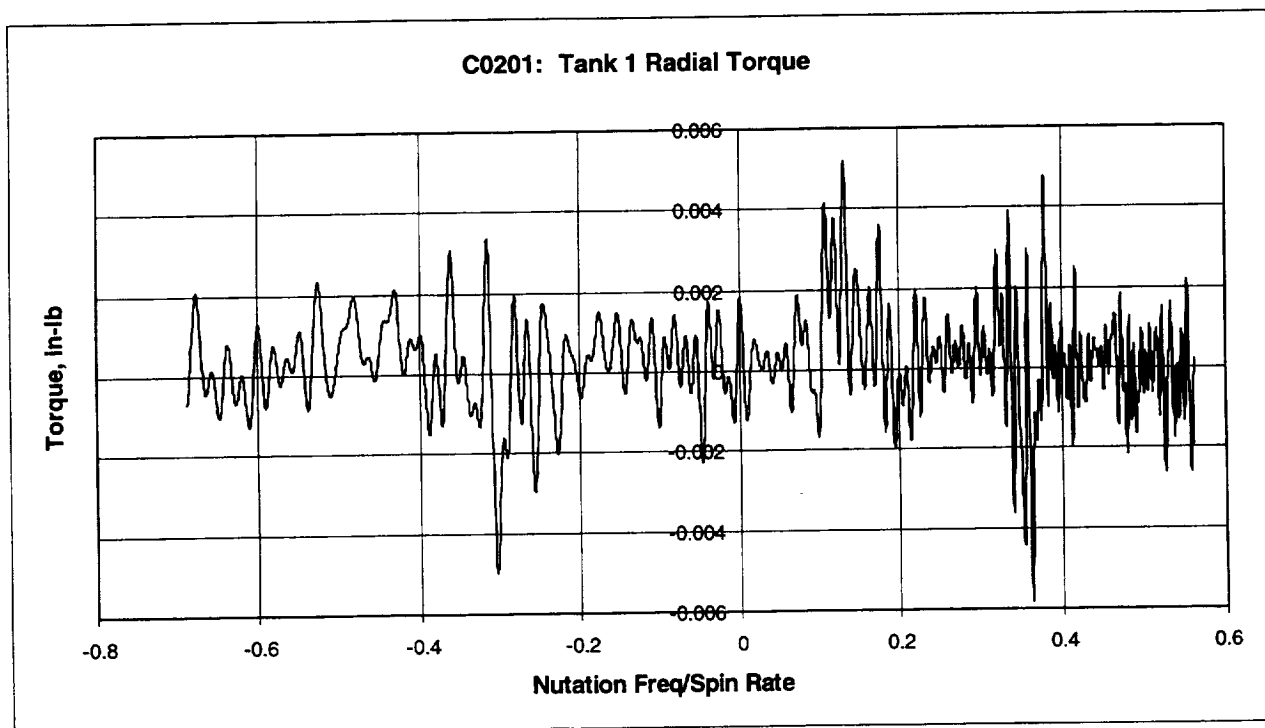
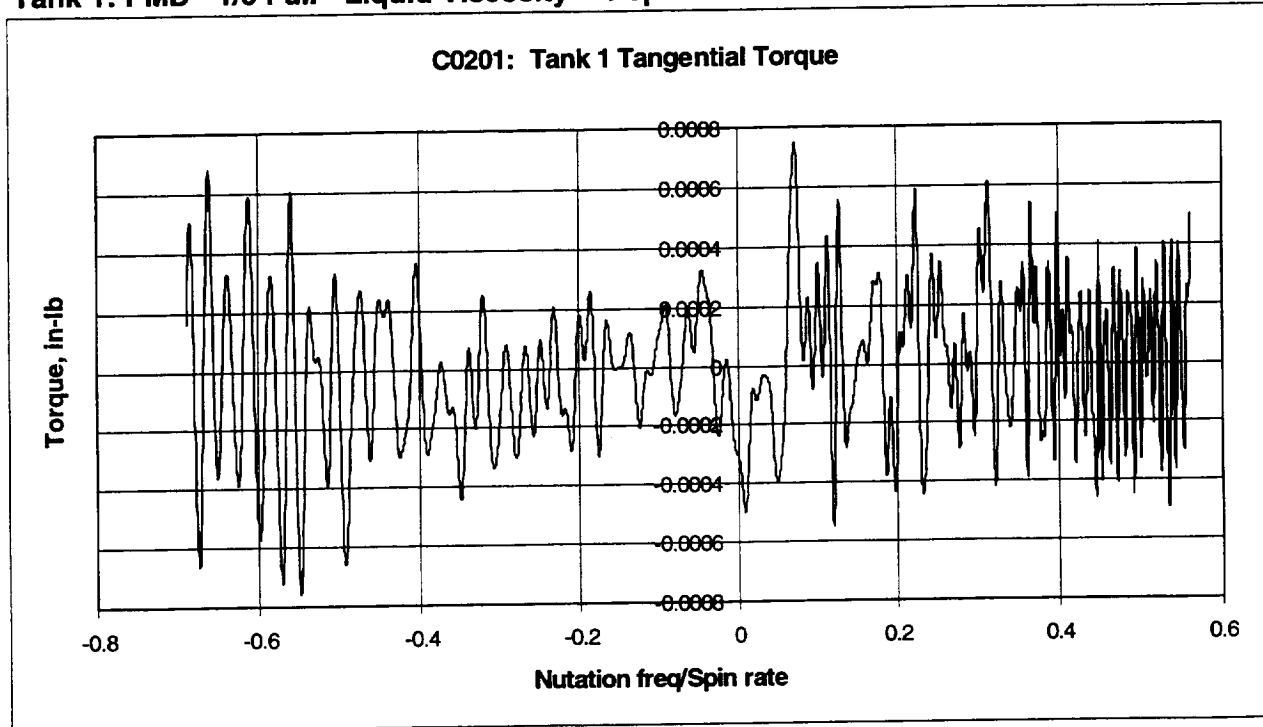


Tank 3 (B0201): 2/3 Full - Liquid Viscosity = 10 cp

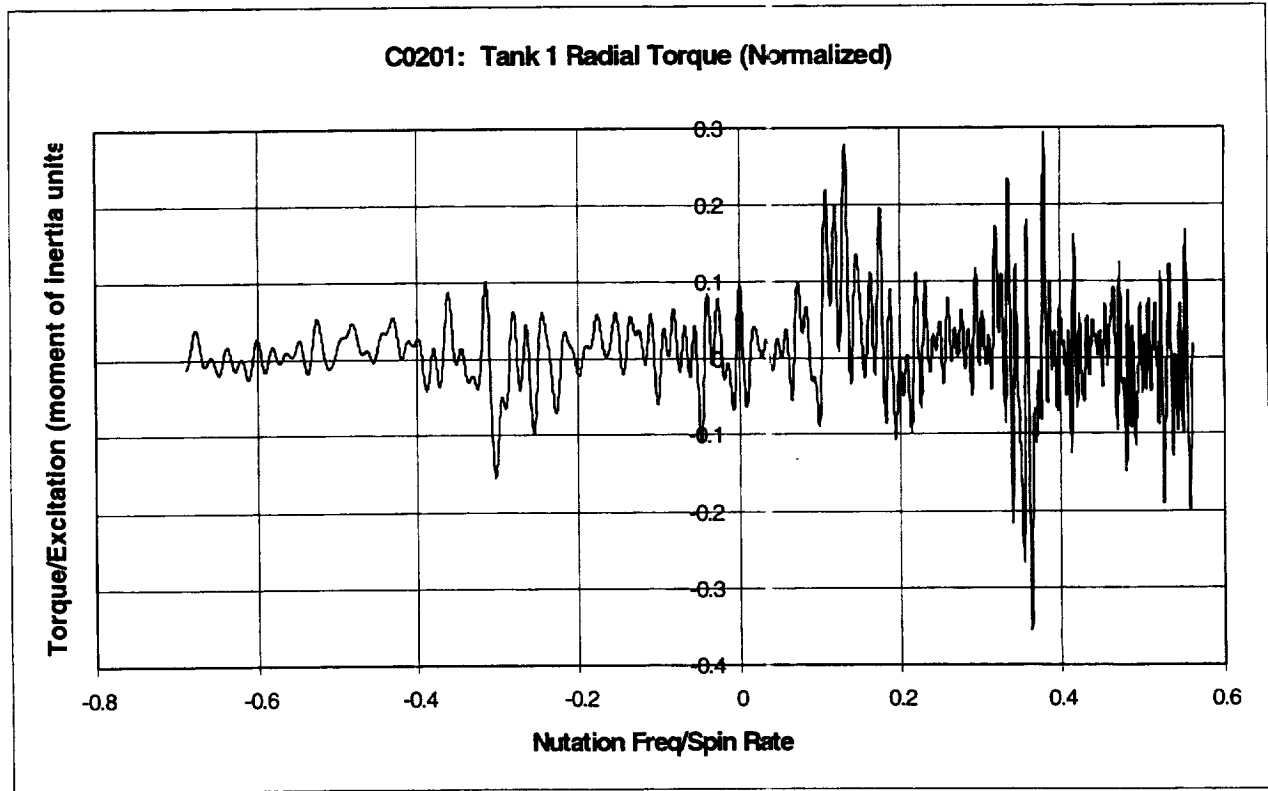
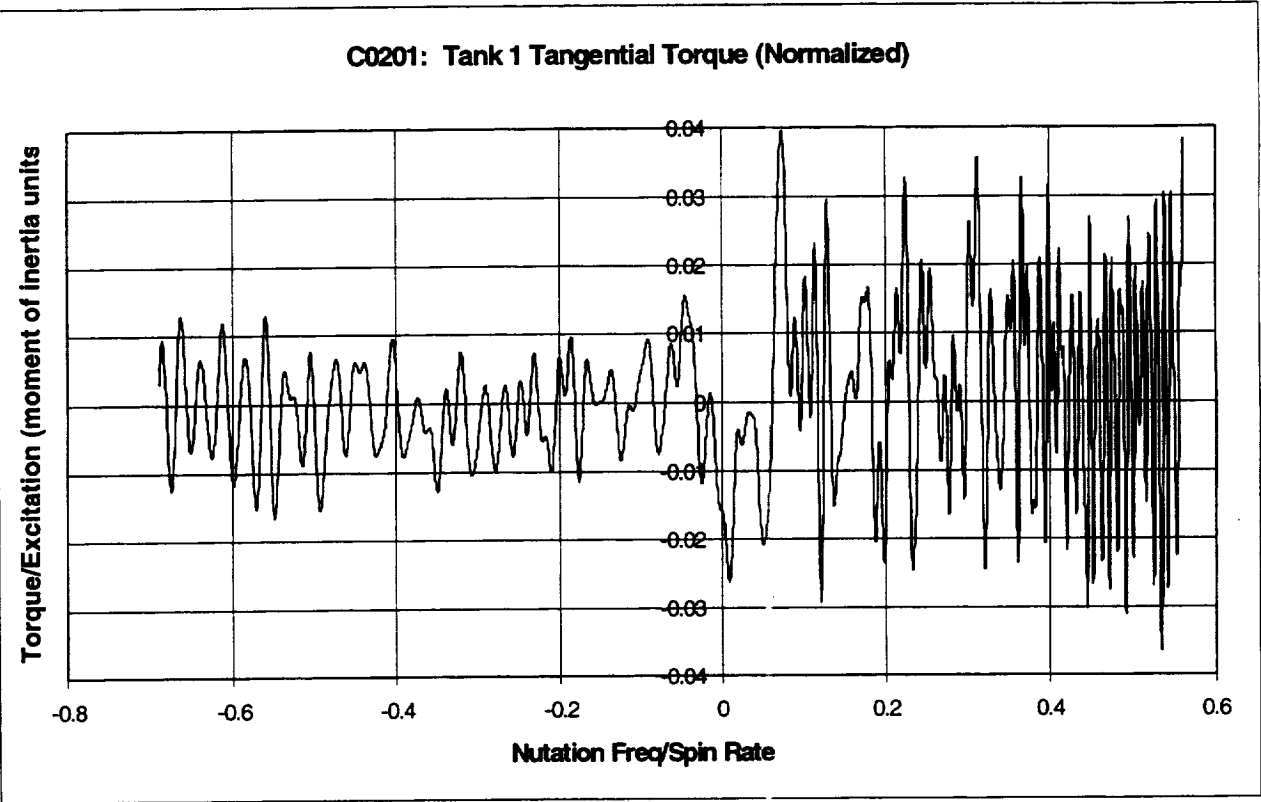


Tank 3 (B0201): concluded

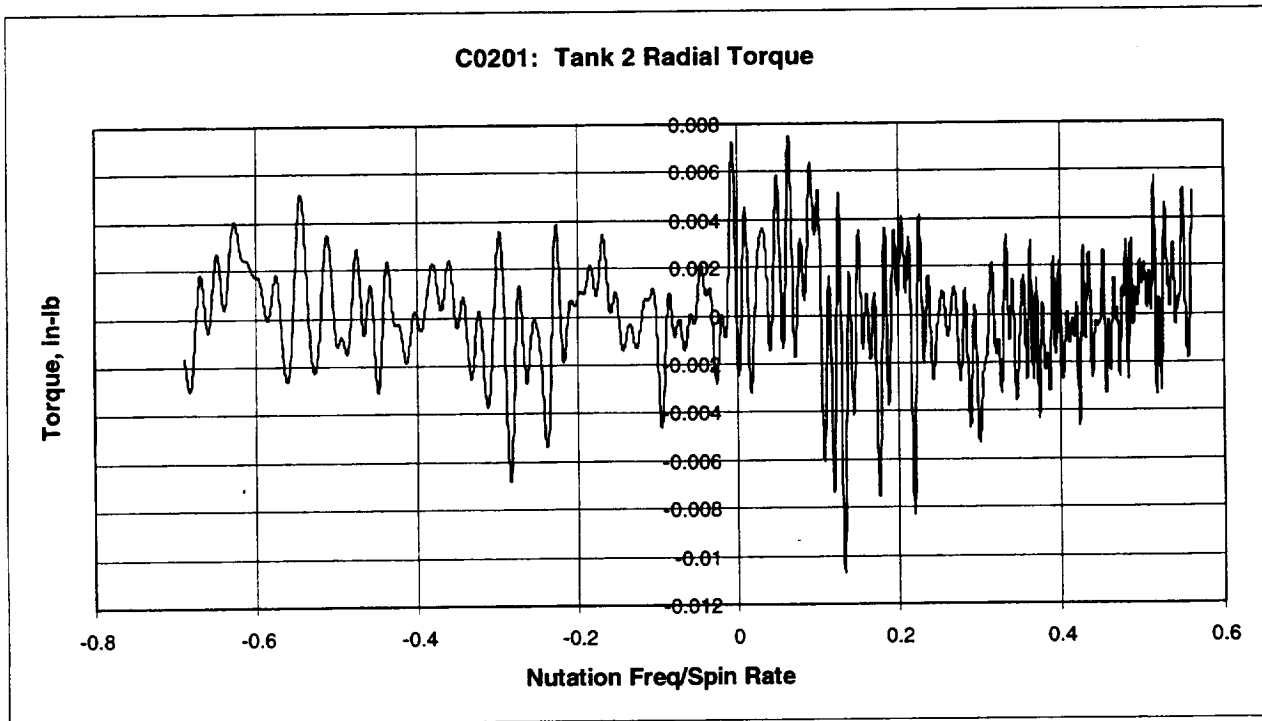
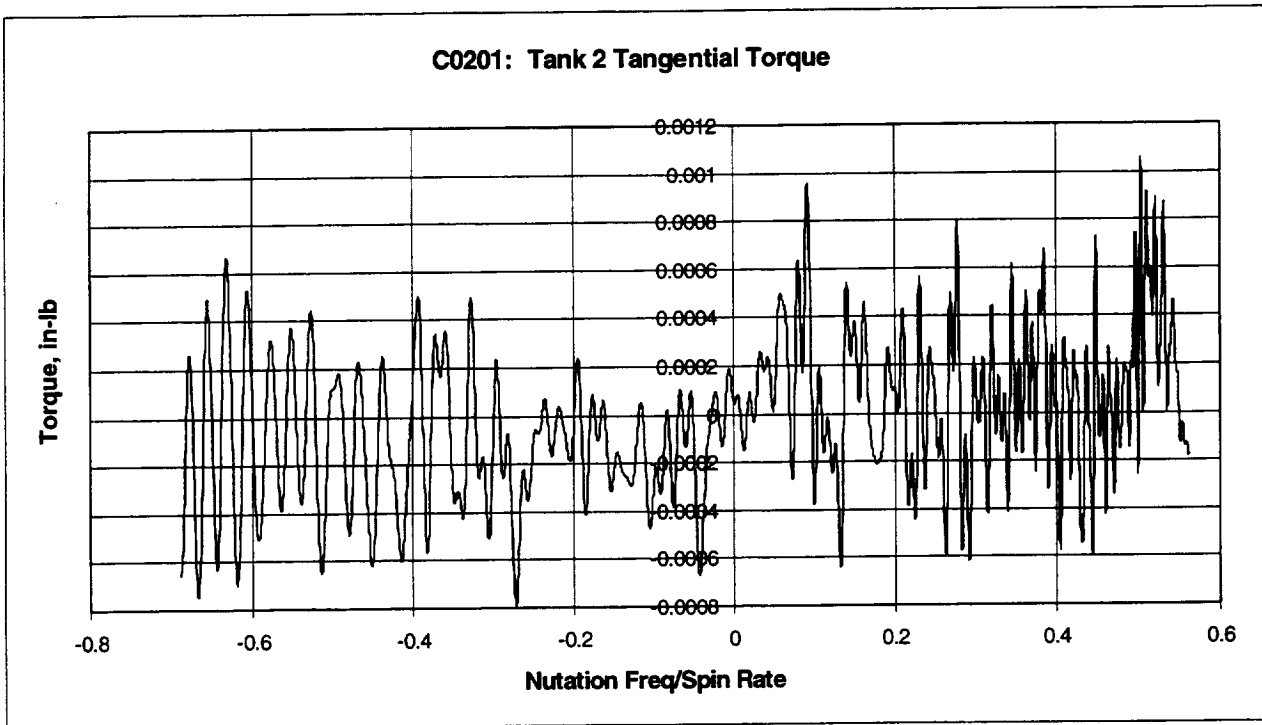


C0201: SWEEP TESTS AT 4.5 RPM - TANK SET C, CYLINDRICAL TANKS 1 AND 2**Nutation Sweep Range: 2.6 rpm \rightarrow 0 \rightarrow 3.1 rpm****Tank 1: PMD - 1/3 Full - Liquid Viscosity = 1 cp**

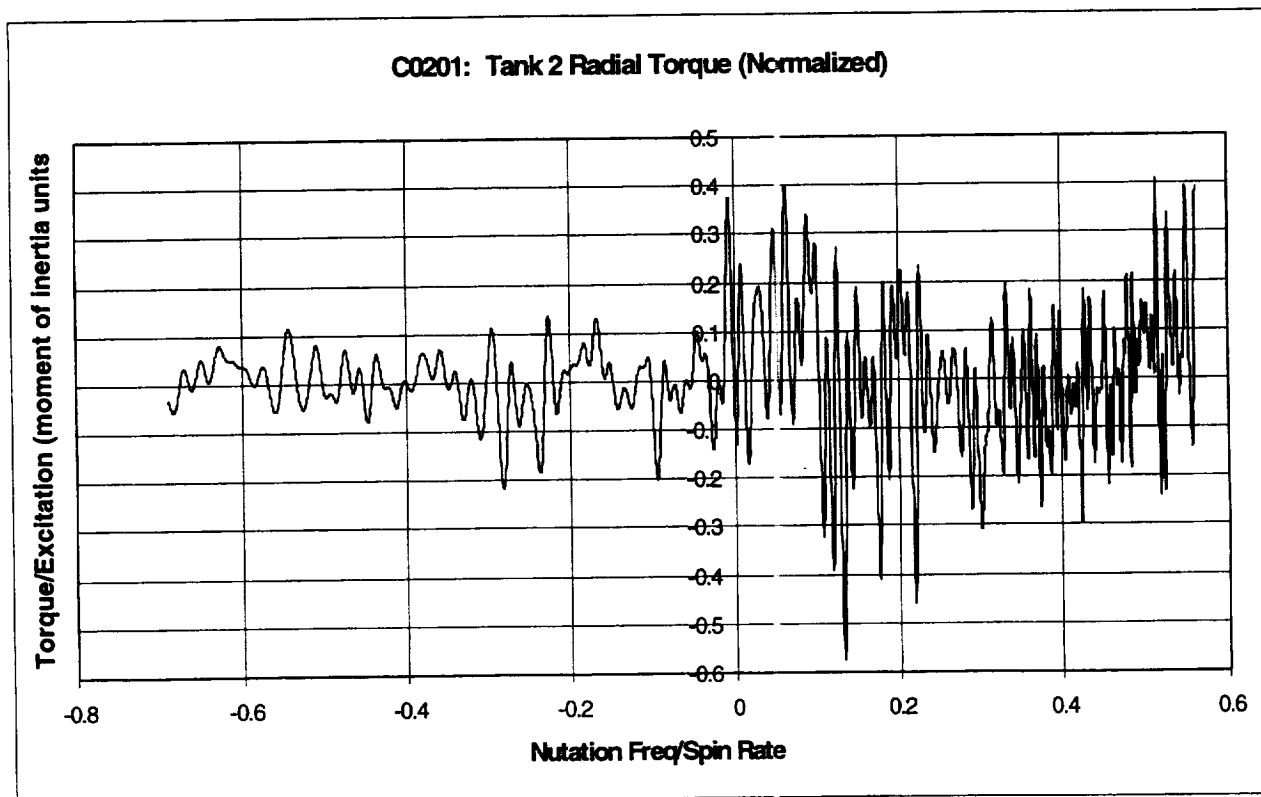
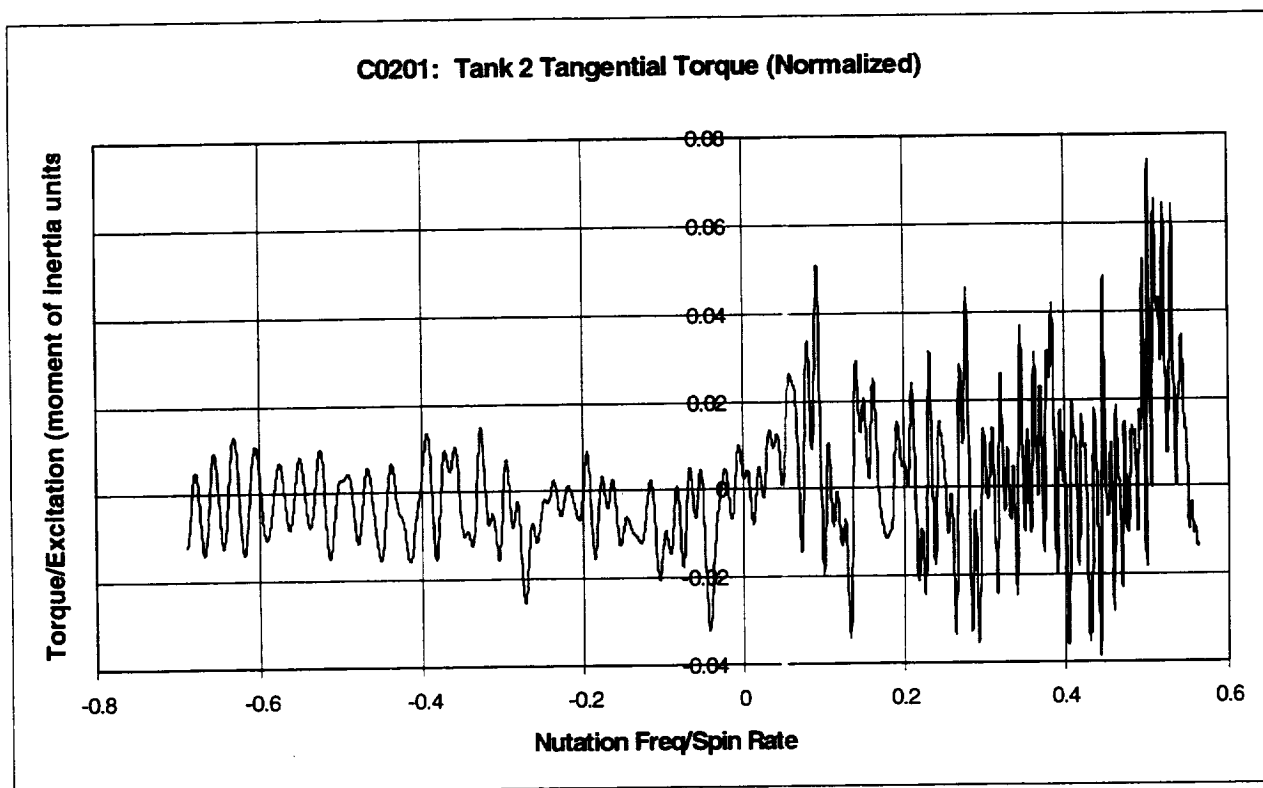
Tank 1 (C0201): concluded



Tank 2 (C0201): PMD - 2/3 Full - Liquid Viscosity = 1 cp



Tank 2 (C0201): concluded



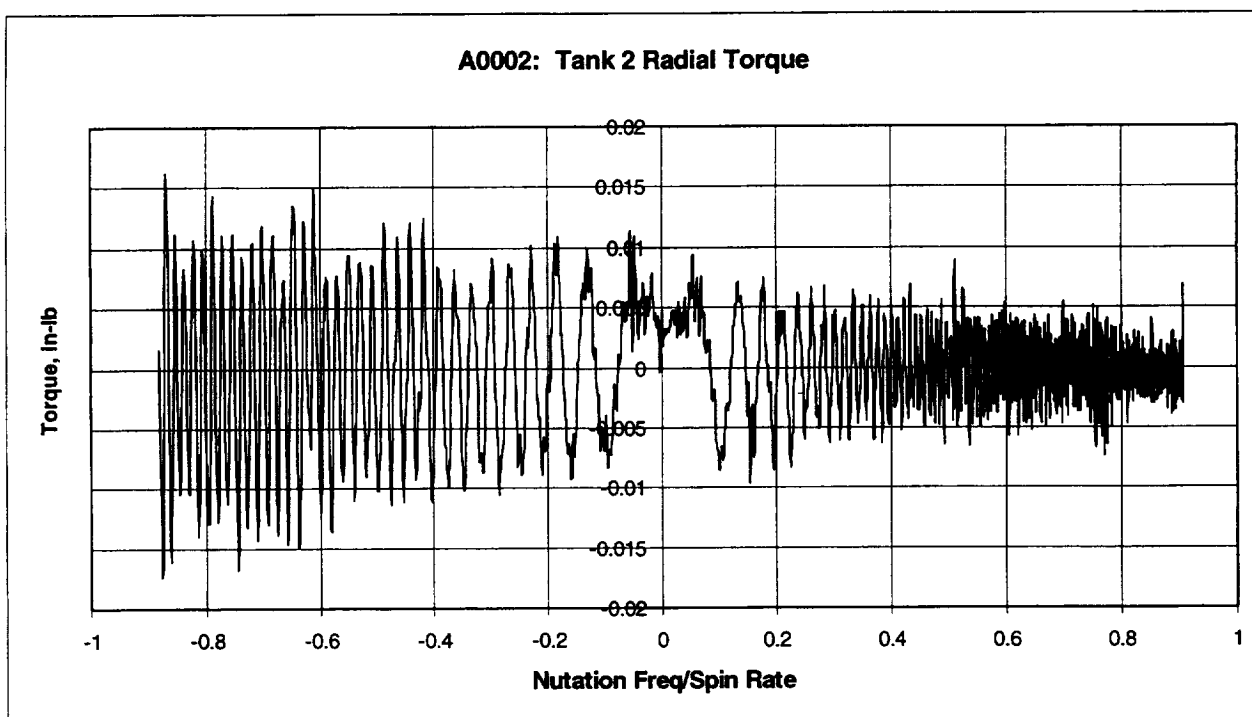
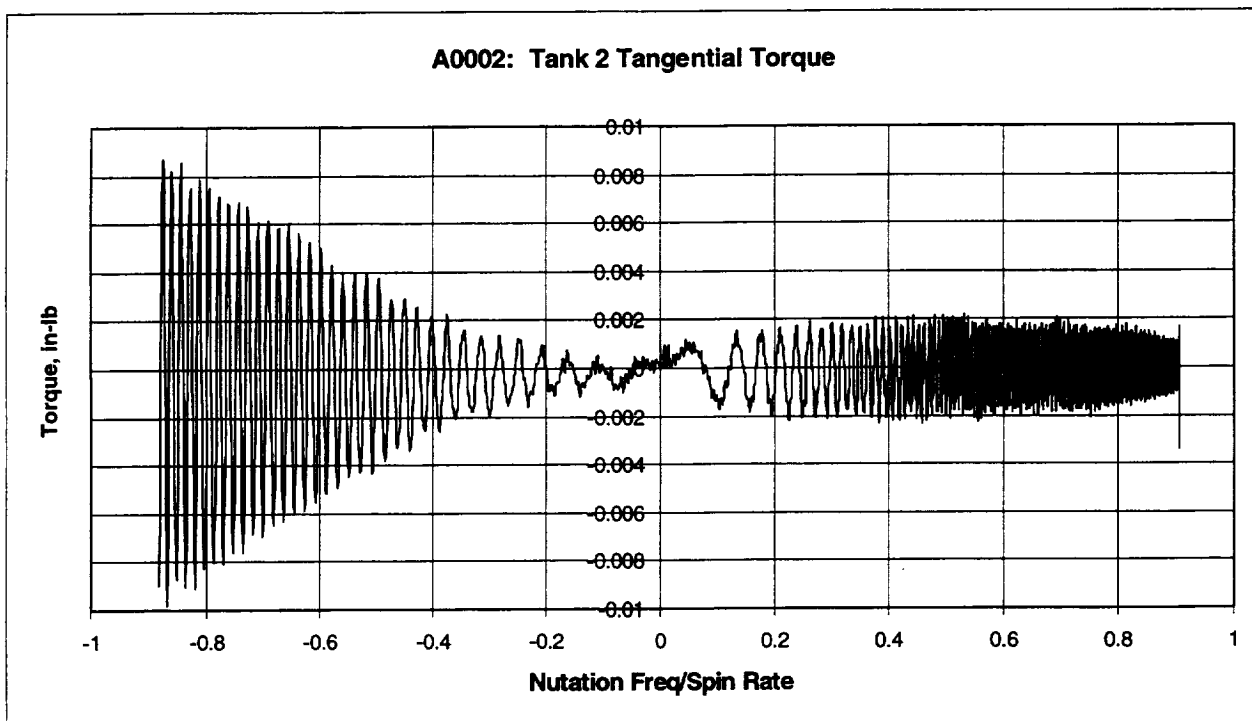
APPENDIX D

**Summary of Radial and Tangential Torque
Histories for Spherical Tanks**

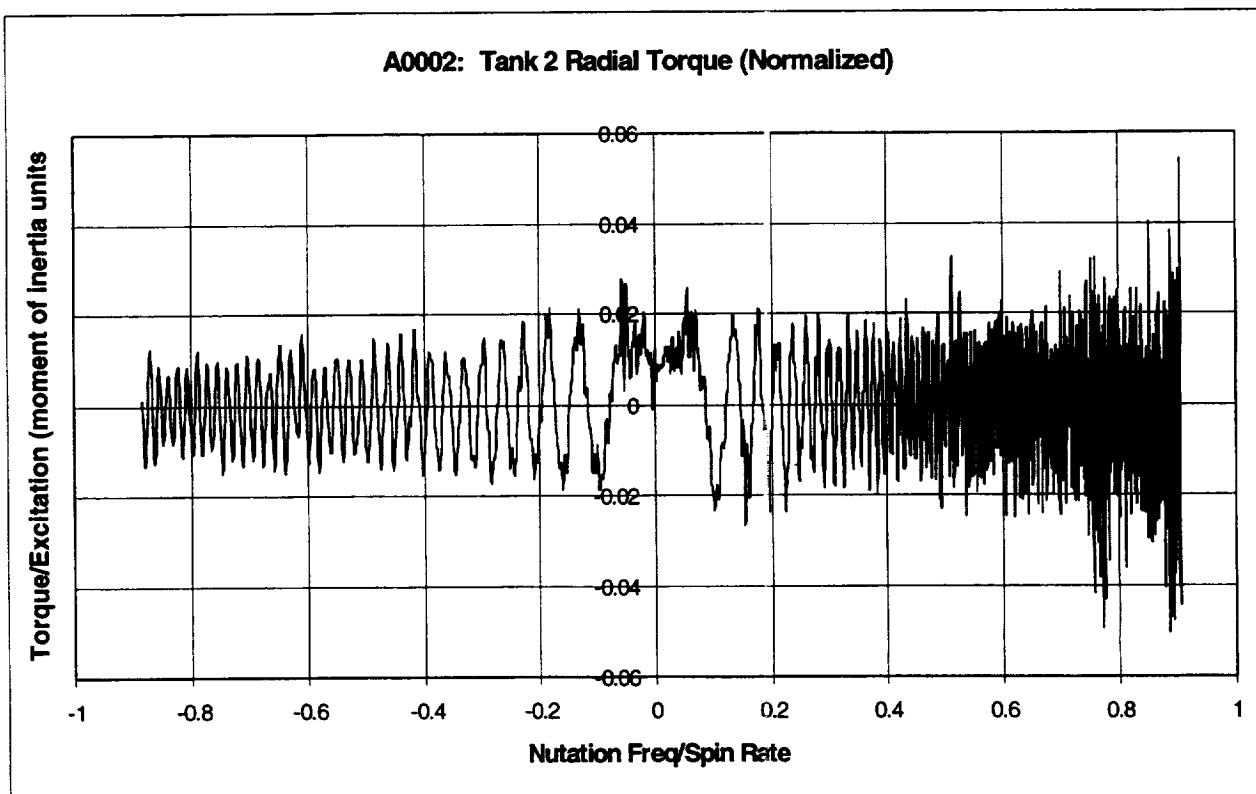
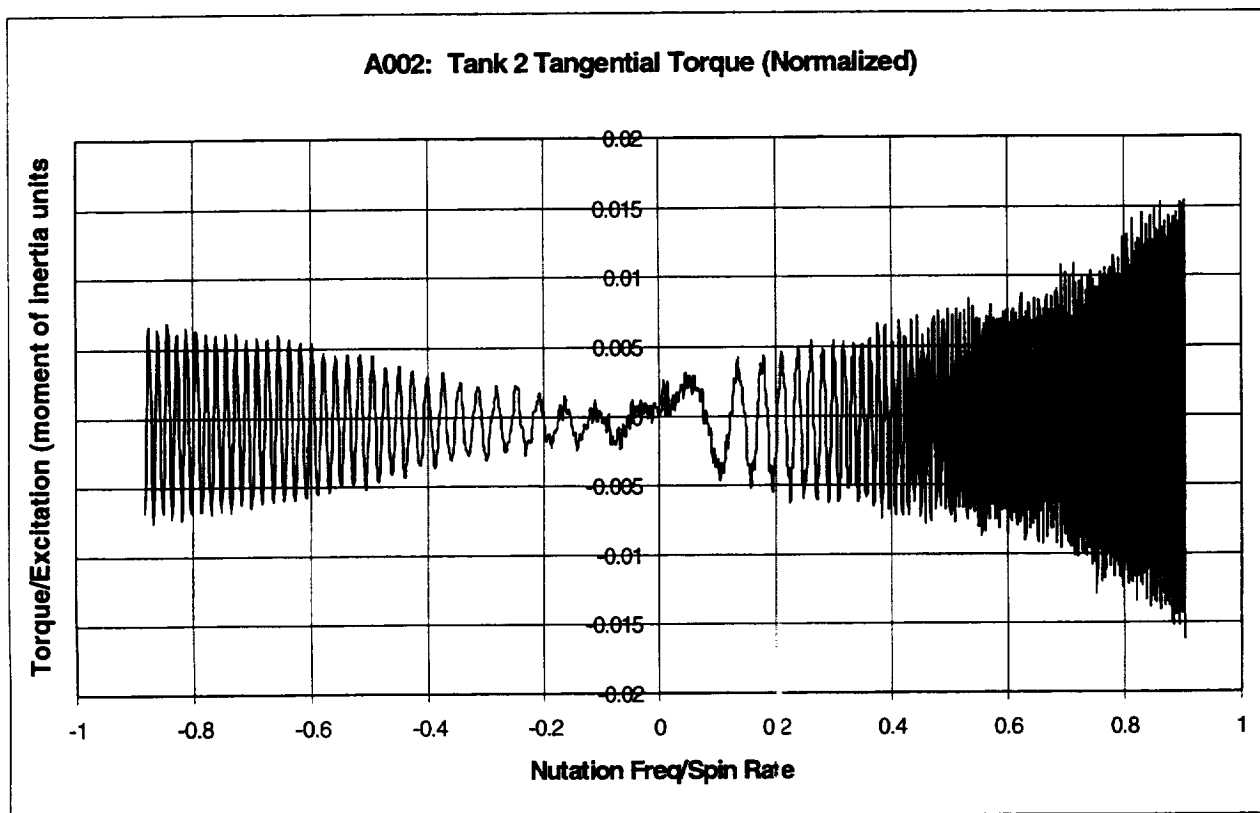
This page left intentionally blank.

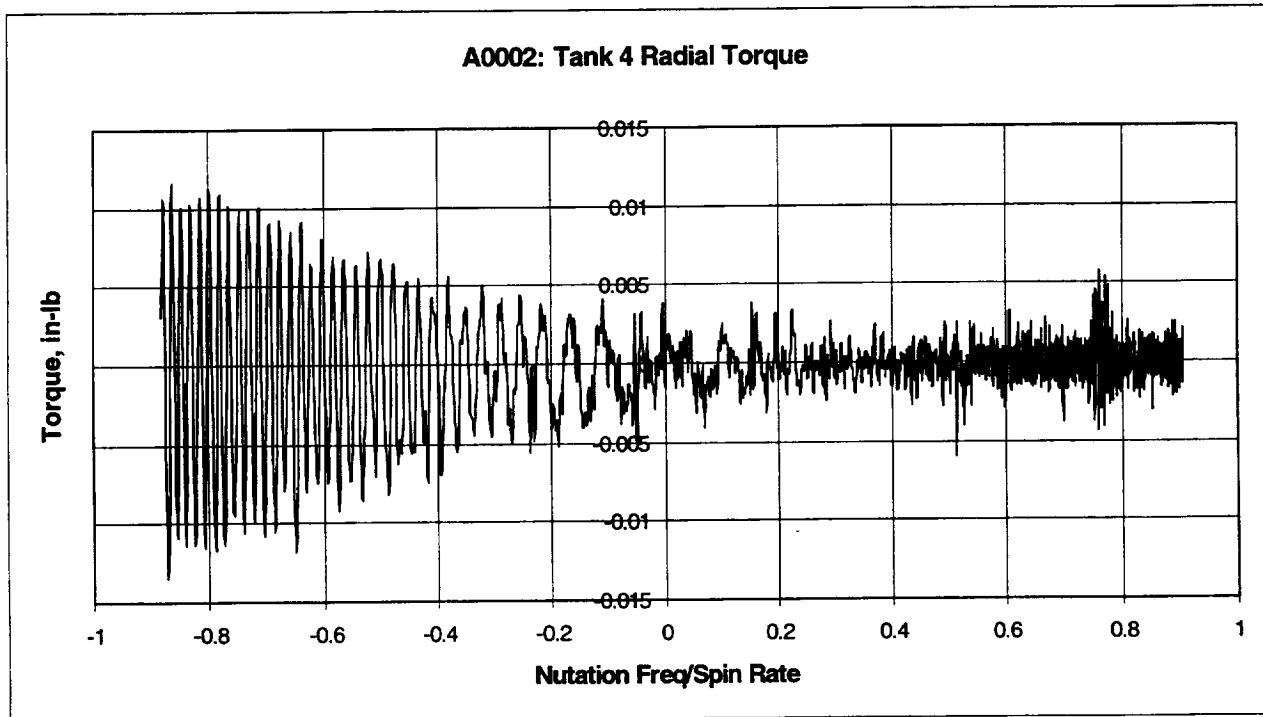
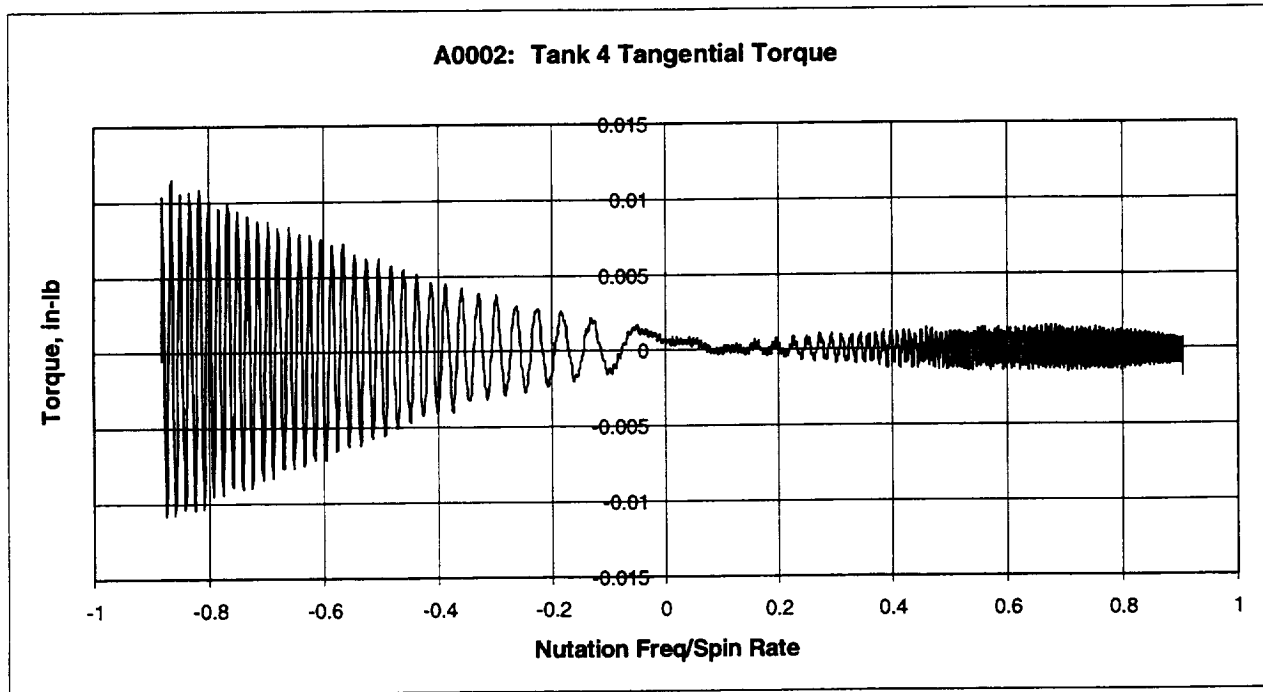
A0002: 20 RPM SWEEP TESTS - TANK SET A, SPHERICAL TANKS 2 AND 4Nutation Sweep Range: 18.1 rpm \rightarrow 0 \rightarrow 17.6 rpm

Tank 2: - 2/3 Full - Liquid Viscosity = 1 cp

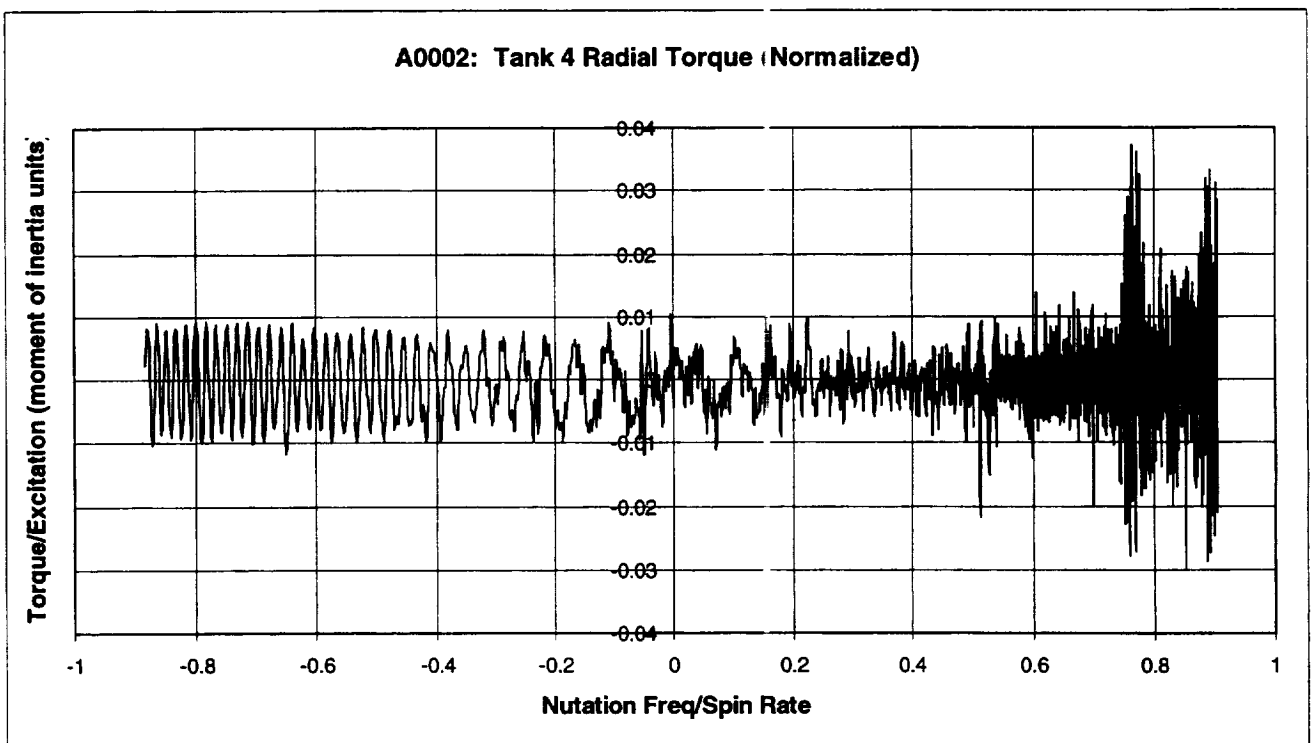
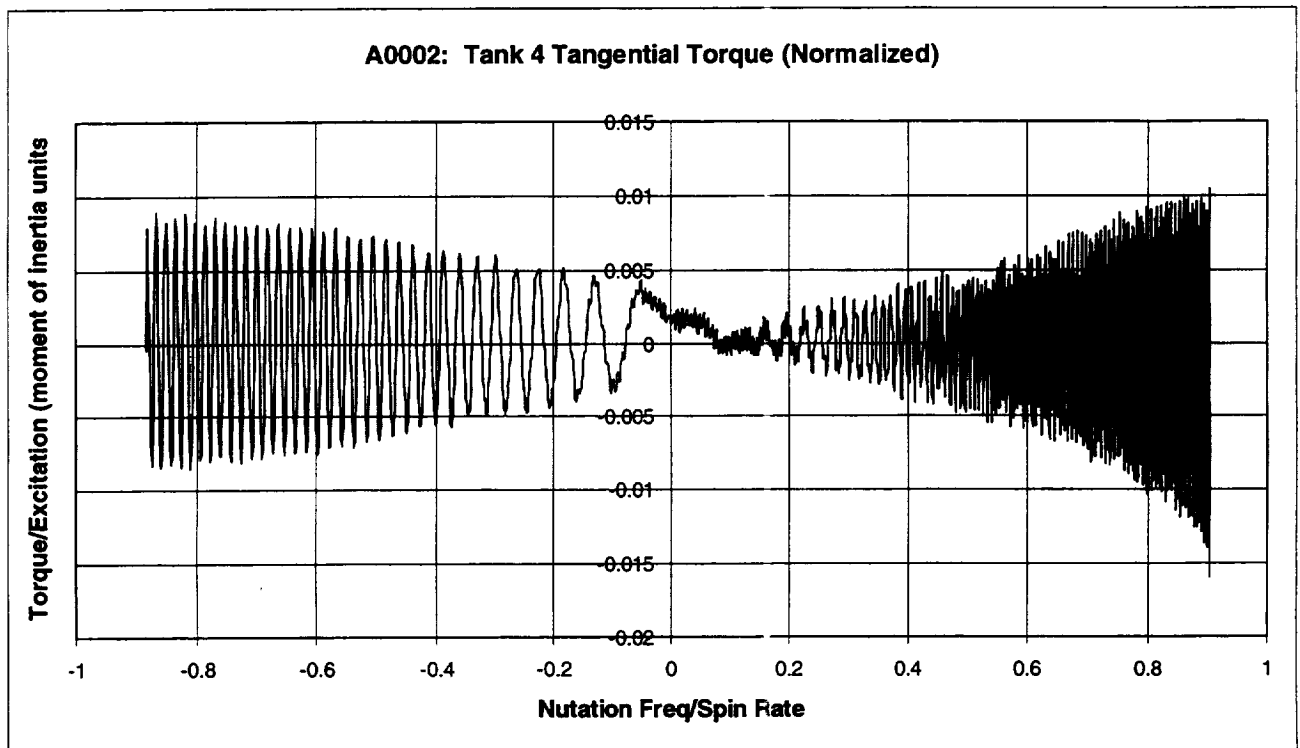


Tank 2 (A0002): concluded



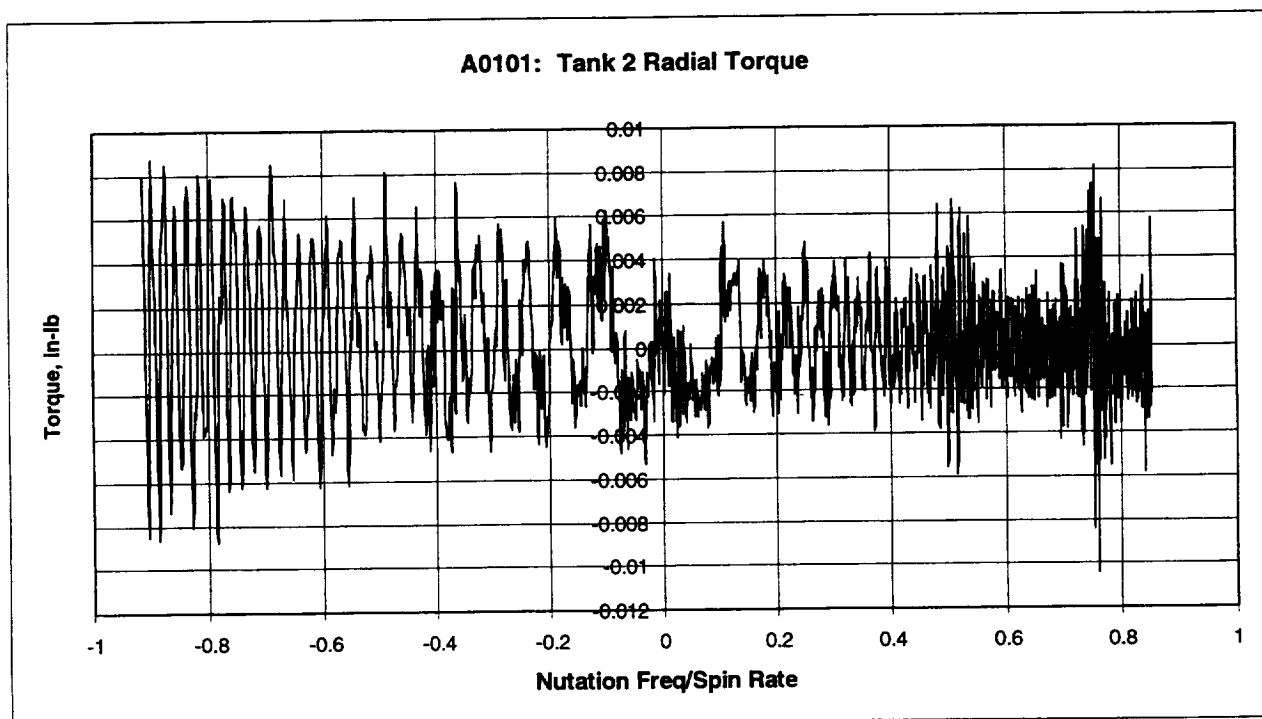
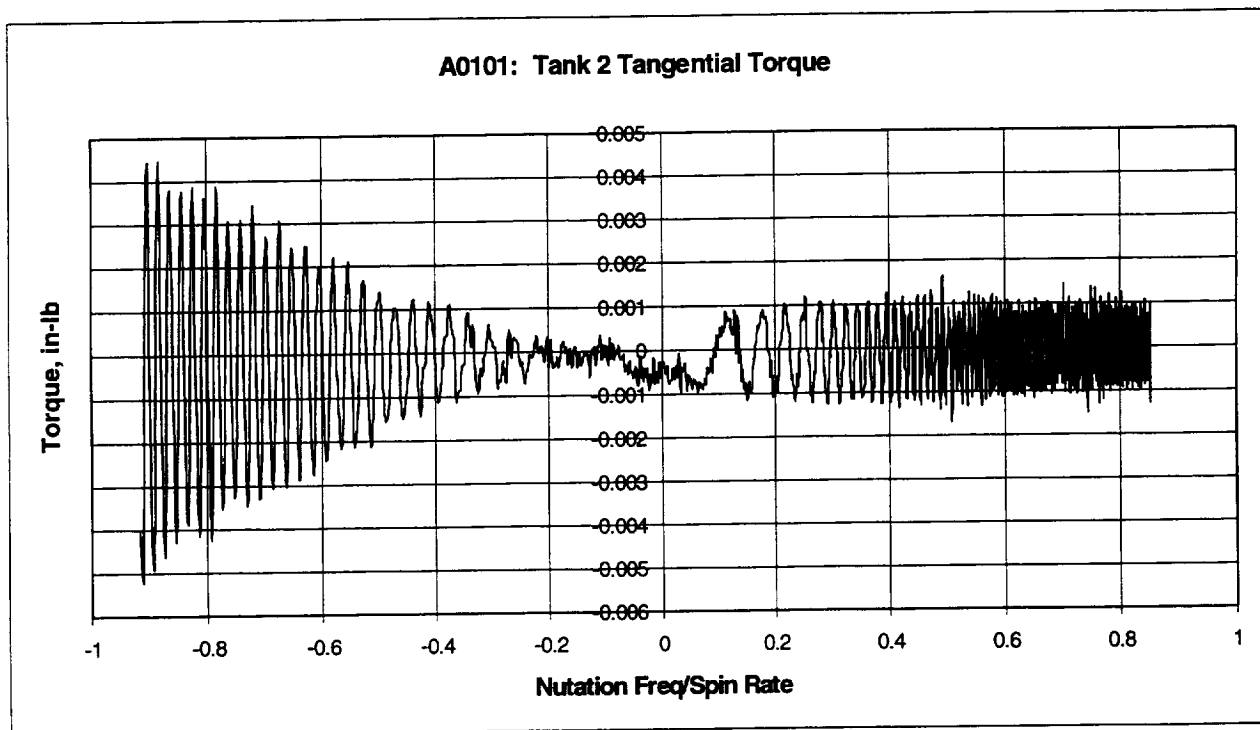
Tank 4 (A0002): 2/3 Full - Liquid Viscosity = 10 cp

Tank 4 (A0002): concluded

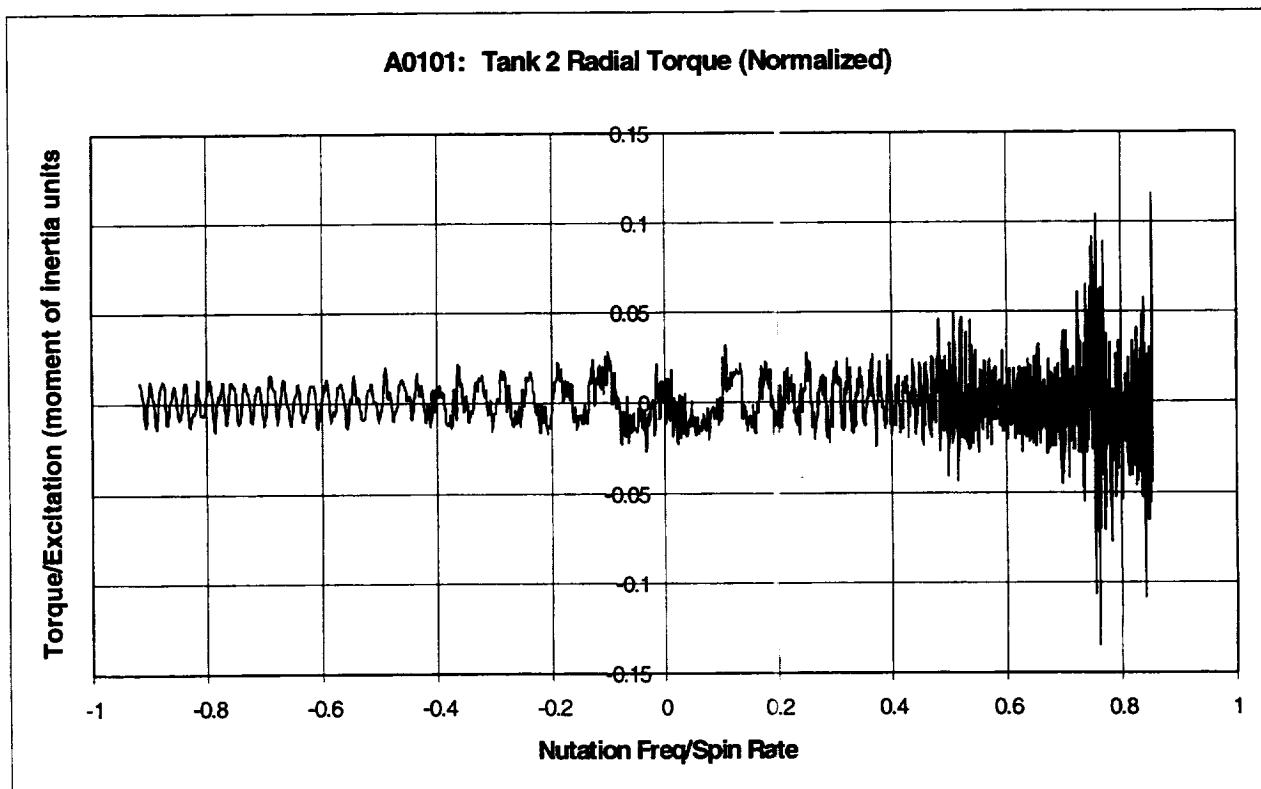
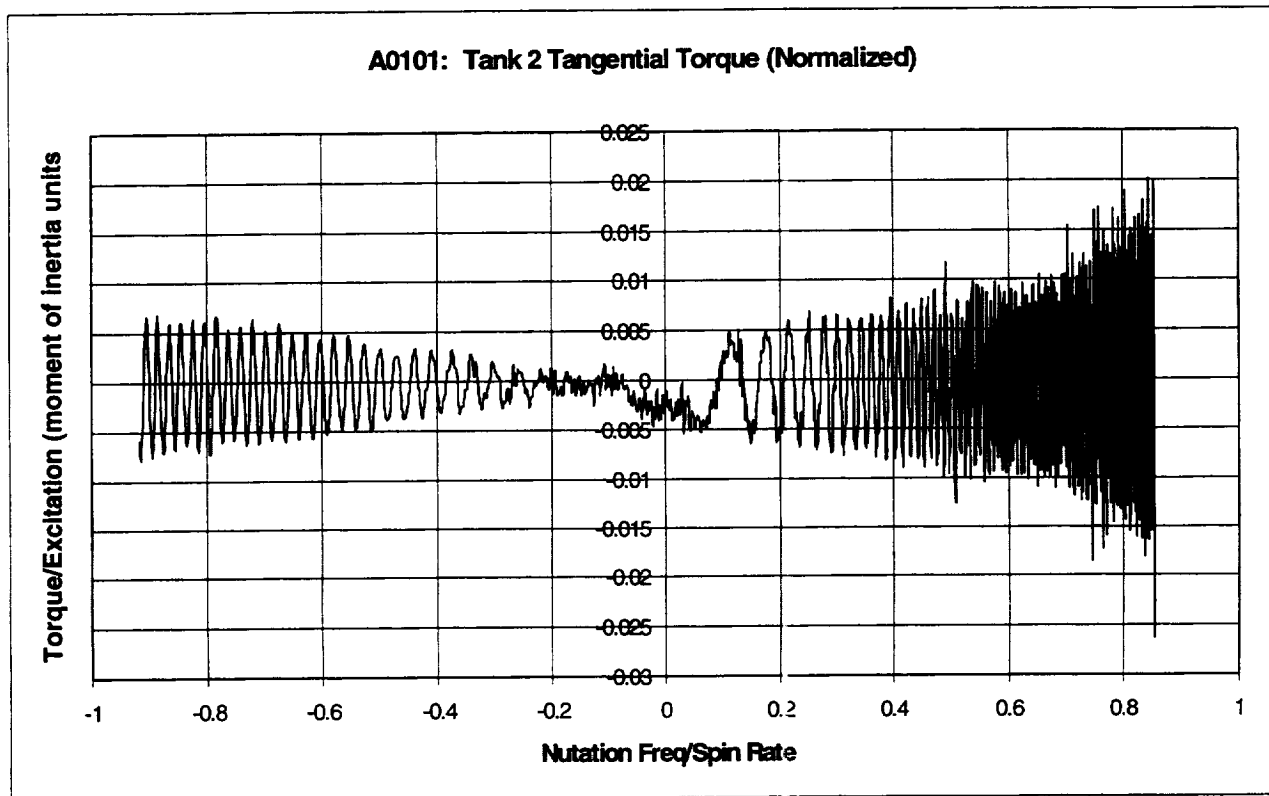


A0101: 14.1 RPM SWEEP TESTS AT - TANK SET A, SPHERICAL TANKS 2 AND 4Nutation Sweep Rate: 12.0 rpm \rightarrow 0 \rightarrow 12.8 rpm

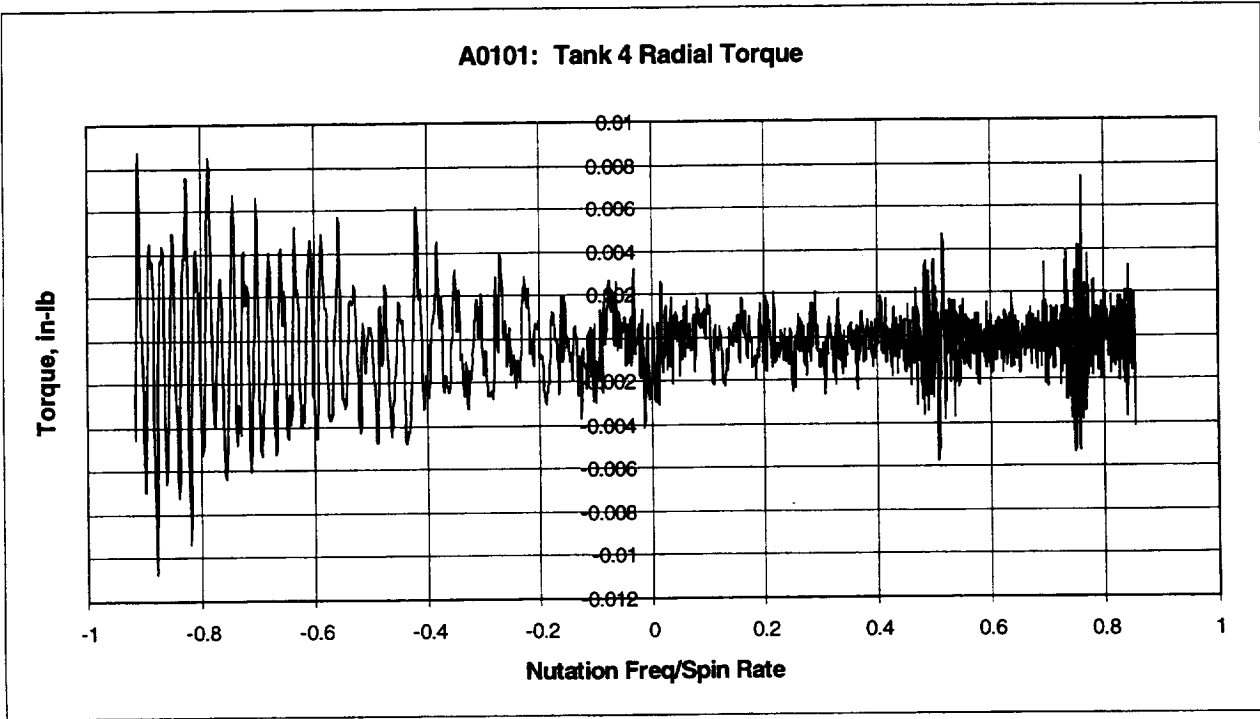
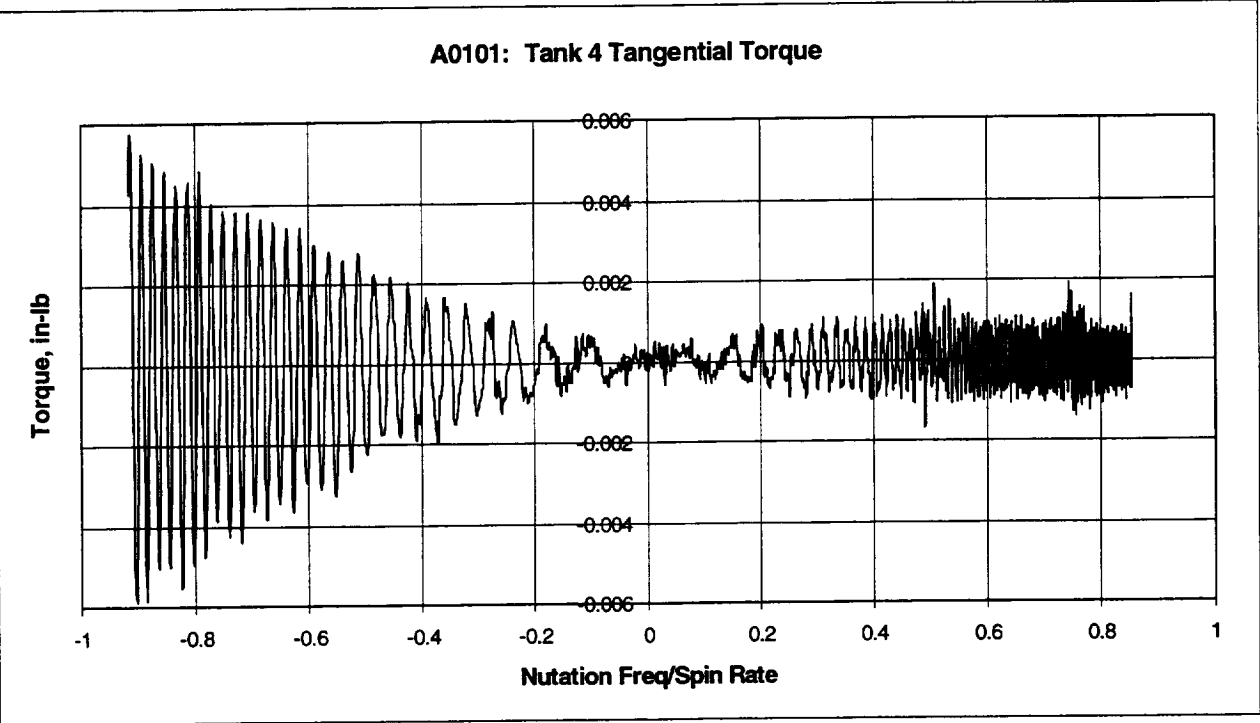
Tank 2: 2/3 Full - Fluid Viscosity = 1 cp



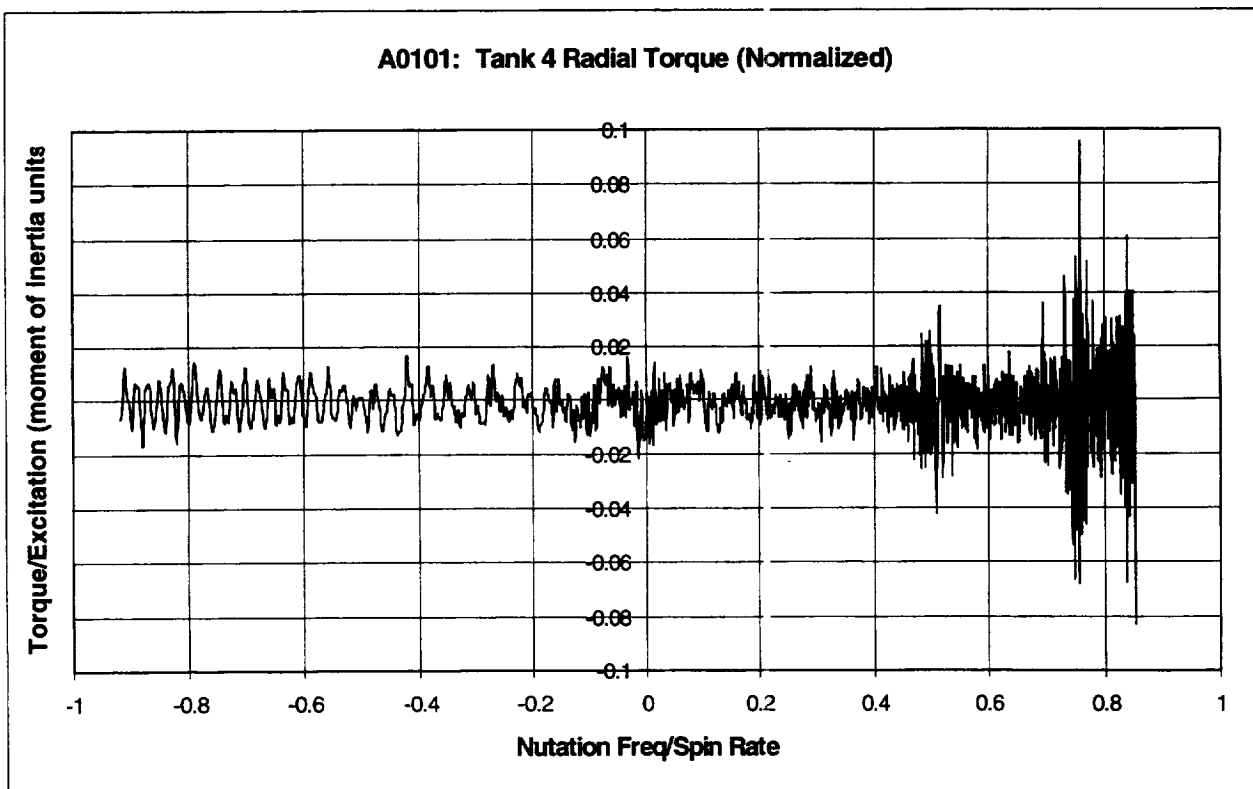
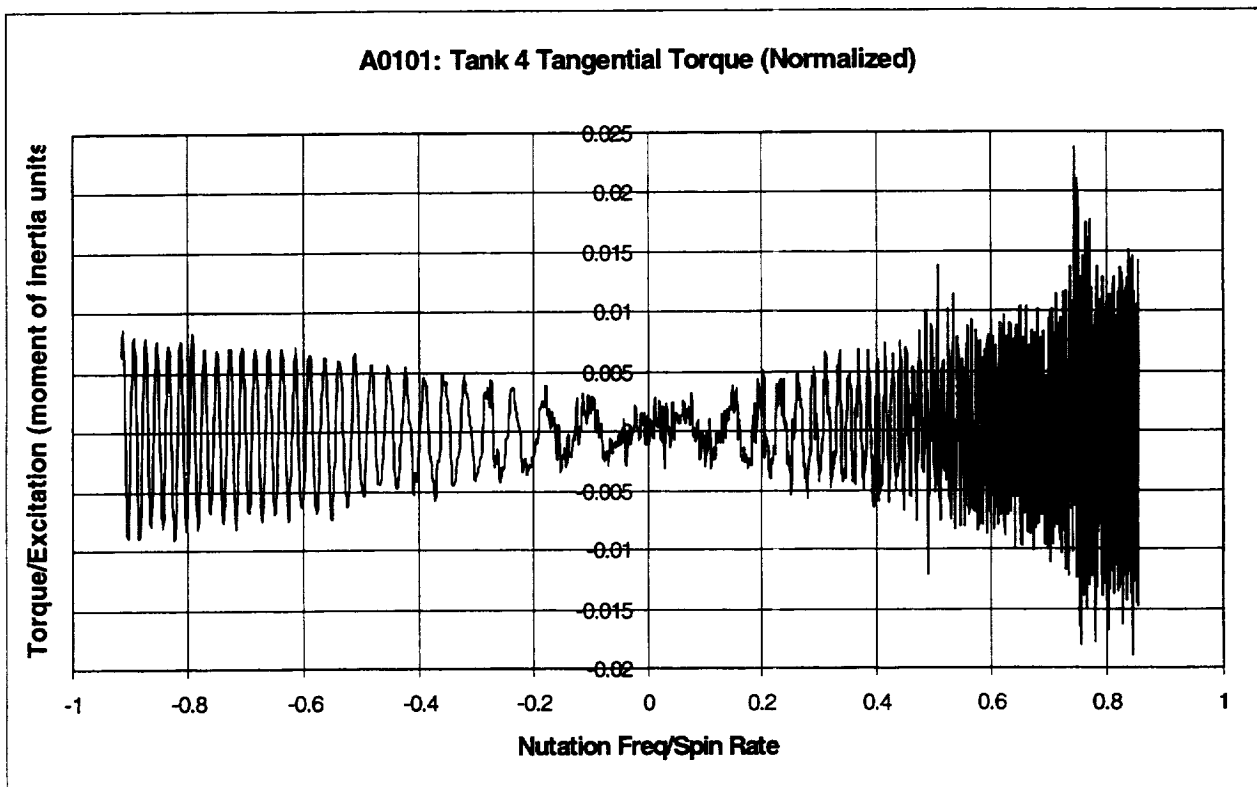
Tank 2 (A0101): concluded



Tank 4 (A0101): 2/3 Full - Liquid Viscosity = 10 cp



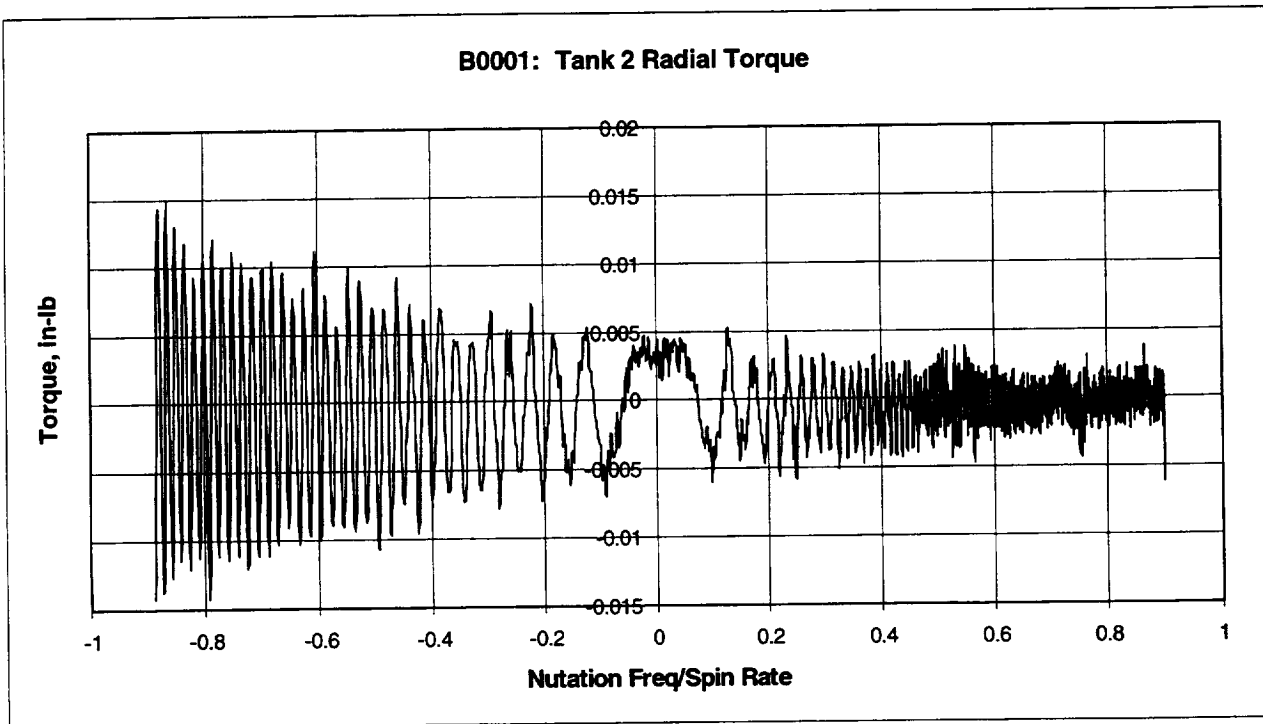
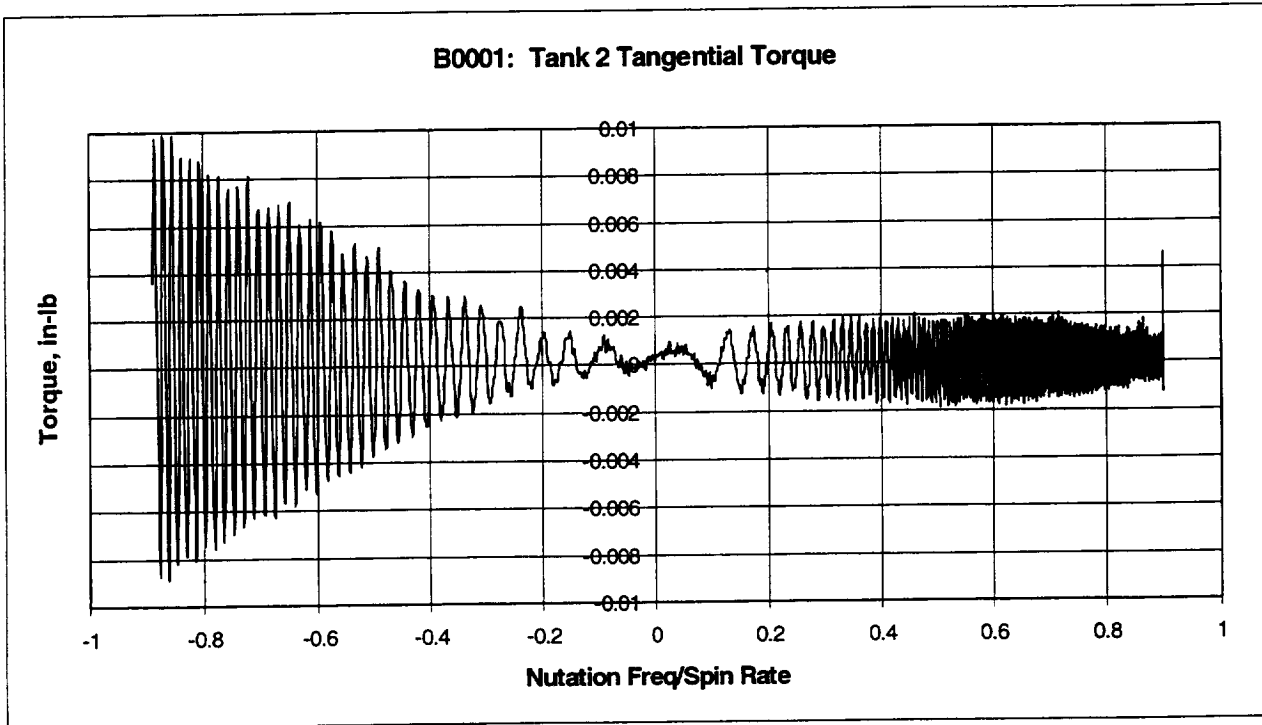
Tank 4 (A0101): concluded

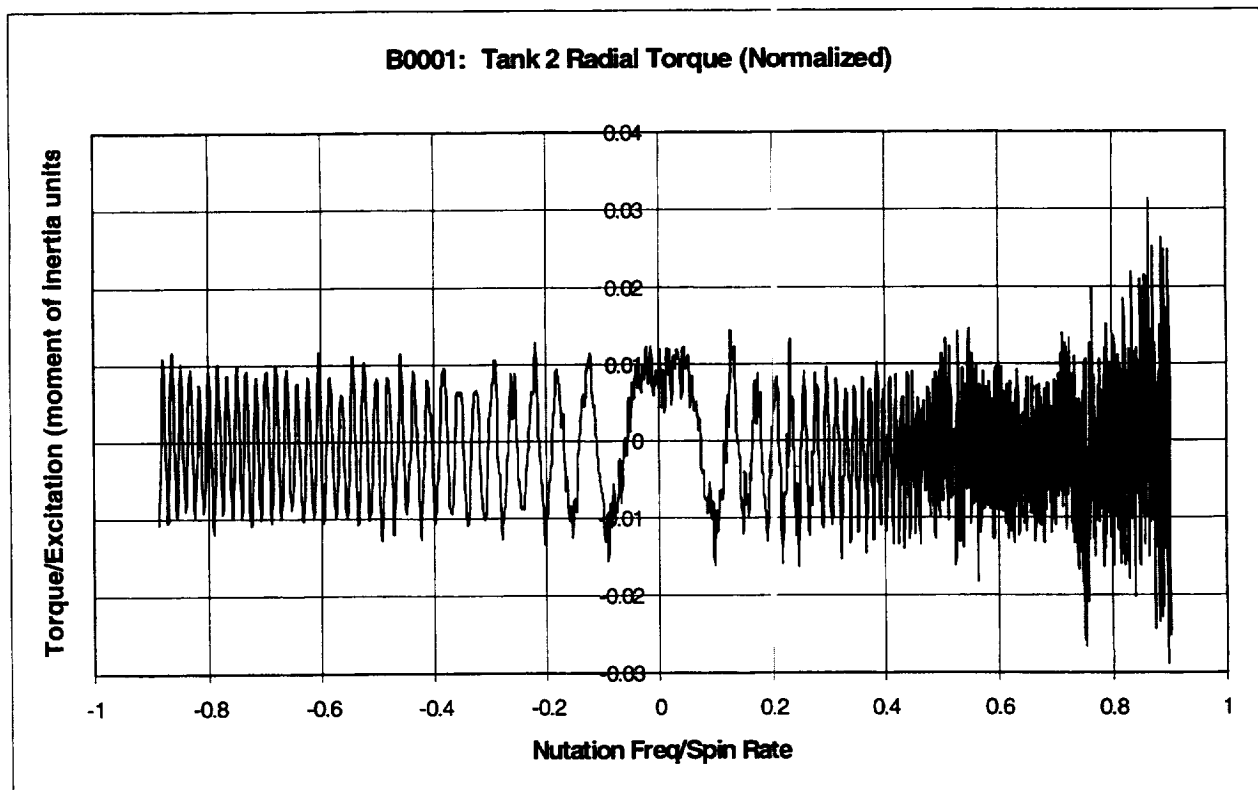
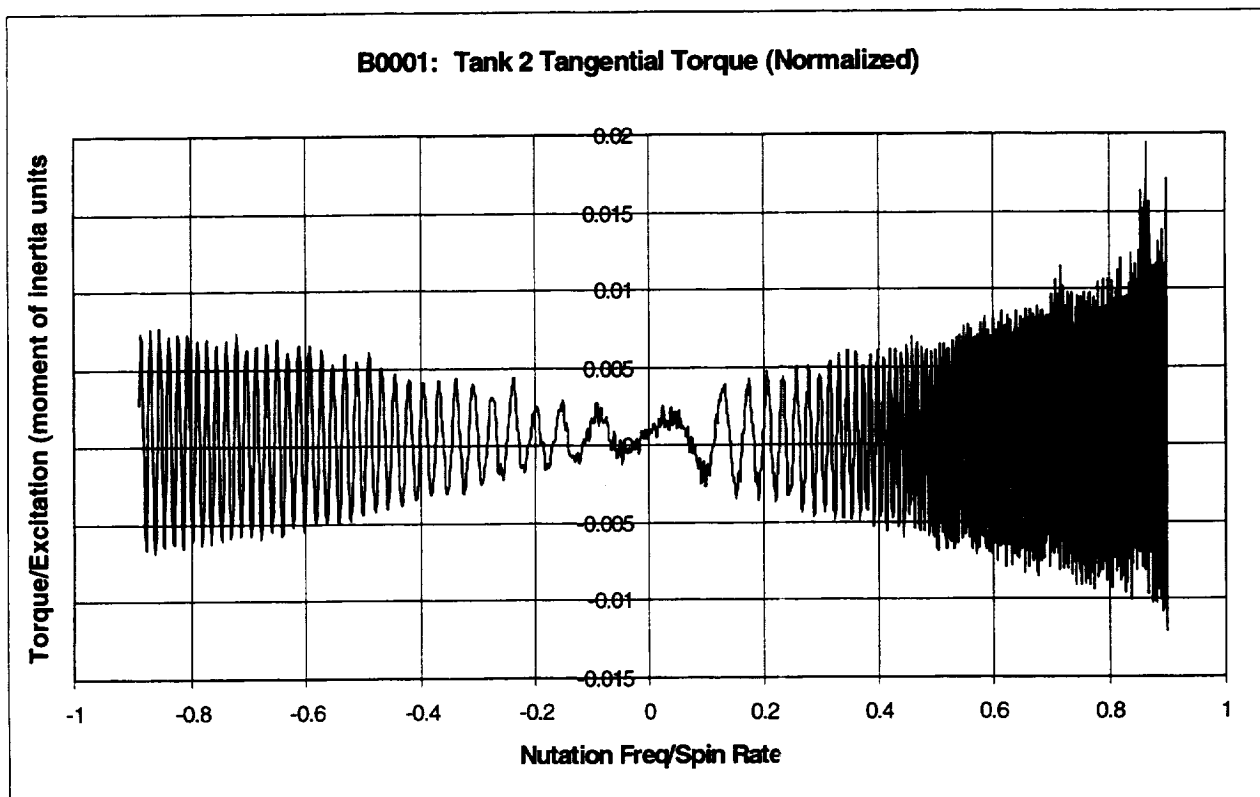


B0001: 20 RPM SWEEP TESTS - TANK SET B, SPHERICAL TANKS 2 AND 4

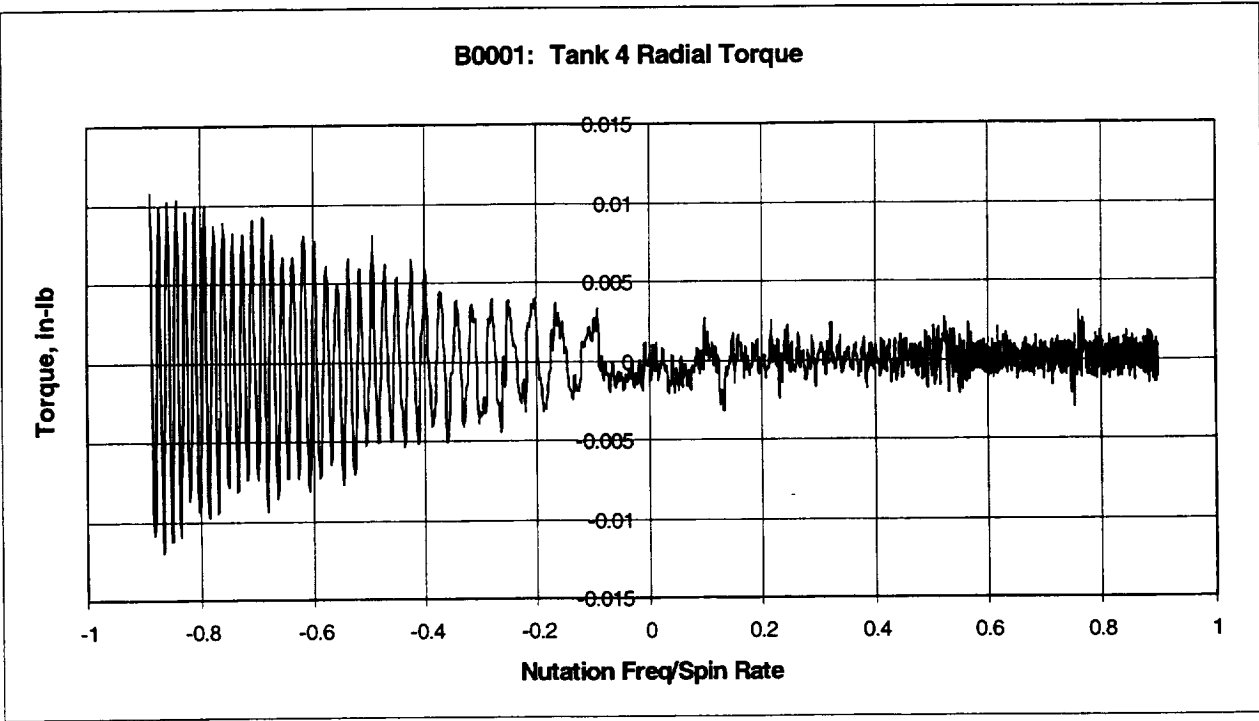
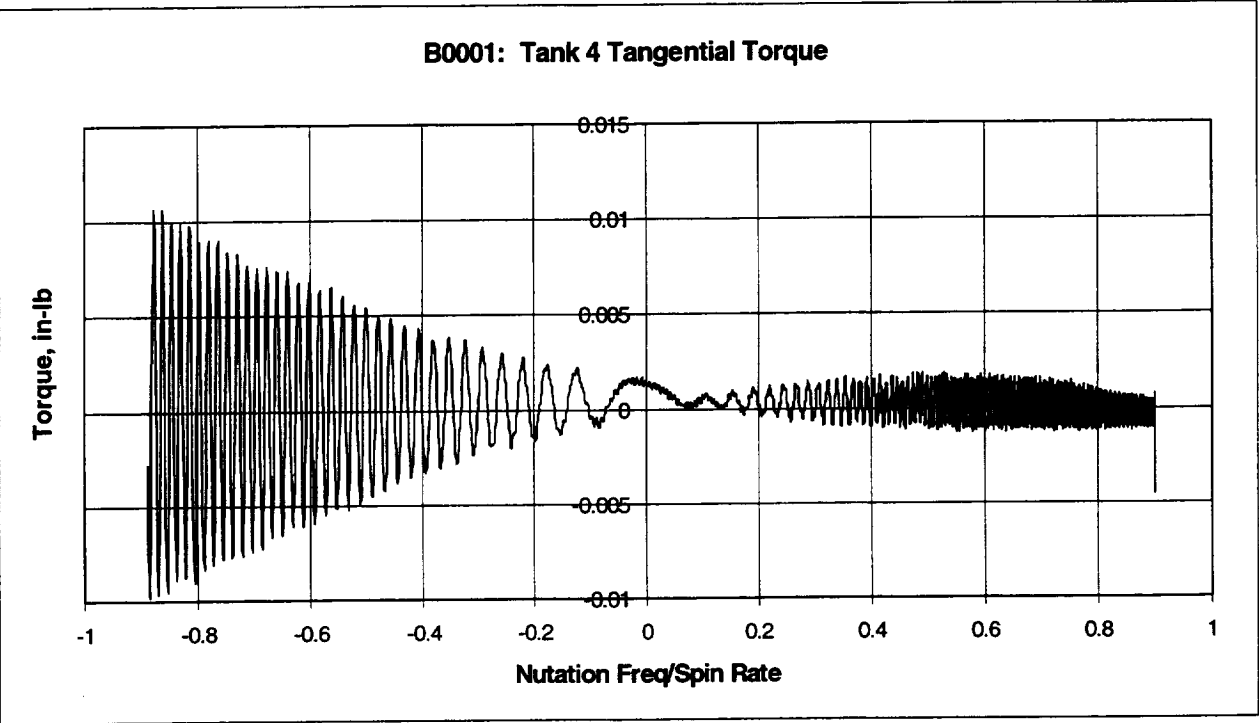
Nutation Sweep Range: 18.1 rpm \rightarrow 0 \rightarrow 17.6 rpm

Tank 2: 1/3 Full - Liquid Viscosity = 1 cp

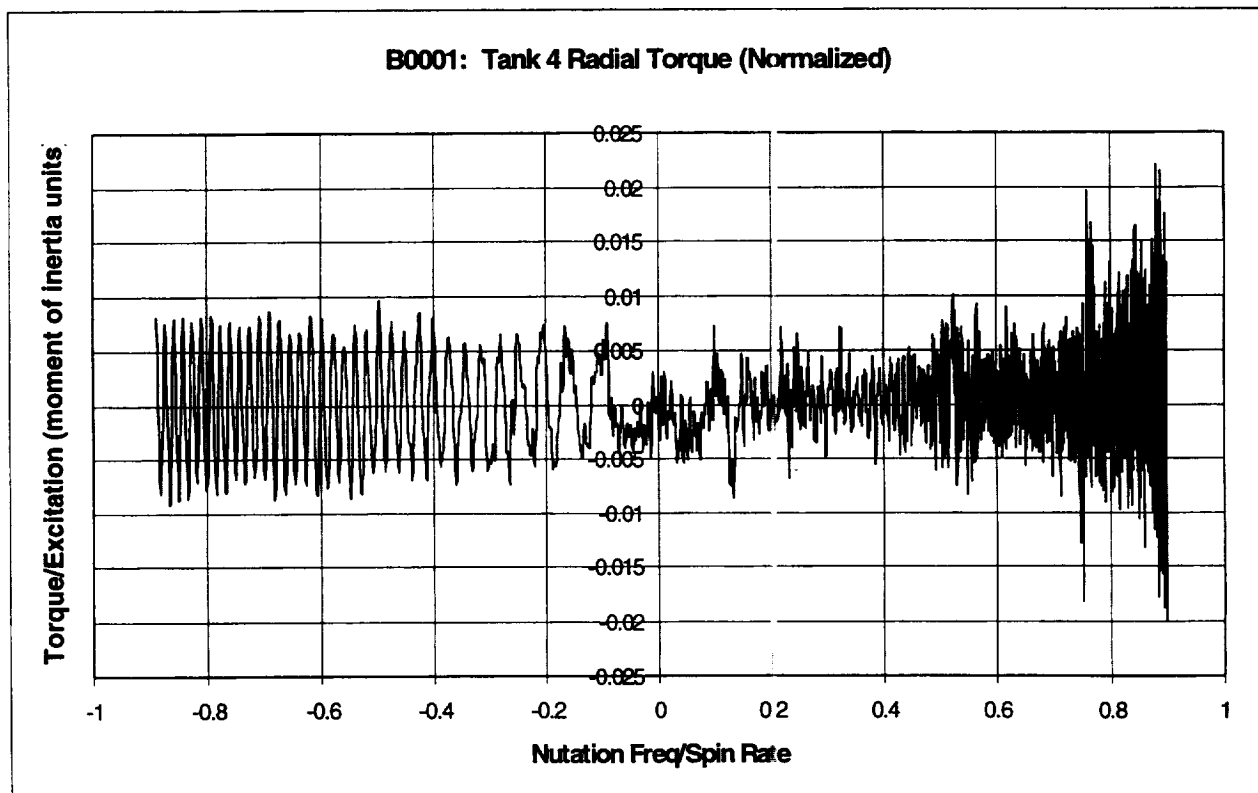
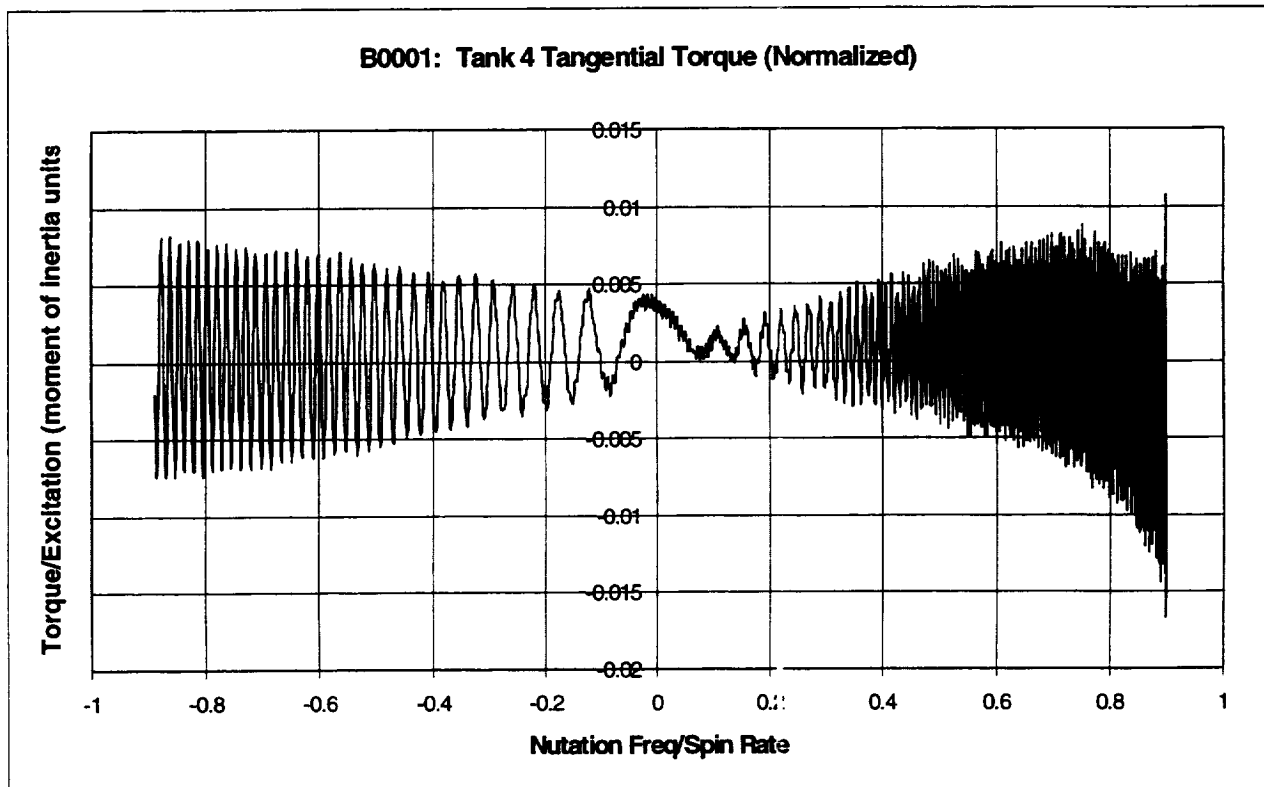


Tank 2 (B0001): concluded

Tank 4: 1/3 Full - Liquid Viscosity = 10 cp



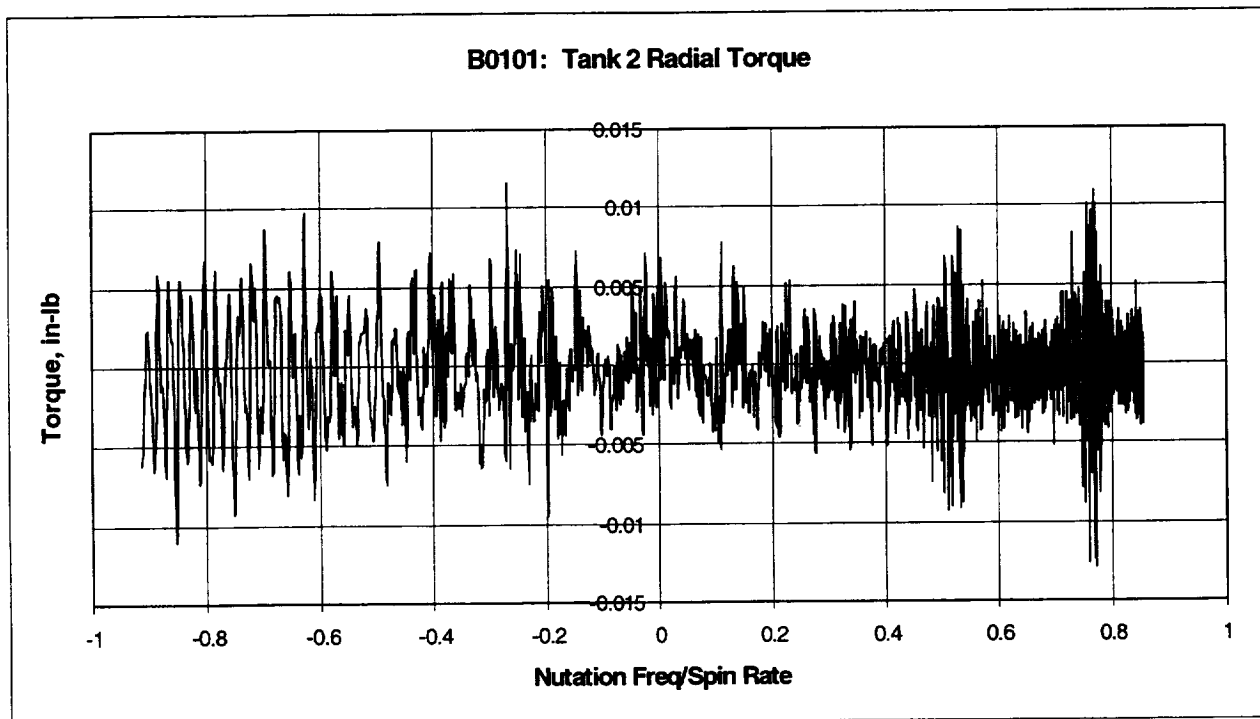
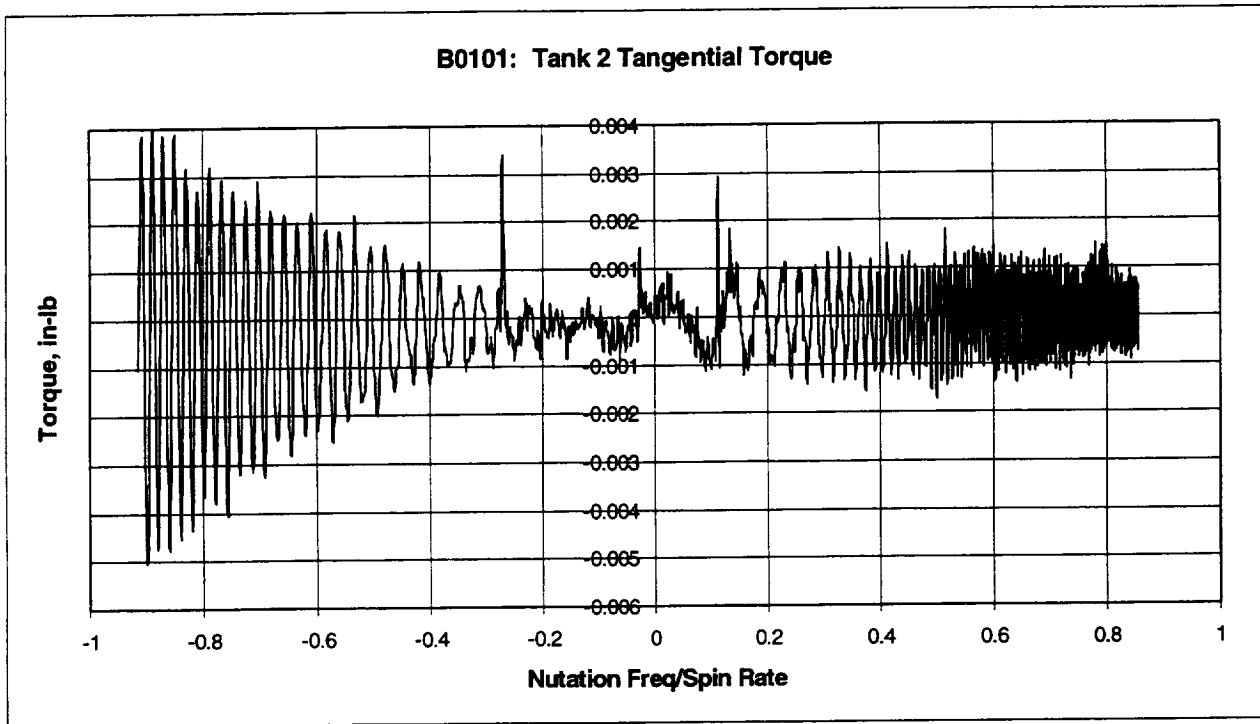
Tank 4 (B0001): concluded

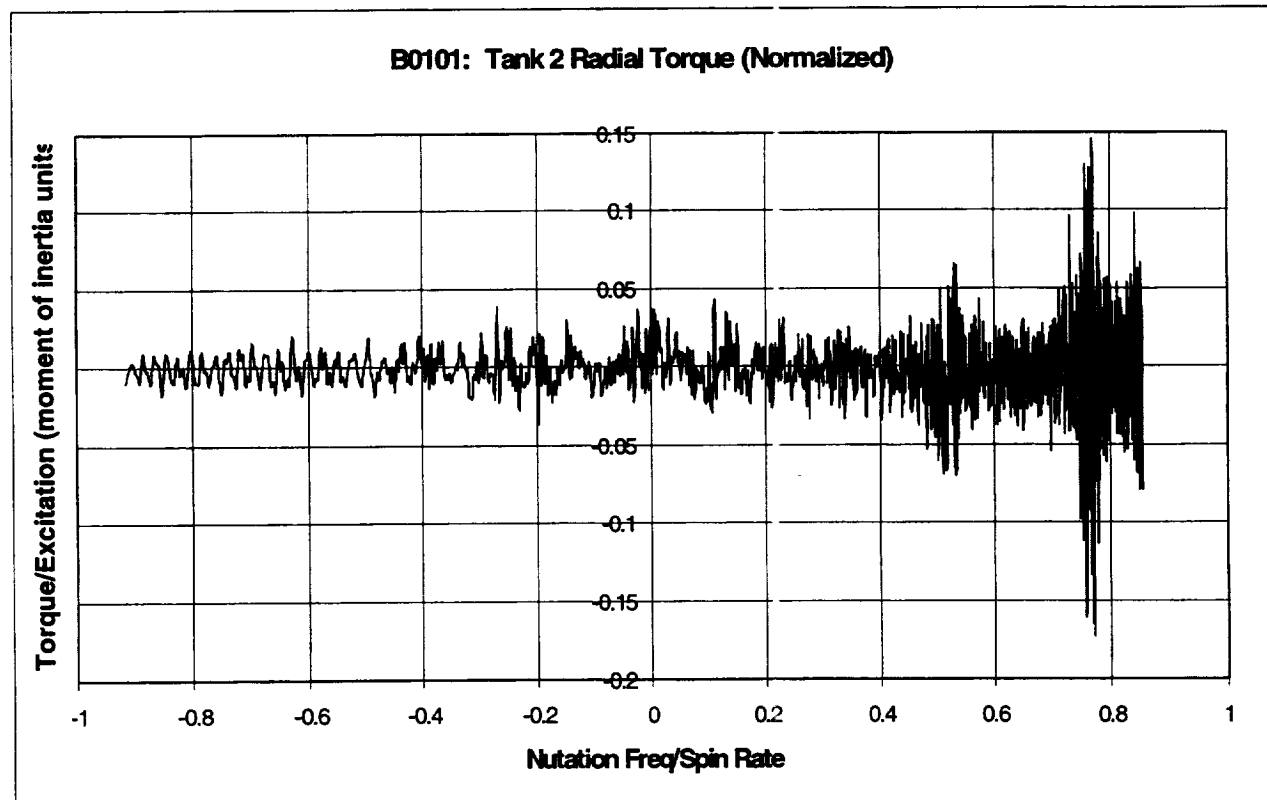
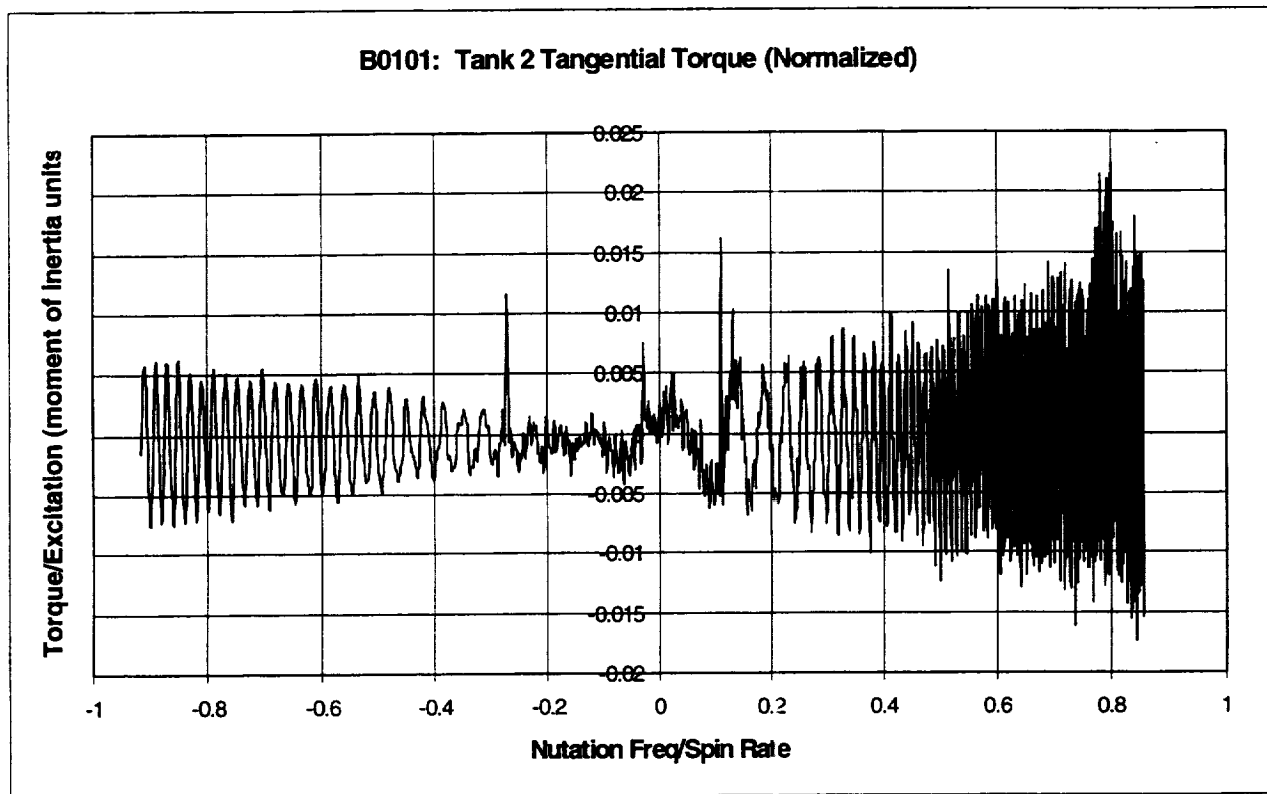


B0101: 14.1 RPM SWEEP TESTS AT- TANK SET B, SPHERICAL TANKS 2 AND 4

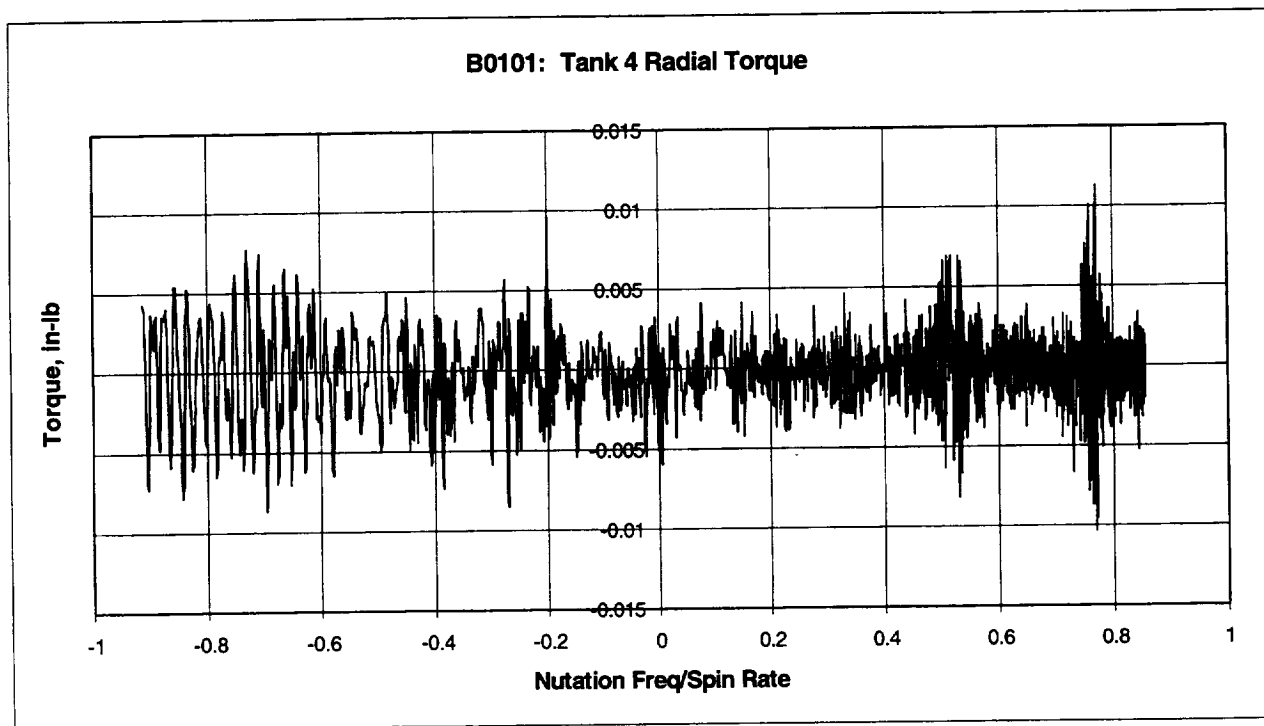
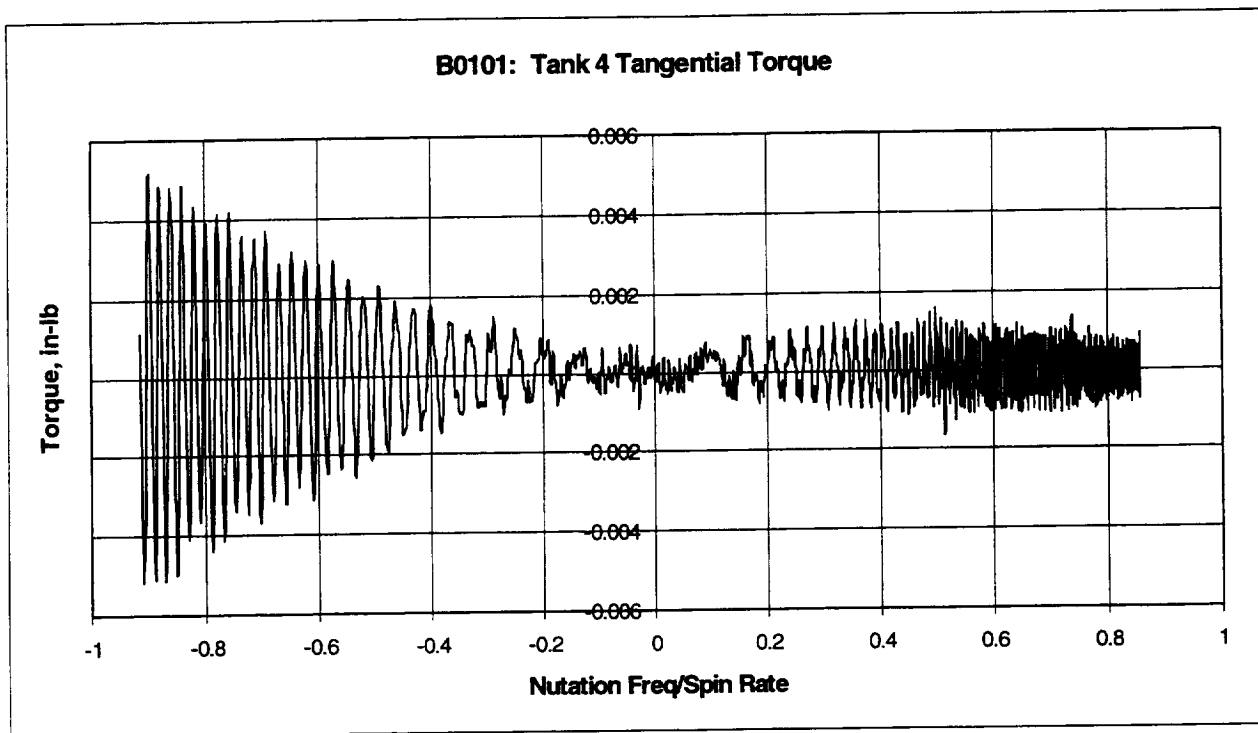
Nutation Sweep Range: 12.0 rpm \rightarrow 0 \rightarrow 12.8 rpm

Tank 2: 1/3 Full - Liquid Viscosity = 1 cp

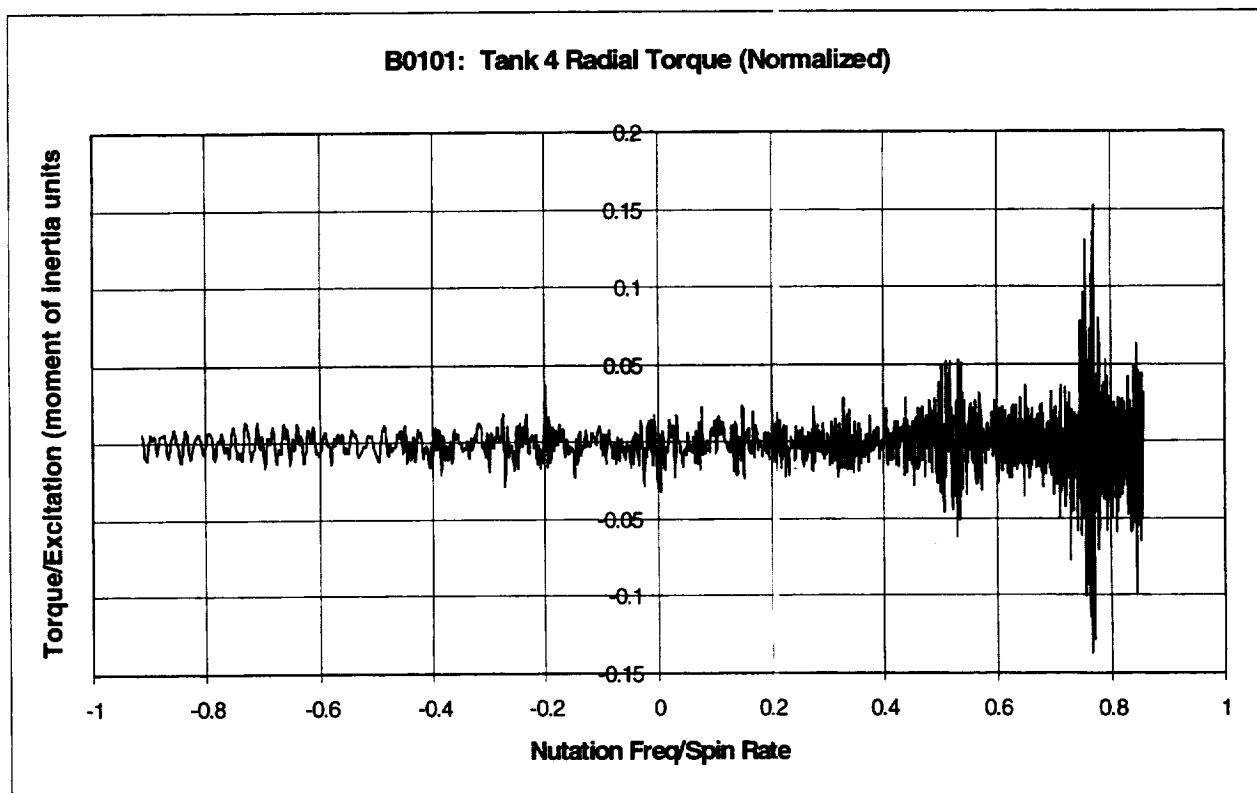
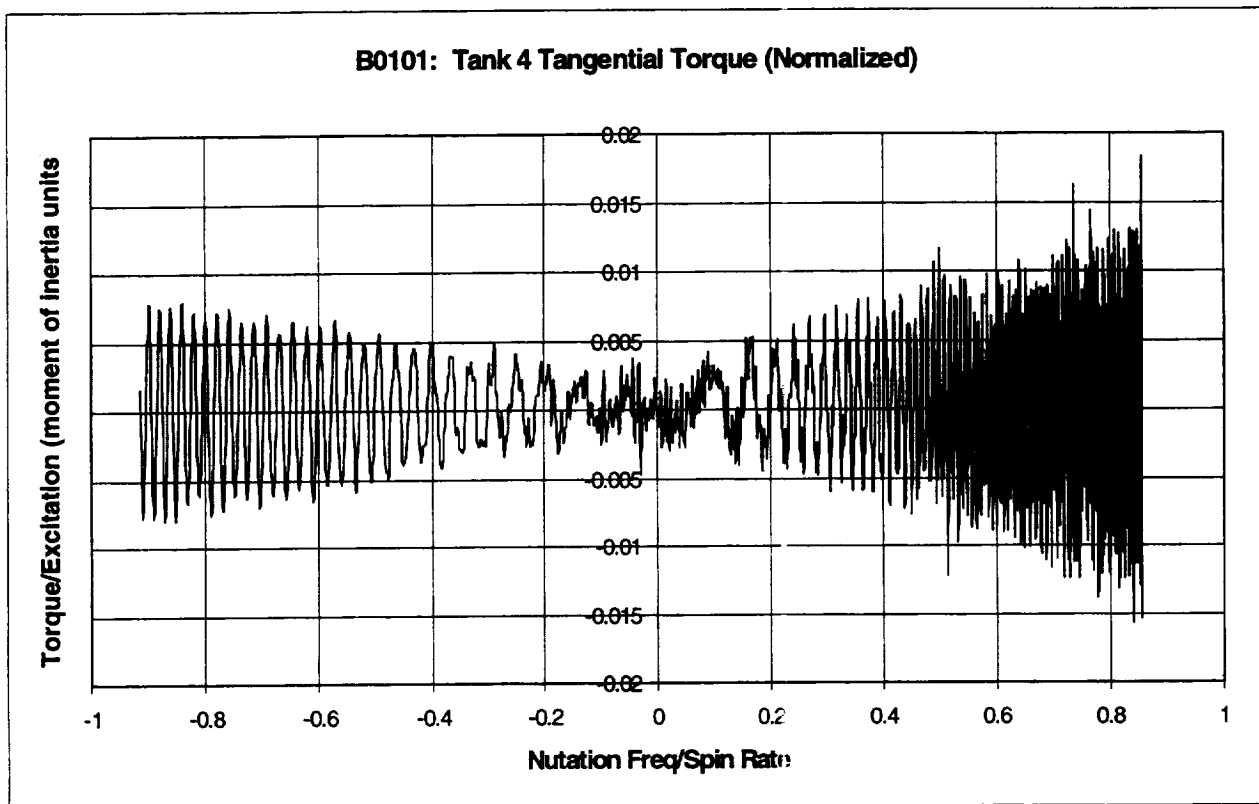


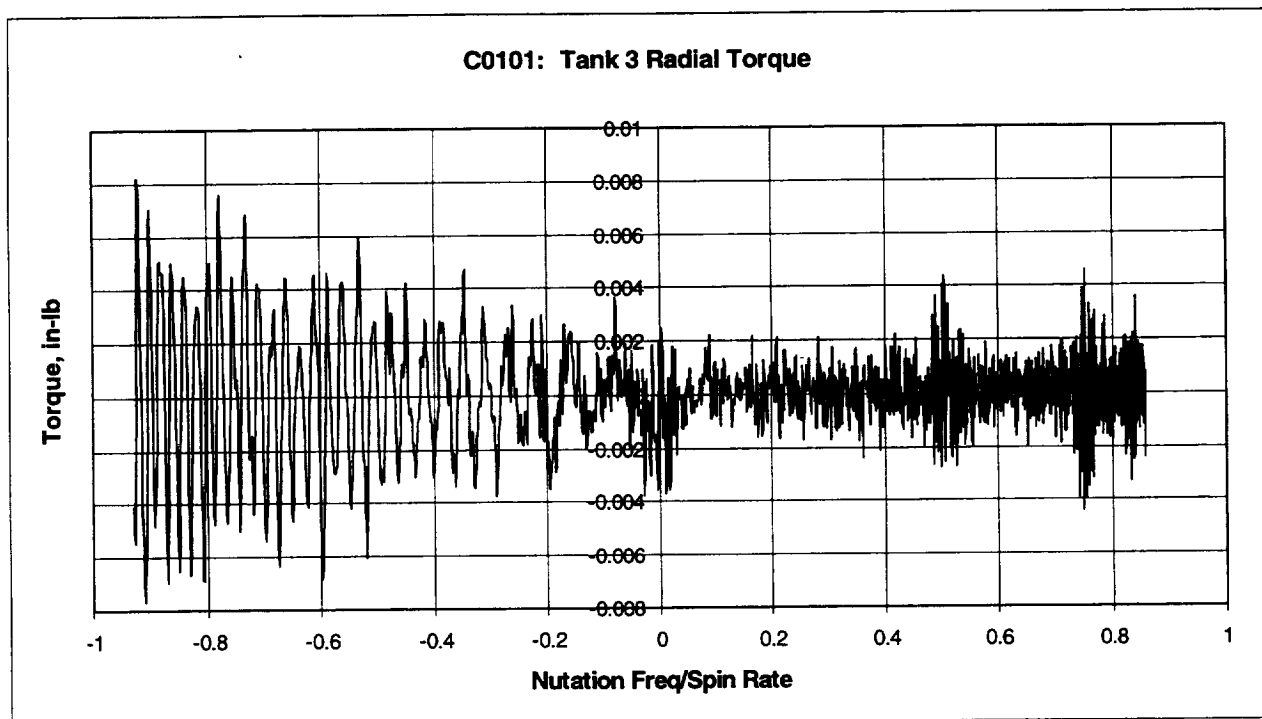
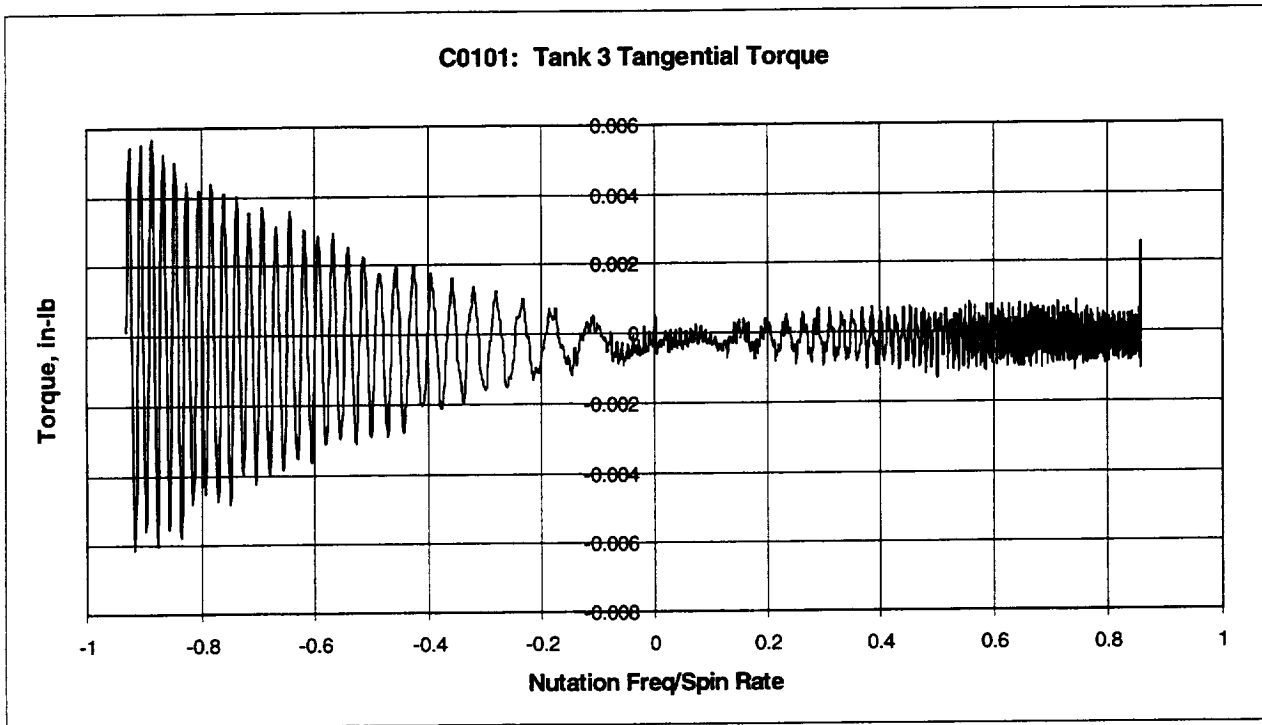
Tank 2 (B0101): concluded

Tank 4: 1/3 Full - Liquid Viscosity = 10 cp

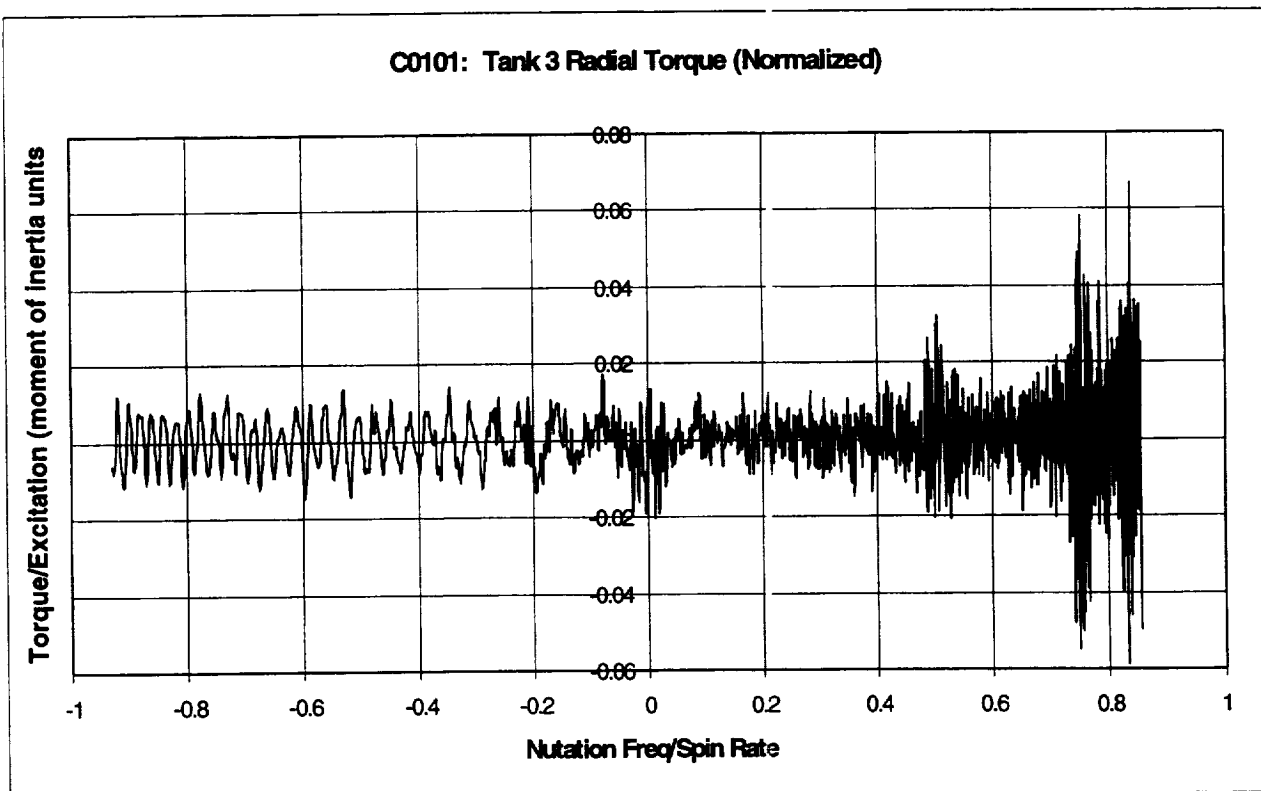
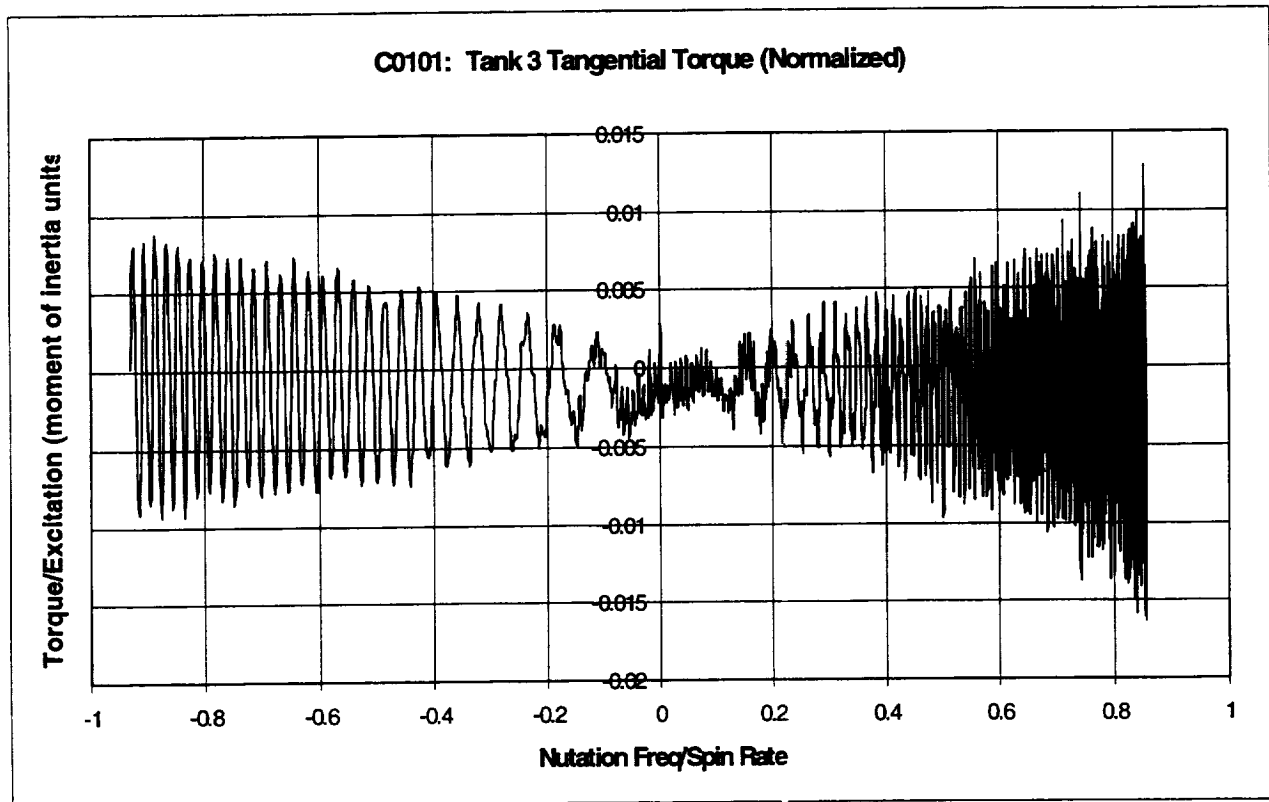


Tank 4 (B0101): concluded

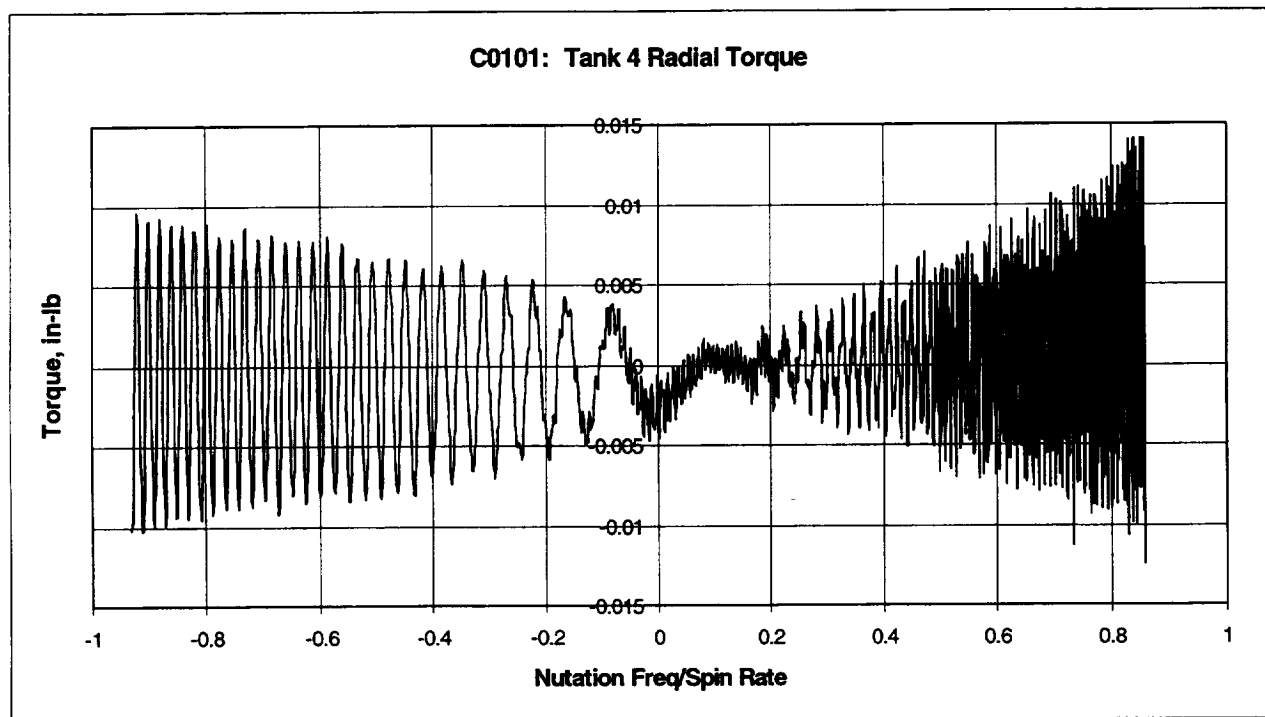
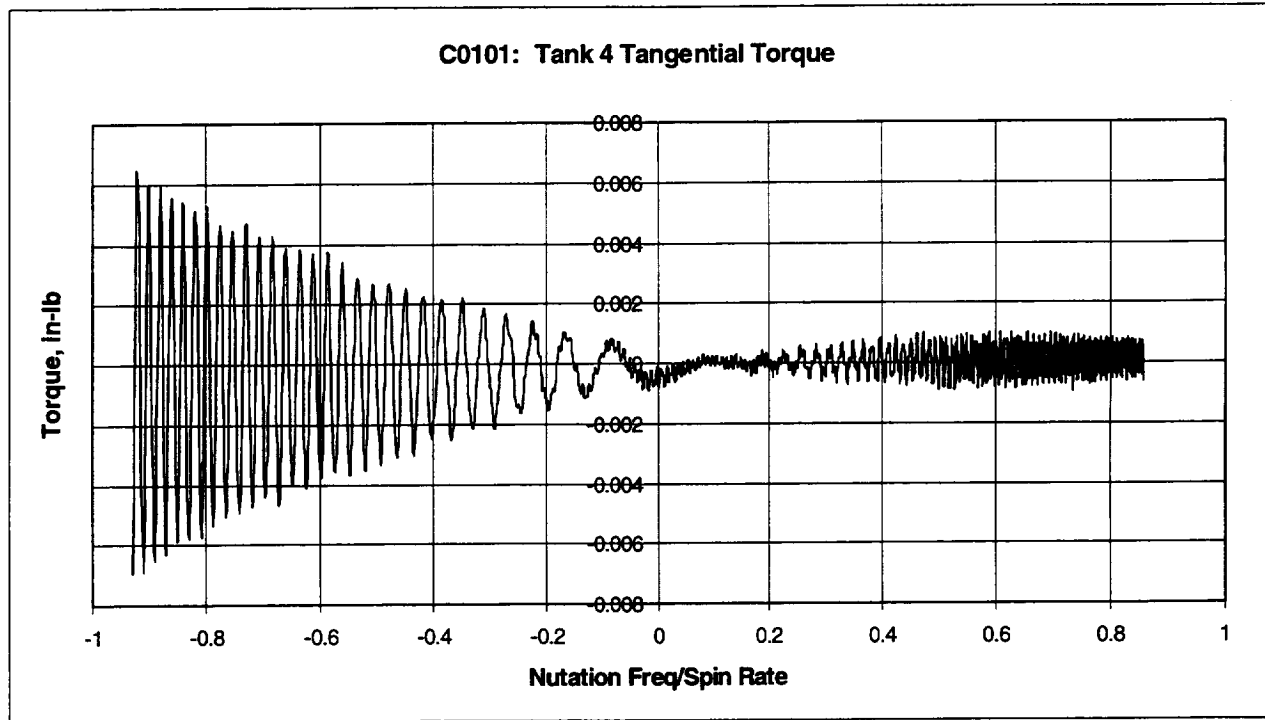


C0101: 14.1 RPM SWEEP TESTS - TANK SET C, SPHERICAL TANKS 3 AND 4**Nutation Sweep Range: 12.0 rpm \rightarrow 0 \rightarrow 12.8 rpm****Tank 3: PMD - 2/3 Full - Liquid Viscosity = 1 cp**

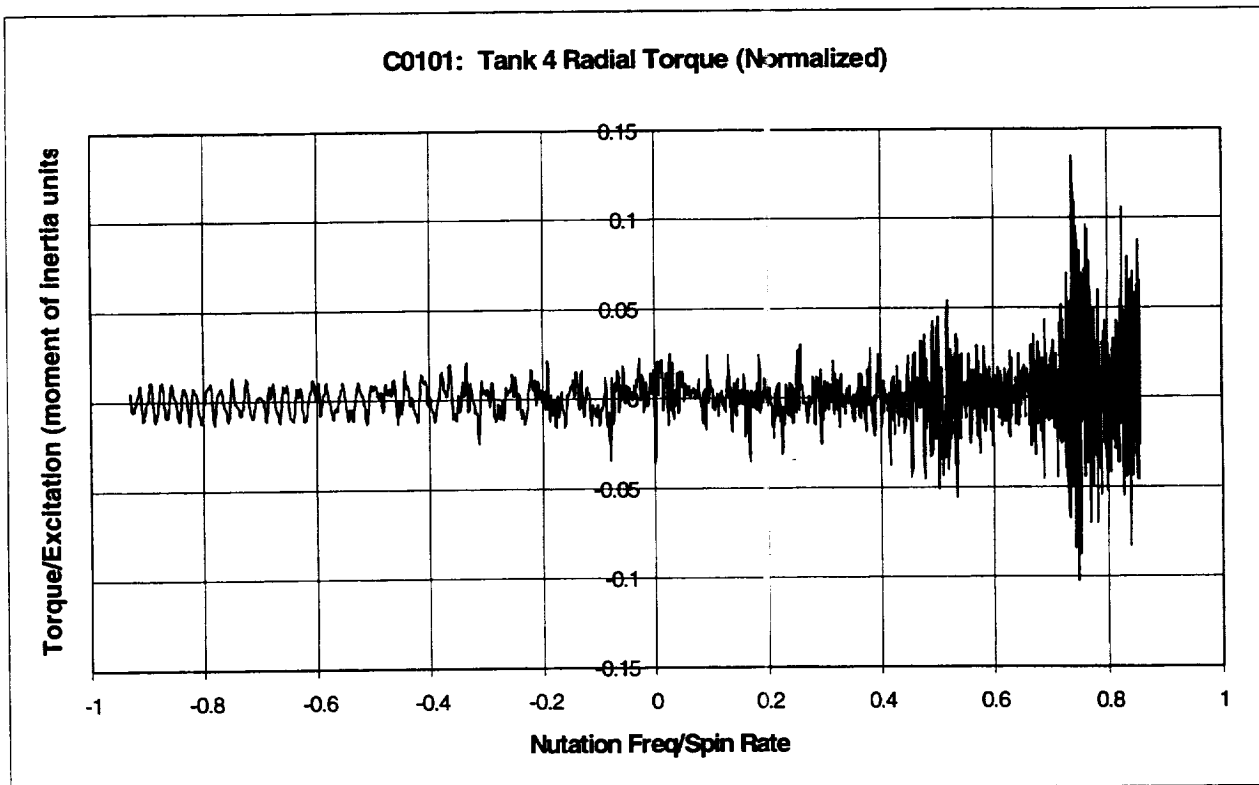
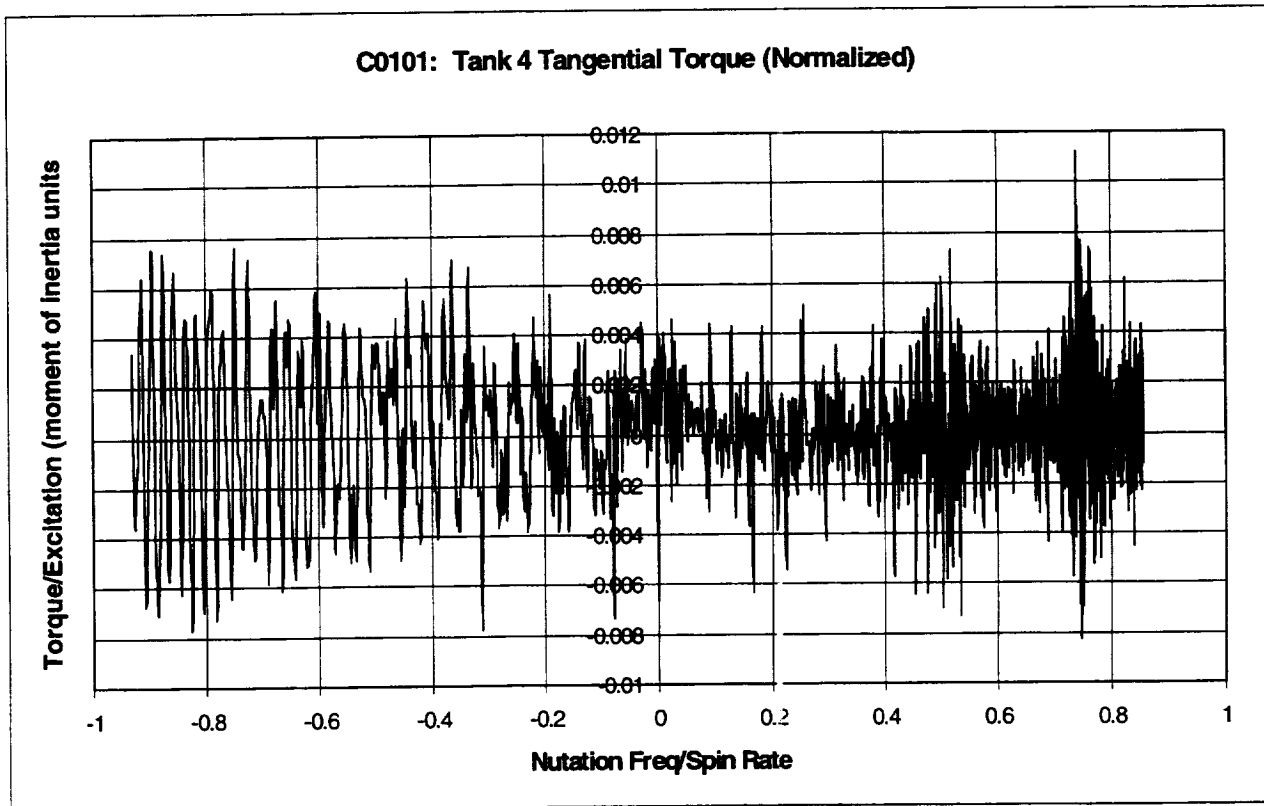
Tank 3 (C0101): concluded

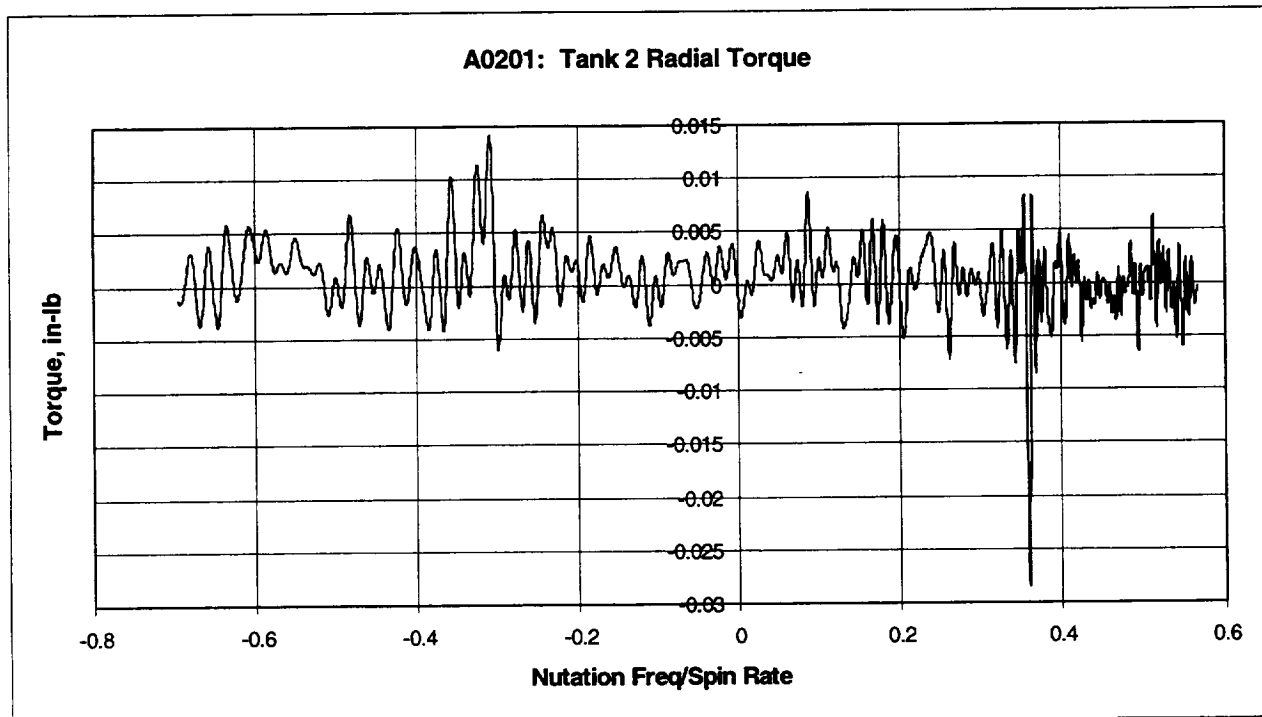
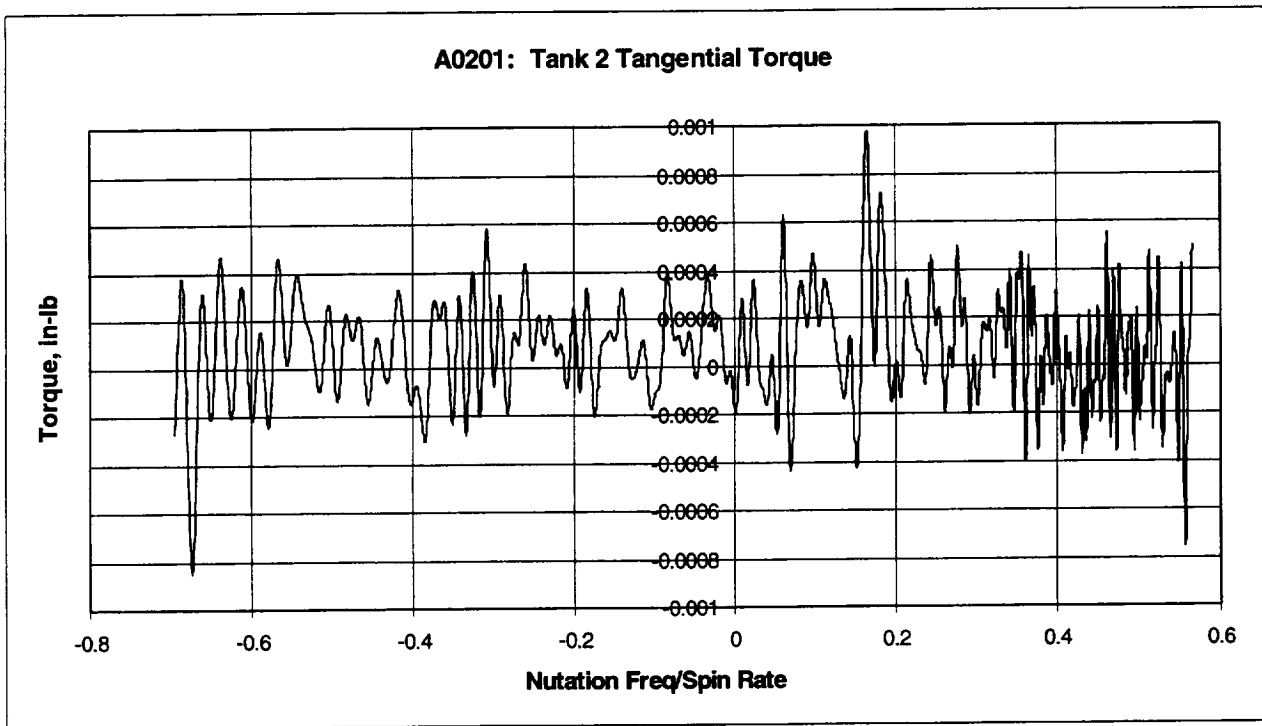


Tank 4 (C0101): PMD - 1/3 Full - Liquid Viscosity = 1 cp

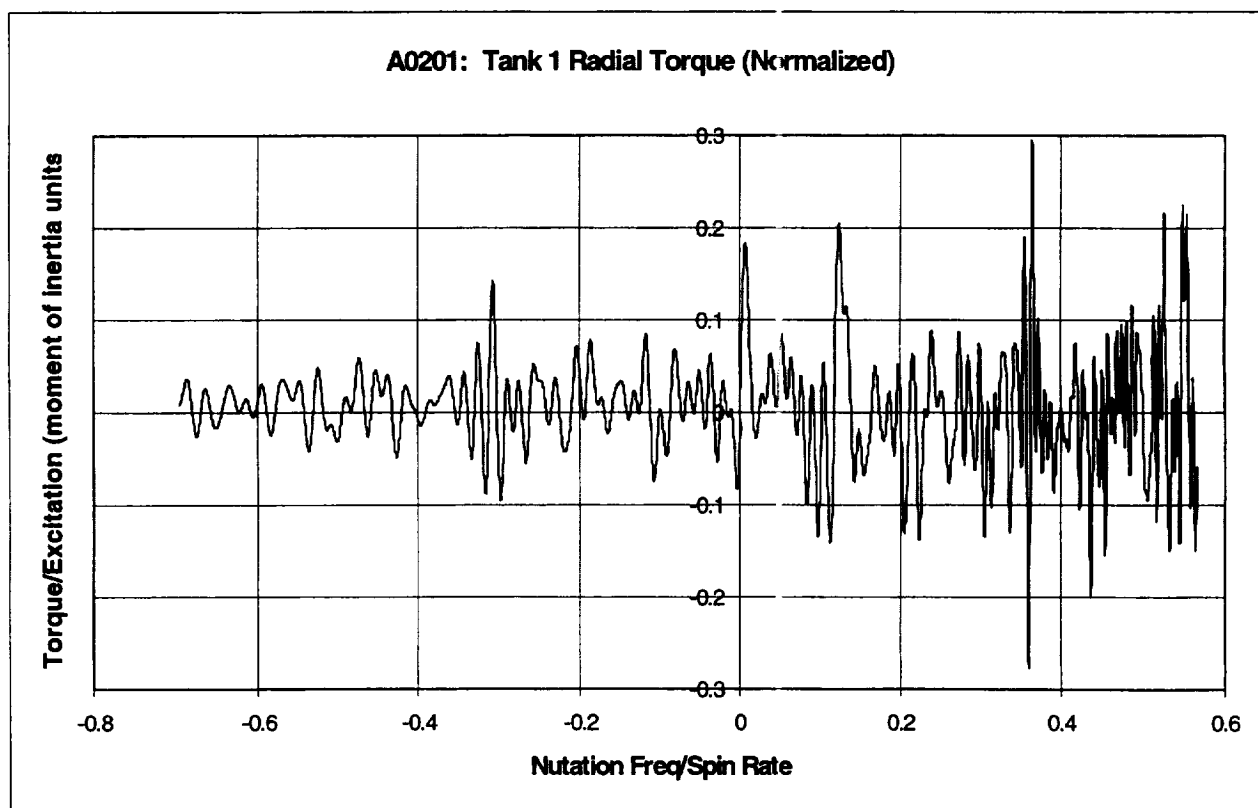
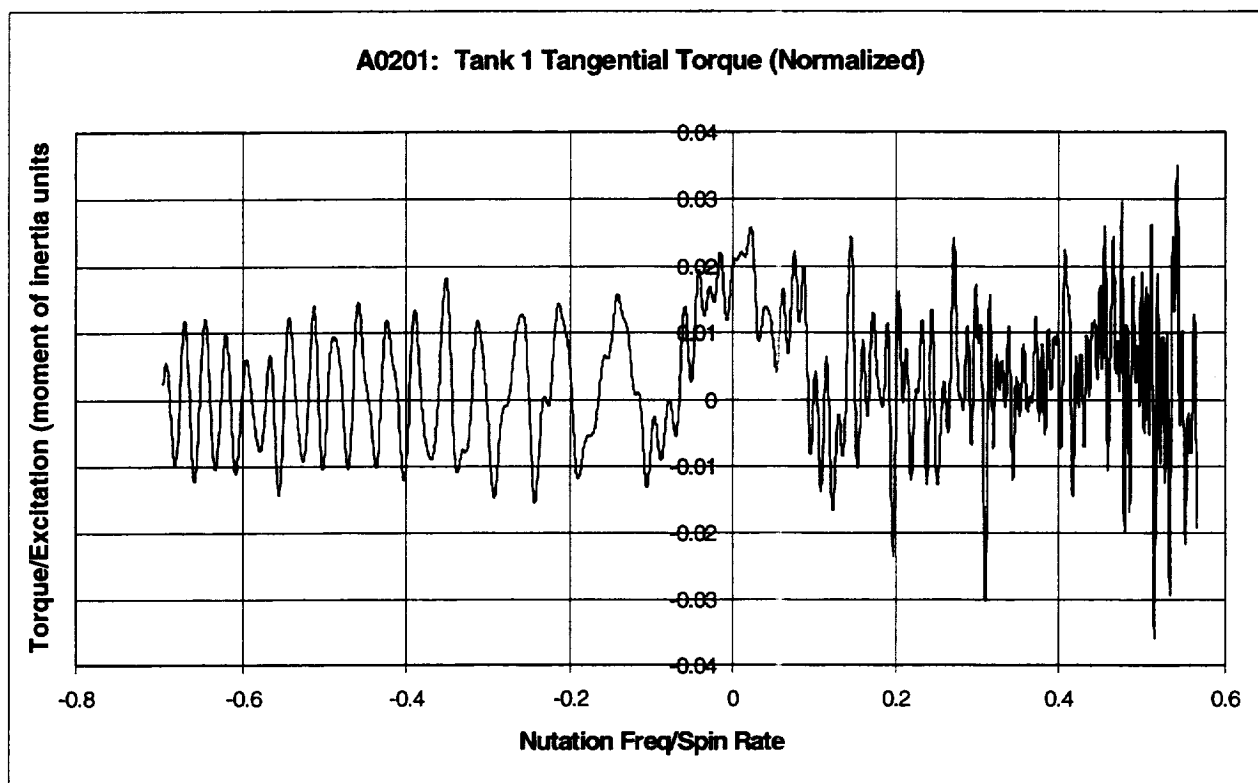


Tank 4 (C0101): concluded

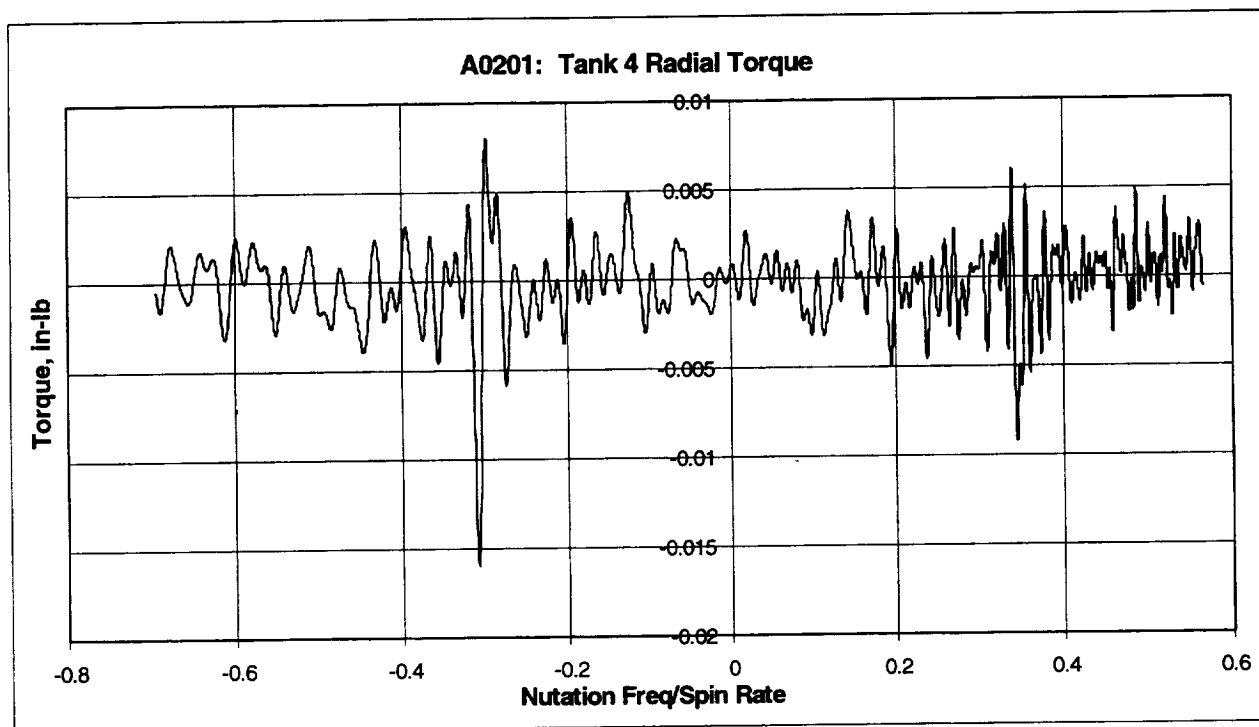
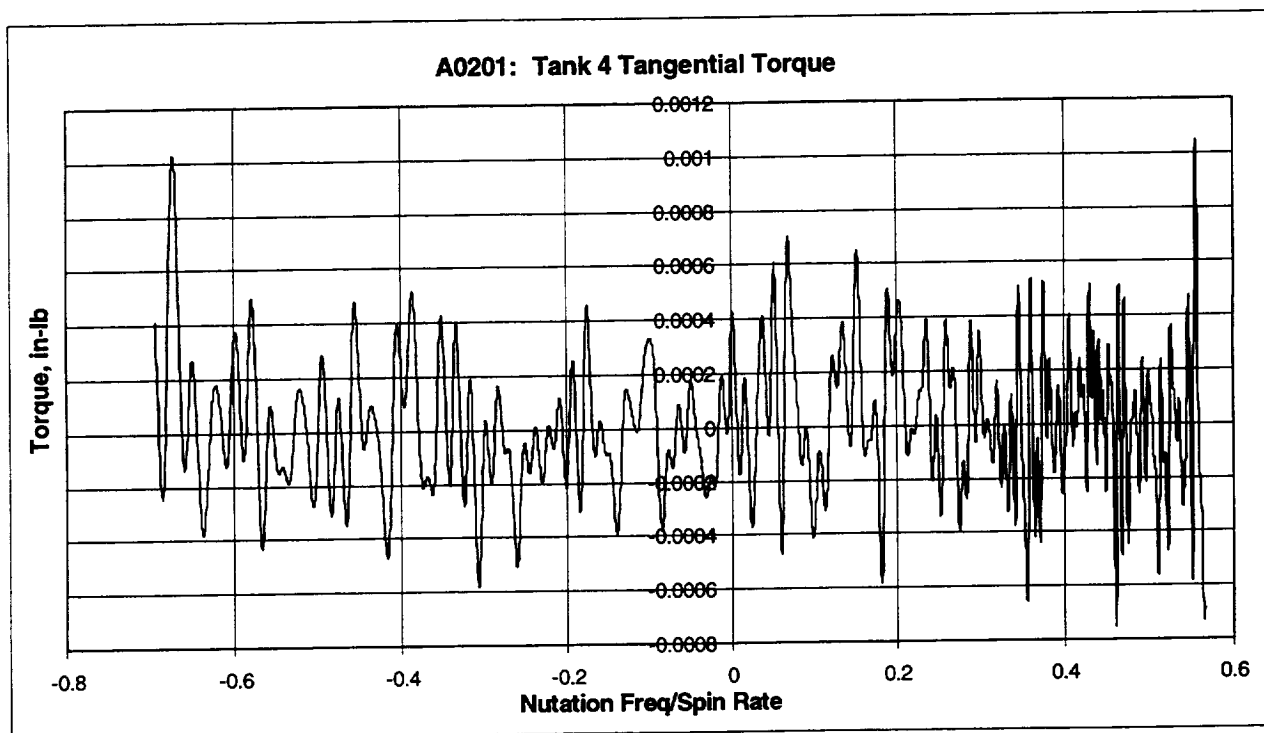


A0201: 4.5 RPM SWEEP TESTS - TANK SET A, SPHERICAL TANKS 2 AND 4**Nutation Sweep Range: 2.6 rpm \rightarrow 0 \rightarrow 3.1 rpm****Tank 2: 2/3 Full - Liquid Viscosity = 1 cp**

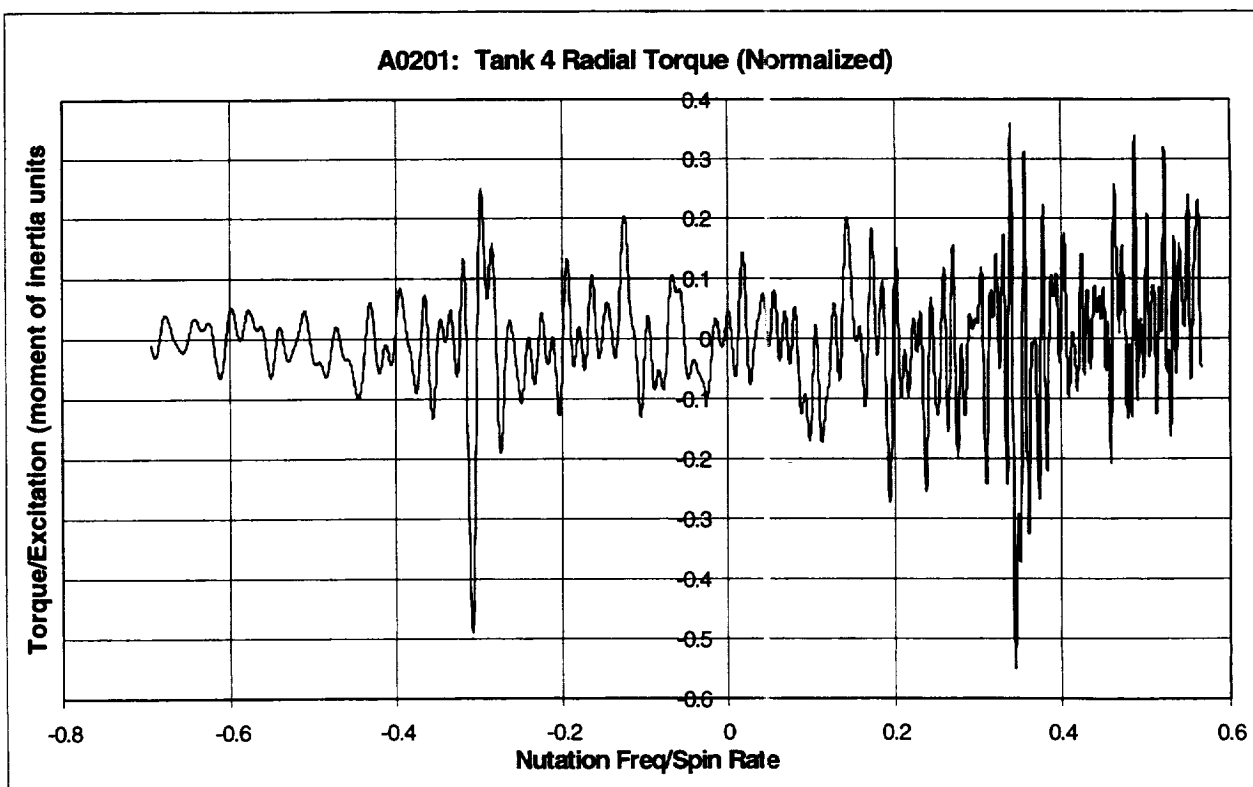
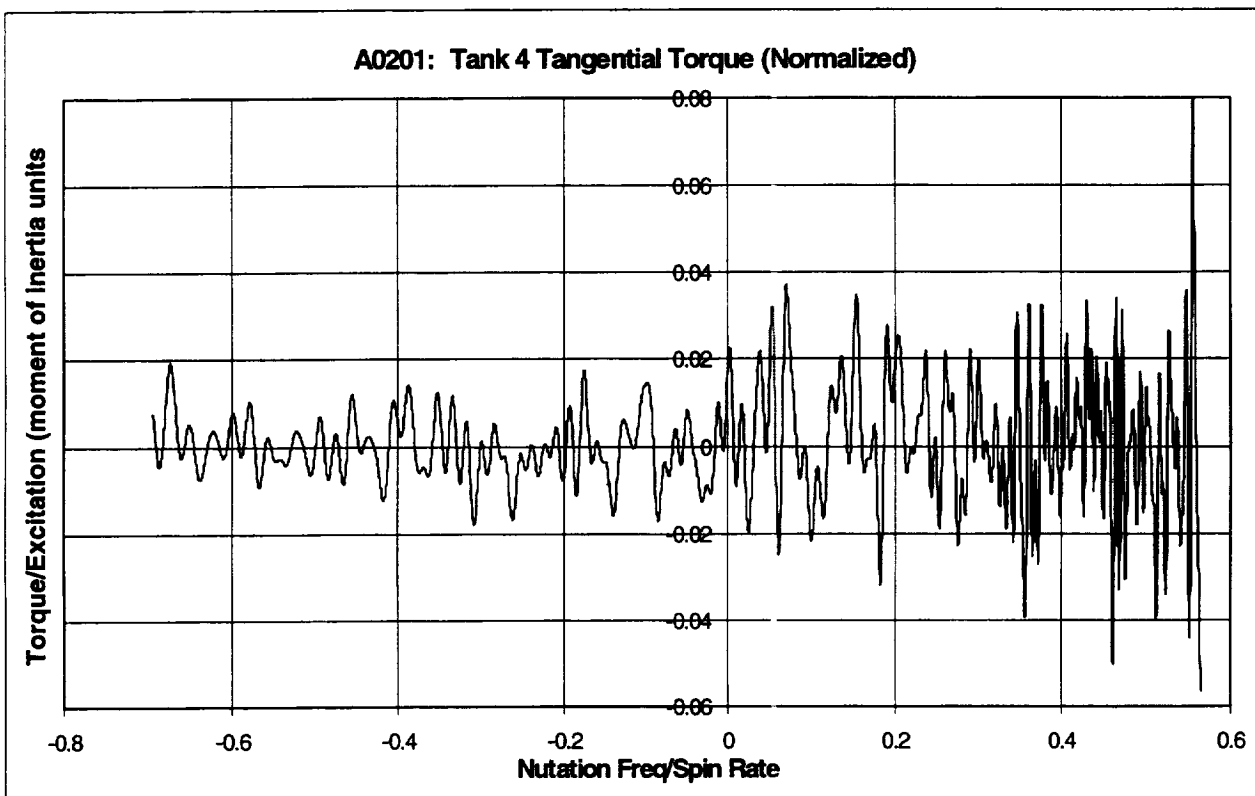
Tank 2 (A0201): concluded



Tank 4 (A0201): 2/3 Full - Viscosity = 10 cp

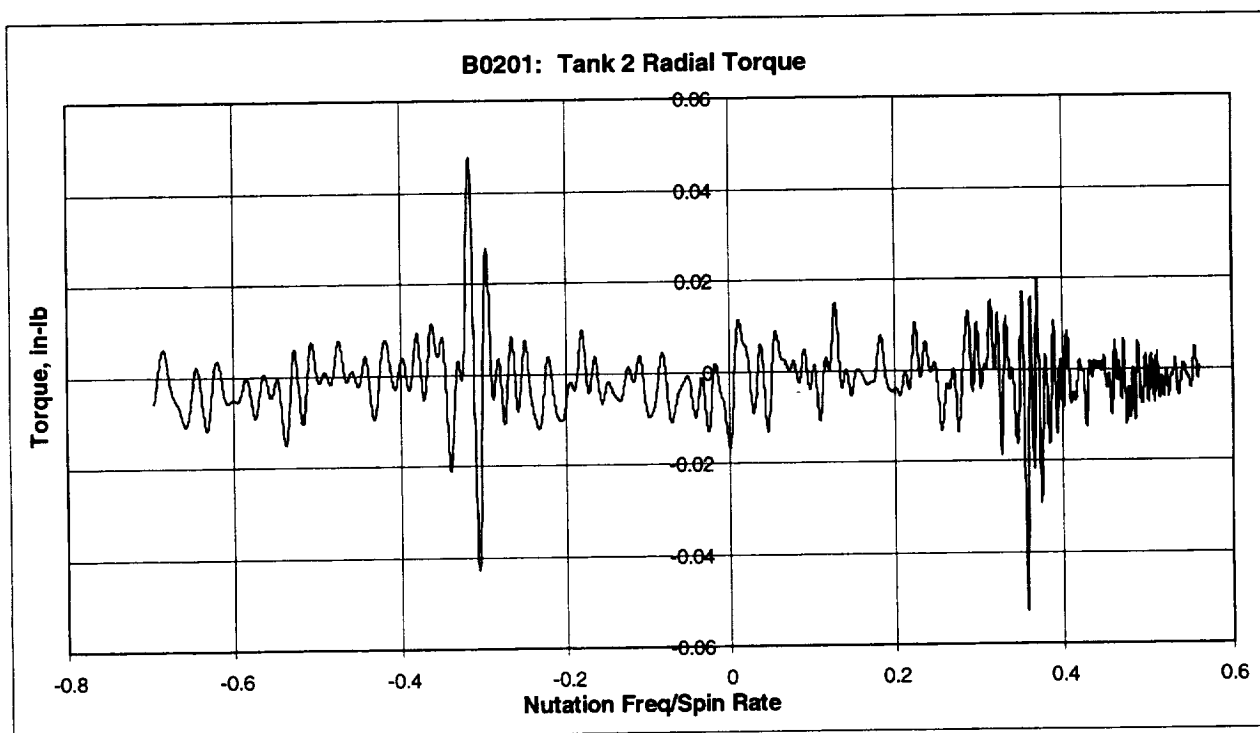
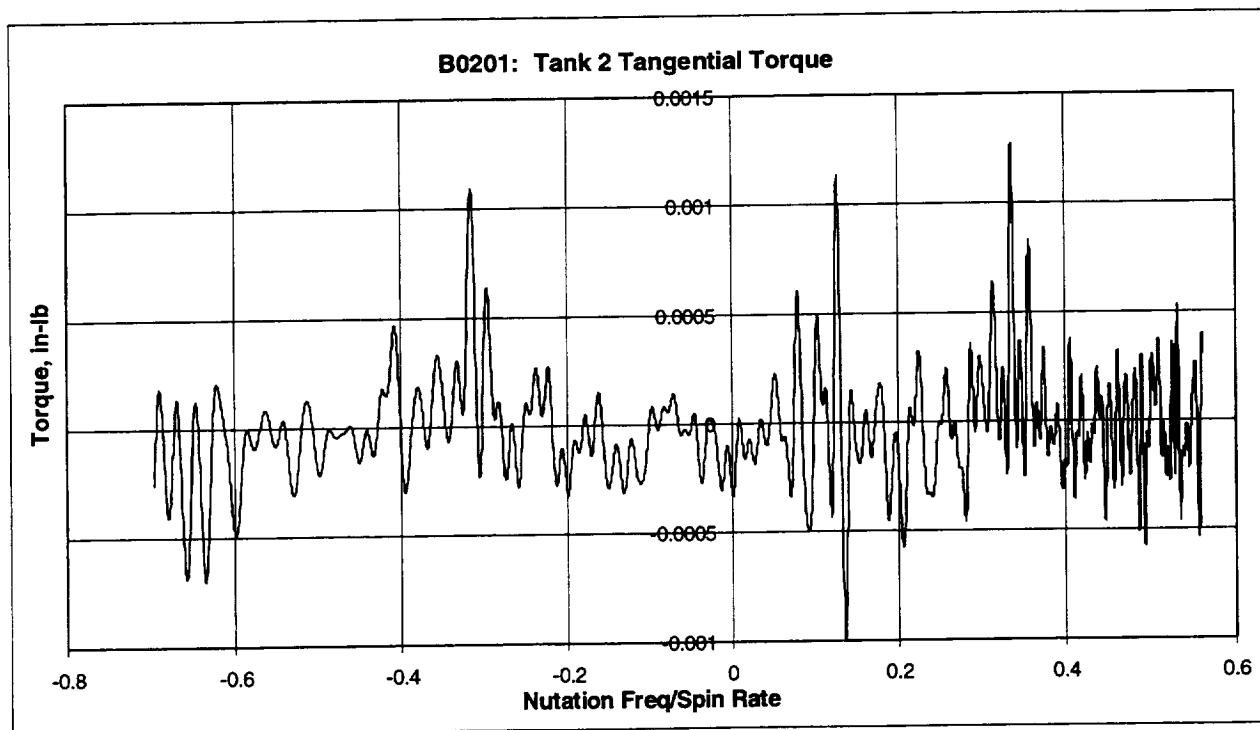


Tank 4 (A0201): concluded

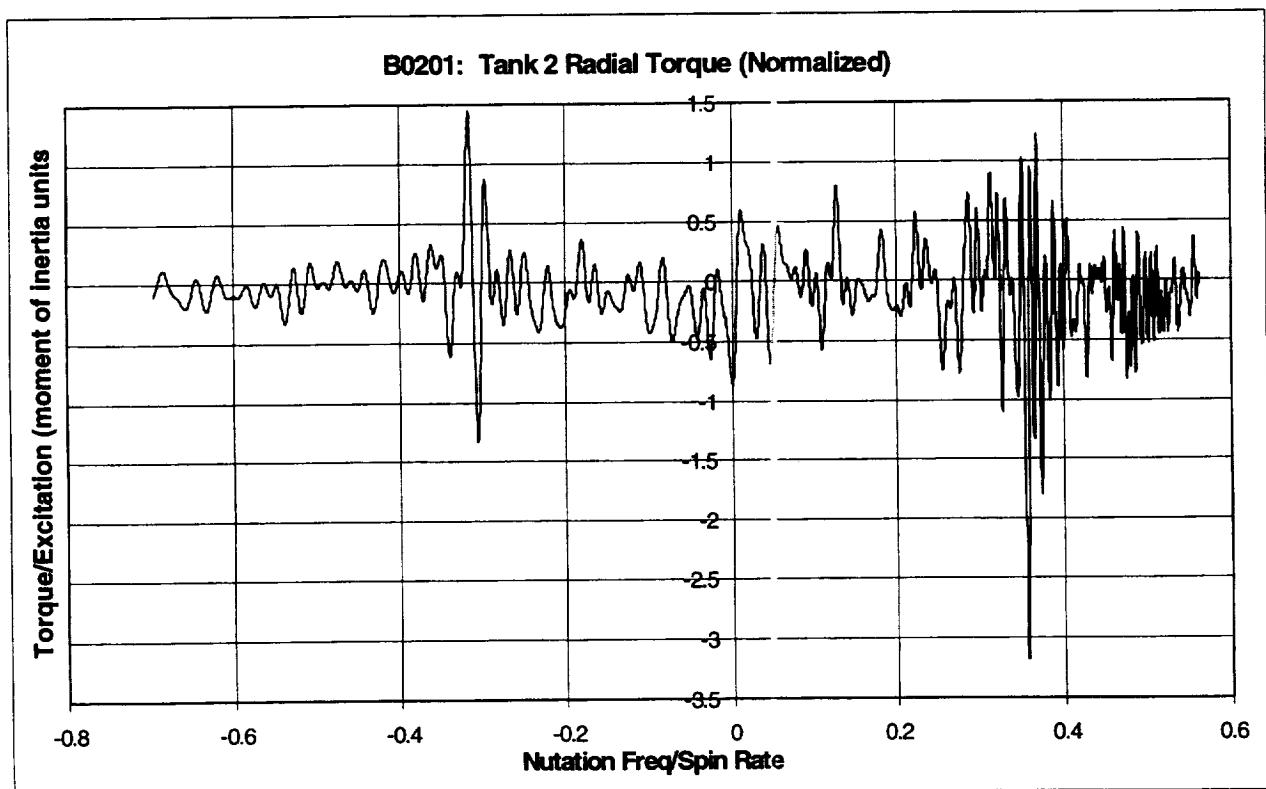
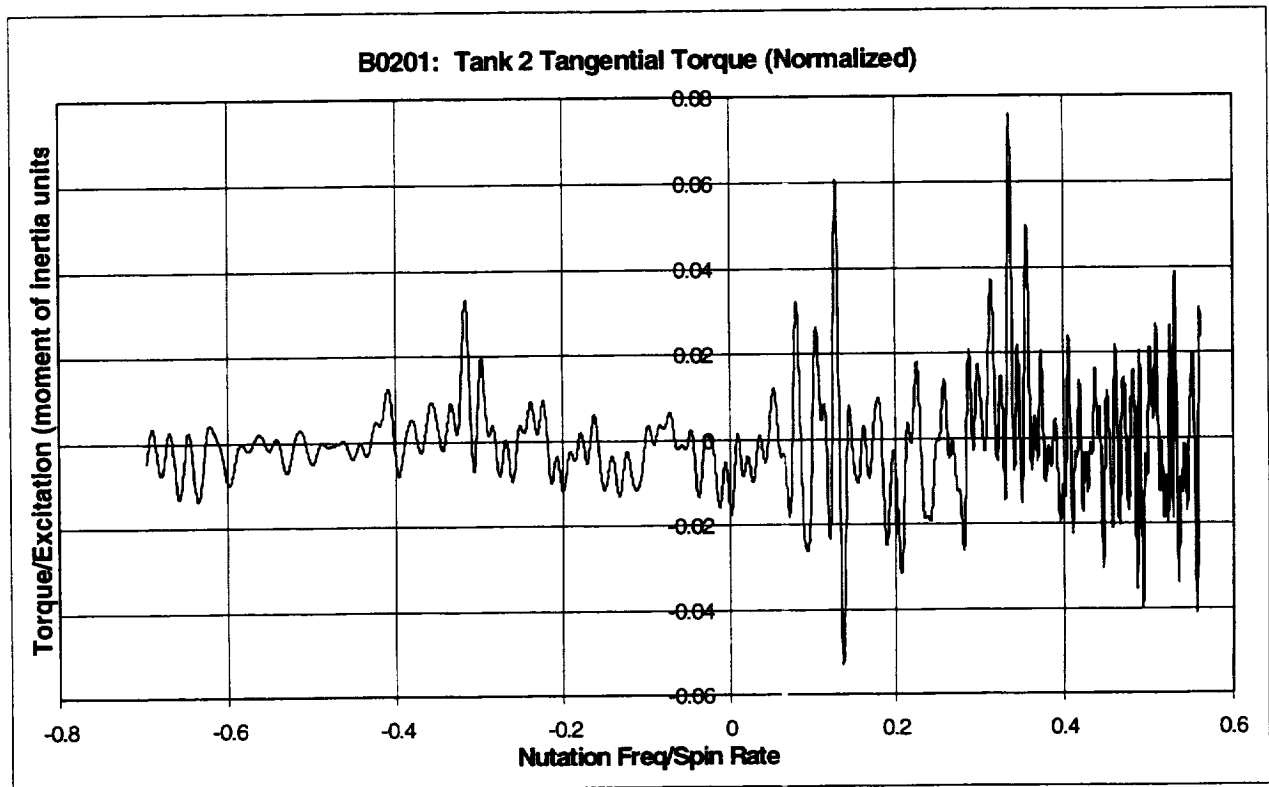


B0201: 4.5 RPM SWEEP TESTS - TANK SET B, SPHERICAL TANKS 2 AND 4Nutation Sweep Range: 2.6 rpm \rightarrow 0 \rightarrow 3.1 rpm

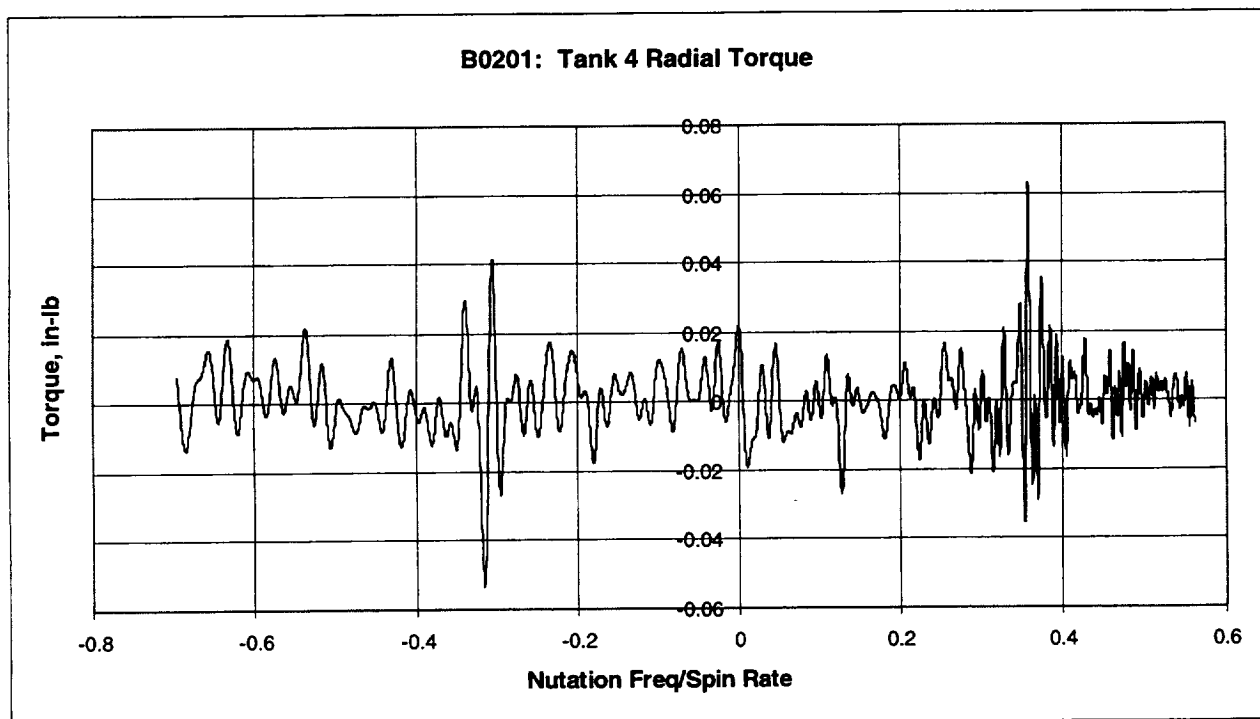
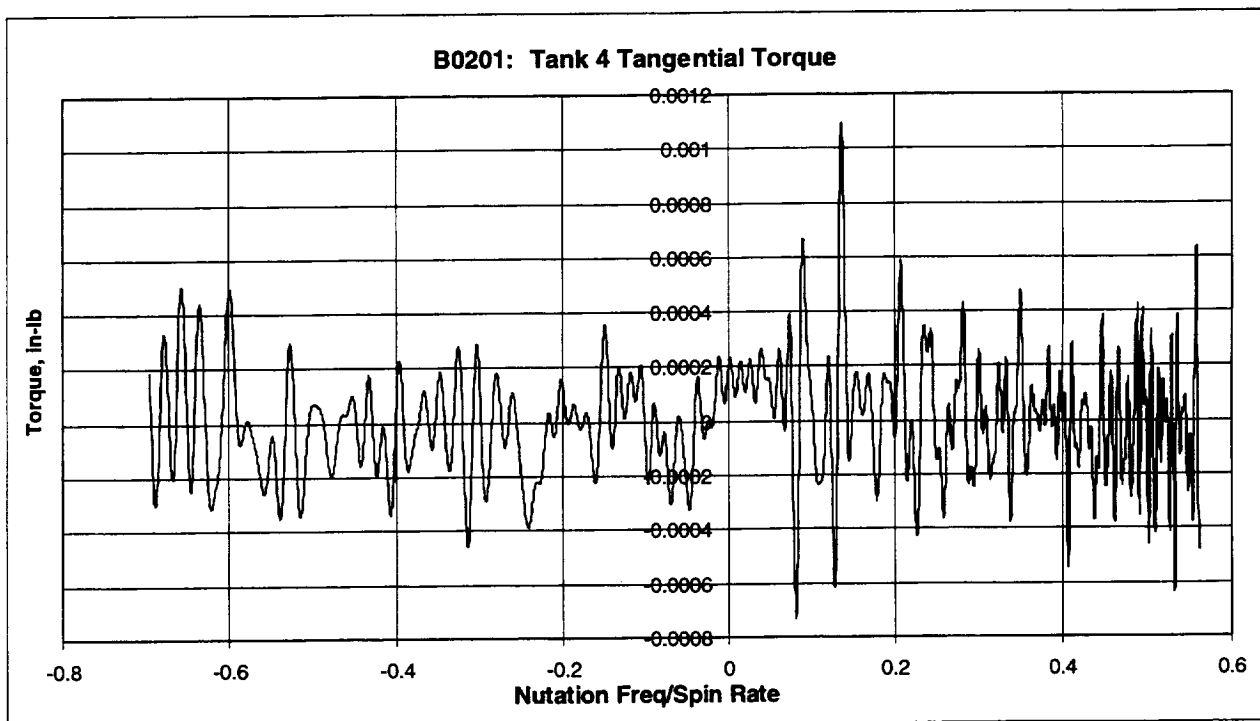
Tank 2: 2/3 Full - Liquid Viscosity = 1 cp



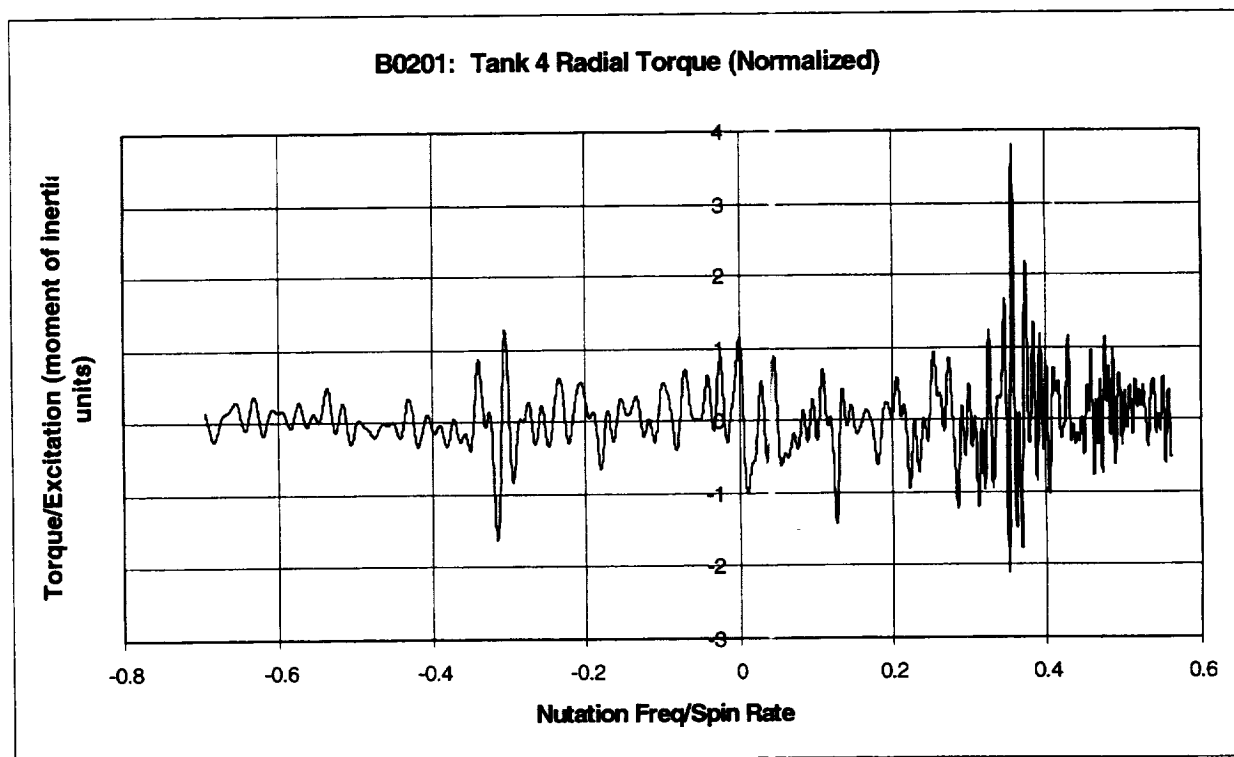
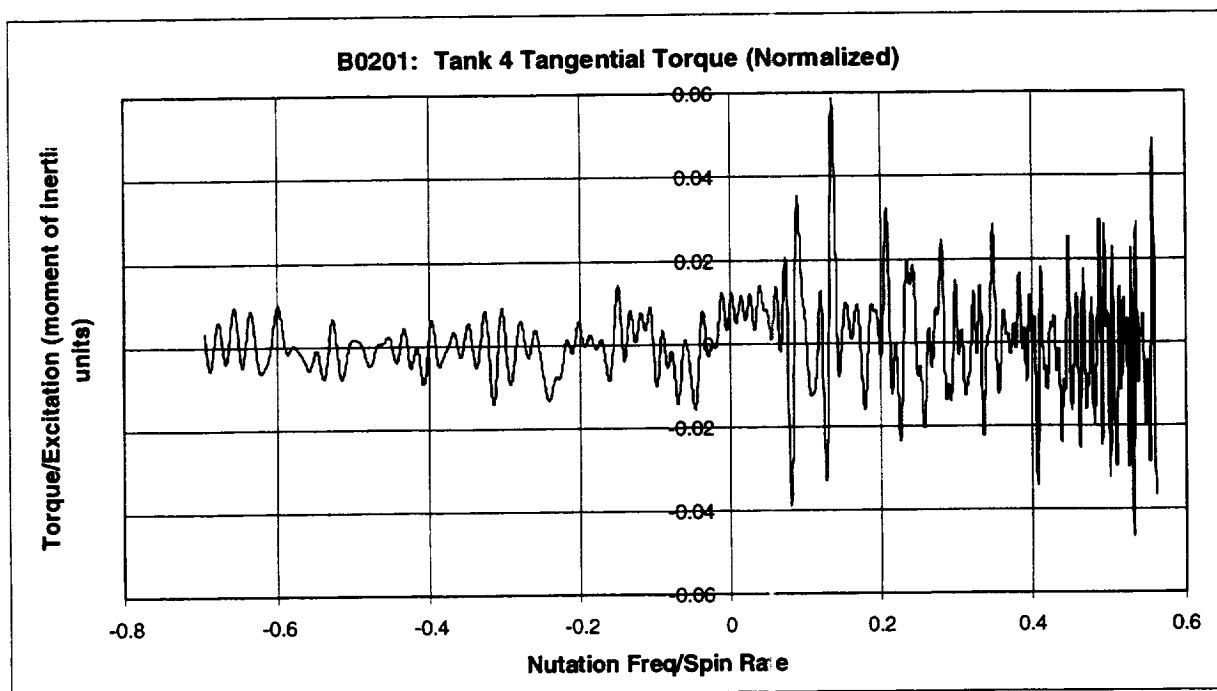
Tank 2 (B0201): concluded



Tank 4 (B0201): 2/3 Full - Liquid Viscosity = 10 cp



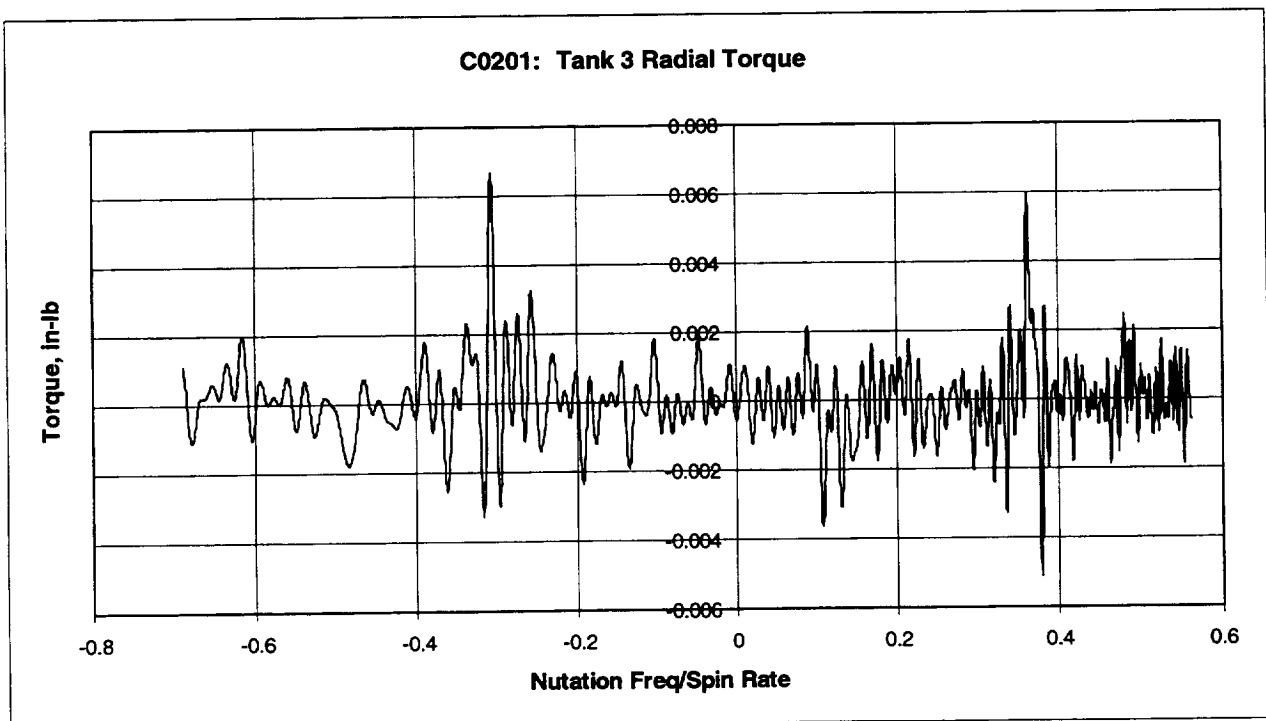
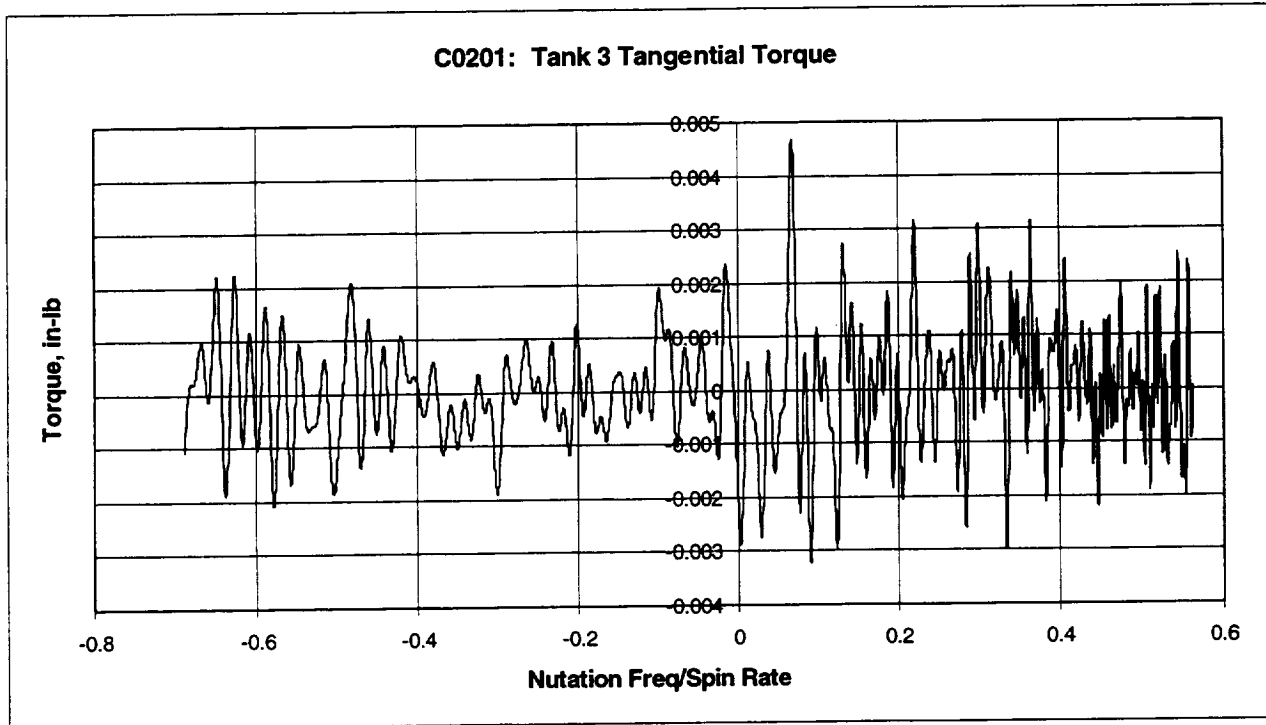
Tank 4 (B0201): concluded



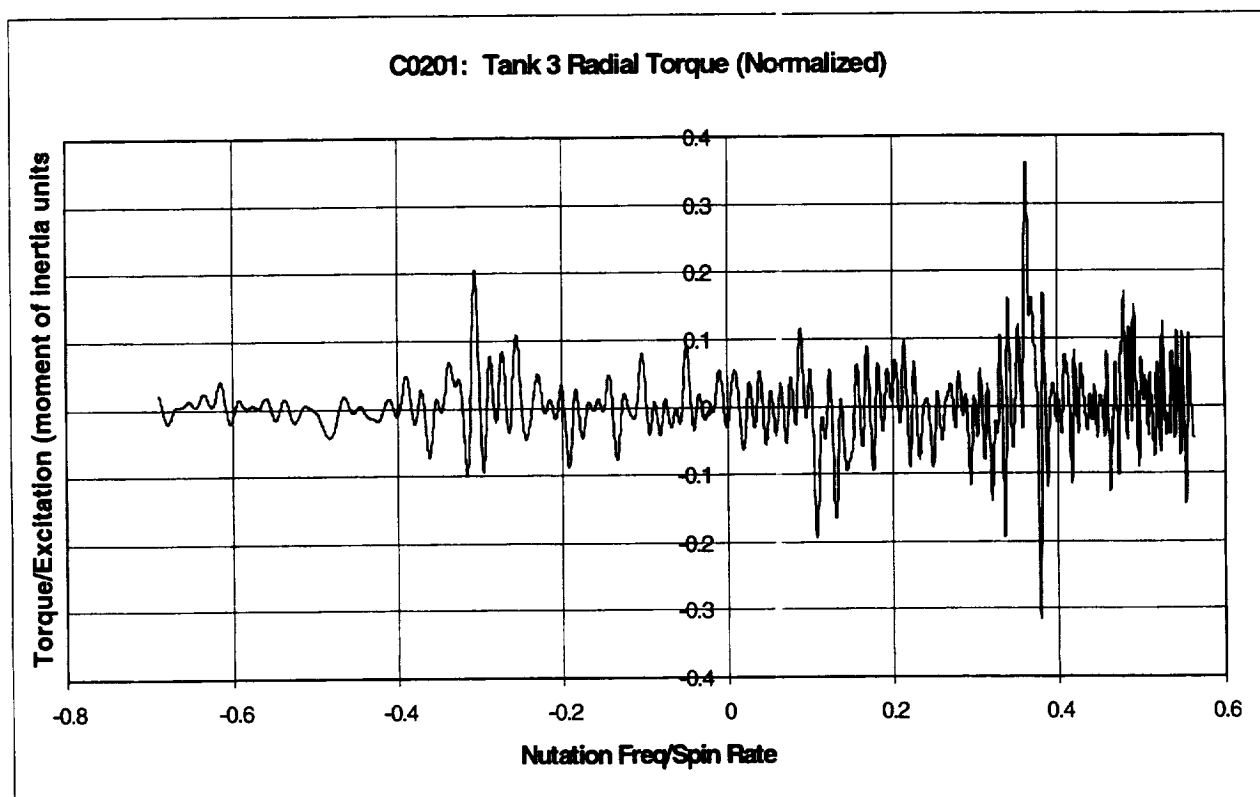
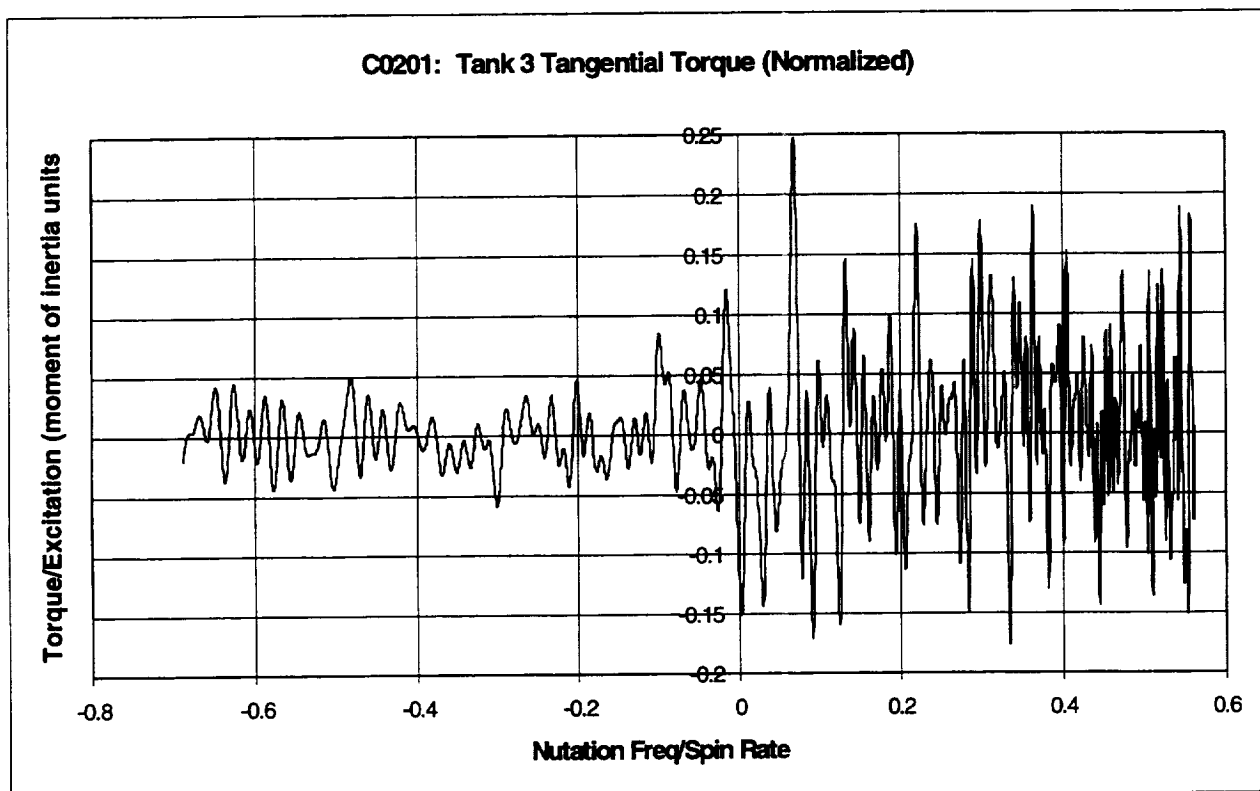
C0201: 4.5 RPM SWEEP TESTS AT - TANK SET C, SPHERICAL TANKS 3 AND 4

Nutation Sweep Range: 2.6 rpm \rightarrow 0 \rightarrow 3.1 rpm

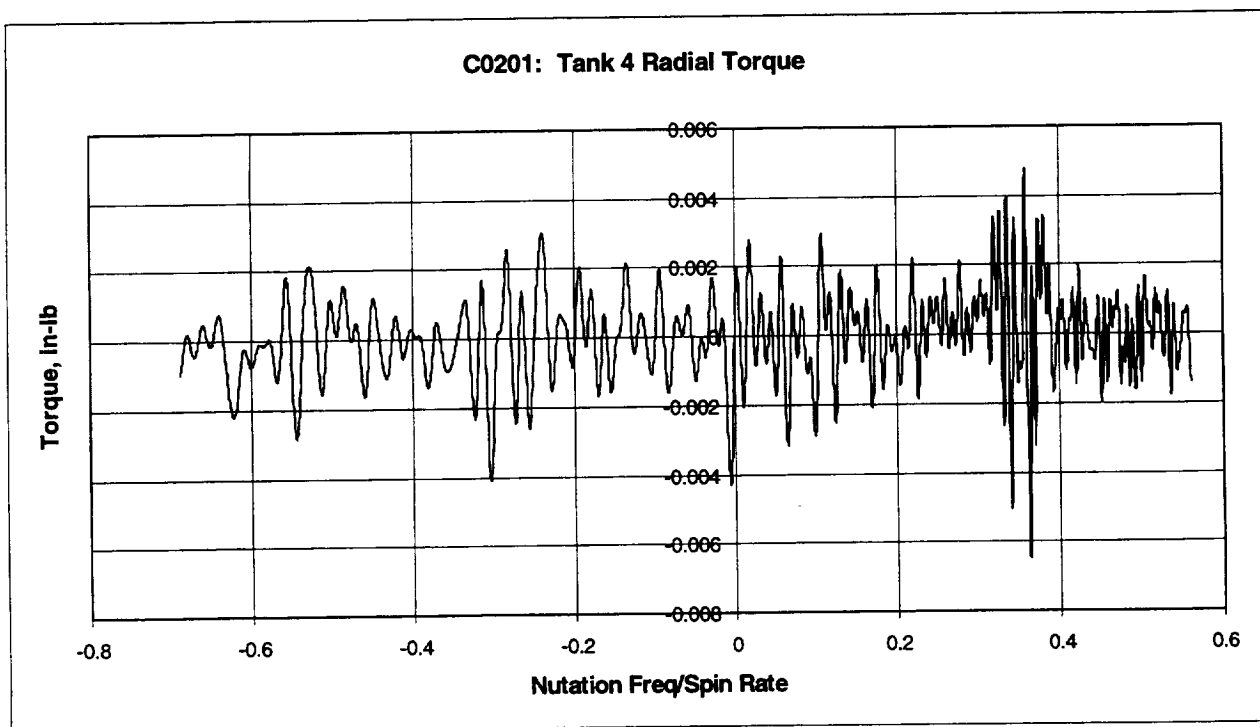
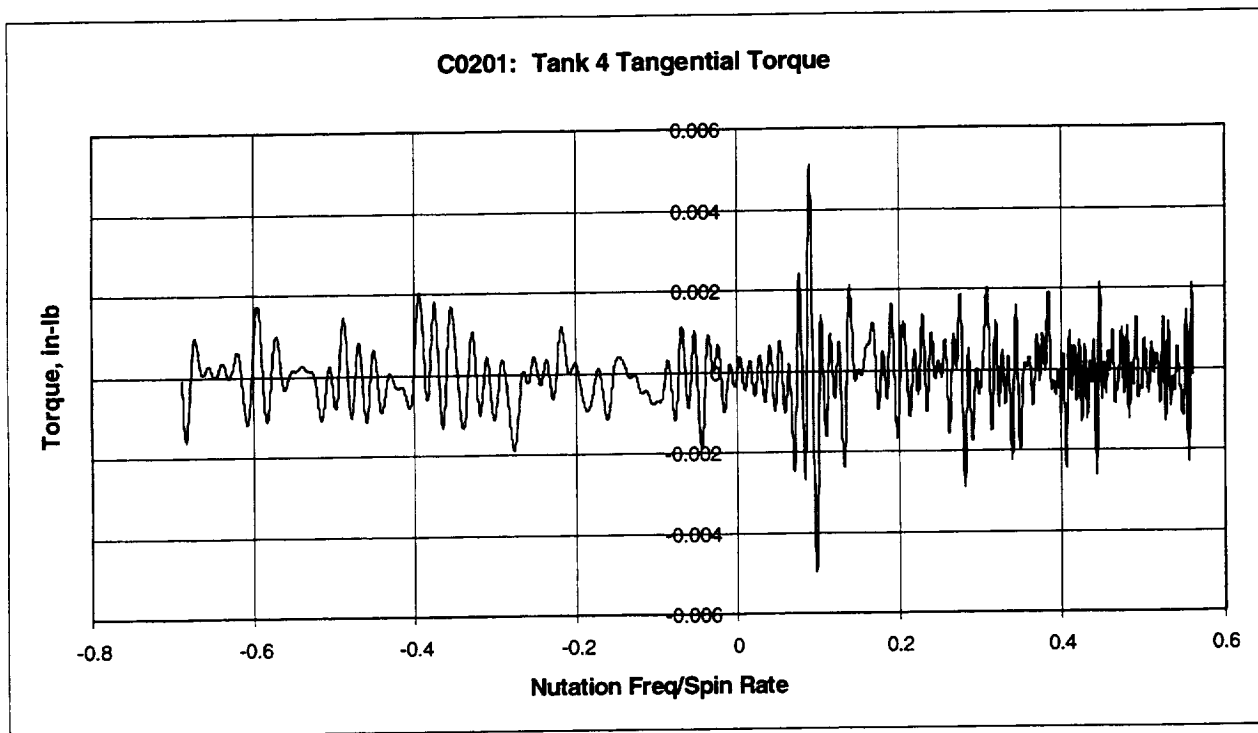
Tank 3: PMD - 2/3 Full - Liquid Viscosity = 1 cp

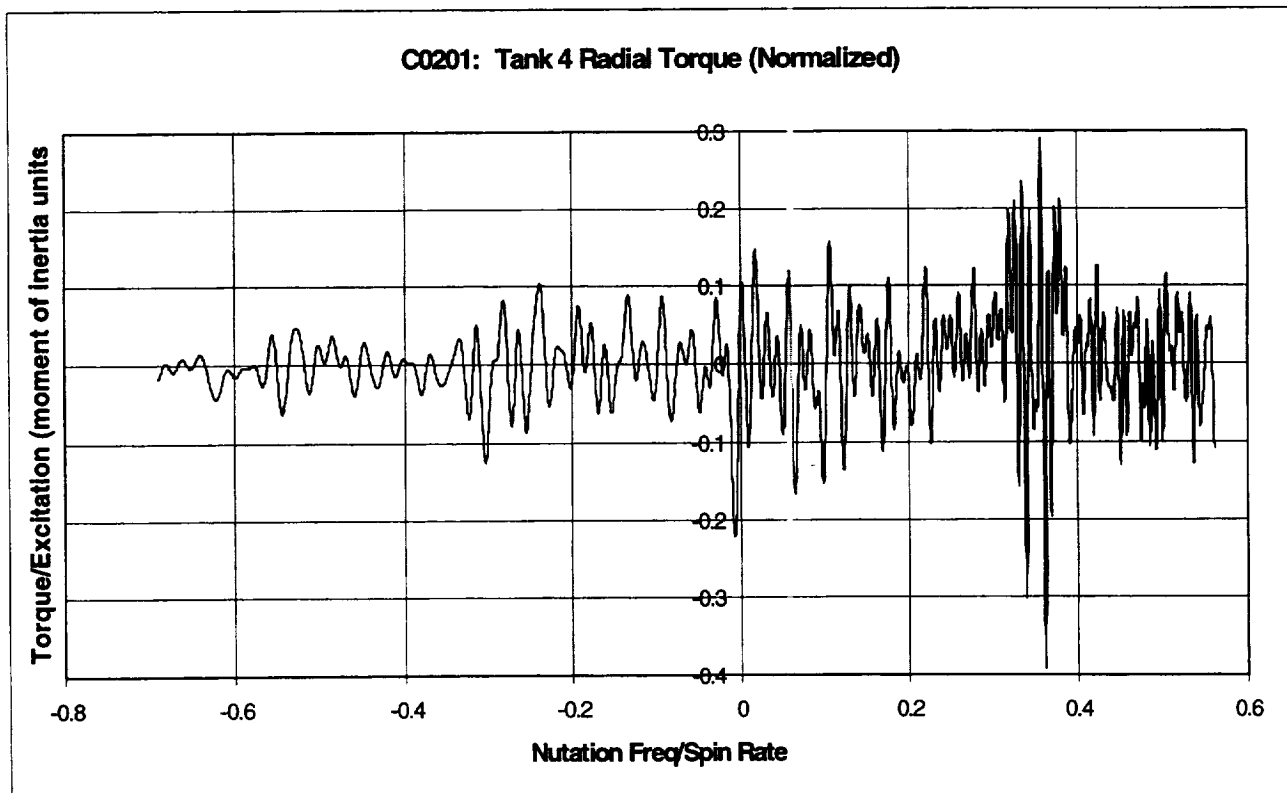
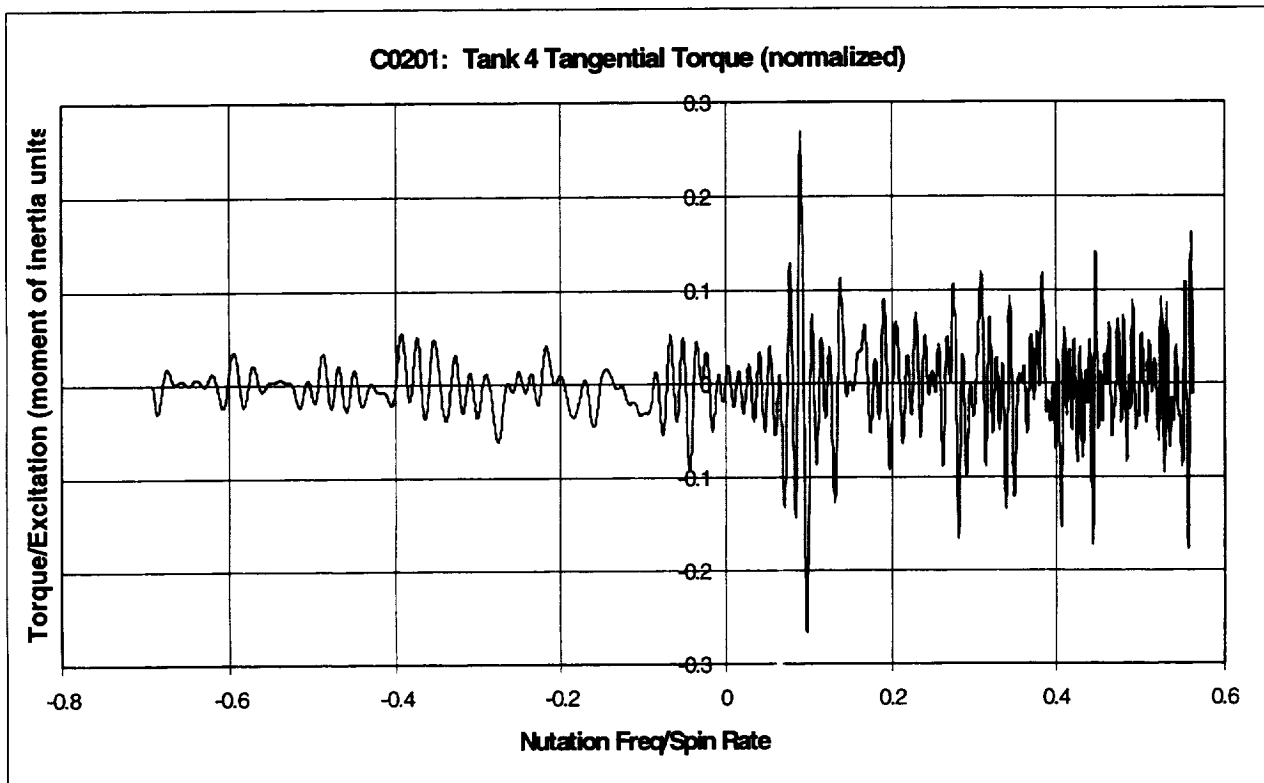


Tank 3 (C0201): concluded



Tank 4 (C0201): PMD - 1/3 Full - Liquid Viscosity = 1 cp



Tank 4 (C0201): concluded

REPORT DOCUMENTATION PAGE			Form Approved OMB No. 0704-0188	
Public reporting burden for this collection of information is estimated to average 1 hour per response, including the time for reviewing instructions, searching existing data sources, gathering and maintaining the data needed, and completing and reviewing the collection of information. Send comments regarding this burden estimate or any other aspect of this collection of information, including suggestions for reducing this burden, to Washington Headquarters Services, Directorate for Information Operations and Reports, 1215 Jefferson Davis Highway, Suite 1204, Arlington, VA 22202-4302, and to the Office of Management and Budget, Paperwork Reduction Project (0704-0188), Washington, DC 20503.				
1. AGENCY USE ONLY (Leave blank)	2. REPORT DATE September 1998	3. REPORT TYPE AND DATES COVERED Final Contractor Report		
4. TITLE AND SUBTITLE Final Report for the Liquid Motion in a Rotating Tank Experiment (LME)		5. FUNDING NUMBERS WU-632-1C-1X-00 NAS3-27252		
6. AUTHOR(S) D.M. Deffenbaugh, F.T. Dodge, and S.T. Green				
7. PERFORMING ORGANIZATION NAME(S) AND ADDRESS(ES) Southwest Research Institute Mechanical and Fluids Engineering Division P.O. Drawer 28510 6220 Culebra Road San Antonio, Texas 78228-0510		8. PERFORMING ORGANIZATION REPORT NUMBER E-11385		
9. SPONSORING/MONITORING AGENCY NAME(S) AND ADDRESS(ES) National Aeronautics and Space Administration Lewis Research Center Cleveland, Ohio 44135-3191		10. SPONSORING/MONITORING AGENCY REPORT NUMBER NASA CR-1998-208667 6322-FNL-01		
11. SUPPLEMENTARY NOTES Project Manager, Penni Dalton, Power and Propulsion Office, NASA Lewis Research Center, organization code 6910, (216) 433-5223.				
12a. DISTRIBUTION/AVAILABILITY STATEMENT Unclassified - Unlimited Subject Category: 20 This publication is available from the NASA Center for Aerospace Information, (301) 621-0390.		12b. DISTRIBUTION CODE Distribution: Nonstandard		
13. ABSTRACT (Maximum 200 words) The Liquid Motion Experiment (LME), which flew on STS 84 in May 1997, was an investigation of liquid motions in spinning, nutating tanks. LME was designed to quantify the effects of such liquid motions on the stability of spinning spacecraft, which are known to be adversely affected by the energy dissipated by the liquid motions. The LME hardware was essentially a spin table which could be forced to nutate at specified frequencies at a constant cone angle, independently of the spin rate. Cylindrical and spherical test tanks, partially filled with liquids of different viscosities, were located at the periphery of the spin table to simulate a spacecraft with off-axis propellant tanks; one set of tanks contained generic propellant management devices (PMDs). The primary quantitative data from the flight tests were the liquid-induced torques exerted on the tanks about radial and tangential axes through the center of the tank. Visual recordings of the liquid oscillations also provided qualitative information. The flight program incorporated two types of tests: <i>sine sweep</i> tests, in which the spin rate was held constant and the nutation frequency varied over a wide range; and <i>sine dwell</i> test, in which both the spin rate and the nutation frequency were held constant. The sine sweep tests were meant to investigate all the prominent liquid resonant oscillations and the damping of the resonances, and the sine dwell tests were meant to quantify the viscous energy dissipation rate of the liquid oscillations for steady state conditions. The LME flight data were compared to analytical results obtained from two companion IR&D programs at Southwest Research Institute. The comparisons indicated that the models predicted the observed liquid resonances, damping, and energy dissipation rates for many test conditions but not for all. It was concluded that improved models and CFD simulations are needed to resolve the differences. This work is ongoing under a current IR&D program.				
14. SUBJECT TERMS Spacecraft propulsion; Spacecraft motion; Nutational oscillation		15. NUMBER OF PAGES 112		
		16. PRICE CODE A06		
17. SECURITY CLASSIFICATION OF REPORT Unclassified	18. SECURITY CLASSIFICATION OF THIS PAGE Unclassified	19. SECURITY CLASSIFICATION OF ABSTRACT Unclassified	20. LIMITATION OF ABSTRACT	